Light-induced protein degradation : a chemical biology approach

Quentin Delacour

Université Pierre et Marie Curie

Ecole doctorale 388 :

Chimie Physique et Chimie Analytique de Paris Centre

Laboratoire PASTEUR

Pôle de Chimie Bio-Physique

Light-induced protein degradation

A chemical biology approach

Présentée par

Quentin Delacour

Thèse de doctorat de Chimie-Physique

Dirigée par

Arnaud GAUTIER et Ludovic JULLIEN

Présentée et soutenue publiquement le vendredi 25 septembre 2015

Devant un jury composé de :

M.	Dr.	Arnaud	GAUTIER	Directeur de thèse
M.	Prof.	Ludovic	JULLIEN	Directeur de thèse
Mme	Dr.	Sandrine	SAGAN	Examinateur
M.	Dr.	Alexandre	SPECHT	Rapporteur
M.	Dr.	Christoph	TAXIS	Rapporteur
Mme	Prof.	Sophie	VRIZ	Examinateur

Light-induced protein degradation

A chemical biology approach

Présentée par

Quentin Delacour

Thèse de doctorat de Chimie-Physique

S.D.G.

List of abbreviations

a.a.: amino-acid
ABA: Abscissic acid
AID: Auxin inducible degron
AFB: Auxin signaling F-box protein
APC/C: Anaphase-promoting complex E3
ARF: Auxin response factors
At: *Arabidopsis thaliana*
ATCC: American type culture collection
B-LID: Blue light inducible degradation
Cdk: Cyclin-dependent kinase
CHIP: C-ter of Hsc70 interacting protein
CHO: Chinese Hamster ovarian
CID: Chemically-inducible dimerization
CMV: Cytomegalo Virus
CRL: Cullin-RING ligase
Cry: *At*Cryptochrome
C-ter: C-terminus of a protein
Cul: Cullin
DBP: Designer binding protein
DD: Destabilizing degron
DHFR: Dihydrofolate reductase
D-MEM: Dulbecco's modified eagle medium
DMNB:4,5-Dimethoxy-2-nitrobenzyl
DMSO: Dimethyl sulfoxyde
DUB: Deubiquitin enzyme
EGFP: Enhanced green fluorescent protein
E1: Ubiquitin activating enzyme
E2: Ubiquitin conjugating enzyme
E3: Ubiquitin ligase enzyme
ER: endoplasmic reticulum
FKBP: FK506 binding-protein
FMN: Flavin mononucleotide
FP: Fluorescent protein
GA: Gibberellic acid
GFP: Green fluorescent protein
HA: Haemaglutinin
HEK293: Human embryonic kidney
HPLC: High-performance liquid chromatography
Hs: *Homo sapiens*
hv: light-illumination
HSP: Heat-shock protein
IAA: Indole acetic acid
IB: Immunoblotting
InsP6: Inositol-6 Phosphate
IRES: Internal ribosomal entry site
J*α*: C-ter helix of *At*LOV2
KikG/R: Kikume green/red
LOV: Light oxygen voltage
LRR: Leucine rich repeats
M: Mock sample
NA: numerical aperture
NAA: Naphtalene acetic acid
NLS: Nuclear localization signal
NPE: 1-(2-nitrophenyl)-ethanol
N-ter: N-terminus of a protein
ODC: Ornithine decarboxylase
Os: *Oryza sativa*
PA-IAA: Photoactivatable IAA
PBS: Phosphate saline buffer
PDB: Protein data dank
POI: Protein of interest
PQC: Protein quality control
psd: photosensitive degron
PROTAC: Proteolysis targeting chimeric protein
ROI: Region of interest
SAC: Spindle assembly checkpoint
Sc: *Saccharomyces cerevisiae*
SD: Standard deviation
shAID: short Auxin-inducible degron
siRNA: small interfering RNA
Skp1: S-phase kinase-associated protein
TEV: Tobacco-etch Virus
TIPI: TEV protease-induced protein inactivation
TIR1: Transport inhibitor response 1
tRNA: transfer RNA
ts: temperature sensitive
UAA: Unnatural amino-acid
Ub: Ubiquitin
UAE: Ubiquitin activating enzyme
UBD: Ubiquitin-binding domain
UCD: Ubiquitin-conjugating domain
UCE: Ubiquitin conjugating enzyme E2
UPS: Ubiquitin proteasome system
UV: Ultra violet
YFP: Yellow fluorescence protein
2,4 D: 2,4 Dichlorophenoxyacetic acid

Contents

Chapter 2: Strategies for the photocontrol of protein activity *in vivo*

Chapter 4: Design of Photo-activatable auxins

Chapter 5: Photo-induced protein degradation in living cells

Chapter 6: Photo-induced protein degradation of a cytoplasmic protein in living cells

Chapter 8: Perspectives

Strategies for photocontrol of protein stability

Chapter 9: Perspectives

Light-activatable degradation could be a relevant perturbation in various contexts

Foreword: What is a *chemical biology* approach?

The frontiers between chemistry and biology disciplines are dynamic. The term *biochemistry* was coined in the early 20th century to describe the field studying chemical processes in living organisms, although the discipline roots back earlier (its birth is often related to the synthesis of urea by Wöhler in 1828)[1]. Biochemistry in its original sense relates to the characterization, purification and reconstitution of biological components. The molecular biology emergence in the second part of the 20th century[2] enabled to close the gap with others biological fields such as *physiology* in a coherent vision of biological processes, so that *biochemistry* now diverges with the latter only by the studied scales.

Chemical biology emerged over the last twenty years as a specific research field at the chemistry/ biology interface, as illustrated in **Fig. 0** with the numbers of references in *Pubmed*[3] database. However, despite its rapid emergence, and the constitution of a *chemical biology* community of researchers, several articles have lined out the difficulty to give an actual positive definition of chemical biology as a research field. This culminated in 2015 with the interview of thirty researchers in the field about the meaning of *chemical biology*[4]. Several characteristics are lined out by commentators to define the *chemical biology* field, such as interdisciplinary research, synergy between chemistry and biology or horizontal focus to study biological questions at the molecular level. Alternatively, other definitions list significant achievements of chemical biology over the last fifteen years. Eventually, many definitions insist on tools and analytical

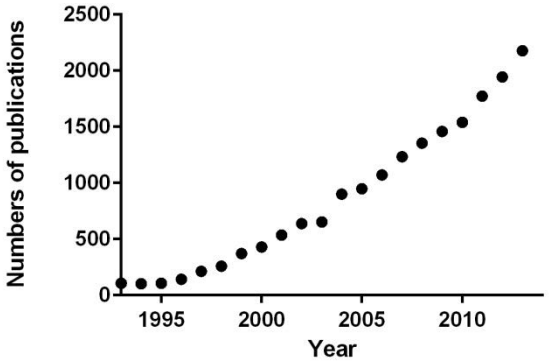

Fig. 0: Number of articles reported in Pubmed from 1992 referring to *chemical biology*.

[1] Morisson K., Weiss G. The origins of chemical biology *Nature Chem. Biol.*, **2** (1), 3-6 (2006).

[2] Morange, M., Histoire de la Biologie Moléculaire, *La Découverte/Poche.*

[3]Alternative clues arguing for the constitution of chemical biology as a specific field are the creation- or change in name- of research journals or research departments explicitly referring to *chemical biology*, the implementation of *chemical biology* degrees in university or the occurrence of *chemical biology* conferences.

[4] *Though our panelists voiced diverse opinions on how chemical biology should be defined, there was a general consensus that modern chemical biology is a distinct discipline by virtue of unique heritage and its subsequent evolution within a dynamic scientific era*. Voices of chemical biology, *Nature Chem. Biol.*, **v. 11**, June 2015. See also: **a**) A decade of chemical biology, *Nature Chem. Biol.*, **v. 6**, December 2010, **b**) Five years of Nature Chemical Biology *Nature Chem. Biol.*, **v. 6**, June 2010, **c**) Chemical biology is, *Chem. Cent. J.*, **1**:5 (2007).

frameworks. Chemical biology is often characterized by its methodologies: commentators listed techniques developed using a chemical biology approach to be applied to biological systems as alternatives to routine biochemical assays[5]. From these definitions, one can retain that an invariant of chemical biology approaches is that they are goal-directed: the experimenter defines a purpose, such as perturbing a specific physiological function with an artifact that he purposefully implements in a living system. This process contrasts with *biochemistry,* which, in a strict sense relates to the description of biological mechanisms.

A common inaccuracy in molecular biology description is finalism that is to attribute a final cause to living organisms and to describe biological processes as goal-directed. However, these were constituted by evolution, consisting in natural selection of pre-occurring variants optimizing fitness in relation to their environment. To address this contradiction between apparent purpose and *''blind''* evolutionary mechanisms, the concept of *teleonomy* was introduced[6], in contrast to *teleology*, in which an agent intentionally models purposed alternatives. Teleonomy was particularly developed by François Jacob in his essay Chance and Necessity (see quote **page 135**).

We thus propose to describe *chemical biology* as a *teleologic* approach of biological studies, to be compared with the *teleonomic* nature of biological processes. In *chemical biology* approaches, the experimenter is an external agent who introduces purpose (obtain given characteristics in a physiological function) to purposeless biological systems. In this dissertation, we propose to illustrate this proposed definition with our work on the implementation of a light-induced protein degradation platform that was published this year (Delacour, 2015). This *teleologic* approach (the experimenters defines the goal) was implemented by hijacking endogenous components of a protein degradation pathway. In this prospect, we will describe the implementation of light-induced degradation in relation to the subjacent biological processes resulting from *teleonomic* evolution.

---

[5] *Chemical biology is focused on the development of new molecules or approaches that are purposefully and intentionally designed to address specific gaps in biological knowledge. In other words, 'tool making' occurs hand in hand with 'tool using'*. Gestwicki J., Voices of chemical biology, *Nature Chem. Biol.*, **vol.11**, June 2015.

[6]*The biologists long-standing confusion would be removed if all end-directed systems were described by some other term, e.g., 'teleonomic,' in order to emphasize that recognition and description of end-directedness do not carry a commitment to teleology as an efficient causal principle*. Pittendrigh C. S., Adaptation, natural selection, and behavior in Behavior and Evolution, ed. A. Roe and G. G. Simpson, University Press, 1958, 390-416.

PART A
INTRODUCTION

Evolution behaves like a tinkerer who, during eons upon eons, would slowly modify his work, unceasingly retouching it, cutting here, lengthening there, seizing the opportunities to adapt it progressively to its new use. […]Evolution does not produce novelties from scratch. It works on what already exists, either transforming a system to give it new functions or combining several systems to produce a more elaborate one.

Francois Jacob, Evolution and Tinkering, *Science*, 196-4295 (1977)

Chapter 1

Strategies for the control of protein degradation

1.0 Motivation: development of a generic perturbation method

The study of the specific role played by a given Protein of Interest (POI) in biological processes relies on perturbative techniques that interfere, at some point, in the gene expression process. An overview of this scheme is proposed on **Fig.1**. Some specifications for the development of such methods are particularly desirable:

- **genericity** : the method should be applicable to any POI, requiring no prior knowledge, and specifically perturbating the POI
- **temporal resolution** : the perturbation timescale should be compatible with the timescale of the biological phenomenon
- **spatial resolution** : down to the single cell or the subcellular level
- **biocompatibility** : applicable *in vivo*, and non toxic

Much of the knowledge about specific POI originates from genetic perturbation studies: introduction of mutations (natural or induced by mutagenesis) modifies the gene expression, either quantitatively (knock-out models, over-expression) or qualitatively (mutants). However, long timescale is necessary for the introduction or isolation of mutations, and subsequent genetic expression; moreover, many mutations on essential genes have important downstream effects[1], and some are lethal in embryonic development. Introduction of genomic targeted techniques such as the CRISPR/Cas9 methodology has been however a significant step forward (Park, 2014).

[1] Compensatory mechanisms resulting from protein redundancy might also oppose visible effects of the depletion.

The discovery and description of gene silencing by interferent RNAs led to the development of siRNA (Novina, 2004). This generic method is currently widespread in molecular and cellular biology as a particularly potent perturbative tool for genetic inactivation (Jankovics 2014). Generic control of RNA synthesis can also be achieved by modulatable transcription promoter (Ouyang, 2010). However, these methods are not fully generic: the knock-out might not be complete, and does not affect preexistent proteins. They are also unavailable to for the yeast model (Carthew, 2001). Moreover, the temporal resolution is limited as these techniques are often used on a 24 hours timescale (Schneeckloth, 2005).

Therefore, perturbation of the protein activity at the protein-level itself is promising for better time-resolved methodologies. Pharmacological inhibitors, which target a POI and modify its activities with variable efficacy and specificity, have been long used in a therapeutic, but also fundamental perspective (Skaar, 2014). However, the drug-discovery process is partly chance-driven, although it is more and more rationalized by chemical biology approaches. Moreover, about 80% of the proteome has no described enzymatic activity (Raina, 2010); these features make the subsequent development of a generic perturbation technique difficult.

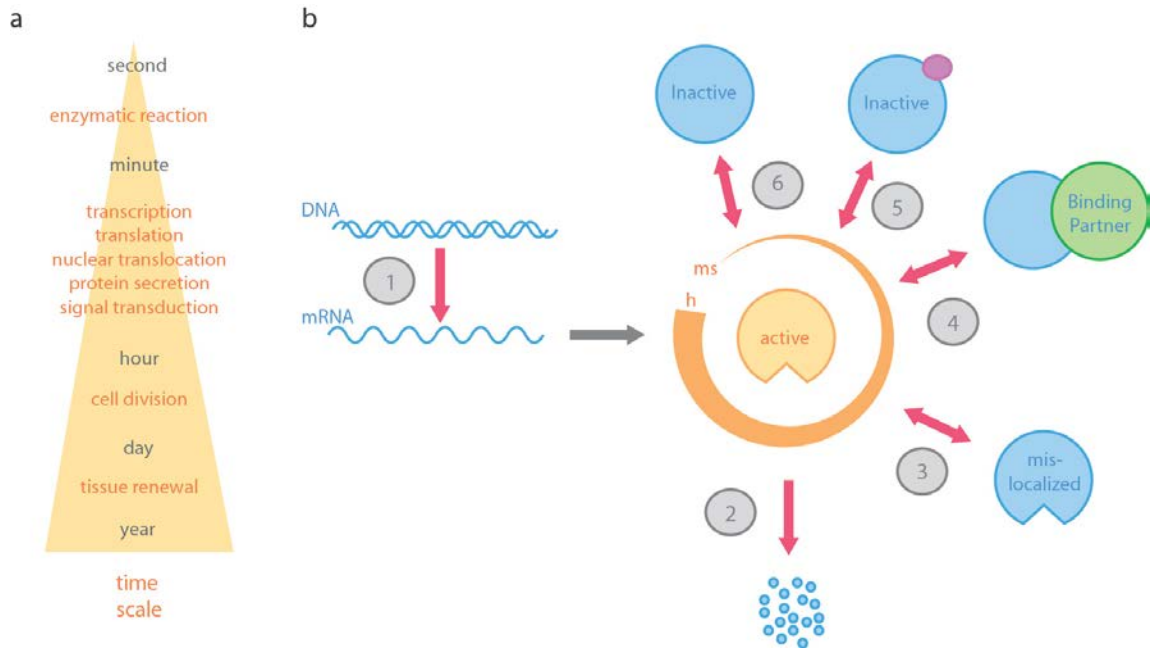

Fig. 1.1: **(a)** Typical timescales of biological processes. Many mechanisms controlling POI activity range between the minute and the hour. **(b)** Overview of processes that can be targeted for perturbing the activity of a POI. Perturbation can be implemented **(1)** at the genetic level, to control transcription or mRNA stability. Alternatively, POI degradation **(2)**, subcellular localization **(3)**, interaction with binding partners that can sequestrate or activate the POI **(4)** would enable to control the active POI availability. The activity of the POI itself can be rapidly controlled by post-translational modifications **(5)** or allosteric changes that can be triggered by small-effectors **(6)** (adapted from (Gautier, 2014)).

Other features of gene expression (**Fig. 1.1.**) that can be targeted to perturb protein activity include:

- Covalent modifications, such as phosphorylation or methylation states
- Interaction with protein partners, homo-dimerization, and aggregation (Skwarczynska, 2012)
- Protein folding and conformational changes
- Cellular localization: for example, conditional addressing of a constitutively cytoplasmic POI to the nucleus or the membrane, where it can interact with an effector partner

Over the last few years, several reported techniques, which will be described in this manuscript, drew attention on the opportunities of hijacking the Ubiquitin Proteasome System (UPS), a ubiquitous protein degradation pathway, to specifically deplete a POI. Such conditional degradation by the UPS would constitute an interesting step towards a generic *On/Off* perturbation method meeting the specifications described earlier.

The possibility of implementing such a technique by using a chemical biology approach in this perspective will be addressed in this work. We will consider the endogenous cellular pathways as functional modules that can be hijacked to trigger designed perturbation. Thus, we propose in this first part a functional description of the UPS in eukaryotes and the implications for a chemical biology process, with top-down perspective towards the specific conditional control of degradation of a POI. We will restrict ourselves to a parsimonious yet generic description of the biological features necessary at each step to implement a functional module for conditional POI degradation.

1.1 The Ubiquitin-Proteasome System (UPS) allows the selective degradation of protein substrates

The control of protein level (proteostasis), along the cell-cycle and in response to variations of the cellular environment, is an essential process for living systems. This control depends on the rates of protein synthesis and folding, protein activity, sequestration, but also protein degradation. In this work, we focus on specific ATP-dependent proteolysis, although protein degradation can be realized by various mechanisms such as lysosomal-dependent mechanisms, which will not be described here.

1.1.1 The Proteasome is an efficient proteolytic complex in eukaryotes

1.1.1.1 The Proteasome is a protein complex with differentiated catalytic/regulatory subunits

ATP-dependent proteases are ubiquitous (present in bacteria[2], archae and eukaryotes), highly conserved proteolytic protein complexes, allowing both Quality Control in protein turnover and specific process regulation (Inobe, 2014). In eukaryotes, a single type is present in the cytoplasm and the nucleus: the 26S Proteasome, a complex of up to fifty subunits and 2.4 MDa, composed of:

– A cylindrical 20S catalytic core, digesting proteins into short peptides of about twenty amino-acids long (**Fig. 1.2).** This core is composed of four stacked heptameric ring, surrounding a central cavity with three different proteolytic sites. This geometry prevents unwanted proteolytic activation, as the catalytic site is isolated from the cytosol.

– One or two 19S regulatory particles (RP), for substrate recognition and transport to the inner core. The base is composed of a ring of six ATPases that unfold and linearize substrates in an ATP-consuming process. It also controls the access to the inner proteolytic site by encapsulating them: only unfolded proteins can pass through the narrow entry channel, excluding globular proteins.

– Two large subunits, Rpn1 and Rpn2 which organize facultative receptors Rpn10 and Rpn13. These additional modules can recognize substrate proteins addressed with a degradation tag[3].

The proteolytic activity of the 20S Proteasome discriminates specific substrates. The question whether the degradation of a protein is only induced by physical interaction with the proteasome, or whether it necessitates specific addressing signaling, long remained open.

[2] Several ATPases (ClpYQ, ClpXP, and ClpAP) functionally related to eukaryotic Proteasome exist in eubacteria.

[3] Several supplementary subunits can be associated for substrate recognition, like protein chaperone Cdc48.

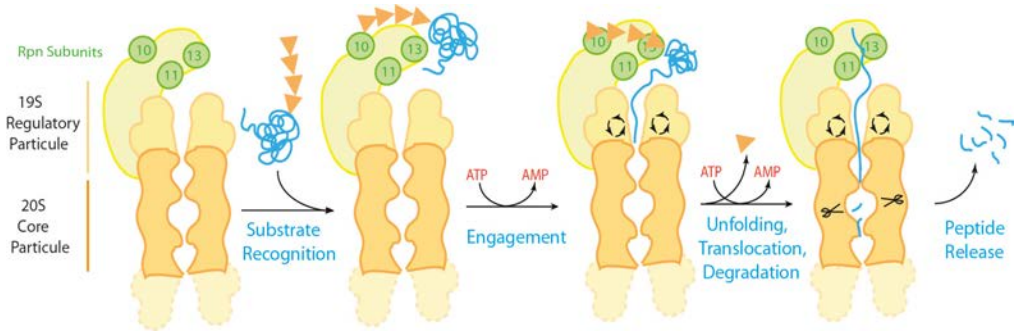

Fig. 1.2: Overview of the substrate degradation mechanism by the proteasome. A poly-ubiquitinated substrate binds with Rpn subunits at the 19S Regulatory Particle. Consequently, the substrate is unfolded and translocated to proteolytic core particle in an active ATP-consuming process, where it is degraded into short peptides.

1.1.1.2 Interaction with proteasome is sufficient for proteolysis: a chemical biology approach

To demonstrate that interaction with the proteasome is sufficient for proteolysis, target reporter proteins were artificially addressed to the proteasome by the rapamycin-heterodimerization system[4] (Janse, 2004). Rapamycin allows the control of the interaction between two proteins FKBP and FRB with high affinity, as detailed in **Fig.1.3.**

FKBP fused to different non-catalytic subunits of the proteasome was co-expressed with FRB fused to a POI in yeast. Addition of Rapamycin conditionally induces the interaction between the two chimeric proteins. This was sufficient to trigger the proteasomal degradation of the FRB-POI, depending on the identity of the proteasomal subunit fused to FKBP. Ubiquitin binding protein Rpn10 displayed the fastest degradation with a half-life of 20 min.

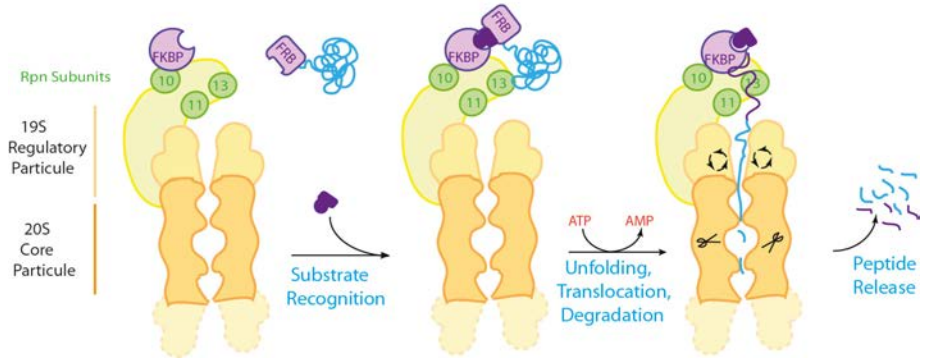

Fig. 1.3: Overview of the proteasome addressing approach reported in (Church, 2014). A POI fused to FRB heterodimerizes with FKBP fused to proteasome regulatory particle Rpn10 upon rapamycin addition. This addressing is sufficient to initiate the unfolding and translocation of the FRB-POI to the proteolytic core where it is degraded.

[4] Rapamycin, a 31 member, 912 Da macrolide antibiotic binds with high affinity (K_D=0.2 nM) to the FK506 Binding Protein (FKBP) and to the mammalian protein Target of Rapamycin (mTOR), which can be restricted to its binding domain called FRB. FRB/FKBP is widely used as a dimerization module, associated with different partner proteins such as Calcineurin 1, or modified Rapamycin ligand. Another dimerization platform is the Coumermycin-induced homodimerization of GyraseB (Farrar, 2000). Other examples based on phytohormones will be described in part **7.2.1.**

It is likely that the physical interaction of the FRB-POI is sufficient for their unfolding by Proteasome ATPase units, a necessary step to access the narrow 20S proteolytic core.[5] This approach confirmed that controlled addressing to the proteasome can be sufficient to degrade a stable POI.

1.1.1.3 Conclusion

The proteasome itself is active for protein degradation, which indicates that substrate selectivity has to be achieved by complementary associated mechanisms, such as polyubiquitin conjugation. Therefore, we will now describe the Ubiquitin-Proteasome System (UPS) to see whether conditional hijacking can be achieved.

1.1.2 Polyubiquitination of protein substrates is a proteasomal degradation addressing tag[6]

The Ubiquitin (Ub)-Proteasome system (UPS) is an essential eukaryotic post-translational regulation pathway. Ub and Ub-like proteins (such as Nedd8 and SUMO) conjugated to protein substrates are able to regulate a broad range of cellular processes such as degradation, control of protein activity or subcellular localization (Novatchkova, 2010).

1.1.2.1 Ubiquitin conjugation is an important post-translational modification mechanism

Ub is a small and highly conserved protein (76 a.a., 8.5 kDa), which can be attached by its Gly76 C-ter to a ε-amino group of Lys residues in a substrate protein. Further addition of Ub residues (polyubiquitination) can take place at one of the seven Lys present in Ub, as detailed on **Fig. 1.4.a**.

Mono- or polyubiquitination of substrate proteins are recognized as signaling tags by specific receptor proteins containing Ubiquitin-Binding Domains (UBD). These receptors can discriminate not only the number of Ubiquitin residues attached, but also their branching mode; this determines the cellular fate of a protein. Much is still to be learned on the regulation of ubiquitination, which involve a complex recognition process; however, in this work, we will focus on the Lys 48 polyubiquitination[7], a cellular signal for proteasomal degradation (Zhou, 2013).

[5] Similar approach led to the rapamycin-controlled degradation of POI by ClpX protease in bacteria (Davis, 2011).

[6] From now on, the proteasome will be considered as a «black box»: once the substrate protein is polyubiquitinated, it is considered to be recognized by the proteasome and degraded.

[7] At least a 4-mer polyubiquitin tag is necessary; other Lys residues such as Lys29 can be involved.

1.1.2.2 Polyubiquitination controls the degradation of protein substrates

Lys48-Polyubiquitination couples a series of post-translational modifications in a substrate protein, which finely tune the degradation rates by the Proteasome. The Ubiquitin-Proteasome System (UPS) is a highly conserved pathway common to all eukaryotic species, tightly controlled by a subset of protein through a cascade of transfer of Ubiquitin monomers (Nagy, 2010). This process is summarized in **Fig. 1.4.b/c.**

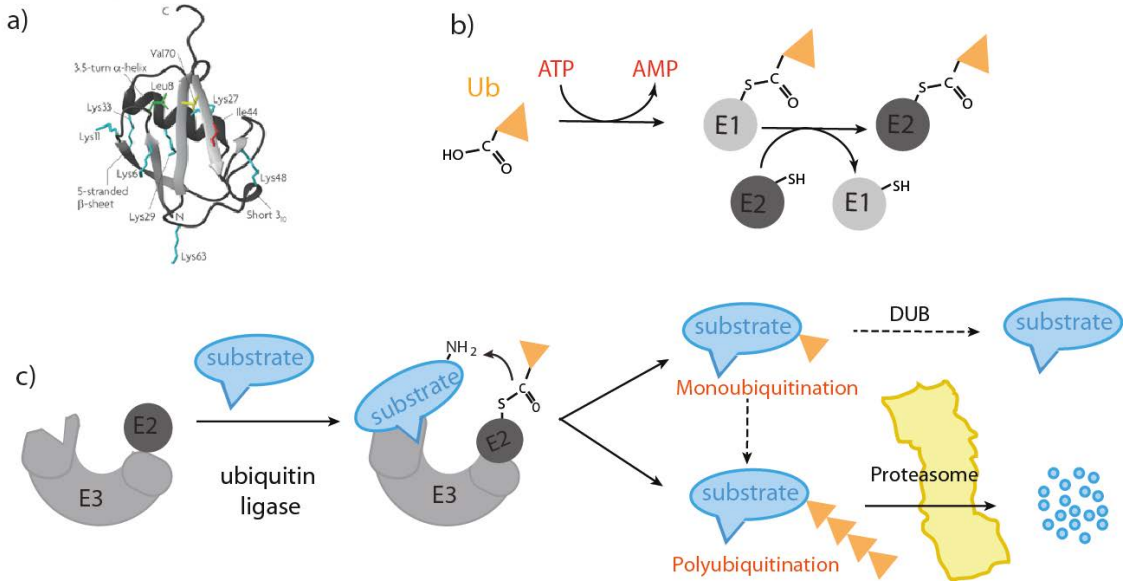

Fig. 1.4: **(a)** Crystallographic structure of Ubiquitin (PDB ref.:1UBQ, adapted from (Dikic, 2009)). **(b-c)** Overview of the UPS degradation pathway. **(b)** An ubiquitin moiety is activated by a thioester link with Ubiquitin Activating Enzyme (UAE) E1, and transferred to an Ubiquitin Conjugating Enzyme (UCE) E2. **(c)** Activated-Ub is conjugated to Lys-residues of a substrate by an ubiquitin ligase, resulting in different cellular outcomes. Polyubiquitinated proteins can be recognized by the Proteasome and degraded.

a) Activation of Ubiquitin transfer by E1 and E2 enzymes[8]

In a first, ATP-dependent step, a thioester linkage is made between Ub at its C-ter and an active site Cys of the Ubiquitin Activating Enzyme (UAE) E1. A trans-thiolation reaction transfers Ub to Ubiquitin Conjugating Enzyme (UCE) E2, through a Cys residue of the conserved Ubiquitin Conjugating Domain (UCD). While there is a single Ub-Activating E1 enzyme in human, 40 UCE E2 variants have been identified, with different structural properties. This variability is seemingly important for the specification of the ubiquitin linkage generated (Metzger, 2014).

[8] A first chemical biology application to the specific targeting of protein substrates by genetically harnessing the UPS components was reported in 1995 (Gosink, 1995). In this approach, different Protein Binding Domains (PBD) were fused to the C-ter of UCE E2. Interaction between the chimeric UCE E2 and the substrate recognized by the PBD (e.g. RNAse A) enhanced the ubiquitination and degradation of the latter in cell lysates *in vitro*. Although the extent of depletion was limited (10% in 4 h), this constituted a proof of principle that interaction with UCE E2 can be sufficient to control the ubiquitination of a substrate.

b) Conjugation of Ubiquitin to Protein substrates by E3 enzymes

The last step involves an ubiquitin ligase E3 which catalyses the transfer of activated thio-ubiquitin E2 to a Lys residue of a target protein[9]. The typology of E3 ubiquitin ligase distinguishes two ubiquitination mechanisms[10] (Metzger, 2014), as explained on **Fig. 1.5**:

- In a first mechanism, the E3 acts as a catalytic intermediate: activated ubiquitin is transferred from E2 to E3, which transfers the ubiquitin to an interacting target protein. This type of ubiquitination is specific of HECT[9] E3 ligases (Marin, 2010).
- Alternatively, the E3 lacks a functional catalytic center, but mediates the close spatial interaction between thio-ubiquitin E2 and the target protein, which authorizes the direct transfer of ubiquitin from E2 to the target protein. This mechanism is present in RING-type E3.

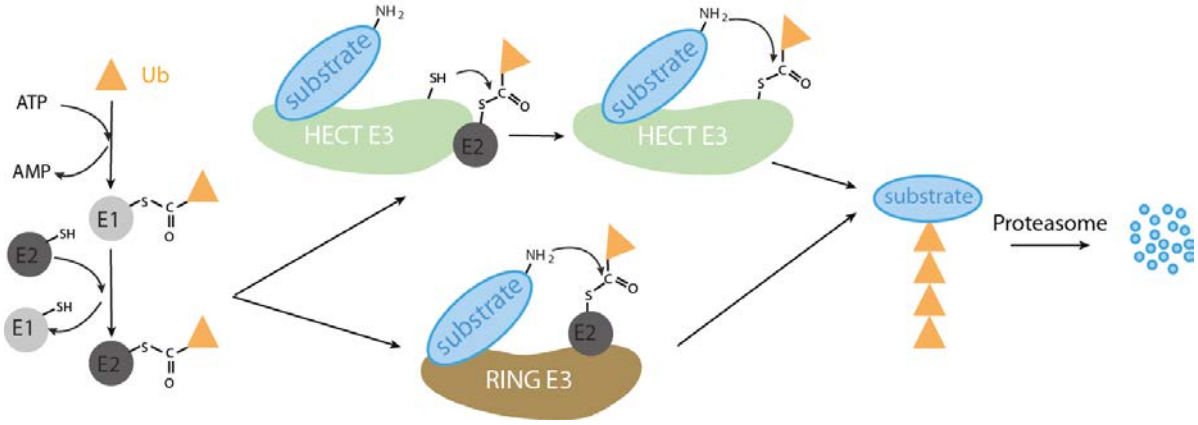

Fig. 1.5: Overview of the two classes of E3 Ubiquitin Ligase mechanisms. **(Top)** Activated Ub-moiety is transferred to a Cys residue of HECT Ubiquitin Ligase, and to Lys residue of a substrate in a second-time. **(Bottom)** In RING ubiquitin ligase, activated-Ub is directly transferred from E2 to substrate, due to the spatial proximity mediated by E3.

c) Final ubiquitination steps allow a complex regulation mechanism

In an increasing complexity, 600 to 1,000 E3 ubiquitin ligases have been identified in human. This dramatic variability is associated with high regulation potential. E3 ubiquitin ligases fundamentally allow homeostasis of the concentration of specific proteins. They are involved in many essential regulation processes such as development, genome maintenance and response to cellular signals (Lipkovitz, 2013). In numerous examples, E3 ubiquitin ligases dysfunctions are associated with human diseases. This is especially true for cancer: for example, specific mutations in the E3 ubiquitin ligase BRCA1 are a hallmark of breast cancer (Nakayama, 2006).

[9] Other ubiquitination positions exist, such as the N-ter of the substrate protein.

[10] HECT: Homologous to E6-AP C-ter; RING: Really Interesting New Gene. In some classifications, two more families, the U-box and PHD-finger, are singularized; in this work, we associate the U-box described on part **1.2.2.1** with RINGs, whereas the PHD finger will not be involved.

Lys48-polyubiquitinated proteins then diffuse before being recognized by the proteasome and degraded [11]. DeUbiquitinating (Dub) Enzymes recognize and remove ubiquitin moieties from ubiquitinated proteins, a process which offers a further level of regulation. (Eletr, 2014)

1.1.3 Perturbation of the UPS pathway by small molecules, a chemical biology approach

1.1.3.1 Motivation

A first approach to perturb the UPS is to develop small molecules inhibiting specific components of this pathway. This pharmacological approach relies on the identification of a specific POI drug target, and might therefore seem incompatible with the development of a generic perturbation pathway. However, important therapeutic stakes, such as p53 are associated with this perspective. Moreover, this is an important requirement for the technology of PROTACs detailed on part **1.3.2.3**. Last, these can constitute interesting examples of chemical biology application for small molecule drug-design. We develop here examples of perturbation at each level of the UPS, as detailed on **Fig. 1.6**. Complete reviews analyze further the associated potentialities ((Bedford, 2011), (Buckley, 2014)).

1.1.3.2 Perturbation of the Proteasome activity globally impairs the UPS

Proteasome inhibition would result in a global impairment of the UPS by preventing the final common step of protein degradation. Paradoxically, the first FDA-approved drugs targeting the UPS were developed against the proteasome. Peptide aldehydes, such as MG 132 [12] are proteasome inhibitors widely used in biological studies (see chapter **3**) to monitor proteasome-dependent degradation, despite poor selectivity and rapid reversibility. These drawbacks were compensated by the conversion into a boronic acid peptide, which led to the development of the more stable and highly specific MG262, which was developed into Bortezomib/Velcade in 2003, a FDA-approved drug for the treatment of multiple myeloma.

[11] In some cases, polyubiquitination might increase the activity of the protein, which might be a strategy to generate short-lived high signals. Alternatively, the E3 Ub ligase can be physically associated with the proteasome.

[12] MG 132 covalently inhibits (K_i= 4 nM) the chymotryptic-like activity of the β5 subunit of the proteasome. Other proteasome inhibitors target the caspase-like (β1) or trypsin-like (β2) activities.

1.1.3.3 Perturbation of the activity of UPS enzymes: from broad impairment to fine control

Inhibition at the E1 level prevents ubiquitin-dependent proteasomal degradation and thus globally impairs the UPS[13]. Pyrazone PYR-41 was the first inhibitor described to covalently inhibit UAE E1 in vivo, preventing global degradation of UPS targets such as P53.

Targeting one of the 40 E2 enzymes introduces an additional step of regulation as these proteins largely determine the ubiquitination chain topology, controlling the fate of target ubiquitinated substrates. This complex regulation process is however widely unknown and few E2 inhibitors have been identified. The first described CC0651 example was selected in a high-throughput screen of inhibitors of $p27^{Kip1}$ ubiquitination, in a cell-free assay reconstituting all components of the ubiquitin machinery. CC0651 inhibits the proliferation of cancer cells by accumulation of the cell-cycle regulatory protein $p27^{Kip1}$.

1.1.3.4 Targeting E3 ubiquitin ligases can trigger specific substrate degradation

With up to 1,000 different genes, E3 ubiquitin ligases exhibit high substrate specificity. This feature renders them highly attractive targets for the selective development of small molecule-based perturbation of the UPS (see Goldenberg, 2010 for identification platform methodology). As most E3 ubiquitin ligases lack an enzymatic activity[14], the inhibition of their activity is mostly achieved by perturbing the surface of interaction between an E3 ubiquitin ligase and its substrate.[15] This is the case in the first described example: *cis*-imidazoline-based Nutlins targets interaction between an E3 ubiquitin ligase MDM2 and its p53 tumor repressor substrate, which is stabilized *in vivo.*

However, other mechanisms for E3 ubiquitin ligase perturbation exist[16]:

(a) inhibition of the E3-substrate interaction with the proteasome

(b) inhibition of the insertion of the substrate adapter into core ubiquitin ligase

(c) perturbation of the core ubiquitin ligase assembly

(d) allosteric change in the substrate adapter protein altering affinity for its substrate

[13] Another orientation is the development of specific inhibitors of the 7 other E1 proteins in human, which share similar structures and mechanisms for activation of Ub-like proteins such as Nedd8. Neddylation being an important regulatory step of Cul-based RING E3 (Duda, 2008), targeting Nedd8-Activating E1 would impair the ubiquitination process.

[14] With the notable exception of HECT E3, see part **1.1.2.2.**

[15] Another attractive target for UPS drug inhibition are the nearly 100 De-Ubiquitin Enzymes (DUB) identified in mammals, which can stabilize substrates by removing Ubiquitin residues.

[16] (a) tryptamine JNJ-26854165 blocks the interaction between p53-MDM2 and the Proteasome, (b) chromone-based SMER3 blocks the insertion of the F-Box protein Met30 in the SCF (Aghajan, 2010); TAME inhibits the insertion of WD40-D-Box-Cdc20 protein into APC Ubiquitin Ligase Complex (Zeng, 2012) (c) thalidomide associates with CRBN, part of Cul4 CRL (d) allosteric change induced by binding of SCFI2 in the WD40 domain of Cdc4, excluding Sic1.

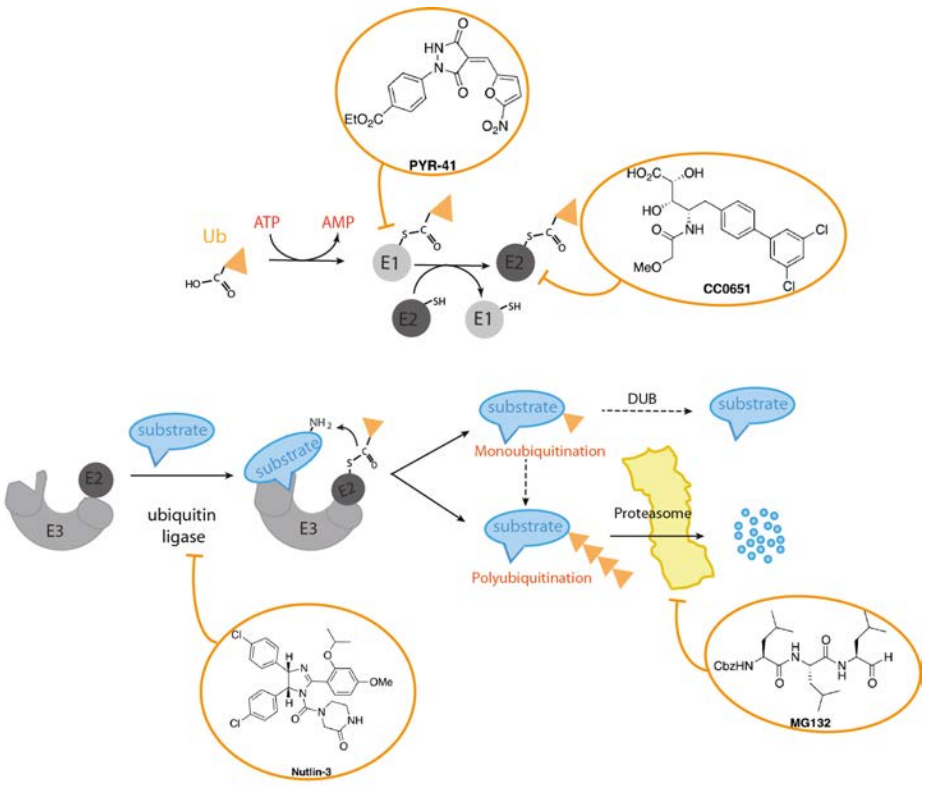

Fig 1.6: Examples of molecules inhibiting specific enzymes of the UPS pathway**:** Pyrazone PYR-41 inhibits globally E1 activating enzyme, CC0651 inhibits E2 Ubiquitin conjugating enzyme, Nutlin-3 inhibits interaction between E3 Ubiquitin ligase MDM2 and p53, MG132 targets the Proteasome.

1.1.4 Complementary signaling can implement substrate selection for proteasomal degradation

It was long thought that polyubiquitin was a necessary tag for proteasomal addressing and degradation initiation. This description has evolved since the identification of ubiquitin-independent degradation substrates, such as Ornithine decarboxylase (ODC) or the emerging field of intrinsically disordered proteins. The current model describes polyubiquitin as a particularly potent adaptor tag, although other signals addressing to the Proteasome might be sufficient to induce degradation (Inobe, 2011), (Asher, 2005).

Consistently, while eukaryotic and archeal proteasomal 20S core proteins present a sequence and structure homology indicating that this process emerged early in evolution, archeal proteasome lack the regulatory 19S RP (Bathelme, 2012). This might indicate that degradation control by ubiquitin conjugation evolved later as substrate selection strategy in eukaryotes (Hagai, 2012), (Zuin, 2014)[17].

[17] Although the UPS can be related to prokaryotic antecedents with Ub-like β grasp domains (Iyer, 2006).

A working analogy can be made between this substrate selectivity in living systems, and our chemical biology approach for conditional degradation of a POI ; in both cases, selectivity of substrate necessitates the implementation of addressing strategies to the degradation effector, the proteasome. In the next two sections, we will thus explore further the two functionalities associated with the UPS: Protein Quality Control and selective regulation, to see whether substrate selectivity can be implemented by hijacking the substrate recognition pathways.

1.2 The UPS Protein Quality Control (PQC) pathway allows the degradation of defective protein substrates

Elimination of misfolded or abherent proteins and homeostasis of available amino-acid pools are essential functions in cells. (Bennett, 2005), (Suraweera, 2012) Moreover, the maintenance of a pool of short-lived proteins in cells also appears as a potent strategy for the rapid generation of spatial gradients or adjusting of the protein composition. We will now describe Protein Quality Control processes associated with the UPS, and their implications for chemical biology approaches.

1.2.1 The *N-end rule* pathway: lessons from a destabilization pathway

1.2.1.1 The *N-end rule* pathway: from instability observations to chimeric POI destabilization

The lifetime of a protein molecule *in vivo* ranges from one minute to several days; this discrepancy between different peptidic sequences was phenomenologically characterized by the universal *N-end rule*, relating the lifetime of a protein to its N-terminal amino-acid identity[18] (Bachmair, 1986). Proteins exposing a residue other than Met are degraded with various rates (Dougan, 2012).

a) The N-end rule pathway in eukaryotes: overview

The eukaryotic N-end rule pathway is related to the UPS, with two sub-divisions: the Arg/N-end rule involving N-terminal arginylation and the Ac/N-end rule, targeting N-terminally acetylated proteins. The N-end rule variations have been widely detailed in recent reviews (Sriram, 2011). In a functional description to implement N-end rule instability in eukaryotes, we only summarize on **Fig**. **1.7** the mammalian Arg/N-end rule. A functional N-terminal degron associates an unstructured N-

[18] Interestingly, the first discovery of the N-end rule pathway resulted from the work by Varshavsky *et al.* in 1986, described below, on the metabolic stability of an engineered Ub-fused protein. This illustrates the fertile interplay that can exist between fundamental description and applied methodology.

terminal extension with internal Lys and a destabilizing N-terminal residue. These features allow protein recognition by E3 RING Ubiquitin Ligases called *N-recognins*, such as Ubr1 in yeast and Ubr in mammals, which ubiquitinate substrates and target them for degradation[19] (Dougan, 2012).

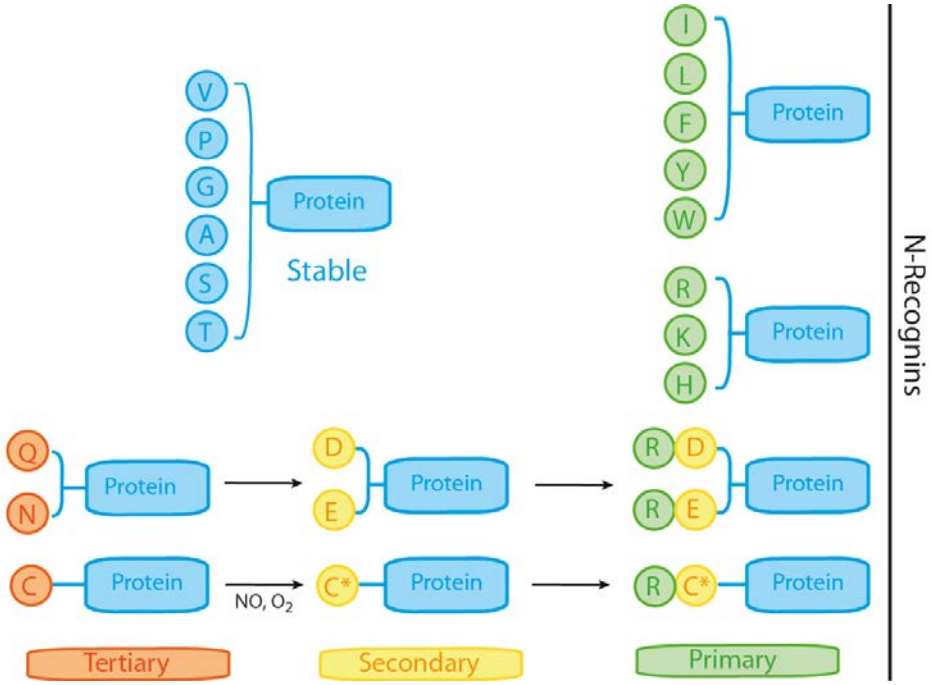

Fig. 1.7: Overview of the "classic" Arg/N-end rule pathway in eukaryotes. The half-life of a Protein is correlated to the identity of its N-terminal residue. At the primary level, some residues are stabilizing (top left), whereas others are destabilizing (top right). At a secondary level, D and E residues are modified by Arginylation, a destabilizing signal. A tertiary level exists as Q and N-terminal residues can be deamidated, resulting in resp. D and E exposition. Alternatively, oxidized N-ter Cys residues are also arginylated. Destabilized residues are processed by a specific class of proteins called N-Recognins (Adapted from (Dougan, 2012)).

b) Application of the N-end rule: implementation of constitutively-degraded variants of a protein

Chemical biology applications originate from a single paper published in 1986 by Varshavsky *et al.* which shed light on the N-end rule (Bachmair, 1986). Instability can be conferred by destabilizing residues (X) located at the N-end terminus of a β-galactosidase protein fused to Ub (chimeric Ub-X-β-Gal). Most of the time, the Ub moiety is rapidly processed by DeUBiquitin enzymes (DUB). This liberates X-β-Gal proteins which are constitutively degraded by the Proteasome at a rate depending on X identity. In particular, N-ter residues Phe, Leu, Asp, Lys, and Arg dramatically reduce the half-life time to a few minutes in yeast. However, introducing a proline residue prevents the DUB cleavage. The mono-ubiquitinated protein is recognized by a TRIP12 HECT E3 ubiquitin ligase (Park, 2009), which processes it by further addition of Ub residues leading to degradation by the proteasome.

c) Instability can be conferred to a POI by destabilizing N- and C-terminal cassettes

[19] HECT-type Ufd4 ubiquitin ligase also mediates polyubiquitination by associating with Ubr1 (Hwang, 2010).

Consequently, shorter protein degron sequences, with a destabilizing N-ter residue and internal Lys residue for ubiquitination, were developed to create N-ter proteins tags that can be fused to any POI to create conditionally unstable variants.

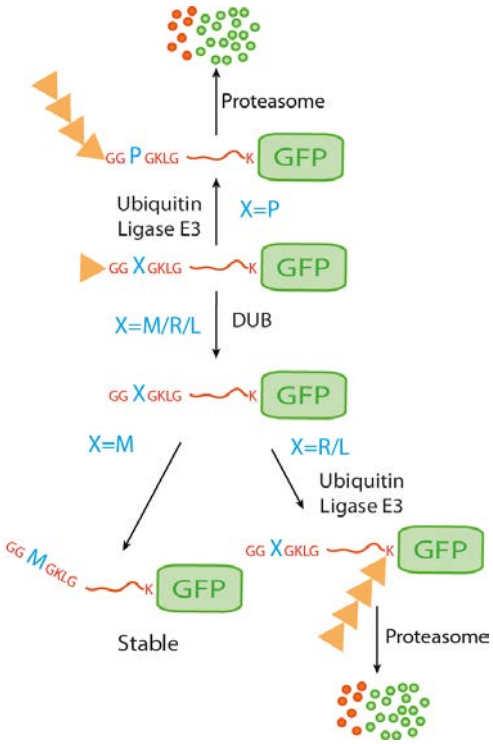

The first example was developed with a 45 residue from an internal sequence of lac repressor (lacI) and was extended to several POI in yeast as a generic and portable destabilization cassette (Park, 1992). This methodology led to the development of short-lived GFP reporters, as explained on **Fig. 1.8.** These constitute an interesting tool for monitoring UPS degradation of instable proteins (Dantuma, 2000), (Houser, 2013).

Fig. 1.8: Targeting of GFP reporters for proteasomal degradation reported by (Dantuma, 2000). The outcome of a GFP fused to an N-ter Ub tag depends on the amino-acid identity of the linker. The Ub tag can either be processed by DUB enzymes (bottom), liberating an N-end sequence driving either polyubiquitination on specific Lys sequence (right) or stabilization (left). Alternatively, the Ub moiety is stable and initiates polyubiquitination, resulting in proteasomal degradation.

Destabilizing C-ter tags, which do not rely on the N-end rule pathway exist, such as sequence derived from Ornithine decarboxylase (mODC) (Li, 1998) or CL1, a 16 amino-acid derived from a ER associated-degradation protein (Gilon, 1998), (Neefjes, 2004). Although the molecular features of their proteasome-dependent degradation might be partially unknown (mODC is degraded in an ubiquitin-independent pathway), these sequences can be used as known destabilizing tags in a chemical biology approach.

Constitutive unstable proteins allow transcriptional pulse-chase experiments, where either transcriptional activation (with an inducible promoter) or repression (with cycloheximide), or global UPS impairment with proteasome inhibitors create a perturbation of the protein content whose proteasomal decay can be monitored. This approach allows however poor temporal resolution due to the transcription and protein folding time, and can be perturbative for other cellular processes. Therefore, a technique to expose conditionally a destabilizing residue would be interesting.

1.2.1.2 Towards the conditional degradation of a POI by N-end rule application

a) Genetic induction of a protease can trigger the N-end rule dependent degradation of a POI

Taxis *et al.* developed the Tobacco-Etch virus (TEV) protease induced protein inactivation (TIPI) degron-system (Taxis, 2009), summarized on **fig. 1.10.b**. In this system, an N-end degron is inactivated by GFP blocker moiety placed at the N-ter, separated by a TEV protease recognition site.

Conditional expression of the TEV protease results in the cleavage of the recognition site and the exposure of destabilizing reside of the N-degron. POI is then degraded by the Ubr1-dependent N-end rule pathway. Although this system relies on genetic induction, the timescale for protein degradation is very rapid (1-3 h)[20]. A chemical biology approach optimized this system by enhancing the bonding and cleavage efficiency of variant TEV proteases (Taxis, 2009).

A TIPI-degron derived from Ornithine decarboxylase (mODC), completed this approach by allowing the degradation of C-ter tagged POI[21] (Jungbluth, 2010). Together, these two systems provide a bidirectional degron which can be placed at both N- and C-ter, or internally, for creation of conditional mutants of essential protein in yeast.

b) A temperature-sensitive (ts) degron triggers temperature destabilization of a POI in yeast

Another example of inducible degradation by the conditional N-end rule destabilization is the development of temperature sensitive (*ts*) degrons, detailed on **Fig. 1.10.a**. A *ts*-variant of human DHFR ($DHFR^{ts}$) was developed in yeast (Dohmen, 1994). This module can be fused at the N-ter of a POI and an Ub moiety (Ub- $DHFR^{ts}$ -POI). The Ub moiety is cleaved by DUB, as previously described, exposing a normally-destabilizing Arg residue at the N-end. The N-end *ts*-degron POI is stable at a permissive 24°C temperature, whereas shifting to 37°C results in the partial unfolding of ^{ts}DHFR, leading to a higher exposure of N-end Arg or internal Lys. This results in the rapid (30 min) proteasomal degradation of the N-end *ts*-degron-tagged POI through Ubr1-dependent ubiquitination.

This N-end *ts*-degron can be easily fused to any POI enabling a very fast and specific degradation. This generic depletion methodology has been widely used for depletion studies in yeast (Kearsey, 2008). A chemical biology approach optimized this system by over-expression of Ubr1 E3 ubiquitin

[20] This might be due to the fact that the TEV protease acts as a catalyst, sequentially proceeding cleavage sites, requiring a very low amount of maturated protein after induction.

[21] It is however to note that the mODC protein is degraded in a proteasome-dependent, but ubiquitin-independent pathway by recognition of its C-ter (Asher, 2005, see part **1.1.4**). This illustrates once again a key principle in chemical biology approaches: the endogenous mechanisms are considered as functional modules unless their deeper comprehension is necessary for the process implementation.

ligase. However, it is limited to species that support a high temperature shift, which is not the case for mammalian cells. Application of this technique in chicken DT40 cells growing at temperature from 35 to 42°C has been reported (Su, 2008).

It was also reported that methotrexate, a high affinity ligand of mammalian DHFR, partially blocked this temperature dependent degradation. This was an interesting step towards the control of protein degradation by small molecules in cells (Prakash, 2009).

c) Small-molecule control of the destabilization of a POI by the N-end rule pathway

Conditional cleavage of Ub residues can be introduced by split-Ubiquitin technologies: N- and C-terminal modified fragments of Ubiquitin protein will complement and fold only if they are fused to partner proteins which can dimerize. The functional reconstituted Ub residue is then cleaved by DUB (Johnsson, 1995), (Lin, 2014).

An interesting combination of split-Ub, DUB enzymes and N-end rule led to the development of the SURF (Split-Ubiquitin for the rescue of Function) methodology detailed on **Fig. 1.9**, which allows the conditional stabilization of a POI by rapamycin in mammalian culture cells. N-ter and C-ter Ub fragments are fused respectively to FKBP and FRB. The POI is fused to C-ter-Ub-FRB together with a degron sequence. In the absence of rapamycin, the degron addresses the POI to proteasomal degradation, whereas the rapamycin-induced dimerization mediates the complementation of the split-Ub, which is recognized and cleaved by DUB, liberating the POI under its native state, a highly attractive feature (Pratt, 2007).

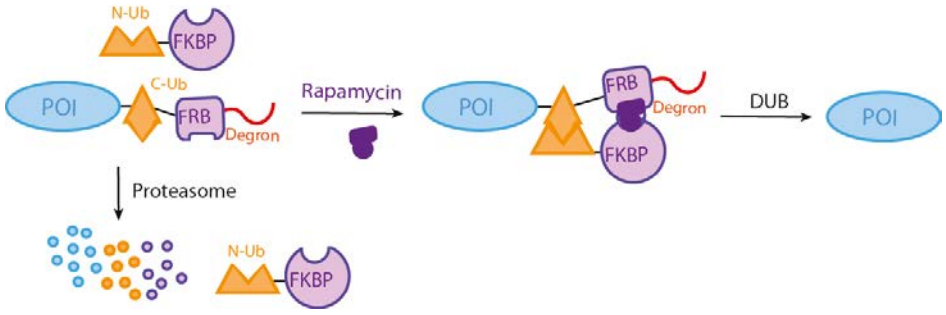

Fig. 1.9: Overview of SURF (Split-Ubiquitin for rescue of Function) methodology. A POI fused to C-ter part of split Ub and FRB is constitutively degraded by a C-ter degron, unless it interacts with N-ter split ubiquitin fused to FKBP in a rapamycin-dependent interaction. Reconstitution of the full-Ub enables processing by DUB, liberating the native POI.

d) Comparison

These methodologies allow the conditional depletion of POI with two different effectors: small molecule can be a simple and efficient way to induce a perturbation. A refinement of this is the genetic induction, where a small molecule addition results in transcription initiation. However, spatial selectivity is poor due to diffusion, and temporal resolution is often affected by the cell-

delivery issue. On the other-hand, temperature-shift is a physical perturbation that can be implemented with excellent spatio-temporal selectivity. However, it can be perturbative for living systems. As an alternative, light-sensitive tools for conditional degron presentation were developed in yeast and mammals (**Fig. 1.10.d**). These methodologies will be presented and discussed on part **7.1.2**.

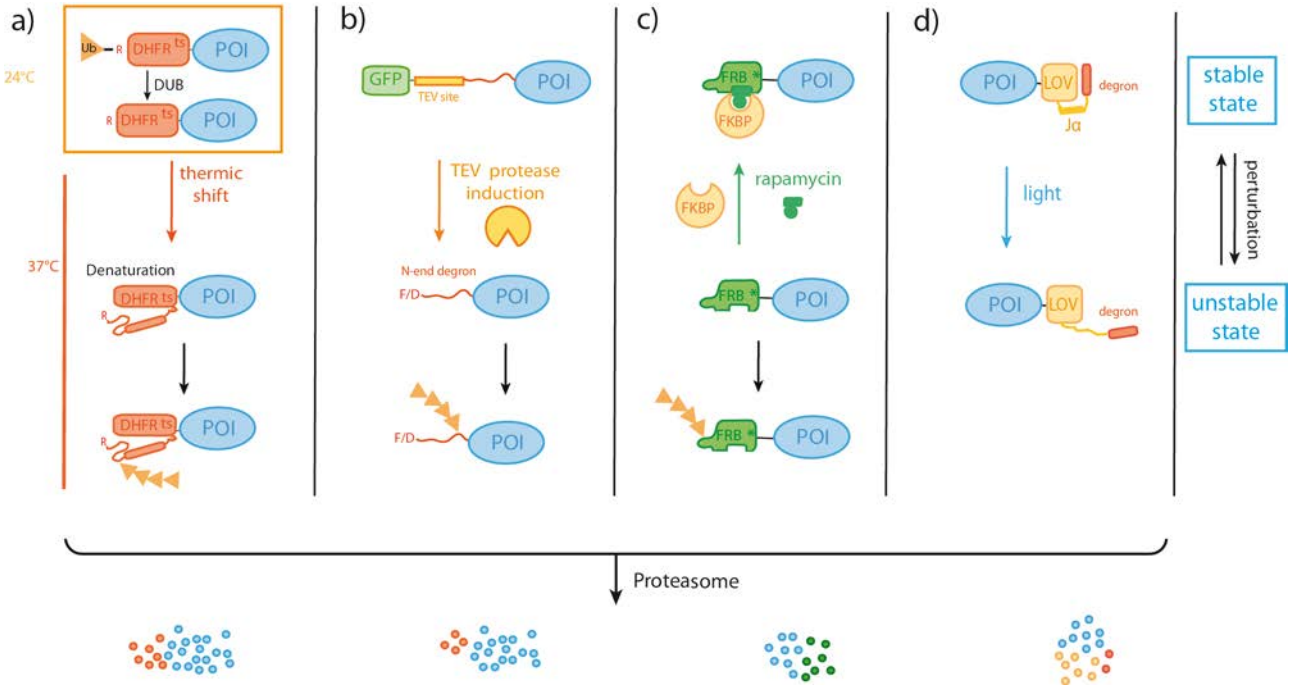

Fig. 1.10: Overview of the strategies to control the stability of a POI by a conditional perturbation (adapted from (Kanemaki, 2013)): **a)** Constitutive N-ter Ubiquitin removal by DUB liberates a POI fused N-end degron which is stable at 24°C in yeasts. Thermal shift from 24°C to 37°C induces a denaturation of the DHFR^{ts}-degron, which is recognized as a N-end rule degron and degraded (**1.2.1.2.b**) **b)** Genetic activation of TEV protease leads to the cleavage of a specific TEV site and the exposition of an N-end rule degron fused to a POI (**1.2.1.2.a**) **c)** A POI fused to an unstable FRB variant is constitutively degraded unless it is stabilized by FKBP in presence of Rapamycin (**1.2.2.2.a**) **d)** blue-light illumination controls the conditional exposure of a degron fused to LOV domain (**7.1.2**).

In this part, we have seen that functional understanding of the N-end rule pathway can lead to the development of constitutively and conditionally unstable proteins. We will now extend this approach to misfolded protein degradation, another PQC process.

1.2.2 Misfolded proteins can be degraded by the PQC pathway

The correct folding of proteins is a crucial issue *in vivo*, as misfolded proteins tend to aggregate, or exhibit a detrimental activity for cells (Bennett, 2005). Several human diseases are associated with a mutation inducing misfolding and causing rapid depletion of an essential protein, such as haemoglobin in haemoglobinopathies (Goldberg, 2003). Conversely, neurodegenerative diseases

such as Parkinson disease can be associated to failure of an E3 ubiquitin ligase Parkin to degrade misfolded protein that aggregate into amyloid plaques (Kitada, 1998).

1.2.2.1 Misfolded proteins are addressed by the UPS pathway *in vivo*

a) The misfolded protein response involves a finely regulated process

Several strategies are present in eukaryotes to address misfolded proteins: a first set of mechanisms involve the repair of misfolded proteins by protein chaperones, while a second strategy is to remove them from the cell[22], by the UPS (or autophagy) (Dantuma, 2010). PQC ubiquitin ligases E3 are able to ubiquitinate misfolded proteins, addressing them for proteasomal degradation (**Fig 1.11**).

This process is evolutionary essential for the cells: the UPS being an efficient tool for protein degradation, it must be only activated on misfolded or damaged proteins, without non-specific destruction of constitutive cell proteins. In eukaryotes, a subcellular compartimentation of the PQC exists: each compartment presents a distinct set of PQC proteins, (see Fredrickson, 2013) for review.

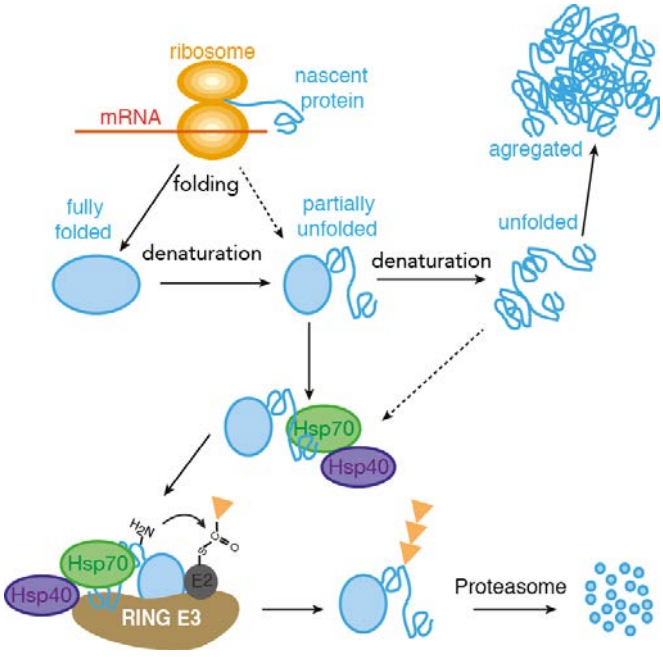

Fig. 1.11: Overview of the misfolded protein addressing in eukaryotes. Misfolded proteins, resulting from denaturation of folded protein or improper folding of nascent peptides are recognized by Heat-Shock proteins (Hsp), and polyubiquitinated by specific RING E3, resulting in eventual proteasomal degradation. This prevents cellular damages associated to unfolded protein aggregation (adapted from (Goldberg, 2003)).

b) The misfolded protein response associates specific E3 ubiquitin ligases to protein chaperones

[22] Historically, this cellular misfolded protein degradation was demonstrated 40 years ago. Incorporation of unnatural Val analogs in Globin proteins in reticulocytes dramatically reduced the lifespan of this normally stable protein.

We here describe briefly the cytoplasmic components for recognition of unfolded proteins. In yeast, the RING-domain Ubiquitin Ligase Ubr1 mediates cytoplasmic PQC degradation, independently of its role in the N-end rule pathway (see part **1.2.1.1**), assisted by Hsp70 and 110 chaperones. In addition, mammalian CHIP (carboxyl terminus of Hsp70-interacting protein) is a U-box E3 which ubiquitinates client protein through direct interaction with Hsp70 and 90 chaperones, which are able to specifically accommodate hundreds of substrates (Taipale, 2012). Other ubiquitin ligases have been described (Fredrickson, 2012).

However, in a chemical biology approach, the simple knowledge that a misfolded protein can be recognized and degraded by endogenous cellular components can be sufficient to implement a controlled degradation, by the conditional destabilization of a protein domain, although the downstream processing mechanism is not fully known.

1.2.2.2 A chemical biology approach: conditional control of POI stability by small molecules

a) Small-molecule mediated stabilization of a constitutively unstable POI

In a first application of the PQC processes *in vivo* detailed on **Fig. 1.10.c**, a POI can be fused to FRB*, an unstable mutant of FRB. This induces the constitutive degradation by the proteasome, unless FRB* is stabilized through a ternary interaction with endogenous FKBP and conditionally-added rapamycin (Stankunas, 2003).

Alternatively, the group of Wandless proposed a *single-ligand single-domain* strategy where a small molecule controls the stability of protein. By a directed-evolution approach, they engineered a mutant version of the human FKBP which is conditionally stabilized by the presence of *Shield1* (Banaszynski, 2006). In absence of Shield1, the constitutively unstable protein is recognized by the PQC pathway, and degraded by the proteasome. This protein sequence thus constitutes a Destabilizing Degron (DD) that can be genetically fused to any POI to confer a small-molecule dependent conditional stability. For example, predictable changes in NIH3T3 culture cells can be observed by the Shield1-induced stabilization of heterologous constitutively active small GTPases. This DD has been widely applied in cell culture and animal studies (Leong, 2012), (Rodriguez, 2012) and constitutes a generic[23] method of destabilizing a POI by addition of a tag (**Fig.1.12.b**).
This potent approach was developed to engineer other DDs for control of fused proteins. Mutants of

[23] However, limitations are observed in certain intracellular contexts: cytoplasmic and nuclear DD fusions are efficiently degraded in mammalian cells; whereas fusions to the mitochondrial matrix or ER lumen lead to constitutive accumulation (Sellmyer, 2012).

E. coli dihydrofolate reductase (*ec*DHFR) that are stabilized by trimethoprim (TMP), a known low-cost inhibitor of the human DHFR were genetically engineered in a DD (Iwamoto, 2010). Besides being an orthogonal alternative, this DD is more efficient for C-ter POI fusion, transmembrane target and nervous system applications compared to Shield1-induced DD.

This method however requires the continuous presence of the stabilizing ligand at a constant concentration, which can be an issue for delivery, for example for the long-term study of a POI in a developing organism. Addition, rather than removal of a ligand would allow a better control of the degradation of a POI.

b) Small molecule-induced destabilization of a stable POI

Two reverse approaches, in which addition of a small molecule destabilizes a constitutively stable protein, were developed by the group of T. Wandless in 2011. In a first strategy (Bonger, 2011), an engineered-variant of FKBP fused to destabilizing 19-residue C-ter sequence constitutes a cryptic degron which is destabilized by the addition of *Shield1* (**Fig. 1.12.a**).

In the second strategy (Neklesa, 2011), a hydrophobic adamantyl-ligand can be added to a HaloTag dehalogenase (a commercial fusion domain recognizing a specific substrate) fused to a specific POI. This hydrophobic group mimics the partially denatured state of a protein, which is recognized by the PQC pathway and degraded (**Fig. 1.12.c**).

Table 1.1 summarizes the properties of the methodologies for small molecule conditional stability.

	Halo Tag destabilization	**Shield destabilization**	**Shield stabilization**	**ecDHFR stabilization**
Reversibility	Partly (50%)	Fully	Fully	Fully
Half-life time	1.5 h	1 h after addition	1 h after removal	several hours
Cellular toxicity	20 µM	None	None	None
IC50	21 nM	3.3 nM	100 nM	90 nM
Working concentration	1 µM	1 µM	1 µM	1-10 µM
Maximal depletion	84%	80%	99%	99%
Tag size	34 kDa	13 kDa	13 kDa	27 kDa
Ref.	*Neklesa, 2011*	*Bonger, 2011*	*Banaszynski, 2010*	*Iwamoto, 2010*

Table 1.1: Compared characteristics of the methodologies for the control of POI stability by small molecules described on section **1.2.2.2**. IC50 = half-maximum inhibitory concentration.

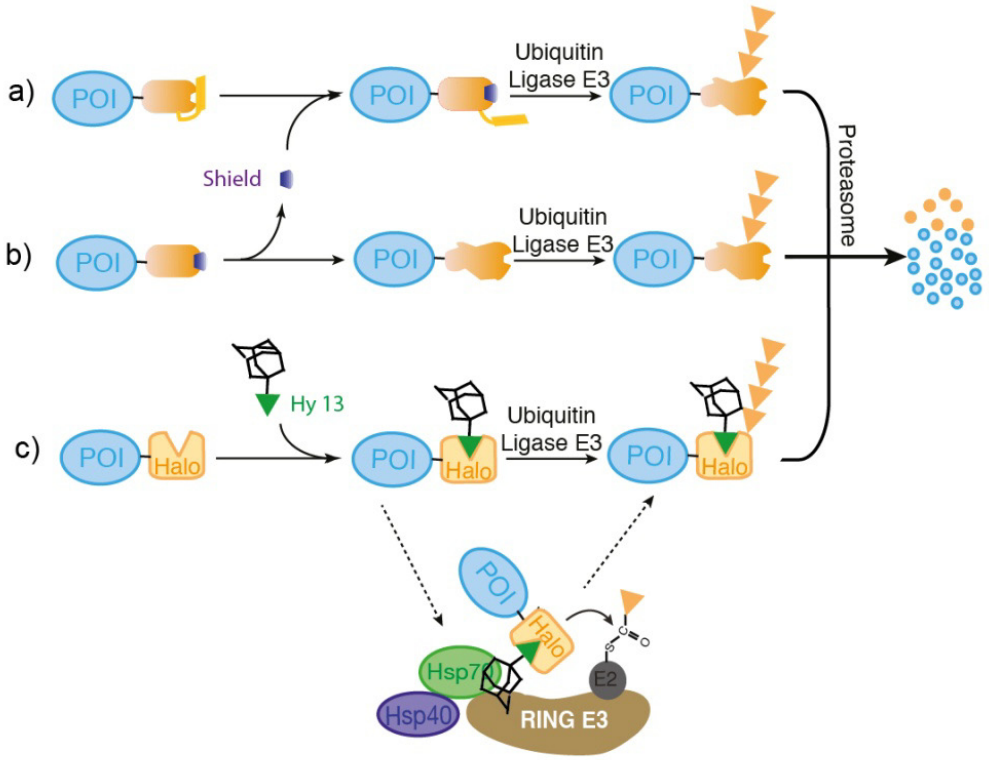

Fig. 1.12: Overview of the methodologies for the control of POI stability by small-molecules (adapted from (Kanemaki, 2013)). Engineered FKBP variants are either (**a**) destabilized (Bonger, 2011) or **(b)** stabilized by the addition of the FKBP ligand Shield1. Alternatively **(c)**, a hydrophobic tag such as adamantate can be addressed to a POI fused to a Halo-tag. Conditional destabilization leads to the recognition of POI by endogenous E3, leading to its proteasomal degradation.

Functional description of Protein Quality Control (PQC) led to the development of POI depletion methodologies, confirming the potentialities coming along this chemical biology approach. However, these PQC processes differ from the regulated ubiquitination of fully folded proteins which acts as a regulation process in cell physiology. A fully-controlled process that does not rely on the introduction of a PQC-recognized module (which can be perturbative for POI function) would be highly interesting. We need now to explore further specific regulation processes associated with E3 Ubiquitin Ligases for selective subsequent developments in POI depletion.

1.3 The UPS allows the selective regulation of functional proteins

1.3.1 Cullin-Ring Ligases (CRL) present a generic, yet modulable strategy for selective degradation of protein substrates

1.3.1.1 CRL is a common strategy for substrate ubiquitination in eukaryotes

Multi-subunit ubiquitin Ligases (E3) assembled on a cullin scaffold were identified in 1997 with protein Cdc4 in *S. cerevisiae* as a substrate archetype for polyubiquitination and proteasomal degradation (Feldman, 1997). This superfamily of Cullin-Ring Ligases (CRL) is widely found in eukaryotes, where it controls a wide range of cellular and physiological processes, and exhibits a high plasticity in substrate specificity (see **Fig. 1.13**) (Cardazo, 2004), (Petroski, 2005).

a) CRL present a common architecture for selective substrate recognition

As the first identified type of RING E3 ubiquitin Ligases, Cul1-based ligases (also called SCF for Skp1, Cul1, F-box) forms an archetypal example on which we will mainly focus. Although some variations can be observed, Cul1 illustrates the common features of Cullins (**Fig. 1. 13**):

- at the C-ter, a highly conserved globular cullin-homology domain, mediating the insertion of a RING subunit, docking the E2 ubiquitin transferase[24].
- at the N-ter, a domain[25] allowing the insertion of an adaptor protein for the recognition of a substrate protein (Schulman, 2000).

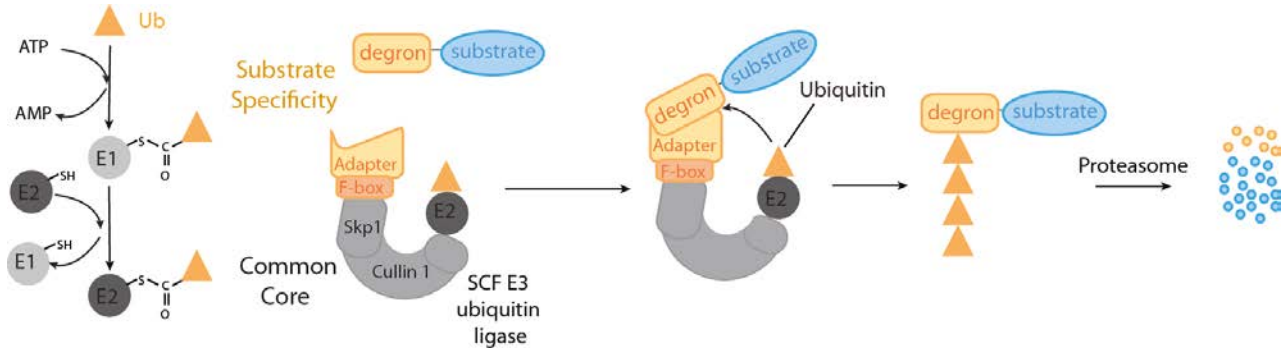

Fig. 1.13: Overview of the specific degradation of protein by SCF pathway. Skp1, Cullin1 and Rbx1 form a common core on which F-box adapters can associate. These bipartite proteins are composed of a conserved F-box domain that associates with Skp1 and a variable Adapter which can specifically recognize target proteins through degron sequence. The association between the substrate and the F-box adapter mediates the physical proximity with activated E2 inserted on the RING Rbx1 protein, which can be sufficient for substrate Lys-polyubiquitination.

In the canonical Cul1 description, substrate receptors are recruited at the N-terminus of Cul1 by the

[24] This interaction seems necessary for the activation of the E2 catalytic activity.

[25] A three repeat of five helix bundle CR domain.

adaptor protein Skp1. This bipartite protein is able to bind the N-ter domain of Cul1 and to integrate a substrate receptor containing a conserved N-ter motif of about 60 amino-acids called the F-box[26]. F-Box, Skp1 and the N-terminal region of Cullin1 binding Skp1 share a high homology with respective orthologs through eukaryotic species, which denotes the importance of the conservation of these substrate-recognition modules (**Fig. 1. 13**).

b) CRL control substrate protein ubiquitination by proximity with E2 enzymes

This whole protein forms a rigid, yet curved structure, acting as a scaffold that spatially connects the Ub-charged catalytic E2 and the substrate protein. This close proximity[27] allows the transfer of Ub moieties to accessible Lys residues of the nearby substrate. This paradigmatic model of a rigid scaffold was however tempered by the structural flexibility, which is necessary to accommodate substrates of variable size and conformation (Qian, 2009). No consensus sequence of ubiquitination on the substrate is necessary, although Lys residues must be accessible for the ubiquitin transfer.

c) Several versions of CRL are concomitantly present in eukaryotic cells

The activity of CRL complexes is tightly regulated in cells[28]. Each CRL can be referred by its Cullin core component. The N-ter regions of the seven homologs Cul proteins in human are not conserved in sequence, but exhibit structural similarities. The Cul1 scaffold enabling the recognition of substrate through conserved adapters seems a common architecture for other Cullin based CRLs, although they have been less studied. Without being exhaustive, we present two alternative models of CRLs in **Fig. 1.14**.

[26] This name comes from Cyclin F where this motif was first identified.

[27] An intriguing feature in the « classical » Cullin scaffold model was the gap space of ~ 50 Å between the substrate adapter and the E2 docked to the Rbx1 domain. A crystallographic structure (Saha, 2008) showed that a small Ub-like protein Nedd8 addition to a conserved Lys residue at the C ter of the Cul induces a major conformational change, displacing the E2-binding RING domain from the Cullin. This illustrates first that Ub and Ub-like modifications can largely modify the structure of a protein, but also that polyubiquitin addition can be regulated by post-translational regulation of E3 Ubiquitin Ligases, cycling between different states.

[28] Homo- or hetero-oligomerization has been described for some F-box protein, which might finely tune the recognition mechanism. A second level of regulation is observed with the instability of the substrate-receptors themselves (de Bie, 2011). In yeast cells, the half-life time for functional F-box proteins is below 30 min. This destabilization might be a consequence of the close proximity of the substrate-receptor to E2-Ubiquitin transferase process, which might transfer ubiquitin moieties to the receptor instead of the substrate in an « auto-ubiquitination » process, although E3 ubiquitin Ligases specifically targeting F-box proteins have been described in mammals. A complex network of interaction exists, as one CRL can ubiquitinate several substrates, but reversely, one substrate can be targeted by several CRLs. This global interactome is still widely unknown.

• in Cul3-based CRLs, substrates are recruited by a single BTB[29] domain, sharing a common fold with Skp1. This BTB domain protein acts both as substrate receptor and adaptor, conjugating the roles played by Skp1 and F-box protein in Cul1 (Genshik, 2013)[30].

• Cul4a-based CRLs recruit substrates by a large adaptor protein DDB1, although the interaction domain is still unclear. Putative substrate receptors are also discussed. These CRLs are associated with UV-lesions detection in the genome (Schrima, 2011).

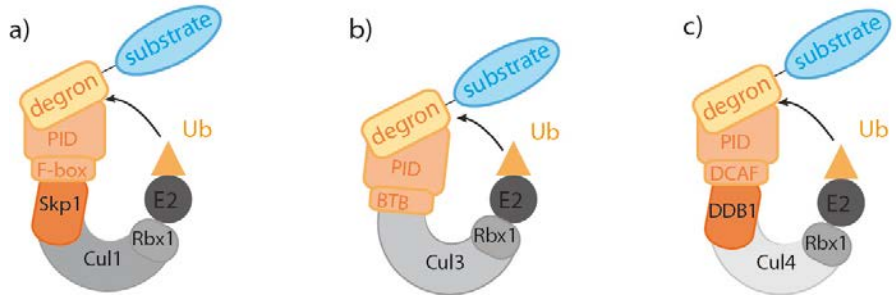

Fig. 1.14: Three CRL complexes architectures. **(a)** Cul1-based CRLs recruit substrates by a Skp1 adapter inserting a substrate adapter by a conserved F-box sequence. **(b)** Cul3-based CRLs recruit substrates by a BTB receptor **(c)** Cul3-based CRLs recruit substrates by a DDB1 adapter inserting a substrate receptor. PID = Protein Insertion Domain.

1.3.1.2 SCF strategy rely on specific substrate recognition

a) SCF specificity rely on F-box adapter diversity: the example of plants

Substrate recognition F-box domains form one of the largest multigene superfamilies[31] in plants, where they are associated with multiple and important developmental functions. At least 694 F-box genes have been identified in *A. Thaliana*, and up to 858 in rice, a number largely exceeding other eukaryotic species, such as budding yeast and human (resp. 14 and 24 genes). This abundance and diversification of F-box genes appears as a plant evolutionary strategy[32].

[29] BTB: Broad Complex, Tramtrack, Bric-à-Brac, DDB1: DNA-Damage-Binding Protein-1.

[30] Up to 439 BTB domain adaptor protein have been identified in human (but only 3 in budding yeast), but it is still unclear whether these might form as many distinct functional E3 ubiquitin Ligases, as BTB-box (like F-box) domains might have other functions in cells. However, as this model was confirmed on various candidate proteins, one can expect this combinatorial sensing to be relevant for cellular processes.

[31] Multigene family proteins are often associated with important morphological aspects in developmental and evolutionary biology. In these processes, proteasome-dependant protein degradation is an effective mechanism for the cellular responses to different external and internal inputs along the development and the life of an organism.

[32] It would however be difficult to presume a general trend of F-box specification in plants; the number of F-Box genes is variable from species to species: 337 F-box genes have been reported in the nematode *C. elegans*.

b) Plant F-box are bipartite proteins for substrate recognition

An F-Box protein can be generally modeled as a bi-modular protein with an F-box domain at its N-term and a Substrate Binding Domain. A genome-wide analysis in plants (Xu, 2009) identified many F-box candidates with others domains in the C-terminal region. Most abundant domains are[33] :

- WD40-Repeat domain: a β propeller structure able to recognize Ser/Thr phosphorylation site
- Leucine-Rich-Repeat Domain (LRR), an arc-shaped α/β repeat structure found in many protein binding contexts as it seems to offer a high modularity for wide substrate recognition. This modular nature allows the specific recognition of a wide range of substrates (**Fig. 1.15**).

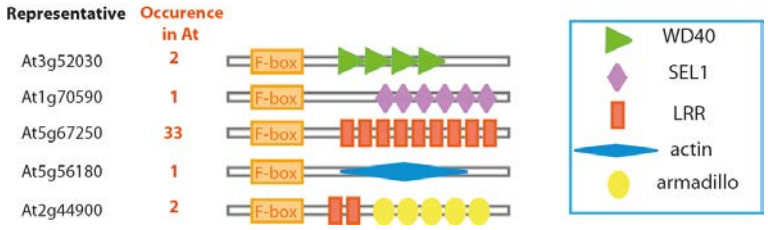

Fig. 1.15: Examples of F-box proteins in *A. thaliana* composed of a common N-ter F-box domain and proteins domains for substrate recognition. These domains vary by their composition, their repetition and their distance to the F-box domain. For each type, a representative example is displayed, along with the numbers of occurrence of this motif in *Arabidopsis* (adapted from (Xu, 2009)).

c) Towards a chemical biology approach

F-box proteins allow a generic, yet adaptable strategy for the degradation of protein substrates by SCF multi-domain complexes. The selectivity of substrate selection is permitted by their modular nature, which is essentially bipartite[34], as illustrated on **Fig. 1.20** for plant F-box proteins:

- the F-box domain (about 50 a.a., although lacking a strict consensus sequence (Kipreos, 2000)) binds to Skp1, mediating the recruitment by the core component of the SCF
- a variable protein-protein interaction domain for specific recognition of distinct substrates

These observations opened the way to chemical biology approaches: selective depletion of specific endogenous POI by combining the activity of E3 ubiquitin Ligases with designer binding proteins.

[33] Mammalian F-box proteins are often denominated by their binding domains: FBWs for F-box with WD-40 Repeat, FBLs for F-box with Leucine-Rich-Repeat (Jin, 2004).

[34] This bipartite nature is comparable with transcription factors decoupling DNA binding and transcription modulation domains which can be derivatized, for example in Yeast Two-Hydrids for monitoring protein interactions.

1.3.2 A chemical biology approach to POI depletion: hijacking the UPS selectivity by chimeric bipartite molecules

1.3.2.1 Chimeric bipartite F-box proteins target POI degradation

Chimeric F-box proteins can insert endogenous SCF complexes through interaction with Skp1 to form functional ubiquitin ligases (Su, 2003). Thus, selective depletion of POI can be induced by genetic engineering of a bipartite chimeric protein, by fusing an F-box protein with a peptide or a protein sequence that is able to bind to a target POI[35]. Harnessing the POI to the artificial E3 leads to its ubiquitination and subsequent proteasomal degradation.

a) Example of application: endogenous β-catenin is ubiquitinated by a chimeric β-TrCP F-box

This strategy was first developed for the specific degradation of pRB (Retino Blastoma Protein) in yeast (Zhou, 2000). We present here (**Fig. 1.16)** the example of depletion of β-catenin, which was implemented by hijacking its SCF-degradation pathway mediated βTrCP (Cong *et al.*, 2003). This F-box protein normally recognizes phosphorylated β-catenin and IκB through WD40 repeats.

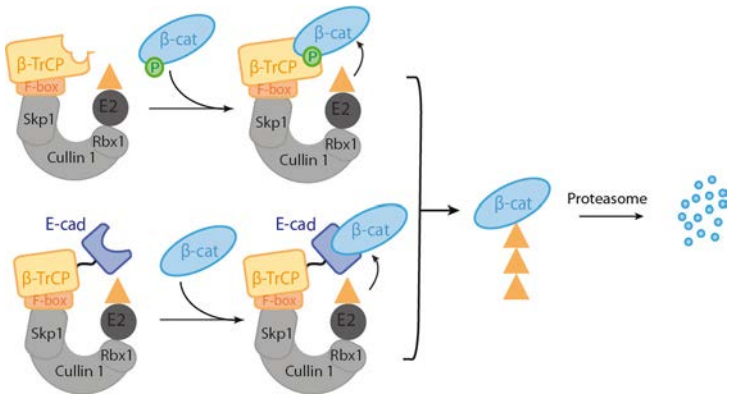

Fig. 1.16: Example of a chimeric F-box strategy for constitutive degradation of an endogenous POI. **(a)** In vivo, the phosphorylated β-catenin (β-cat) is recognized by $SCF^{\beta\text{-TrCP}}$ and degraded. **(b)** A chimeric protein associates the N-ter β-TrCP F-Box and an E-cadherin (E-cad) domain that recognizes unphosphorylated β-cat and targets it for degradation.

A chimeric F-box protein was engineered by fusion of the C-ter of β-TrCP (containing the F-box) with the β-catenin binding domain of E-cadherin (90 a.a.) separated by a Gly-Ser linker preventing the steric hindrance. Expression of this chimera induced a protein knock-out of unphosphorylated β-Catenin in mice, allowing a model to study the effect of β-Catenin silencing in some cancers.

[35] This approach has also been realized with HECT E3 ubiquitin ligase (Colas, 2000). A PBD aptamer with high affinity for Cdk2, selected from yeast-two hybrids combinatorial libraries, was fused to the catalytic domain of a HECT E3 ubiquitin Ligase. This chimeric protein expressed in yeast induced the polyubiquitination of the target Cdk2 protein. This did not however lead to proteasomal degradation, but rather to changes in the subcellular localization. This outcome might be explained by the fact that endogenous Cdk2 is not subject to ubiquitin dependent proteolysis; addition of an Ub residue might not therefore be sufficient to destabilize the Cdk2 proteins (Colas, 2000).

Optimization of the chimeric F-Box protein for improved interaction included elimination of the binding sites of endogenous substrates in the F-Box domain protein, a minimal POI binding domain to prevent unspecific interaction and adaptation of the linker length for increased flexibility.

b) Extension to chimeric U-box proteins as an optimization strategy

The hijacking of the multimeric SCF Ubiquitin Ligase system raised concern that over-expression of engineered F-box proteins might overwhelm the endogenous SCF machinery, inhibiting the ubiquitination process (Zhou, 2005). As an alternative, Portnoff *et al.* proposed the use of the single chain U-box type E3 derived from CHIP (see part **1.2.2.1**), with a broad substrate activity. This U-box protein fused to a PBD forms a functional E3 ubiquitin ligase without needing endogenous partner adapters (Portnoff, 2013).

1.3.2.2 Chimeric bipartite adapter proteins rely on specific POI binding domains

The first generations of engineered E3s necessitated natural protein domains that were known to specifically interact with the target protein; consequently, the example set were limited and did not allow a generic technique for the depletion of any POI.

a) Single-Domain Antibody fragments

An approach to overcome this problem is the use of single-chain antibody fragments called nanobodies[36]. A chimeric F-box protein was engineered by fusing the N-ter of an endogenous F-box to single-domain GFP antibody fragment VhhGFP4 (**Fig. 1.17**) (Caussinus, 2011).

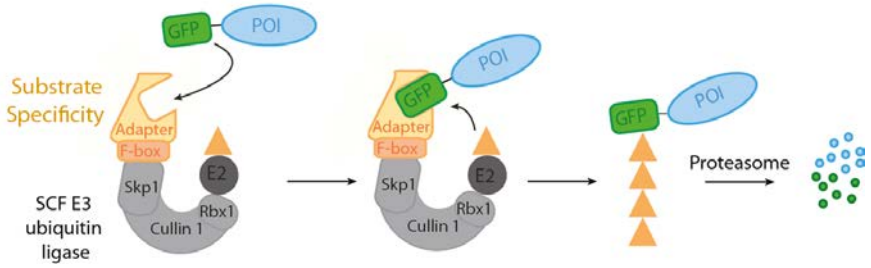

Fig. 1.17: Overview of the strategy described in (Caussinus, 2012) for the constitutive degradation of a POI fused to a GFP. A chimeric protein associates an F-Box and a GFP antibody fragment that recognizes GFP tagged proteins and targets them for degradation.

[36]The nanobody development addressed the limitations of antibodies fragments in cells, which cannot fold in the cytoplasm due to disulfide oxidation. They often use single-domain antibody derived from immunized llamas.

This method (deGradFP) allowed the degradation of GFP-tagged histones in mammalian cells and fruit flies. Temporal-controlled expression with a region-specific promoter in *Drosophila* confirmed the specificity[37] and the fast kinetics (2-3 hours) of the degradation. Although this method was developed against a chimeric fusion protein, the wide use of GFP as a fusion reporter tag makes the depletion of GFP- POI promising (Morin, 2001).

b) DARPins

Another possibility to implement POI binding domain is the development of DARPins, which are engineered ankyrin-repeat proteins selected from randomized libraries, allowing the development of small Designer Binding Proteins (DBP) with high specificity for any target POI. Brauchle *et al.* adapted the deGradFP technique to engineer a chimeric F-box protein fused to an anti-GFP DARPin which reproduces the characteristics of DeGradFP (Brauchle, 2014).

c) Peptide aptamers

Peptide aptamers, which are affinity binders composed of short stretches of variable peptide regions constrained within a protein scaffold constitute a third alternative. A chimeric F-box protein containing a peptide aptamer selected against β-catenin was able to significantly deplete this protein (Yeh, 2013). This constituted an important step towards a generic, fully encoded method to deplete any POI. This was confirmed later by Portnoff *et al.* who developed chimeric proteins called ubiquibodies by fusioning Chip U-Box to DARPins DBP, which can degrade endogenous proteins in various cell lines (Portnoff, 2013).

These examples show the potentialities coming along the development of fully-encoded and generic techniques to induce knock-out of any POI[38]. This requires the expression of a chimeric adaptor protein, which can be either constitutively expressed, or induced by a conditional promoter. This limits however the time resolution of this protein depletion technique. A small-molecule methodology, PROTACs, offer an alternative strategy for depletion of endogenous proteins.

[37] It is notable however that deGradFP could not degrade GFP alone, indicating that this adaptor-mediated depletion were not completely generic for small protein substrates.

[38] This methodology can be combined with RNAi silencing, or genomic edition with CRISPR/Cas9 (Park, 2014) for faster and complete protein depletion.

1.3.2.3 PROTACs: a small-molecule approach to conditional POI depletion

a) Overview of the bipartite molecule approach

Proteolysis-targeting chimeric molecules (PROTACs) are bifunctional heterodimeric molecules composed of two ligand-recognition motifs separated by a linker sequence. A first ligand, mostly a peptide, is known to interact with an E3 ubiquitin ligase complex, whereas the second ligand targets a specific POI (Sakamoto, 2001). PROTAC molecule mediates the formation of a ternary complex with the POI and the E3 ubiquitin ligase. This induced-colocalization can mediate the polyubiquitination of the POI by the ubiquitin ligase and its eventual degradation by the proteasome (Raina 2010).

The first described PROTAC conjugated ovalacin, a covalent MetAP-2 covalent binder to a phosphopeptide derived from lκBa binding the mammalian F-box $SCF^{\beta\text{-}TrCP}$ (transducin repeat-containing protein, see section **1.3.2.1**) [39]. MetAP-2 is recruited by the $SCF^{\beta\text{-}TrCP}$ *in vitro*, polyubiquitinated and degraded by the proteasome (Carmony 2012) (**Fig 1.18**).

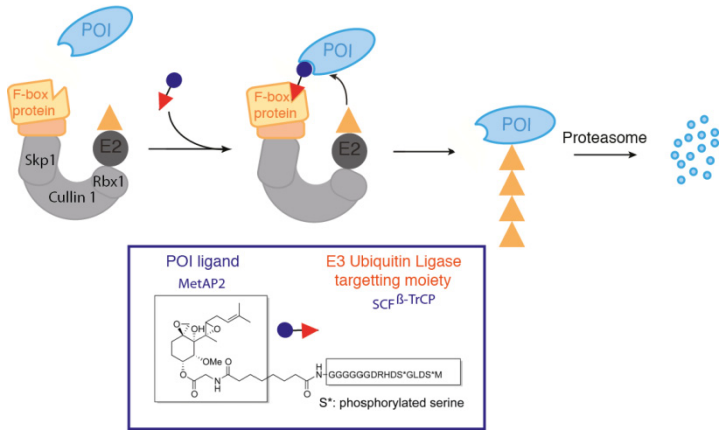

Fig. 1.18: Overview of PROTAC strategy for conditional degradation of an endogenous POI. A bipartite molecule with ligand-recognition motifs mediates the heterodimerization between a POI and a functional F-box protein part of an SCF complex. This interaction can be sufficient to target the POI for proteasomal degradation. This principle is illustrated with artificial addressing of MetAP2 to $SCF^{\beta\text{-}TrCP}$ by a PROTAC molecule associating ovalacin and a specific peptide targeting $SCF^{\beta\text{-}TrCP}$.

b) Implications of the PROTAC strategy for a small-molecule based perturbation of a POI

An essential condition for the development of PROTAC against a specific POI is to have a described high-affinity ligand, which limits the field of target POI. It also requires the design and synthesis of the PROTAC molecule, however with no molecular biology manipulations needed, as

[39] A subclass of PROTACs, SNIPER, relies on the bestatin esters, which recruit the E3 Ubiquitin Ligase cellular Inhibitor of Apoptosis Protein 1 (cIAP1). However, this molecule is rather unstable and not very specific. Alternatively, many PROTAC molecules target Von-Hippel Lindau protein (VHL), a Cullin 2-based E3 ubiquitin-ligase.

it targets endogenous proteins. One drawback of PROTACs is their poor cell-penetrability[40], which initially limited their applications to cell extracts or necessitated microinjection. Introduction of a Cell-Penetrating-Peptide sequence (CPP) allowed *in vivo* delivery.

c) Possible modulation of a PROTAC activity

Interestingly, an example of ligand-induced modulation of a PROTAC platform was reported with the development of PhosphoPROTACs. In this case, the POI-targeting ligand is a peptidic sequence phosphorylated by membrane receptors in response to external stimulus by growth factor, which modifies the affinity of the PROTAC for the POI[41] (Hines, 2013).

PROTACs constitute an interesting example of perturbative technologies using small molecules (a field sometimes called *chemical genetics*). Due to its elegant approach, which hijacks the endogenous degradation machinery, they offer a robust platform for protein knock-outs which could be developed by chemical libraries screenings. The described examples offer highly potential candidates for therapeutic applications.

However, as PROTACs rely on specific artificial POI ligand, they do not present a fully generic method for POI depletion. Natural small molecule-mediated modulation of the activity of a SCF E3 ubiquitin ligase has been described in metal homeostasis (Salahudeen, 2009), (Kobayashi, 2011). Identification of these processes might be a significant step towards the development of fully generic POI depletion. We will now detail this process for the Auxin-Induced Degradation.

[40]However, PROTAC molecules are still permeable, in contrast to RNAi, which require a transfection agent to be efficiently delivered *in vivo*. They also present a dose-dependent knockdown. Another advantage is that PROTAC specifically target a three-dimensional protein conformation. This theoretically allows to specifically target conformational subpopulations of a protein, which can be difficult achieved by either RNAi or small drugs relying on functional inhibition of the enzymatic activity. It can also target non-enzymatic proteins.

[41] For example, NGF (nerve growth factor) selectively stimulates the TrkA-dependant phosphorylation of a PROTAC containing the TrkA phosphorylation-sequence. This modification enhances the affinity of the PhosphoPROTAC for PI3K, recruited at a VHL E3 ubiquitin Ligase and degraded within 6 hours (Hines, 2013).

1.4 Auxin-induced degradation, a conditional small-molecule system for specific protein depletion

1.4.1 Nuclear Auxin-Response in plant involves controlled degradation strategies

1.4.1.1 The phytohormone auxin regulates genetic expression by controlled degradation

a) Nuclear Auxin Response is a transcriptional switch mediated by auxin

The plant hormone auxin, a small tryptophan-derived indole molecule, is involved in almost all developmental processes in plants, promoting different cellular processes in a tissue-dependent concentration response[42]. Auxin has been identified as a regulator of the stability of a family of transcriptional repression factors Aux/IAA (dubbed so relative to the expression in presence of auxin IAA), with 29 members in *Arabidopsis Thaliana (At)*. These Aux/IAA proteins bind to and repress the activity of DNA-binding transcriptional activators ARF (Auxin-Response Factors) through a conserved dimerization domain (Wright, 2015). In the presence of auxin, degradation Aux/IAA proteins are degraded by the Proteasome in a few minutes, leading to a de-repression of ARF-mediated transcription (**Fig. 1.19**) (DeRybel, 2009).

b) Nuclear Auxin Response involves the SCF^{TIR1} E3 Ubiquitin Ligase

SCF Ubiquitin Ligase had been reported as responsible for the ubiquitination of Aux/IAA. More accurately, the F-box protein TIR1 (Transport Inhibition Response 1) was identified in 2005 as an auxin receptor, which evoked a direct link between auxin perception and its protein degradation response, excluding intermediate transmission pathways:

- auxin promotes the interaction between TIR1 and Aux/IAA in a pull-down reaction[43], independent of temperature, and without involving a stable modification of either protein;
- competitive binding experiments showed that auxin directly binds to TIR1
- interaction between synthetic protein in cell-free expression system (Dharmasiri, 2003), or in insects cells extracts could be induced by auxin. (Dharmasiri, 2005).

[42] Historically, the existence of auxin was postulated by Charles Darwin in 1881 to explain phototropism in plants, but it was isolated and its structure was solved only some fifty years later (DeRybel, 2009).

[43] A 17 amino-acid peptide from the core of domain II in Aux-IAA, corresponding to a region identified with mutations disrupting the interaction with TIR1, is sufficient to pull-down TIR1 in presence of auxin (Kepinski, 2005).

1.4.1.2 Auxin directly mediates heterodimerization of TIR1 and Aux/IAA

A crystallographic structure of *At*TIR1 in the presence of auxin and a 13-amino-acid peptide from Domain II of Aux/IAA protein *At*IAA7 (Tan, 2007), lighted-up the mechanism of perception of auxin: the eighteen Leu-rich repeat (LRR) domains at the C terminus of TIR1 form a mushroom-like pocket binding auxin. This small molecule acts as "molecular glue", enhancing the interaction between the two partners, through docking of a hydrophobic pocket[44]. Surprisingly, another molecule, inositol hexakisphosphate (InsP6) is bound at the interaction core of TIR1. Several synthetic auxins, such as 1-Naphalene-Acetic Acid (NAA) or 2, 4-Dichlorophenoxyacetic Acid (2, 4-D) can also trigger this dimerization. This auxin-mediated interaction leads to the poly-ubiquitination of Aux/IAA through conserved Lys residues, and its fast proteasomal degradation.

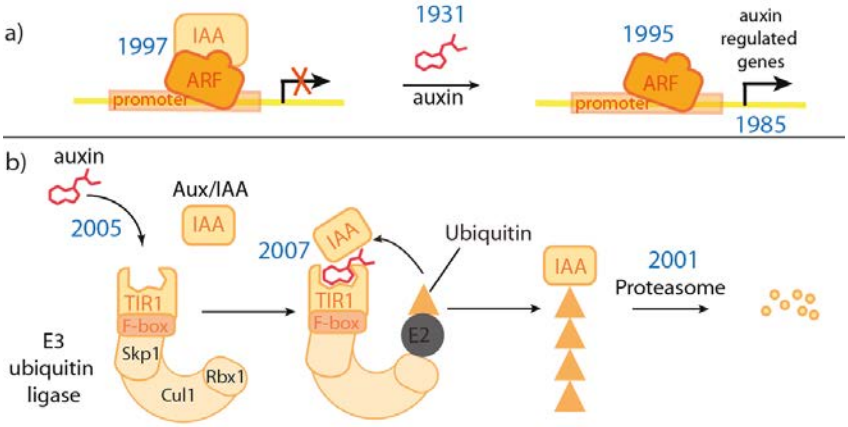

Fig. 1.19: Overview of the Nuclear-Auxin Response in plants. The expression of ARF genes is regulated by ARF transcriptional activators. The phytohormone auxin activates ARF expression by inducing the proteasomal degradation of ARF-repressors Aux/IAA. Auxin mediates the direct heterodimerization between Aux-IAA and SCF^{TIR1}, leading to the polyubiquitination and eventual proteasomal degradation of Aux/IAA.

In conclusion, auxin directly regulates the interaction between an F-box and its substrate[45] *(and not by allosteric conformation change). This would constitute an interesting platform for a small molecule conditional protein degradation.*

[44] A recent paper highlighted the role of nitric oxide NO in the auxin-dependent degradation: NO enhances TIR1-Aux/IAA interaction, while NO depletion blocks Aux/IAA protein degradation. This modulation is mediated by the S-nitrosylation of critical Cys residues localized on the LRR loops. These finding suggest that auxin sensing might be finely regulated by small molecules other than auxin, and post-transcriptional mechanisms (Terrile, 2013).

[45] This direct interaction constitutes an interesting example of natural ligand-induced dimerization, to compare with the widely used artificial rapamycin dimerization system. Would it be possible to make a dimerization system with TIR1 and Aux/IAA? In the original biological context, as well as in heterologous yeast or mammalian system, TIR1 is associated with endogenous Skp1 to form a functional E3 through its F-Box ; auxin-induced association between TIR1 and Aux/IAA results in the polyubiquitination and proteasomal degradation of IAA as the F-Box sequence is implicated in the interaction with Aux/IAA (Dharmasiri, 2005), it is difficult to have a stable association with no degradation ; this system might be possible in a system where TIR1 does not associate with endogenous ubiquitin Ligase proteins, such as bacterial or cell-free expression system, or to engineer TIR1 to prevent association with Skp1.

1.4.2 Auxin-Inducible-Degron (AID), a chemical biology methodology for conditional protein degradation

This feature was derivatized by the team of Kanemaki (Nishimura, 2009) to elaborate an elegant strategy to control the degradation of POI by a chemical biology approach. This exploits the universality of ubiquitination and proteasomal degradation processes in eukaryotes, the genericity of the SCF E3 ubiquitin ligase and the specificity of phytohormone perception in plants (**Fig. 1.20**).

1.4.2.1 The auxin-inducible degron allows conditional degradation in yeast

a) AID methodology relies on heterologous expression of plant proteins in yeast

Heterologous F-box protein *At*TIR1 expressed in yeast can associate with endogenous Skp1 (see part **1.3.1.1**), due to the high conservation of Skp1 and F-box sequences through eukaryotes, to form a functional RING SCF ubiquitin ligase, as was confirmed by immunoprecipitation. As TIR1 possesses no orthologs in non-plant cells, this artificial ubiquitin Ligase is orthogonal to yeast; it can however interact with and ubiquitinate a heterologous Aux/IAA protein in an auxin-dependent manner **(Fig. 1.20**). *At*Aux/IAA17 protein was selected among the 29 members of the Aux/IAA family (presenting a differential affinity to auxin-dependant TIR1 binding) for its short life-time (about 10 min in presence of auxin).

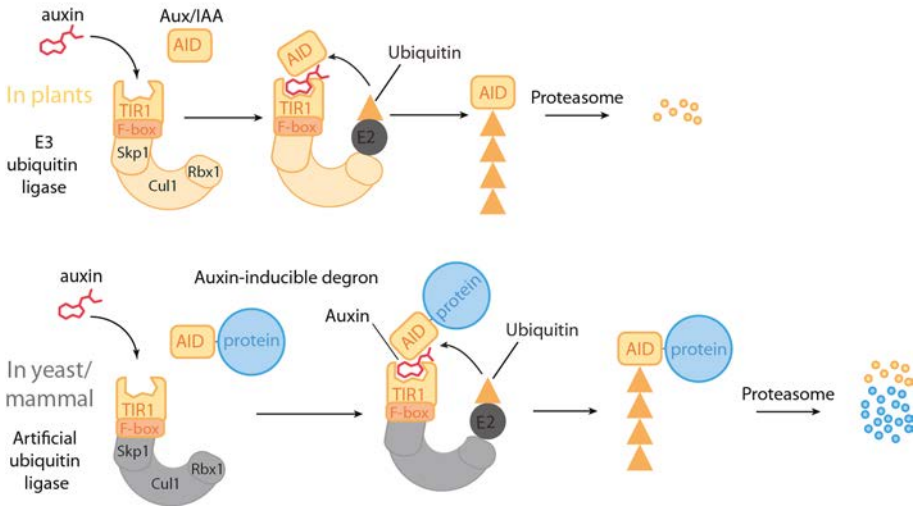

Fig. 1.20: Overview of the Auxin-Inducible Degradation depletion method. In plants, the transcriptional repressors Aux/IAA are degraded by SCF^{TIR1} in presence of auxin which mediates direct heterodimerization. *At*TIR1 heterologously expressed in yeast or mammalian cells associates with endogenous SCF components to form a functional artificial Ubiquitin Ligase E3, which associates to an AID-tagged POI in an auxin-dependent fashion. Consequently, the AID-POI is degraded by the proteasome.

b) AID allows auxin-dependent POI depletion

The complete sequence of *At*Aux/IAA17, which will later be called the AID for Auxin Inducible Degron, can be fused to POI. Addition of 500 µM auxin in yeast cells heterologously expressing *At*TIR1 and nuclear AID fused to a reporter GFP (AID-GFP-NLS) led to the rapid (30 min) and complete (97%) proteasomal degradation of the AID-GFP-NLS (Nishimura, 2009).

c) AID is a generic POI depletion methodology

The AID methodology presents several interesting features for the development of a perturbation technique. First, degradation is reversible, as auxin removal (by change of medium) disrupts the TIR1-AID interaction and thus stops the AID degradation, which is re-expressed within one hour. Another interesting feature for the development of a generic method is that the AID tag can be incorporated either at the N- or C-ter of the target POI. Last, the extent of depletion is finely tunable, as the depletion process is a direct auxin-dose response.

Over the six years following the publication of this strategy, the AID protocol has been widely exploited in yeast cells (more than 50 reported applications in *Pubmed*) as a perturbation technique to explore the function of POI. It is often used to confirm the predicted role previously postulated with other molecular biology methods such as siRNA or immunoprecipitation.
Several methodological papers have reported improvements of this technique in yeasts, such as subcellular addressing, fusion with endogenous ubiquitin ligase components, or optimization by using mutants and orthologs variants of TIR1 and IAA. These methods will be presented and discussed on chapter **3**.

d) AID requires the co-expression of two heterologous proteins

One of the characteristics of the AID approach is that it necessitates the expression of two proteins, contrary to the techniques evoked in part **1.2** (where expression of a single POI fused to a destabilizing domain is sufficient to induce degradation, relying on endogenous machinery). A main issue of this heterodimerization system is to control stoichiometry of the two heterologous proteins:

- Overexpression of TIR1 would saturate insertion of TIR1 in endogenous SCF
- Overexpression of AID-POI would saturate the SCF-TIR1 ubiquitin Ligase, therefore slowing down the kinetics of degradation.

Kanemaki *et al.* proposed the use of IRES (internal ribosome entry site)-based bicistronic plasmid for the co-expression of the two proteins[46].

[46] The stoichiometry of expression can be adjusted by regulation of the strength of the IRES.

1.4.2.2 The AID methodology can be extended to mammalian culture cells

The application of perturbative techniques from yeast to mammalian culture cells is highly desirable, but not always possible, as illustrated by the *ts*-degron methodology (see part **1.2.1.2**).

a) Optimization of the F-box protein TIR1 is needed for AID application to mammalian cells

Indeed, heterologous expression *At*TIR1 and AID-GFP-NLS did not lead to notable auxin-dependent degradation in mammalian cells at 37°C (Nishimura, 2009). The authors postulated that *At*TIR1, normally functioning at 24°C was temperature sensitive, and introduced *Os*TIR1 isolated from rice species (*Oryza sativa*) growing at warmer temperature[47]. Heterologous *Os*TIR1 efficiently induced the proteasome-dependent degradation of AID-GFP-NLS at 37°C in variable mammalian culture cell lines by addition of 500 µM auxin.[48] The authors claimed a half-life as low as 10 min in Human Embryonic Kidney (HEK) cells.

b) Mammalian AID is a generic protein depletion platform

In 2012, the team of D. Cleveland confirmed the potentiality of this approach by conditionally depleting various protein targets in different cellular contexts, in mammalian culture cells, as summarized on **Table 2** (Holland, 2012). Although application to mammalian cells have been associated with particularly interesting kinetics, few applications have been reported to this day.

Protein identity	**Plk4**	**CENP-A**	**TRF2**	**Cyclin B1**	**H2B**
Localization	nuclear	cytoplasmic	nuclear	cytoplasmic	nuclear
Localisation	centrosomic	centromeric	telomeric	diffuse	diffuse
Half-life (min)	9	18	13	17	40

Table 1.2: Reported POI targets for AID-degradation in (Holland, 2012). For each example, the localization of the heterologous POI-AID is reported with the half-life upon 500 µM auxin addition.

1.4.2.3 Fine regulation of auxin-mediated response by combinatorial auxin-sensing variants

a) A complex regulation of nuclear-signal proteins is associated with fine auxin sensing

TIR1 is a member of the AFB gene family where four members have been recognized as auxin receptors[49]. A complex regulation of the Aux/IAA genes exists, showing that a fine tuning and

[47] This was not true however for the *Gh*TIR1 from tropical cotton (*Gossypium Hirsutum*) closely related to *At*TIR1.

[48] Natural Auxin (Indole Acetic Acid, IAA) or artificial Auxin (Naphtalene Acetic Acid, NAA).

[49] Members of the AFB family share homology with the Jasmonic acid receptor COI, which might indicate a common hormone sensing which evolved to specific perception of different molecules.

plasticity exists in the AFB-dependent auxin reception (Parry, 2009). In particular, the TIR1 and AFB1 proteins share a 70% homology; both exhibit variable affinity to Aux/IAA proteins conditioned by the presence of auxin at very variable ranges.

Combinations of pairs taken among the 4 AFB receptors and the 29 Aux/IAA proteins in *Arabidopsis* assemble at different auxin concentrations, as monitored in yeast two-hybrids assays (Villalobos, 2012). This feature allows a large dynamic range of auxin sensing by differential sensitivity of co-receptor pairs. These characteristics have been exploited to develop quantitative ratiometric assays to measure auxin dynamics with large and adaptable ranges (Wend, 2013).

b) The whole plant auxin-response pathway can be functionally expressed in yeast

As an illustration of the potentiality associated to this chemical biology approach (expressing ectopic proteins as functional modules in model system), the entire *Arabidopsis* nuclear auxin signal has been recapitulated in yeast (Pierre-Jerome, 2014), by expressing the modular elements of auxin-reception pathway (**Fig. 1.21**):

- an auxin receptor of the AFB family (6 members)
- a transcriptional repressor of the Aux/IAA family (29 members)
- an Auxin-Response transcription Factor (23 members) associated with a plant ARF promoter

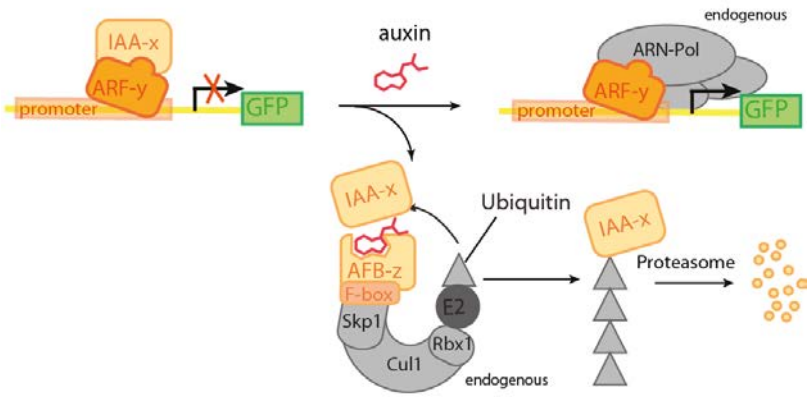

Fig.1.21: Overview of the strategy reported by (Pierre-Jerome, 2014). The *Arabidopsis* nuclear auxin response can be recapitulated in yeasts by a heterologous expression of a combination of three components taken among the variants existing in *A. thaliana*: an ARF transcriptional activator, an Aux/IAA transcriptional repressor and an AFB F-box protein. These heterologous plants proteins associate with endogenous transcription and UPS systems due to high conservation of specific association sequence among eukaryotes to form functional artificial systems.

These ectopic proteins inserted into the UPS and transcriptional machinery, due to conservation of common features through eukaryotes, specificity of interaction and orthogonality of the heterologous proteins. Combined with a mathematical model, this allowed a fine evaluation of the

combinatorial constants of interaction of the core elements of the Auxin Response Components. This reconstituted system might allow better understanding of how a simple pathway orchestrates a large number of responses in response to auxin, depending on cellular context.

1.5 Conclusion

In this chapter, we described the mechanisms controlling the stability of a given protein by regulation of the UPS-dependent degradation in eukaryotes. This allowed first the development of constitutive unstable versions of POI; but subsequently, several examples of conditional degradation were described, relying on a perturbational actuation method. As mentioned on section **1.2.1.2.d**, both chemical and temperature-shift strategies suffer from intrinsic limitations[50] which prevent the development a specific and generic degradation methods.

Light activation is a relatively non-invasive and specific perturbation. The wavelength and intensity of illumination can be finely tuned. Moreover, precise patterns of illumination can be controlled in time and space with lasers, down to a subcellular resolution. Light appears therefore as a promising method for specific control of degradation. In the next chapter, we will thus describe strategies for the photocontrol of protein activity.

[50] Chemical strategies imply addition or removal of a small molecule. Alternatively, temperature-shift is highly-specific, but can only be applied to a limited number of eukaryotes and is highly perturbative.

Chapter 2

Strategies for the photocontrol of protein activity *in vivo*

On Chapter **1**, we described the mechanisms controlling the stability of a given protein by regulation of the UPS-dependent degradation in eukaryotes. In this chapter, we will thus describe strategies to control the activity of POI *in vivo*, with a specific perspective for the implementation of a light-controlled proteasomal degradation. We will first describe photosensing protein modules existing in living systems, for the subsequent development of optogenetic actuation tools[51]. Then, in a second part, we will present chemical tools enabling light-control.

2.1. Photosensible protein modules trigger effector responses upon light illumination

2.1.1. Description of photosensible protein modules

Photochemical reactions in cells take place in protein complexes converting the incoming radiation in either energy (photosynthesis), or information through an ontology of proteins called *photoreceptors*, distributed in all kingdoms, including non-photosynthetic organisms (Miesenbock, 2011). These proteins can be described as a combination of a receptor (sensing light-variation in the environment), and an effector module.

[51] In a restricted sense, optogenetics refer to the control of physiological activity by genetically encoded light-sensitive proteins. A strict application of the definition might exclude some important achievement, such as the development of caged-neurotransmitters, as it does not correspond to a genetically encoded technique. In this work, we will rather use *photoactuation*, as the control of physiological function *in vivo* by light illumination (Deisseroth, 2011).

UV and visible light quanta are associated with energies up to 400 kJ/mol, comparable in magnitude to the strength of a single or a double bond. Photon absorption by an extended conjugated π electron systems[52] can trigger a photochemical reaction: *cis-trans* isomerisation, bond cleavage (photolysis) or bond formation, or charge dissociation (Moglich, 2010). This results in transmission of a global conformational change in the holoprotein, which either alters directly the activity of an endogenous effector domain, or modifies the affinity of the photoreceptor protein for a binding partner. In both cases, a discrepancy in activity exists between the dark ground and the light-activated state. This process is reversed in the dark by thermal return[53] (Tischer, 2014).

Consequently, these photosensitive domains offer interesting opportunities for light-actuation that can be fused to POI for the control of a physiological pathway by light. This led to the blooming development of optogenetics[54] over the last few years, which have been extensively described in complete reviews (Goguen, 2011), (Kim, 2013), (Gautier, 2014). We will give next a short description of four existing light-sensitive proteins adapted into optogenetic methodologies.

2.1.2. Examples of photosensible protein modules

2.1.2.1 LOV-domain modules

The light-oxygen-voltage (LOV) domain[55] proteins are blue-light sensing modules, associated to phototropic responses in plants (Krauss, 2009). The LOV module consists of a core domain of about 110 a.a. binding a photoreactive cofactor flavin mononucleotide (FMN). Illumination with blue light leads to the formation of a covalent bond between the flavin and a conserved Cys residue. This conserved mechanism triggers however various conformational changes at N-or C-termini, resulting in different outputs (Zoltowski, 2009). Thermal hydrolysis of the cysteinyl-flavin bond allows the

[52] Generally a chromophore cofactor is bound to the protein; however, receptors in UVR8 are endogenous Trp residues mediating the switch from dimeric to monomeric state upon activation, in absence of cofactor (Tischer, 2014).

[53] An inherent limitation of light-sensitive domains is that equilibrium exists between dark and activated states due to thermodynamic properties: a fraction of protein is active in dark, resulting in background activity (Vendrusolo, 2008).

[54] The most dramatic methodologic developments are undoubtly channelrhodopsin-based tools, enabling the photocontrol of ionic fluxes and membrane polarization, with applications in neurophysiology. As it is not directly relevant for our approach, it will not be described in this dissertation. An example of review is found in (Dugué, 2012).

[55] LOV domains are part of a larger class of PAS (PER-ARNT-SIM) sensory domains, which can be associated with various multi-domains effector proteins, including DNA-binding proteins or histidine-kinases. Four major LOV families are currently identified in Plants and fungi (Krauss, 2009).

return to dark-state. This diversity of conformational modulations is associated with an extended library of LOV variants and mutants exhibiting different kinetic and thermodynamic properties. Therefore, LOV-domains were identified as promising candidates for the development of optogenetic tools (Pathak, 2013). Possible implementations described on **Fig. 2.1** include (**a**) photo-controlled homodimerization (Zoltowski, 2009), (**b**) light-dependent unfolding modulating the activity of a fused POI (for example, DHFR in (Lee, 2008)), or (**c**) conditional exposition of a fused sequence by unfolding of the Jα-helix (for example controlling the sequestration of an addressing peptide) (Strickland, 2012).

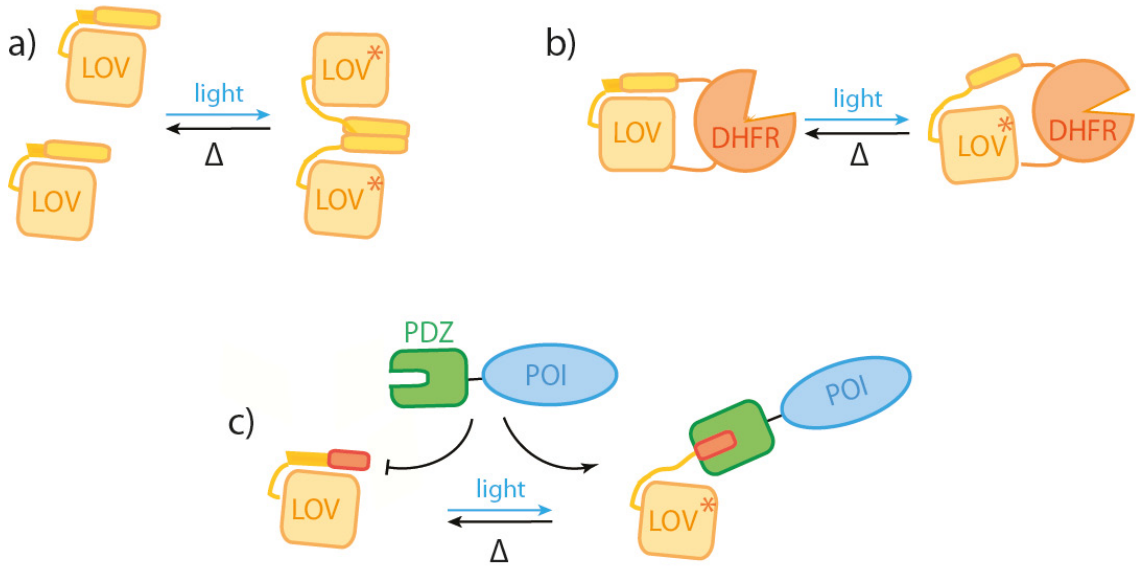

Fig. 2.1: LOV-domain based light-sensitive modules for implementation of optogenetic process *in vivo*: **(a)** Light-dependent homodimerization; **(b)** Light-dependent conformational change of POI (DHFR) fused to a LOV-domain. **(c)** Light-dependent heterodimerization by differential sequestration of a PDZ recognition peptide fused to a LOV-domain.

2.1.2.2 Cryptochrome-based modules

Cryptochromes are a class of proteins binding a FAD cofactor, which are implicated in circadian clock regulation in animals, and in growth control in plants; in these systems, blue-light absorption induces reduction of the FAD chromophore, inducing a reversible conformational change in the C-terminal helical domain[56], which thermally returns to the ground state in minutes (Kim, 2013). Interestingly, blue-light mediates differential affinity of *At*Cry2 to a binding partner CIB1 (calcium and integrin-binding protein). This was derivatized in a photoactivatable dimerization platform (Kennedy, 2010) that has since been validating on multiple approaches (Pathak, 2013) (**Fig. 2.2.a**). Interestingly, aggregation of Cry-fusion proteins was observed in certain conditions (Tischer, 2014).

[56] This mechanism however also involves a triad of conserved Trp residues.

2.1.2.3 Phytochrome-based modules

Plant phytochromes are a class of light-responsive proteins with N-terminal sensory module binding a linear tetrapyrole chromophore, which undergoes *cis-trans* isomerisation induced by red-light, resulting in a global conformational change in the protein, from red-absorbing (Pr) at 650 nm to far-red absorbing (Pfr) state. Either thermal return or far-red illumination at 750 nm converts Pfr back to its red state (Kim, 2013). Pfr differentially bind to PIFs (phytochrome-interacting factors). Photoactivatable tools for heterodimerization of POI were implemented with PIF3 and PIF6 (**Fig. 2.2.b**) (Pathak, 2013). Development of red-absorbing photoactuators is highly desirable because of the low toxicity and high tissue-penetration of red-light; however, they require addition of exogenous chromophore, and exhibit slower kinetics than blue light-based systems (Tischer, 2014).

2.1.2.4 FP Dronpa monomeric state is reversibly controllable by light

The group of Lin designed variants of the photoswitchable fluorescent protein Dronpa whose oligomerization state is light-dependent (Zhou, 2013). 145N Dronpa variants associate into a fluorescently-active tetramer, which dissociate upon cyan (500 nm) illumination. Variants 145N and 145K associate into a dimer. This dimer also dissociates upon 500 nm illumination, but is reformed by thermal return or 400 nm illumination (**Fig. 2.2**). This propriety was derivatized for the light-control of protein activity: Dronpa monomers fused to a POI associate into a dimer (or tetramers with POI dimerization) which can mask (« cage ») an active site, activated by a 500 nm illumination. This elegant approach allows reversible photoactivation process, although protein engineering with Dronpa can be challenging [57].

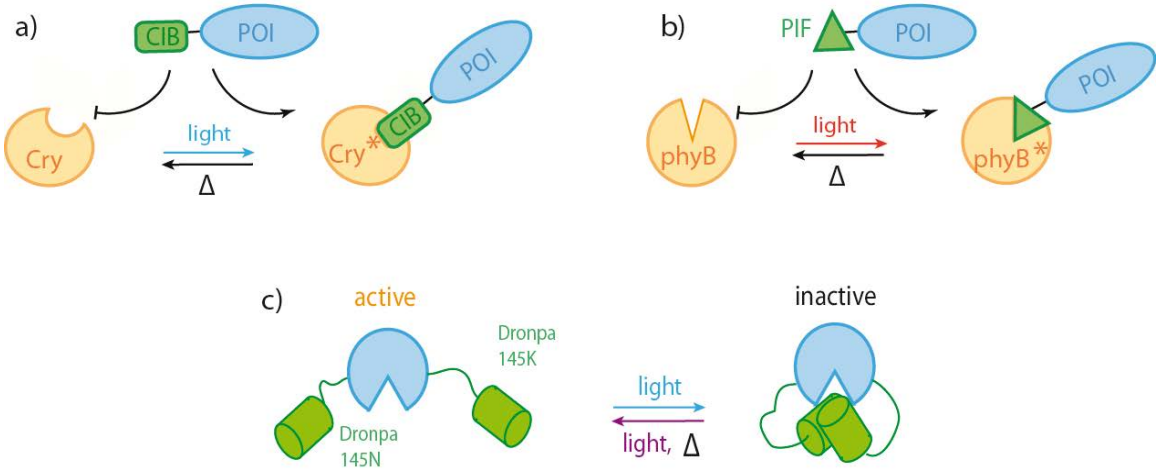

Fig 2.2: Light-sensitive modules for implementation of light-controlled heterodimerization of POI *in vivo*: (**a**) Blue-light-dependent interaction of Cry and CIB. (**b**) Red-light-dependent interaction of PhyB and PIF, reversed by far red-light (c) Blue-light-dependent interaction of Dronpa variants 145N and 145K can hinder a POI active site.

[57] Another plant protein UVR8 (UV-B resistance), stably dimeric in the dark, dissociates upon UV illumination, enhancing its affinity for COP1 (Constitutively Morphogenic 1) (Kim, 2013). UVR8-COP1-based photo controlled dimerization platform have been implemented in mammalian cells, although prolonged use of UV light can be an issue.

2.1.3 Classification of optogenetic systems based on photosensible protein modules

2.1.3.1 By physiological function target

Development of the photosensing proteins described above led to numerous applications for POI control in vivo, that we cannot extensively describe here. We identified ten classes of cellular functions that can be controlled by optogenetic tools, presented on Fig **2.4**.

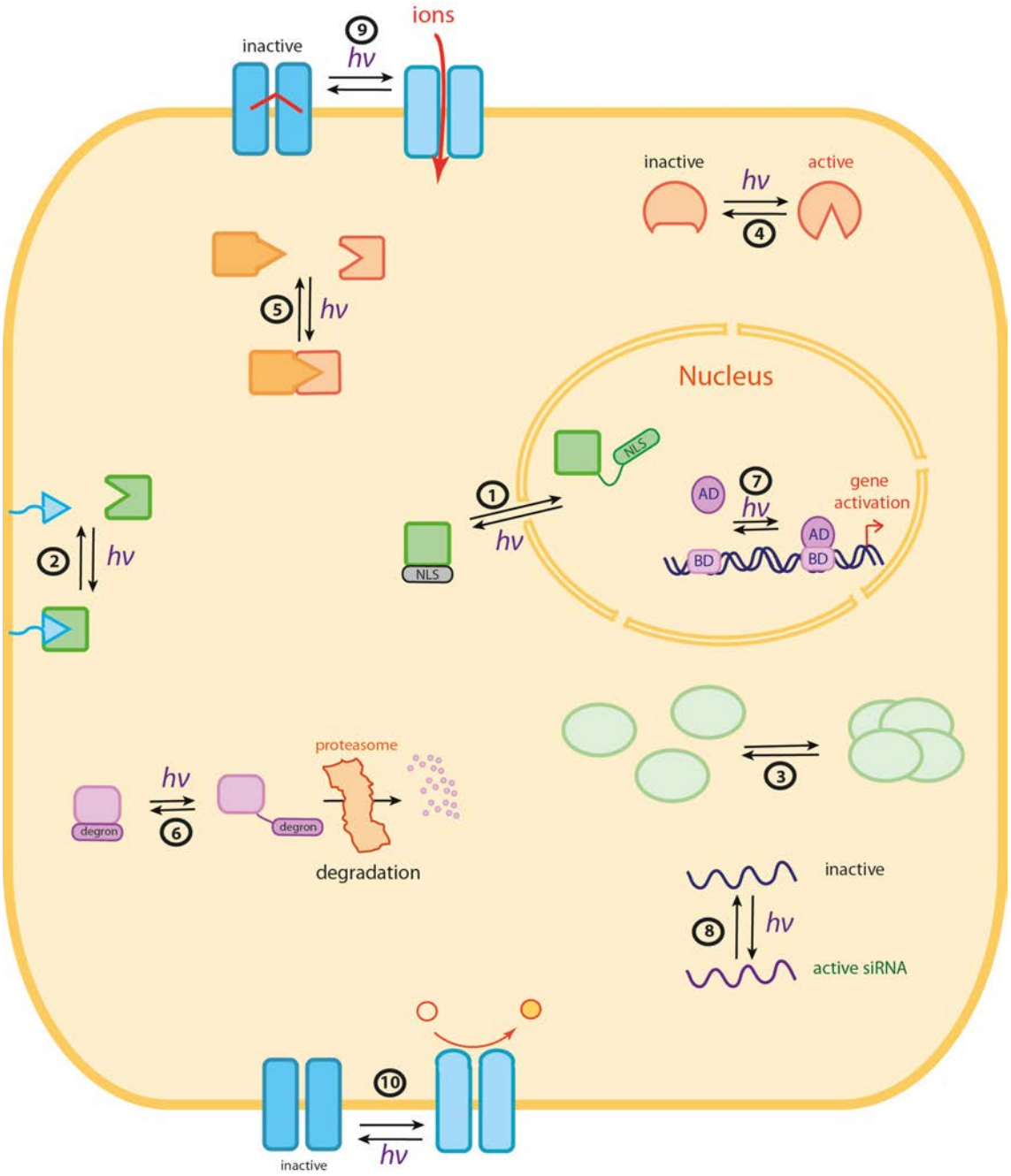

Fig. 2.3: Overview of the light-controlled physiological processes implemented by optogenetics for in eukaryotes

- **Subcellular localization (green)**: nuclear addressing **(1)**, membrane addressing **(2)** or sequestration **(3)**
- **POI activity (red):** either controlled by conformational change **(4)** or heterodimerization **(5)**
- **POI turnover (violet):** proteasomal degradation **(6)**, transcription initiation **(7)**, or small-RNA control **(8)**
- **Membrane protein control (Blue)**, including ion channel activation **(9)** or membrane receptor activation **(10).**

Table 2.1 proposes reference examples for each physiological function and photosensor type:

#		LOV domains	Cryptochrome	Phytochrome	Others
1	**Nuclear Import**	*Niopek, 2014*			*Crefcoeur, 2013 (UVR8)*
2	**Membrane addressing**	*Strickland, 2012*	*Kennedy, 2010*	*Levskaia, 2009*	*Zhou, 2012 (Dronpa)*
3	**Sequestration**		*Taslimi, 2015*	*Yang, 2013*	*Chen, 2013 (UVR8)*
4	**Protein Activity**	*Wu, 2009*	*Idevall, 2012*	*Folcher, 2014*	*Zhou, 2012 (Dronpa)*
5	**Heterodimerization**	*Strickland, 2012*	*Kennedy, 2010*	*Levskaia, 2009*	*Zhou, 2012 (Dronpa)*
6	**Proteasomal degradation**	*Renicke, 2013*			
7	**Transcription activation**	*Polstein, 2012*	*Kennedy, 2010*	*Shimizu, 2002*	*Muller, 2013 (UVR8)*

Table 2.1: Reference examples of light-sensitive modules applications for the light control of physiological processes.

2.1.3.2 By actuation mechanism

Photoactuation with light sensing domains involves two mains classes of mechanisms. :

- Fusion of POI to a LOV domain can result in the allosteric modulation of protein activity by light illumination (Strickland, 2012). Alternatively, a short domain fused to *As*LOV2-Jα can be cryptic in the dark due to cryptic docking, whereas illumination leads to the dissociation of Jα from the LOV core and the presentation of the functional domain (Lee, 2008).
- Optical dimerization systems, based on the light-induced differential affinity to binding protein (**Fig. 2.2**). An efficient dimerization method would control the functional accumulation or depletion of POI in space, controlling therefore the function. Alternatively, the activity of a split protein can be controlled by complementation dependent on fused dimerizers. As a general trend, these systems allow fast-kinetics of dimerization, within the minute time-scale (Tischer, 2014).

2.1.4 Conclusion

Photosensing modules exhibit thus high potential for the light-control of physiological functions, with growing use. The possibility to implement light-controlled proteolysis by inserting photosensing modules will be discussed on chapters **7** and **8**. However, the implementation of light-sensitivity by genetic manipulation can be difficult.

In multicellular organisms such as metazoan or higher plants, physiological activity can be controlled by small molecules. For example, in section **1.4.2.1**, we described the plant transcriptional switch mediated by the small molecule auxin, which mediates protein heterodimerization and proteasomal degradation. Therefore, a simple strategy for the control of physiological processes by modulating the disponibility of effector molecules by light would be valuable. We will next present strategies for the photo-activation of small molecules.

2.2- Chemical actuators enable photocontrol of physiological activities

2.2.1 Classification of chemical actuators

Small chemical actuators combine light-sensing and effector parts on physically distinct chemical entities. Two classes of molecules can be distinguished by the reaction resulting from photon absorption by the chromophore: either *cis-trans* isomerization; or bond-cleavage of the chromophore; in both cases, this process results in a differential accessibility of an active effector molecule (Shao, 2009), (Ahmed, 2013). Synthetic photoactuators molecules are attractive, as a variety of chromophores with diverse photochemical properties can be conjugated to a molecule of interest, using reasonably simple synthetic approaches.

2.2.1.1 Photoswitchable effectors

In the first case, photoisomerization can enable the presentation of a hindered active molecule. Azobenzene is a widely used example of small-molecule modulation with light. The stable trans-conformation can be converted to a *cis* geometry upon 360-400 nm light-illumination. This process is reversible, longer wavelength converts the azobenzene back to its *trans* conformation, and can be repeated many times (Shao, 2009). We present in **Fig. 2.5** an example of azobenzene-based module for pH modulation previously developed in our group. Alternatively, conjugation of proteasome inhibitors with azobenzene led to the development of platforms for photo-controlled impairment of the UPS (Hansen, 2014).

Further development led to hybrid approaches that combine genetic encoding with synthetic photoactive compound. For example, azobenzene moieties conjugated to accessible endogenous Cys residues of endogenous porines allowed light-control of permeability as photoisomerizable tethered ligands (PTL) (Kramer, 2005).

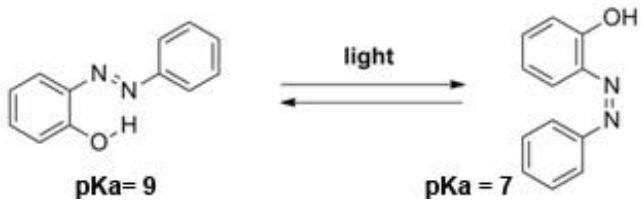

Fig. 2.4: Example of azobenzene-based photoswitchable effector developed in our group. pK_A of an azobenzene-based platform is modulated by light-illumination (Emond, 2011).

2.2.1.2 Caged effectors

In the second case, the chromophore is cleaved by photolysis, leading to the liberation of an active diffusible protein effector. This defines the class of caged molecules (Deiters, 2010).

Photocaging of bioactive molecule has been introduced by the pioneer work on deoxy-nucleotide phosphate protection by *o*-nitrobenzyl caging group (Engels, 1976), (Kaplan, 1977). Many biological effectors have since been caged, along with commercial availability (Corrie, 2005). For example, glutamate and γ-aminobutyric acid (GABA) are highly-interesting candidates to interrogate spatial control of neurotransmission (Matsuzaki, 2010).

Caged-compounds combine practical advantages of small-molecule addition, but enable spatio-temporal control by light illumination. Moreover, caging strategy can be applied to many types of biological effectors, including oligonucleotides, metabolites, or peptides, a feature which is inaccessible to photosensible protein modules methodologies (Riggsbee, 2010). For example, this strategy allows light-control of RNA interference (Chaulk, 2007). We present in **Fig. 2.6** two examples of caged biological effectors developed in our group.

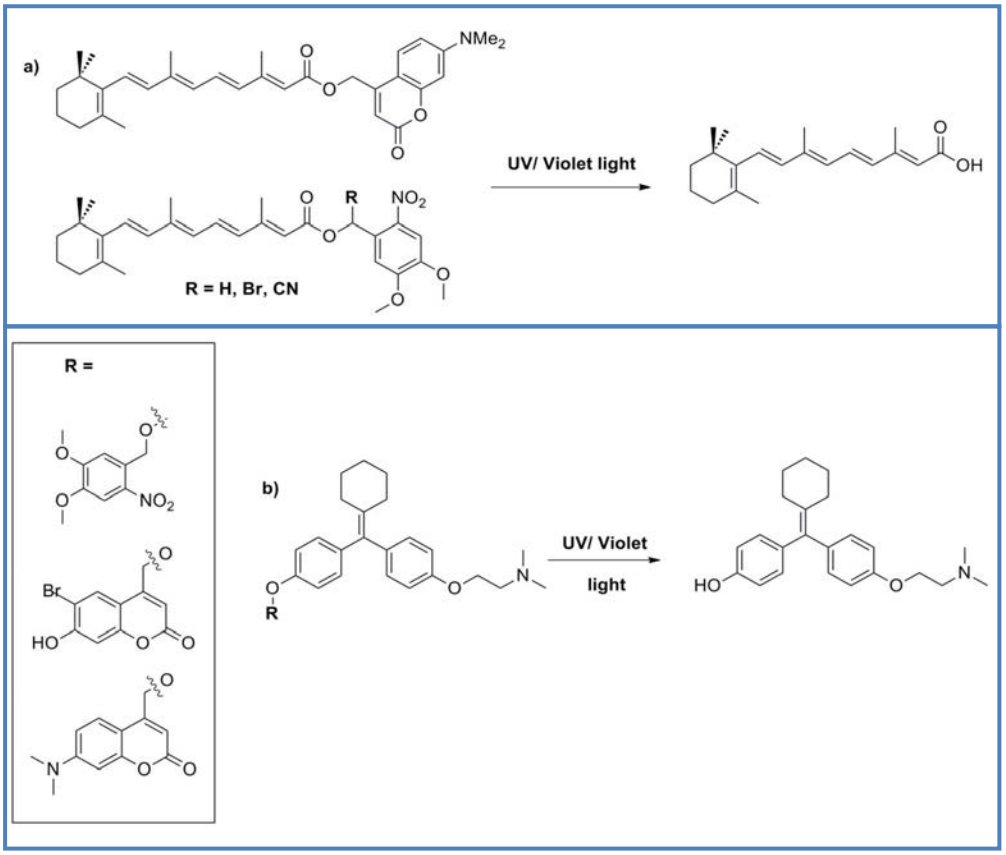

Fig 2.5: Example of caged effector molecules developed in our group. **(a)** Retinoic acid, an important morphogenetic regulator was caged with Dimethoxy-nitrobenzene (DMNB) or Coumarin caging group. One-(365 nm) or two-photon (750 nm) liberation could trigger visible alteration phenotype in zebrafish eye development (Neveu, 2008). **(b)** cyclofen-OH, a photochemically stable inducer of the receptor specific for 4-hydroxy-tamoxifen (ER(T2)), was caged with various caging groups for photoinducing the nuclear translocation of proteins in zebrafish embryos (Sinha, 2010).

2.2.1.3 Genetically encoded caged proteins: chemical genetics approaches

Unnatural mutagenesis allows the incorporation of caged amino-acids (such as Tyr, Cys, Ser and Lys) at specific positions (Riggsbee, 2010). This can be realized in mammalian cells by engineering orthogonal pairs of aminoacyl-^{t}RNA synthetase/^{t}RNA enabling the site-specific incorporation of a caged amino-acid into a heterologous POI gene where the codon for a critical residue has been replaced by a non-sense codon[58]. Although it relies on a complex heterologous co-expression, this constitutes a fully-encoded method to implement conditional POI control with high spatio-temporal resolution. Interestingly, light-illumination liberates the native functional protein, a highly desirable feature. This strategy was used, for example, for the fast (< 1 min) photocontrol nuclear translocation by caging a key Lys residue in a Nuclear Localization Signal (NLS) sequence (Gautier, 2010). Alternative physiological targets of caged proteins and caged small molecules effectors are listed in **Table 2.2**:

	Caged proteins	Caged molecules
Nuclear Import	*Gautier, 2010*	*Sinha, 2010*
Membrane addressing		*Umeda, 2011*
Sequestration		*Robinson,2010*
Protein Activity	*Gautier, 2011*	*Veldhuizen, 2003*
Heterodimerization		*DeRose, 2013*
Proteasomal degradation		*This work*
Transcription activation	*Pinheiro, 2008*	*Neveu, 2008*
si RNA activation		*Chaulk, 2007*

Table 2.2: Reference examples of caged proteins and caged small molecules applications for the light control of physiological processes displayed on **Fig. 2.4**.

2.2.2 Specification of a good caged compound

The desirable characteristics of a caged compound can be listed (adapted from (Bochet, 2002), (Corrie, 2005), (Kao, 2008), (Gurney, 2010), (Civillico, 2011). Ideally, a caged compound is inactive in the dark, whereas light-illumination restores the biological activity.

[58] As an example, we describe the caged lysine unnatural amino-acid (UAA) incorporation strategy used in (Gautier, 2010). The pyrrolysyl-tRNA synthetase of *M. barkeri* (a methanogenic bacterium) and its cognate amber codon tRNA are functional and orthogonal to the endogenous translational machinery in mammalian cells (Chen, 2009). A chemical biology approach by directed evolution of the active site of the synthetase led to a selective synthetase/tRNA pair enabling to incorporate a caged Lys UAA in the POI.

2.2.2.1 The caged compound must be inactive in the dark

a) chemical stability

A first requirement is that the caged compound is not affected by hydrolysis in water. Esters are more sensitive to hydrolysis than ethers or carbamates, resulting in spontaneous release of the active compound (Fedoriak, 2005). For example, cAMP caged with 2-nitrobenzyl are sensitive to hydrolysis, resulting in steady-low level release of free cAMP (Lester, 1982).

b) *in vivo* stability

Endogenous enzymes such as esterases can potentially recognize and hydrolyze caged-substrates *in vivo*. This issue will be addressed with the development of caged auxins in plants in Chapter **4**.

c) Inactivity in the dark

Some potent effectors, such as glutamate are biologically active at very low concentrations. Therefore, high purity in caged-molecule is necessary to prevent residual active compound to prevent background activation in the dark. Although the caged-molecules are relatively stable, manipulators should handle these products with special care to prevent activation by ambient light. For example, a reported caged-version of the small inducer of gene expression doxycyclin presents background activation when used at usual concentration of free-doxycyclin activation, hypothetically due to mild-affinity with the effector protein Tet (Cambridge, 2006).

2.2.2.2 The caged compound must be activatable upon light illumination[59]

a) Efficiency of photoliberation

Two important parameters characterize the overall caged compound efficiency: first, the absorption coefficient ε ($M^{-1}.cm^{-1}$), quantifies the ability of a molecule to absorb light (according to Beer-Lambert's law)[60], the first-step of the uncaging process. Second, the quantum-yield of uncaging φ is defined as the ratio of the numbers of absorbed photons leading to an efficient photochemical release[61] compared to the total numbers of photons absorbed. Both these numbers need to be

[59] The intensity is either quantified by surfacic power (in $W.m^{-2}$), or by the photon flux (in mol $photons.m^{-2}.s^{-1}$). Typical surfacic power of 10^{-1}–10^{3} $mW.cm^{-2}$ is obtained with violet light in epifluorescence microscopy.

[60] Alternatively, the single-photon absoption cross-section σ (in cm^2 or $Å^2$) caracterizes the effective capture area of a molecule is proportional to ε.

[61] Dissipation can however occur *via* other photophysical processes, such as quenching, non-radiative transfer or

maximized, to prevent light damage associated with high-illumination. Therefore, the product ε.φ, called *action cross-section*, can be used to characterize the system.

b) Kinetics of photoliberation

Ideally, photolysis should be triggered by a short pulse, and the photochemical reaction post-illumination should be fast in comparison to the biological phenomenon studied; however, fast and efficient release are not always compatible. As photorelease is a sequential process of reactions with possible by-products, fast photochemical reactions do not necessarily lead to the expected active product. Assuming a global single-exponential decay, the actual rate of uncaging *k* (or alternatively, the typical time constant τ, or the half-life time $t_{1/2}$) has been reported for several caged bioactive molecules, with typical range from 10^2 to 10^7 s^{-1}. Therefore, a compromise has to be made according to desired specifications.

c) Photoliberation can be highly-localized

The caged compound must be evenly distributed through the system of interest. Light allows highly precise patterns of activation. In one-photon activation, a beam of near-UV light triggers, with maximal release at the focal plane. Higher spatial selectivity can be obtained by two-photon excitation.

2.2.2.3 The caged compound must be compatible with cellular physiology

a) Biological toxicity

The caged compound must be biologically inert and non-toxic: DMNPE caged ATP (Nichols, 1990) addressed the instability of previous caged-ATP candidates with 2-nitrobenzyl (section **2.2.2.1.a)**, but inhibited ATP-sensitive K+ channels.

b) Light toxicity

UV-light-illumination can also be toxic, especially below 350 nm, a range at which *o*-nitrobenzyl uncaging is the most efficient, due to strong absorption by endogenous cellular components. However, this issue can be addressed by the introduction of electron-donating substituents enabling red-shifted absorption. Two-photon excitation is another strategy for efficient uncaging in the « therapeutic optical window », between 700 nm and 900 nm, where both light-absorption and scattering are minimal. Photolysis can generate toxic side products, such as nitrosobenzaldehyde,

fluorescence. Competition between these phenomena and efficient photolysis is quantified globally by quantum-yield.

the photoilluminated product of *o*-nitrobenzyl caging group. Introduction of methyl alpha substituent results in a less-toxic ketone by-product.

c) Intracellular uptake

Addition of a hydrophobic caging chromophore to a molecule that is itself moderately soluble, such as serotonin or cAMP can be a challenge when the caged molecule has to be delivered at high concentrations. The introduction of a large caging group can be an issue for biological uptake. However, the protecting cage can also confer membrane permeability to hydrophilic molecules.

The choice of a photocaging group relies on a compromise, depending on the specifications for photoactivation, as reported caging groups exhibit different photochemical, stability, and delivery issues. Nitroaryl- derivatives, especially 6-nitroveratryloxycarbonyl (NVOC), and 2-4 dimethoxy-nitrobenzyl (DMNB) are commonly used in reported photoactivation examples.

PART B
RESULTS

"We must, therefore, conclude that when seedlings are freely exposed to a lateral light, some influence is transmitted from the upper to the lower part, causing the latter to bend." [1]

Charles Darwin, The Power of Movement in Plants (1880)

''Au début de l'enquête, on est dans le noir, on tâtonne... ''

Georges Simenon, Maigret et les témoins récalcitrants

[1] Light perception by plant shoots triggers a differential growth response, a process called phototropism. This led Charles Darwin who studied this phenomenon to propose that the origin of this light-driven asymmetry was a diffusible factor, which was purified fifty years later and named auxin. Interaction of auxin with light roots thus back in the very initial phytohormone observations (Abel, 2010).

Presentation of part B

In chapter **1**, we reviewed the existing methodologies for controlling the stability of a Protein of Interest (POI) by hijacking the Ubiquitin-Proteasome System (UPS). This led to the development of the Auxin-Inducible Degradation (AID) methodology, which enables to deplete heterologous POI in yeast or mammalian cells by conditional addition of a small molecule auxin (natural IAA, or synthetic NAA). This perturbation is easy to implement, but allows poor spatio-temporal resolution, whereas homogenous distribution or intracellular delivery can be an issue. In chapter **2**, we described the existing methods for the light-control of physiological processes. In particular, the availability of small effectors can be modulated by light using a caging methodology.

In this work, we propose to implement light-control on the AID methodology by a photoactivable caged version of the effector of degradation, auxin, as summarized on **Fig. B.** Light illumination would liberate the inactive caged auxin. This would lead to the heterodimerization of heterologous POI tagged with an AID degron and F-Box protein *Os*TIR1, resulting in polyubiquitination and eventual proteasomal degradation of AID-POI.

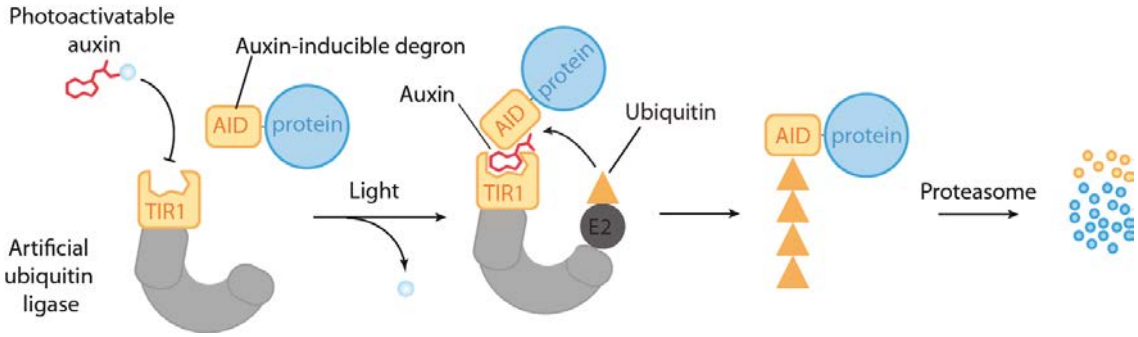

Fig. B: Overview of a light-controlled AID for conditional depletion of POI in mammalian cells. Caged auxin is inactive in the dark, whereas its photolysis by UV illumination mediates the direct interaction between heterologous POI-AID and F-box *Os*TIR1, leading to the subsequent polyubiquitination and degradation of the POI-AID.

We will describe in chapter **3** the optimization process for the AID platform in mammalian cells. Then, in chapter **4**, we will describe the design of a caged auxin candidate meeting the specifications described on part **2.2.2**. These tools will be combined in chapter **5** for the light-control of nuclear protein degradation. Eventually, in chapter **6**, we will extend this methodology to cytoplasmic proteins.

Chapter 3

Development and Optimization of the AID depletion system in mammalian cells

3.1 Specifications for the implementation of an AID methodology in mammalian cells

The Auxin Inducible Degron (AID) methodology, presented in section **1.4.2** enables the proteasomal degradation of a given POI by conditional addition of auxin, as recapitulated on **Fig. 3.1**. This strategy necessitates the co-expression of two heterologous proteins: *Os*TIR1 and POI fused to an AID degron (the complete sequence of *At*Aux/IAA17)[2].

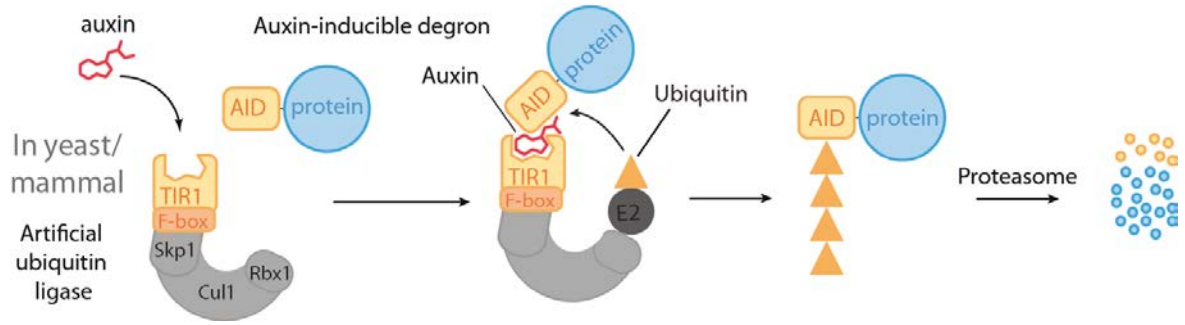

Fig. 3.1: the AID process allows conditional depletion of POI in mammalian cells. Addition of the small molecule auxin mediates the direct interaction between heterologous POI-AID and F-box TIR1, forming a functional ubiquitin ligase with endogenous SCF components. This leads to the subsequent polyubiquitination and degradation of the POI-AID.

[2] Contrary to the techniques presented in part **1.2**, where expression of a single POI fused to a destabilizing domain is necessary, and which rely only on the endogenous degradation machinery.

3.1.1 AID methodology necessitates dual expression of heterologous proteins

3.1.1.1 Bicistronic vector strategy allows dual protein expression

We first elaborated a strategy to control the relative levels of the two proteins heterogously expressed proteins. In transient transfection systems, the expression efficiency is related to the uptake of exogenous plasmid by culture cells, which is a stochastic event. Co-transfection of two different plasmids reduces the individual control of the relative expression of proteins. We thus used an alternative co-expression strategy (except in chapter **6**).

In the original AID methodology (Nishimura, 2009), Kanemaki *et al*. used a bicistronic IRES vector[3]. In this strategy, explained on **Fig. 3.2.a**, a single transcript under the dependence of a CMV (Cytomegalovirus) promoter allows the expression of two cistrons separated by an Internal Ribosomal Entry Site (IRES). This element acts as a ribosome recruitment site (other than the 5'), allowing initiation of translation from an internal region of the mRNA, eventually enabling the translation of two proteins from a single mRNA (see the *IRESite* database for complete reference).

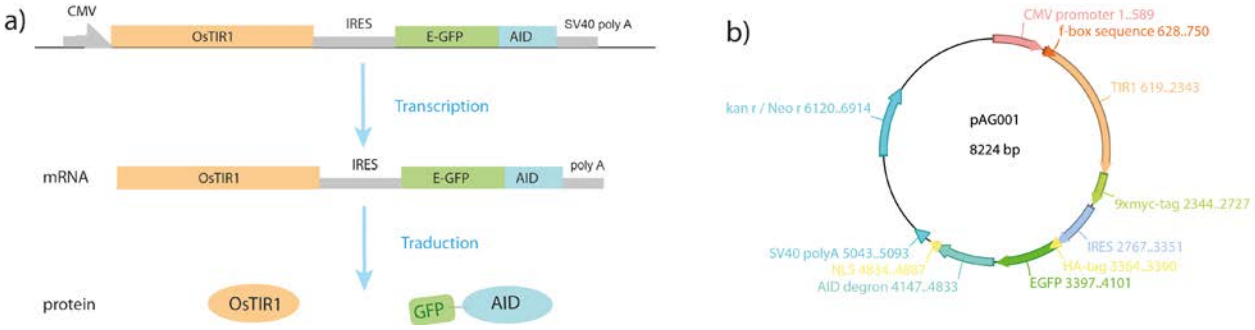

Fig. 3.2: **a)** A bicistronic strategy allows dual expression of proteins separated by an IRES sequence from a single mRNA regulated by a CMV promoter. **b)** Map of pAG1 plasmid allowing *Os*TIR1-9cMyc/EGFP-AID-NLS expression in mammalian cells.

3.1.1.2 A single plasmid strategy for AID implementation

We chose this bicistronic plasmid strategy for dual protein co-expression in mammalian cells. The pNHK60 plasmid (*Os*TIR1-9cMyc-IRES-EGFP-AID-NLS) described in (Nishimura, 2007) (courtesy of Pr. Kanemaki) and enabling the expression of *Os*TIR1 and EGFP fused to AID and a

[3] Another strategy in mammalian cells has later been described (Holland, 2012): mammalian cell lines stably expressing *Os*TIR1 were constructed by retroviral transduction. Heterologous POI fused with AID under the dependence of a conditional doxycyclin promoter can be expressed by single plasmid transient transfection. This constitutes a generic platform for conditional degradation of various POI targets. An elegant alternative was proposed for the development of the AID methodology in *Trypasonomas*, an eukaryotic unicellular organism where IRES sequences are inefficient. Instead, the P2A peptidic sequence can be inserted between the two proteins. This sequence is cut through a co-translational process, ensuring dual protein expression in a strict 1:1 stoichiometry (Kreidenweiss, 2013).

nuclear localization signal was modified by insertion of sequence coding for a HA epitope at the N-terminus of EGFP-AID-NLS[4], giving new plasmid pAG1 (*Os*TIR1-9cMyc-IRES-HA-EGFP-AID-NLS), displayed on **Fig. 3.2.b**.

3.1.2 Specification of cell line model for evaluation of the AID methodology

3.1.2.1 Mammalian cell line and culture medium selection

We first chose Chinese Hamster Ovarian (CHO), a classically-used mammalian cell line model for recombinant protein expression, characterized with a rapid growth (*American Type Culture Collection (ATCC)* database). A mammalian cell culture medium had then to be selected; first, it must be fit for cell survival and growth. Dulbecco-Modified Eagle Medium (D-MEM) is classically used. Addition of animal serum is often necessary, but can be an issue in protocols depending on the addition of small molecules (some serum proteins, such as albumin, are known to adsorb hydrophobic molecules (Fasano, 2005)). This question will be further discussed on chapter **5**. Some cell lines, such as CHO, also need to be supplemented with non-essential amino-acids *(ATCC)*.

3.1.2.2 Culture medium must be auxin-free[5]

Native presence of free auxin in culture serum might induce unwanted AID depletion. As the phytohormone auxin is highly abundant in plant, it might therefore be present in herbivorous species serum such as fetal bovine serum (FBS); however, no variation of EGFP fluorescence signal was observed between CHO cells co-expressing *Os*TIR1-9Myc and EGFP-AID-NLS cultivated in D-MEM with 1%, 5% or 10% FBS (data not shown).

3.1.2.3 Culture medium must be compatible with light illumination

One last requirement is that the UV light used for actuation does not interfere with the medium. Phenol red, a pH indicator dye classically used in culture media such as Dulbecco Modified Eagle medium (D-MEM), has been described to give toxic by-products upon UV illumination (Stoien, 1974), and can absorb a non-negligible part of the light used for actuation. On chapters **5** and **6**, we switched to a phenol red free medium for light induced depletion in microscopy.

[4] HA tag is a widely used epitope derived from Human Influenza Haemaglutinin. However, immunoblotting experiments directed against this epitope did not allow reliable quantification (data not shown).

[5] Interestingly, natural auxin IAA was first isolated and purified from human urine in the 1930s (Abel, 2010).

3.1.3 Validation of the AID methodology in a mammalian cell line

3.1.3.1 Implementation of auxin-conditional control of POI in CHO cells

We first tested whether we could implement conditional depletion by addition of auxin in CHO culture cells. However, transient transfection of plasmid pAG1 in CHO cells was associated with both poor transfection efficiency and low expression level. We thus looked for an alternative to optimize AID expression[6]. As a first strategy, we constructed a stable CHO cell line. We took advantage of the Gentamycin resistance gene present in the pAG1 plasmid. CHO cells were transfected with pAG1, and a polyclonal cell line was established by G418 selection[7]. Monoclonal cell lines were established by isolation and selection of individual clones.

This stable cell line enabled to validate the auxin-induced depletion. Addition of 500 µM of natural (Indole Acetic Acid, IAA) or synthetic auxin (Naphtalene Acetic Acid, NAA) for 2 hours led to a quantitative depletion of EGFP-AID-NLS assessed by EGFP epitope in immunoblotting. No significant variations were observed for the heterologous *Os*TIR1-9Myc and endogenous actin protein levels assessed by immunoblotting (**Fig. 3.3.a/b**). This excluded that the observed EGFP-AID-NLS depletion might be attributed to a differential transfection efficiency or sample loading in Western-Blot experiment.

This observation was further validated by monitoring EGFP fluorescence in fixed CHO cells in confocal microscopy. Specific nuclear EGFP fluorescence was observed in CHO cells co-expressing heterologous EGFP-AID-NLS and *Os*TIR1-9Myc, but not after incubation with 500 µM IAA and NAA for 2 hours (**Fig. 3.3.c**). We thus validated that quantitative protein depletion could be implemented by addition of auxin in mammalian culture cells, reproducing the observations reported by (Nishimura, 2009). However, low expression levels were observed (see auto-fluorescence in **Fig. 3.3.c**); moreover, the cell-line was poorly-stable and derived rapidly in absence of G418. For these reasons, we preferred to change cell line for higher expression level and prevent detrimental activity by transient expression in culture cells.

[6] Although high heterologous protein expression is desirable to enhance the specificity of the signal measured, several papers reported concerns that over-expression of UPS-interacting proteins might lead to the saturation of the UPS, impairing both endogenous and artificial protein degradation (Sellmeyer, 2009), (Zhou, 2000).

[7] The neo gene (from bacterial transposon Tn5) encodes an aminoglycoside phosphotransferase (APT 3'). Heterologous expression in mammalian cells confers resistance to G418, a Gentamycin-related antibiotic. Consequently, cells having incorporated a transfected plasmid by homologous recombination can be selected in one to three weeks by addition of G418, at a concentration range toxic for WT cells (100-1000 µg.mL^{-1}, depending on plasmid and cell type).

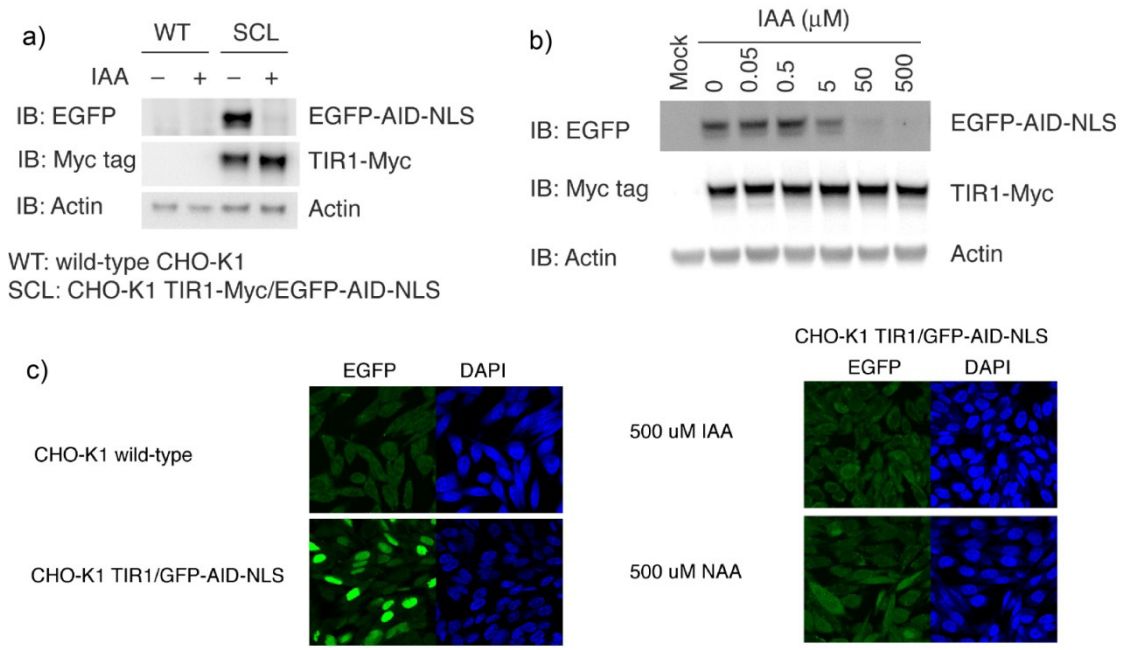

Fig 3.4: **(a-b)** WT CHO cells (left) and CHO cells stably expressing EGFP-AID-NLS and *Os*TIR1-Myc (SCL = Stable Cell Line, right) were incubated with (+) or without (–) 500 µM IAA for 2 hours **(a)**, or with various concentrations of IAA for 2h **(b).** Cell lysates were analyzed by immunoblotting (IB) with the indicated antibodies. **(c)** Cells incubated as in **(a)** were fixed, stained with DAPI, and visualized in confocal microscopy.

3.1.3.2 Implementation of auxin-conditional control of POI in HEK cells

A second strategy to optimize the heterologous protein expression was to switch to another cell line enabling a good model expression system. Human Embryonic Kidney 293 (HEK293) cell lines are fast-growing and offer excellent transfection efficiencies and high expression of heterologous protein (*ATCC*). Moreover, HEK293 cells are a classical model for proteasome-dependent degradation, as UPS components are endogenously present at high levels (Gastaldello, 2008).

We first confirmed that conditional depletion could be induced by addition of auxin in HEK293 cells co-expressing EGFP-AID-NLS and *Os*TIR1-myc. Addition of 500 µM IAA led to significant depletion of EGFP-AID-NLS in 2 hours assessed by EGFP epitope in immunoblotting (**Fig. 3.4.a**). To determine the timing and extent of auxin-induced depletion, we monitored the EGFP fluorescence signal in individual HEK293 cells co-expressing EGFP-AID-NLS and *Os*TIR1-myc in confocal time-lapse microscopy[8]. In presence of 500 µM IAA at 37°C, we observed a depletion of the EGFP fluorescence, with a half-life of 36 ± 3 min, whereas control cells incubated with DMSO showed no significant depletion (**Fig. 3.4.b/c**).

[8] Confocal microscopy enables increased optical resolution and contrast, due to selection of focused light by a pinhole positioned at the confocal plane; it both allows precise visualization of 2-D slices and 3-D reconstructions. As precise evaluation of fluorescence was desirable for reproducible depletion, we selected this visualization methodology.

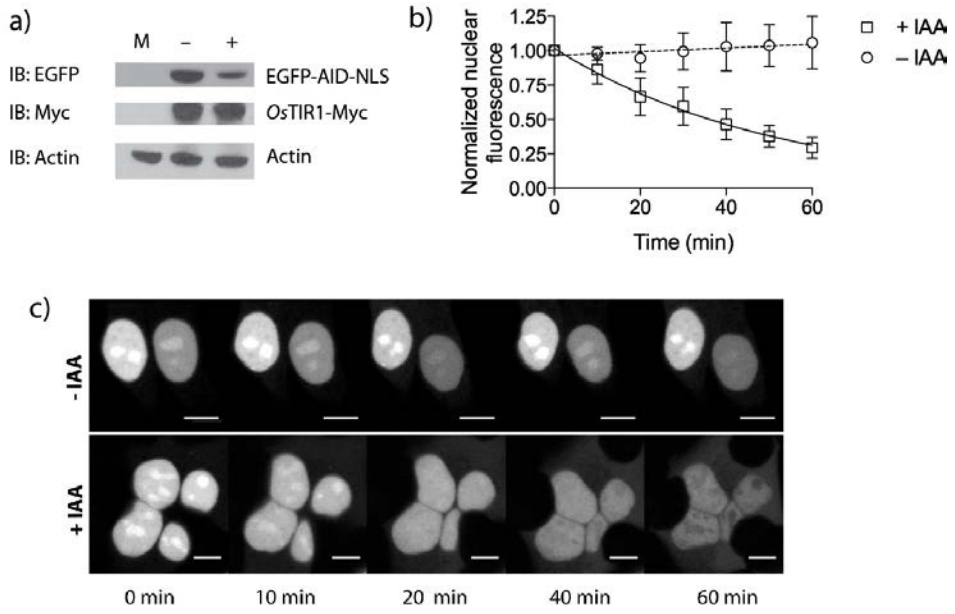

Fig. 3.4: **(a)** HEK293 cells co-expressing EGFP-AID-NLS and *Os*TIR1-Myc were incubated with (+) or without (–) 500 µM IAA for 1 hour. Cell lysates were analyzed by immunoblotting (IB) with the indicated antibodies. M: Mock samples. **(b)** The nuclear fluorescence of HEK293 cells co-expressing EGFP-AID-NLS and *Os*TIR1-Myc was quantified by confocal microscopy at various times after 500 µM IAA addition (square). Plots show the normalized nuclear fluorescence intensity in function of time (mean ± SD, n = 10). Least squares fits (lines) gave the half-lives of EGFP-AID-NLS. Control experiments without IAA (circle) are shown. **(c)** Confocal micrographs of representative cells at various times post-IAA addition, or post-DMSO control addition.

3.2 Optimization of the AID methodology for efficient POI depletion in HEK293 cells

3.2.1 Subcellular addressing is an important parameter for efficient POI depletion in AID methodology

3.2.1.1 Slow POI depletion is observed upon auxin addition in HEK293 cells

The rather slow degradation timescale reported in section **3.1.3.2** contrasted with the half-life of 10 minutes for AID-GFP-NLS previously assessed by immunoblotting experiments (Nishimura, 2009) in similar conditions. Moreover, it also contrasts with observations by Holland *et al.* who reported shorter half-lives (< 18 min) for five AID-tagged POI in mammalian cells ((Holland, 2012), see section **1.4.2.2**). However, Holland *et al.* reported a considerably longer half-life of 40 min for Histone H2B-AID, which is close to our observations for AID-GFP-NLS[9]. This discrepancy

[9] Contrary to the other nuclear AID-tagged protein (TRF2 and CENP-A), H2B and AID-GFP-NLS are diffuse in the nucleus; It might be possible that TRF2 and CENP-A might be expressed at lower levels than H2B, facilitating their complete depletion. Alternatively the positively-charged H2B-AID is relatively inaccessible for ubiquitination, as it is

between the reported auxin-dependent degradation rates and our observations is an issue for the development of an efficient conditional depletion platform, which we will address next.

3.2.1.2 Heterologous *Os*TIR1 and AID-GFP-NLS are not colocalized in HEK cells

We first wondered whether the poor degradation efficiency reported above might originate from poor nuclear addressing of heterologous *Os*TIR1-myc. As this process depends on auxin-mediated direct interaction, it is important that the two co-expressed proteins have the same subcellular localization. As heterologous AID-GFP-NLS is localized in the nucleus (**Fig 3.4**), *Os*TIR1-Myc has thus to be addressed in sufficient quantity to this compartment to ensure functional interaction.

The heterologous *Os*TIR1-Myc is a 78 kDa protein, which is largely above the exclusion size for passive diffusion through the nuclear pore (Lange, 2007). Nuclear accumulation of *Os*TIR1-myc protein necessitates therefore a nuclear import mechanism, depending on the presence of a Nuclear Localization Signal (NLS). No strong endogenous NLS was predicted in the sequence of *Os*TIR1-9Myc by bioinformatics tools (*cNLS mapper*). We postulated therefore that heterologous *Os*TIR1-9Myc is present principally in the cytoplasm, and poorly imported in the nucleus. Immunocytochemistry experiments in fixed HEK293 cells confirmed this hypothesis (**Fig. 3.5.a**).

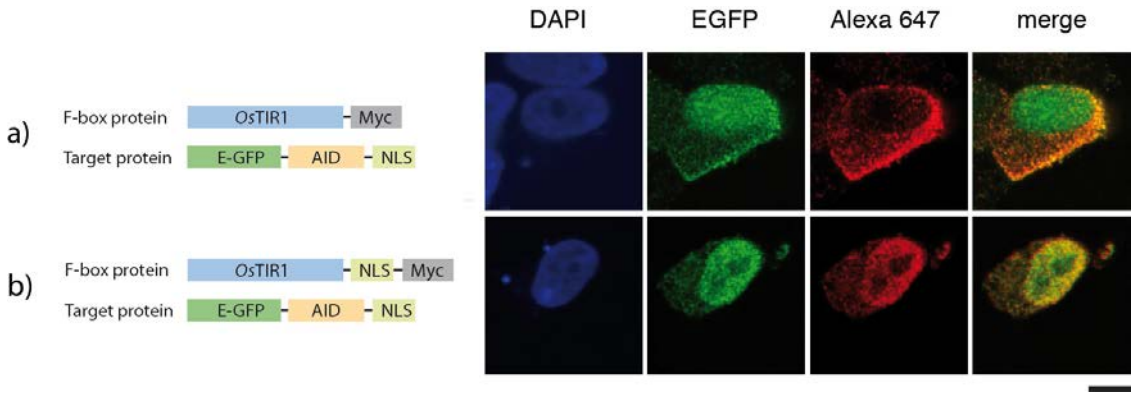

Fig. 3.5: Graphical map of the heterologous proteins expressed in pAG1 and pAG38, and micrographs of fixed HEK293 cells that expressed **(a)** *Os*TIR1-Myc and EGFP-AID-NLS (first row), and **(b)** *Os*TIR1 fused to a Myc-tag and a nuclear localization signal (*Os*TIR1-NLS-Myc) and EGFP-AID NLS (second row), were stained with DAPI and immunostained with an anti-Myc primary antibody and an Alexa 647-conjugated secondary antibody. Selective detection of the EGFP signal shows the cellular localization of EGFP-AID-NLS, while selective detection of theAlexa 647 signals shows the cellular localization of *Os*TIR1-Myc and *Os*TIR1-Myc-NLS. Scale bar 10 µm.

tightly associated with the chromatin.

3.2.2 Co-localization of TIR1 and AID-GFP-NLS increases the degradation rate

3.2.2.1 *Os*TIR1 can be addressed to the nucleus by NLS fusion

Consequently, a NLS sequence was fused to *Os*TIR1-Myc in a new plasmid construction (pAG 38, *Os*TIR1 NLS--cMyc-IRES-HA-EGFP-AID-NLS). This NLS is expected to lead to the nuclear accumulation of heterologous *Os*TIR1-Myc-NLS. This was confirmed by immunocytochemistry experiments in fixed HEK293 cells[10] (**Fig. 3.5.b**).

3.2.2.2 Co-localization of TIR1 and AID-GFP-NLS increases the rate of degradation twofold

We next confirmed that this construction was functional for auxin-conditional depletion in HEK293 cells co-expressing EGFP-AID-NLS and *Os*TIR1-9cMyc-NLS. Addition of 500 µM IAA for 2 hours led to a significant depletion of EGFP-AID-NLS in EGFP immunoblotting (**Fig. 3.6.a**).

To demonstrate that localization of *Os*TIR1 might affect the degradation efficiency, we quantified by time-lapse confocal microscopy the auxin-induced depletion of EGFP fluorescence signal in individual HEK293 cells co-expressing EGFP-AID-NLS and *Os*TIR1-Myc-NLS (**Fig. 3.6.b/c**). In presence of 500 µM IAA at 37°C, we observed a significant depletion of the EGFP fluorescence, with a half-life of 19 ± 2 min, which is in good accordance with other examples reported in the literature (Nishimura, 2009) (Holland, 2012).

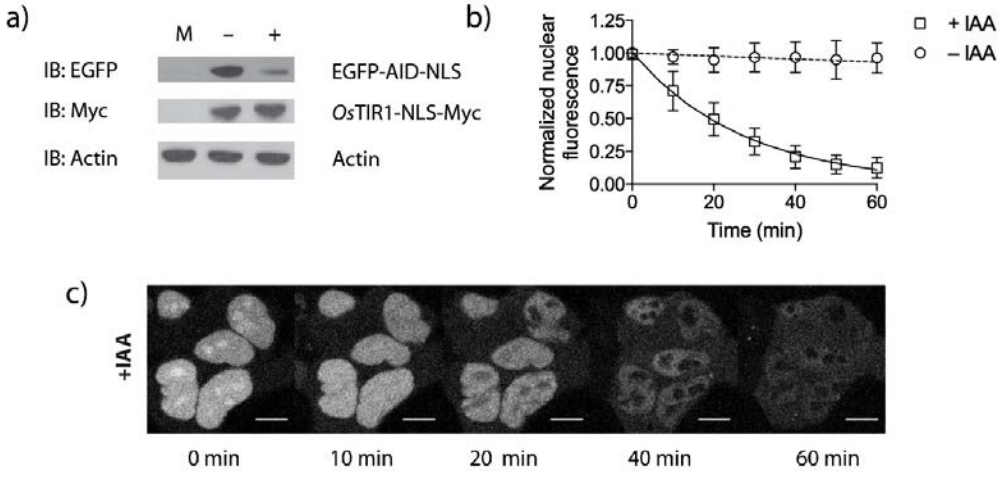

Fig. 3.6: (**a**) HEK293 cells co-expressing EGFP-AID-NLS and *Os*TIR1-NLS-Myc were incubated with (+) or without (–) 500 µM IAA for 1 hour. Cell lysates were analyzed by immunoblotting (IB) with the indicated antibodies. M: Mock samples. (**b**) The nuclear fluorescence of HEK293 cells co-expressing EGFP-AID-NLS and *Os*TIR1-NLS-Myc was quantified by confocal microscopy at various times after 500 µM IAA addition (square). Plots show the normalized nuclear fluorescence intensity in function of time (mean ± SD, n = 10). Least squares fits (lines) gave the half-lives of EGFP-AID-NLS. Control experiments without IAA (circle) are shown. (**c**) Confocal micrographs of representative cells at various times post-IAA addition.

[10] It was reported (Holland, 2012, Fig 6) in the case of centromeric POI tagged with AID that addition of auxin led to the reversible recruitment of cytoplasmic *Os*TIR1 at the centrosome.

3.2.2.3 Observations

Concomitantly with the acceleration of degradation kinetics, we observed fluorescence distribution changes upon auxin addition, highlighted in **Fig. 3.7**:

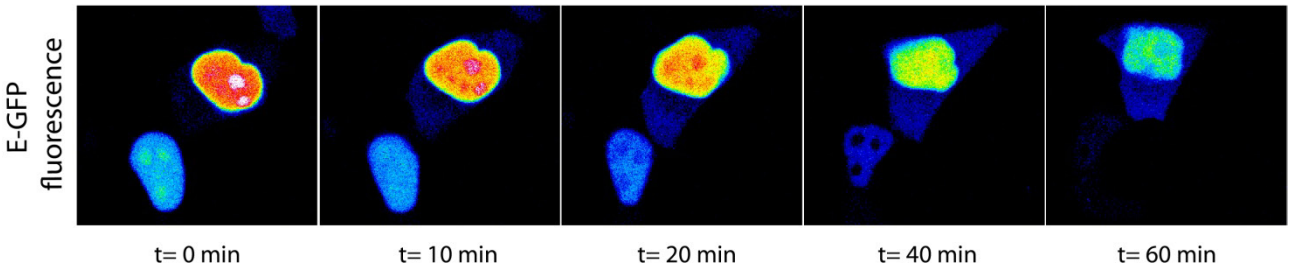

Fig. 3.7: Confocal micrographs of representative HEK293 cells co-expressing EGFP-AID-NLS and *Os*TIR1-Myc were incubated with 500 µM IAA at various times.

Although the heterologous EGFP-AID-NLS is a nuclear protein, an increase of the cytoplasmic fluorescence is observed upon conditional auxin addition, concomitantly with the global depletion (**Fig. 3.7**). A possible explanation to this phenomenon is that the degradation of the polyubiquitinated EGFP-AID-NLS by the proteasome is incomplete, as it requires active unfolding of the target protein. EGFP proteins undergo a post-translational maturation forming an active chromophore, which might not be efficiently unfolded by the proteasome **(Fig. 3.8.c**). Consistently, a specific signal below 30 kDa is observed in immunoblotting of HEK cells expressing EGFP-AID-NLS, which increases upon auxin addition **(Fig. 3.8.a**). This signal might be due to EGFP protein resulting from degradation, free to diffuse in cytoplasm due to absence of NLS signal.

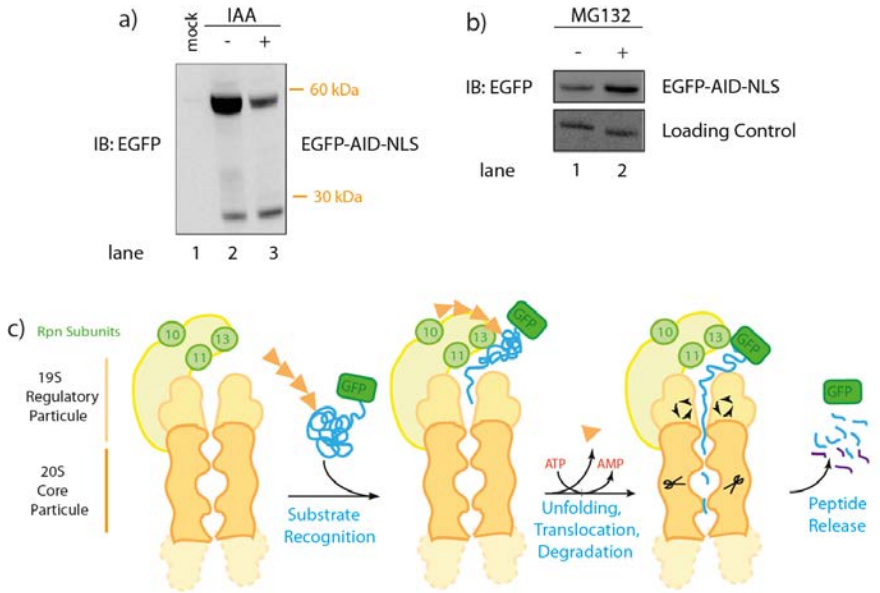

Fig. 3.8: **(a)** HEK293 cells co-expressing EGFP-AID-NLS and *Os*TIR1-NLS-Myc were incubated with (+) or without (–) 500 µM IAA for 1 hour. Cell lysates were analyzed by immunoblotting (IB) with α-GFP antibody. **(b)** HEK293 cells co-expressing EGFP-AID-NLS and *Os*TIR1-NLS-Myc were incubated with (+) or without (–) 50 µM MG132 for 2 hours. Cell lysates were analyzed by immunoblotting (IB) with α-GFP antibody. **(c)** Proposed mechanism for incomplete degradation of EGFP fusion proteins. The β-barrel EGFP cannot be unfolded and access the proteolytic core.

As this signal is present in absence of auxin, we suspected that background degradation of EGFP-AID-NLS took place in absence of auxin. Consistently with this, an increase of the EGFP-AID-NLS signal was observed in HEK293 cells expressing *Os*TIR1-NLS-myc incubated with proteasome inhibitor MG132 for 2h (**Fig. 3.8.b)**. In the same time, we observed a rapid fluorescence loss in the nucleoli[11].

3.2.2.4 Discussion

The almost two-times acceleration of the degradation rate between *Os*TIR1 and *Os*TIR1-NLS confirmed that colocalization of *Os*TIR1 and AID-tagged POI is an important parameter for the optimization of the AID depletion platform, as summarized in **Fig. 3.9**.

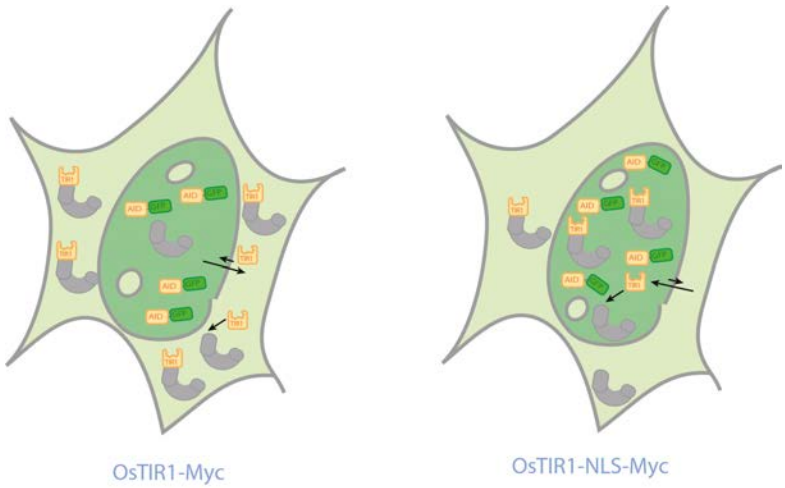

Fig. 3.9: Comparative graphic showing the importance of colocalization for EGFP-AID-NLS and *Os*TIR1-myc; poor nuclear addressing of *Os*TIR1-myc prevents formation of functional ubiquitin ligase degrading nuclear EGFP-AID-NLS, in contrast with nuclear *Os*TIR1-NLS-Myc.

Histoimmunostaining experiments (*Human Protein Atlas, proteinatlas.org*) showed that Cullin1 is a predominantly nuclear protein, although it can be inhomogenously associated with vesicles in the cytoplasm. Cytoplasmic aberrant expression of Cullin1 is associated with the development of aggressive carcinoma (Do, 2014). Therefore, it is expectable that the formation of a functional SCF^{TIR1} is more efficient in the nucleus.

One can interrogate how a slow but functional specific degradation process can take place without colocalization of the two heterologous proteins. We propose here two hypotheses:

[11] The heterologous EGFP-AID-NLS is a nuclear protein accumulating in the nucleoli (**Fig. 3.4**). Upon auxin addition, fluorescence is rapidly depleted from the nucleoli in 10 to 20 minutes before global depletion affects the nucleoplasm (**Fig. 3.6.c** and **3.7**). A hypothesis to explain this feature might be that nucleolar EGFP-AID-NLS have a higher diffusion coefficient than nucleoplasmic one (which might interact with DNA) (Boyd, 2011); therefore, they are more accessible to auxin-dependent polyubiquitination, and degraded first. Alternative hypothesis is that specific degradation take place in the nucleoli. However, this is not consistent with the nuclear distribution of UPS protein (Human Protein Atlas). Otherwise, it was reported that specific polyubiquitination of p53 in the nucleoli can drive their nucleolar export (Boyd, 2011). However, no specific differential depletion was seen with proteasome inhibitor MG132 (which does not prevent polyubiquitination) upon auxin addition (see **5.2.3.3**).

- Heterologous *Os*TIR1-myc contains a mild NLS sequence. This might be sufficient to address a minority fraction of the protein to the nucleus, where it can form functional SCF^{TIR1}, however in default to EGFP-AID-NLS, explaining the slow degradation rate
- A dynamical exchange can exist between nuclear and cytoplasmic addressing, although largely unbalanced in favor of nuclear localization. This mechanism might explain the slower degradation rate, which necessitates the nuclear export of EGFP-AID-NLS.

We later found another confirmation of this strategy reported in the literature: nuclear addressing of heterologous *At*TIR1 by fusion with NLS addressed limitations of the classical AID methodology in yeast and accelerated the auxin-dependent degradation of nuclear proteins[12] (Kanke, 2011).

3.2.3 Probing F-box/Skp1 fusions for AID optimization

3.2.3.1 F-box/Skp1 fusions were reported to enhance AID depletion in yeast

In the same paper (Kanke, 2011), the authors expressed concerns that heterologous *At*TIR1 might fail to incorporate efficiently within endogenous SCF components. In the AID methodology (Nishimura, 2009), endogenous Skp1 (S phase kinase associated protein 1) mediates the interaction between heterologous *At*TIR1 (or *Os*TIR1 in mammalian cells) through its N-terminal F-box domain and the Cullin1 to form a functional E3 ubiquitin ligase complex[13] (see section **1.3.1**). Therefore, an improved AID (*i*AID) was developed by fusing *Sc*Skp1 to *At*TIR1-NLS. This strategy was expected to enhance the probability of forming a functional ubiquitin ligase by decreasing the numbers of partners, and thus accelerate the kinetics of ubiquitination. Indeed, auxin addition accelerated the depletion of AID-GFP-NLS reporter from 50% to 90% in one hour (Kanke, 2011).

3.2.3.2 F-box/Skp1 fusion enhance AID depletion in mammalian cells

We adapted this strategy to our degradation system, by fusing the entire *Hs*Skp1 sequence (160 a.a., 19kDa) to *Os*TIR1-9Myc and *Os*TIR1-9Myc-NLS in new plasmid constructions (resp. pAG 39 and pAG 40). This strategy is summarized in **Fig. 3.10.a**.These constructions allowed EGFP-AID-NLS degradation by conditional 500 µM auxin addition within 2 hours. Consistently with section **3.2.2.1**, nuclear addressing of *Hs*Skp1-*Os*TIR1 by NLS fusion enhanced depletion efficiency (**Fig. 3.10.b**).

[12] In yeast cells expressing *At*TIR1, heterologous Mcm4-AID (a chromatin-bound protein essential for replication) is degraded in presence of auxin, but this depletion is slow (3 hours) and incomplete (up to 75%).

[13] Skp1 is involved in the regulation many cellular processes such as cell-cycle regulation. In a context where Skp1 proteins are inabundant, others F-Box proteins such as Skp2, which is differentially expressed through the cell-cycle, might compete with heterologous *Os*TIR1 so that the ubiquitination of substrates is a limiting step.

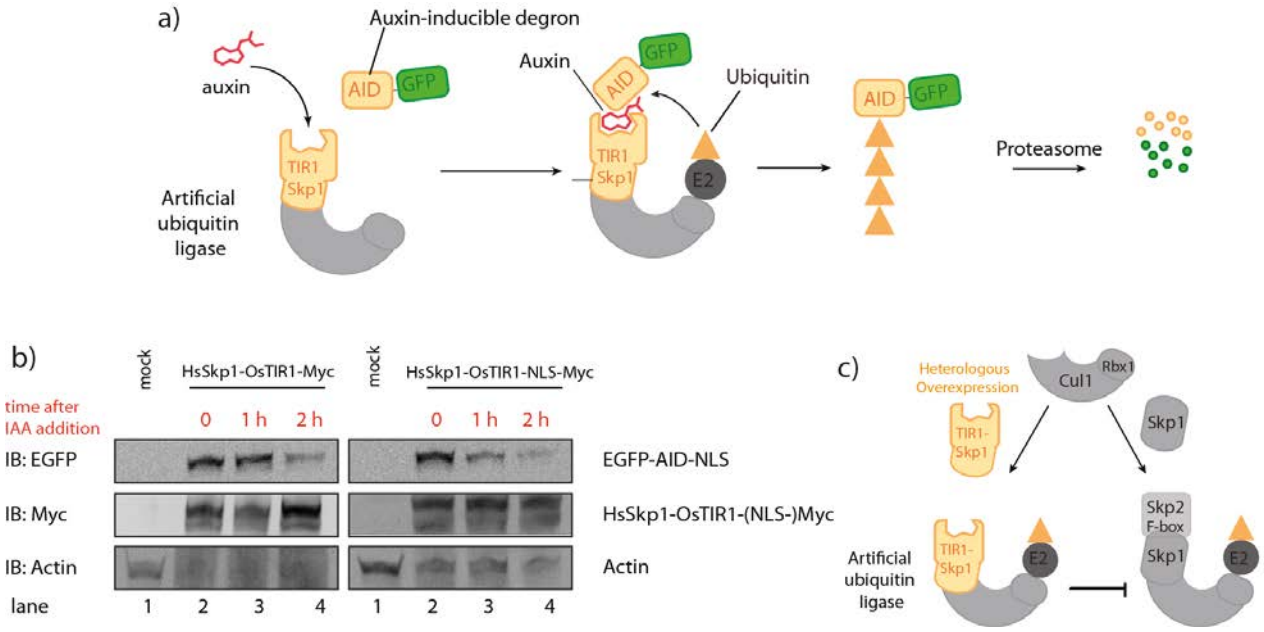

Fig. 3.10: **(a)** Graphical abstract of the heterologous proteins *Hs*Skp1-*Os*TIR1-(NLS)-myc strategy **(b)** HEK293 cells co-expressing EGFP-AID-NLS and either *Hs*Skp1-*Os*TIR1-Myc or *Hs*Skp1-*Os*TIR1-NLS-Myc were incubated with (+) or without (–) 500 µM IAA for 1 or 2 hours. Cell lysates were analyzed by immunoblotting (IB) with the indicated antibodies. M: Mock samples. **(c)** Proposed mechanism for the growth defect observed with pAG39 or pAG40. Overexpression of Skp1 fusion might saturate endogenous Cullin1 scaffold and prevent interaction of endogenous Skp1 with essential cell-cycle protein Skp2.

However, transient transfection with both pAG39 and pAG40 visibly inhibited HEK cells growth and affected the nuclear shape. Skp1 is an essential cell-cycle regulation factor (cf section **9.1**). It is therefore expectable that overexpression of a Skp1-fusion protein might saturate the endogenous SCF complexes, displaying major perturbations in the cell-cycle. Consequently, we abandoned this strategy for further optimization.

3.3 Acceleration of POI depletion kinetics using AID F-box variants

3.3.1 TIR1 homologs allow auxin-conditional degradation in heterologous system

3.3.1.1 TIR1 homologs exhibit differential range of auxin-response depletion kinetics in plants

The F-box protein TIR1 is the paradigmatic, first identified auxin nuclear receptor in *A. Thaliana* (Dharmassi, 2005), (cf section **1.4.1**). This culminated in 2007 by the publication of the structure of a TIR1-Auxin-Aux/IAA complex, which showed that auxin mediates the direct interaction between TIR1 and an Aux/IAA protein (Tan, 2007). However, *At*TIR1 is part of a larger six-gene clade of

Auxin-signaling F-Box protein (AFB) with conserved F-Box and LRR domains[14] (Bargmann, 2014). Complex combinatorial association in AFB and Aux/IAA protein pairs results in variable response to auxin in plants. In a yeast heterologous co-expression system, *At*AFB2 promoted faster degradation than *At*TIR1 for most *At*Aux/IAA tested[15] (Villalobos, 2012). In particular, this was the case for *At*Aux/IAA17 (the AID), with three-fold acceleration of degradation rate (Havens, 2012).

3.3.1.2 Development of mammalian AID methodologies based on TIR1 homologs

Therefore, we wondered whether we could optimize our depletion system in mammalian cells by replacing heterologous *Os*TIR1 by *At*AFB2, to accelerate the kinetics of degradation of AID-tagged POI. However, based on the reported development of *At*TIR1-based AID methodology (Nishimura, 2009), it is expectable that heterologous *At*AFB2 is functional at 24°C, but not at 37°C. Consistently with the approach of Kanemaki, we also proposed to introduce the putative AFB2 found in *Oryza sativa*[16]. We thus replaced *Os*TIR1-Myc-NLS by *At*AFB2-Myc-NLS and *Os*AFB2-Myc-NLS in new plasmids constructions (resp. pAG52 and pAG53) (**Fig. 3.11.a**).

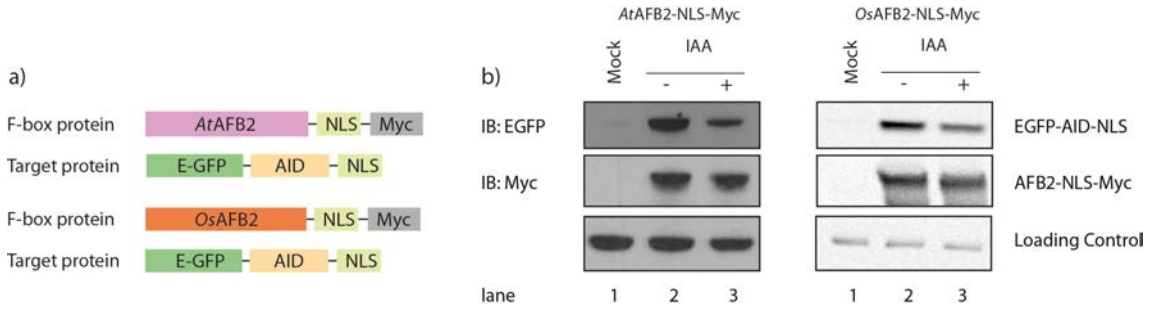

Fig. 3.11: **(a)** Graphical map of the heterologous proteins expressed in pAG52 and pAG53. **(b)** HEK293 cells co-expressing EGFP-AID-NLS and either *At*AFB2-NLS-Myc (left) or *Os*AFB2-NLS-Myc (right) were incubated with (+) or without (–) 500 µM IAA for 1 hour. Cell lysates were analyzed by immunoblotting (IB) with the indicated antibodies.

We next confirmed that these constructions were functional for auxin-conditional depletion in HEK293 culture cells. Addition of 500 µM IAA for 1.5 hour led to a significant depletion of EGFP-AID-NLS in EGFP immunoblotting for both constructions, although to a lesser extent for *Os*AFB2-Myc-NLS (**Fig. 3.11.b**), which was consequently abandoned.

[14] All members of this family are auxin receptors, as identified by pull-down experiments. However, individual TIR1/AFB proteins display different biochemical properties, especially regarding their auxin-dependent affinities to Aux/IAA proteins (Villalobos, 2012).

[15] Yeast heterologous systems have been proposed as semi-synthetic platform to estimate the association kinetics displayed by variable pairs of Aux/IAA and AFBs, resulting in different kinetics of auxin-induced degradation assessed by YFP reporter tags (Villalobos, 2012), (Havens, 2012).

[16] The candidate gene TIR1-like *Os*04g0395600 displayed the highest homology (67%) with *At*AFB2 in BLAST sequence alignments.

3.3.1.3 Kinetic comparison of F-box *At*AFB2 and *Os*TIR1 for auxin-induced degradation

We then compared the kinetics of AID-GFP-NLS depletion when using *At*AFB2-NLS instead of *Os*TIR1-NLS. Incomplete degradation was observed in time-lapse confocal monitoring of EGFP-AID-NLS in HEK293 cells expressing *At*AFB2-NLS (**Fig. 3.12**) (compare with **Fig. 3.6**). This feature prevented further investigations.

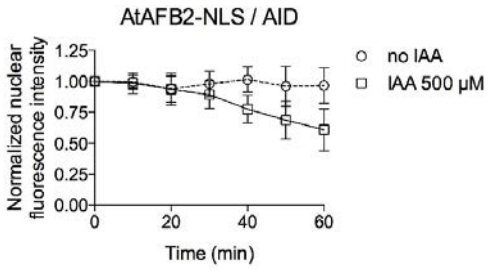

Fig. 3.12: **(a)** The nuclear fluorescence of HEK293 cells co-expressing EGFP-AID-NLS and *At*AFB2-NLS-Myc was quantified by confocal microscopy at various times after 500 µM IAA addition (square). Plots show the normalized nuclear fluorescence intensity in function of time (mean ± SD, n = 10). Least squares fits (lines) gave the half-lives of EGFP-AID-NLS. Control experiments without IAA (circle) are shown.

3.3.1.4 Conclusion

This approach validated however that *Os* and *At* TIR1 homologs can deplete *At*Aux/IAA17 in heterologous mammalian systems. Moreover, this observation contrasts with reports by (Nishimura, 2009) that *At*TIR1 is not functional in mammalian cells due to non optimal temperature conditions. Further optimization work could involve the systematic evaluation of the degradation rates between combinations of AFB/Aux-IAA proteins as was done in yeast cells (Havens, 2012) to identify efficient pairs for auxin-conditional degradation in mammalian cells. However, in next section, we describe another strategy for degradation acceleration based on TIR1 mutants.

3.3.2 Point mutations in TIR1 accelerate auxin-conditional degradation

3.3.2.1 Identification of TIR1 mutants for enhanced Aux/IAA degradation in yeast

Variants of *At*TIR1 displaying enhanced affinity for Aux/IAA proteins were identified in a mutation screen in yeast two hybrids (Yu, 2013). Point mutations D165E and M468L enhanced the auxin-induced interaction with all members of the *At*Aux/IAA family tested[17]. Consequently, remarkable acceleration of the degradation kinetics (five to six times faster that wild-type *At*TIR1) was

[17] The kinetics of degradation were assessed by exogenous expression of the TIR1 variants with Aux-IAA tagged with Yellow-Fluorescent Protein: auxin-induced depletion was determined by flow-cytometry exhibited. Regrettably Aux/IAA 17, corresponding to the AID degron was not tested.

observed for each mutant. These mutations seem to act independently, as the effect on the double-mutant was synergic. Remarkably, D170E and M473L mutations are located in the Leucine Rich Regions (LRR) outside the contact interface with Aux/IAA, or in the hydrophobic auxin-binding pocket, as one could have expected[18] (**Fig. 3.13.b**). These mutations might hypothetically induce structural changes in the auxin-binding pocket of TIR1 (Yu, 2013).

```
AtTIR1   155  CRNLKELDLRESDVDDVSGHWLS 177
OsTIR1   150  CKLLRELDLQENEVEDRGPRWLS 172
AtAFB2   150  CRHLRDLDLQENEIDDHRGQWLS 172
              C+ L++LDL+E++++D    WLS

AtTIR1   464  FAGDSDLGMHHVLSGCDSLRKLE  487
OsTIR1   459  FAGDSDKGMMHVMNGCKNLRKLE  482
AtAFB2   459  FAGDTDKGMLYVLNGCKKMKKLE  482
              FAGD+D GM +V++GC  ++KLE
```

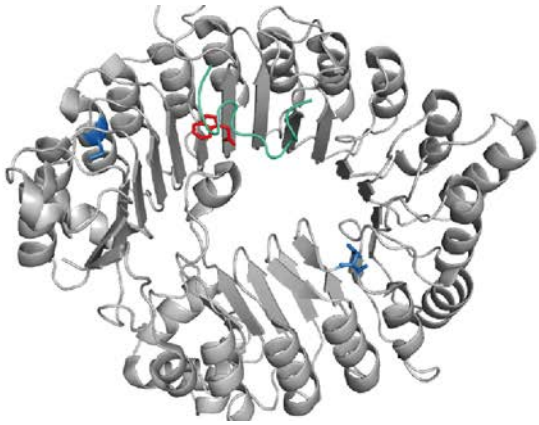

Fig. 3.13 (a) BLAST alignment between *At*TIR1, *Os*TIR1 and *At*AFB2 highlighting D165 and M468 conserved neighboring regions. **(b)**: *At*TIR1 visualization in Pymol highlighting positions D165 and M468 (blue), auxin (red) and Aux/IAA7 peptide (green) (PDB reference:2P1Q).

Identification of F-box variants with enhanced partner binding properties might be interesting for optimization of protein degradation platform in a chemical biology approach[19]. We therefore looked to introduce these mutations in mammalian cells in order to accelerate auxin-dependent degradation.

3.3.2.2 Introduction of point mutations in TIR1 variants in mammalian AID methodology

However, it was reported that heterologous *At*TIR1 is not functional at 37°C. Application of the AID methodology from yeasts to mammalian cells necessitated replacing F-box protein *At*TIR1 by its ortholog *Os*TIR1, compatible with higher temperatures ((Nishimura, 2007), see part **1.4.2.2**). As the mutations globally affect *At*TIR1 structure (Yu, 2013), one can however postulate that these variants might be more plastic and functional in mammalian cells.

Alignment between orthologs *At*TIR1, *Os*TIR1 and *At*AFB2 sequences showed that the mutations positions were conserved and corresponded to high homology regions (**Fig. 3.13.a**). We postulated

[18] An Alanine scan confirmed that these positions were important for auxin-induced recognition of Aux/IAA. Yeast two -hybrids experiments showed that the mutations induced a greater affinity for Domain II of Aux-IAA (Yu, 2013).

[19] However, although these mutations dramatically accelerated the degradation of Aux/IAA proteins, no application to the yeast AID methodology has been yet reported.

that introduction of these mutations in *Os*TIR1 might enhance the degradation kinetics. Single mutants *Os*TIR1^{D170E} and *Os*TIR1^{M473L}, and double mutants *Os*TIR1$^{D170E\text{-}M473L}$ directed were synthesized by directed mutagenesis. Similarly, we previously showed (section **3.3.1.3**) that *At*AFB2 was functional, although less-efficient than *Os*TIR1. Thus, we also introduced *At*AFB2^{D170E}, *At*AFB2^{M473L}, and *At*AFB2$^{D170E\text{-}M473L}$ as heterologous F-box variants.

3.3.2.3 *Os*TIR1 mutants were selected as potential targets for enhanced AID depletion kinetics

We first assessed that the new constructions were functional. Depletion of AID-GFP-NLS was observed in immunoblotting analysis after incubation of 500 µM IAA for one hour in HEK293 cells expressing various *Os*TIR1 mutants, comparable to WT *Os*TIR1 (**Fig. 3.14.a**). Parallely, significant depletion was observed for the *At*AFB2 variants, although less efficient than the WT *At*AFB2 (**Fig. 3.14.b**). As this platform is already less efficient for AID methodology, we did not pursue further this strategy. In both proteins, a lesser extent of depletion was associated to the double-mutant, in contrast to the reported cumulative effects of the two mutations in *At*TIR1 in yeasts (Yu, 2013).

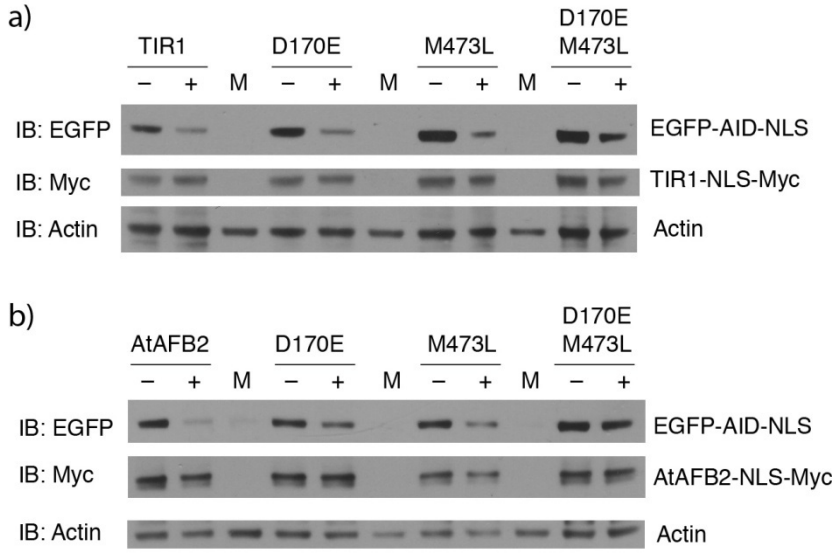

Fig. 3.14: HEK293 cells co-expressing EGFP-AID-NLS and an F-box protein-NLS-Myc were incubated with (+) or without (–) 500 µM IAA for 1 hour. Cell lysates were analyzed by immunoblotting (IB) with the indicated antibodies. M: Mock samples. (**a**) F-box = *Os*TIR1 or its mutants D170E, M473L, or D170E-M473L (**b**) F-Box = *At*AFB2 or its mutants D170E, M473L, or D170E-M473L.

3.3.2.4 Introduction of D170E mutation to *Os*TIR1 enhances the degradation rate

To confirm that the three *Os*TIR1 mutants were functional for auxin-dependent depletion, and interrogate whether enhanced depletion rates might be observed, the kinetics of degradation of AID-GFP-NLS in single HEK293 cells expressing *Os*TIR1 mutants were quantified by the decay of the EGFP signal in time-lapse microscopy (**Fig. 3.15**). In presence of 500 µM IAA, we observed a half-life of 15 ± 1 min with *Os*TIR1^{D170E}-NLS, 25 ± 2 min with *Os*TIR1^{M473L}-NLS, and 30 ± 2 min with

*Os*TIR1$^{D170E-M473L}$-NLS, in contrast to the half-life of 19 ± 2 min reported on section **3.2.2.2** with *Os*TIR1-NLS. Hence, introduction of the D170E mutation accelerated the kinetics of degradation by 20%, ensuring 90% of protein depletion within 45 minutes. Contrastingly, slower depletions are observed with mutations M473L and D170E-M473L.

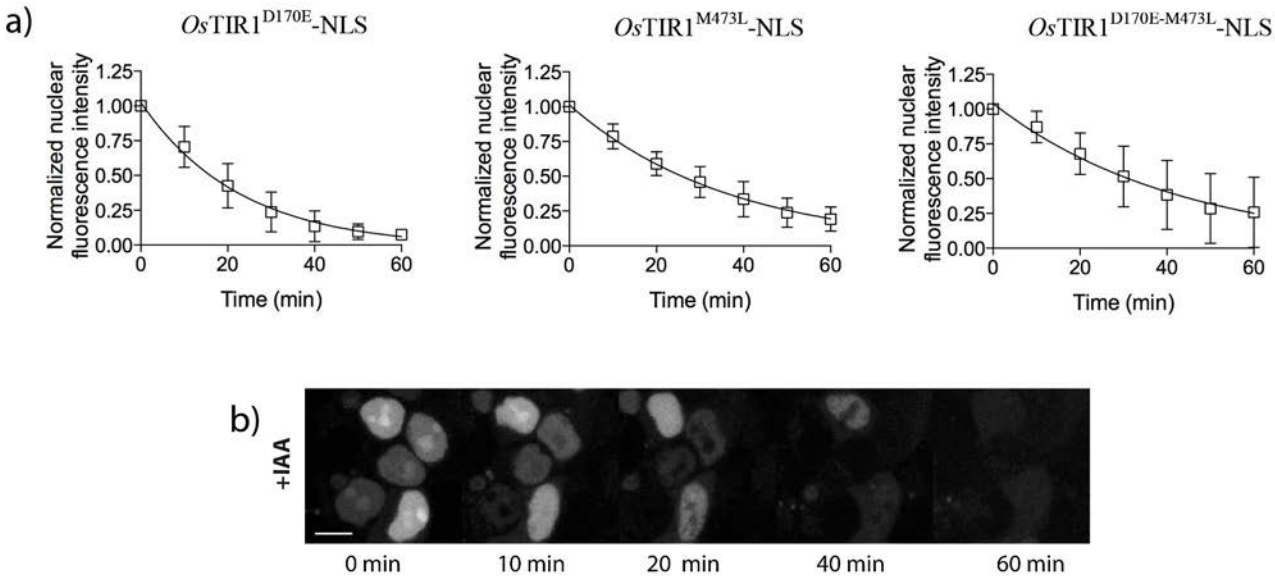

Fig. 3.15: (**a**) The nuclear fluorescence of HEK293 cells co-expressing EGFP-AID-NLS and *Os*TIR1-NLS-Myc mutants D170E, M473L, or D170E-M473L were quantified by confocal microscopy at various times after 500 µM IAA addition (square). Plots show the normalized nuclear fluorescence intensity in function of time (mean ± SD, n = 10). Least squares fits (lines) gave the half-lives of EGFP-AID-NLS. (**b**) Confocal micrographs of representative cells co-expressing EGFP-AID-NLS and *Os*TIR1-NLS-Myc mutant D170E at various times post-IAA addition, in minutes.

In this part, we evaluated the possibility of accelerating the auxin-dependent degradation rates by replacing the F-box protein *Os*TIR1 by homologs (section **3.3.1**), or by mutants (section **3.3.2**). This illustrates the fact that chemical biology approaches enable ever-optimizing strategy with constant shuttling with literature reports. We eventually selected the *Os*TIR1^{D170E}-NLS clone as a degradation platform for further applications described in the next chapters.

3.4 Conclusion

In this chapter, we illustrated an optimization approach for the implementation of Auxin-Inducible Degradation in mammalian cells. Several modifications were proposed to address the slow initial depletion kinetics: this included subcellular addressing of heterologous proteins for optimal colocalization, and introduction of F-box variants for enhanced auxin-induced heterodimerization. Although most of these approaches were not successful, combination of two modifications enhanced two-fold degradation kinetics, as a half-life of the reporter-AID protein of 15 ± 1 min was

observed with *Os*TIR1^{D170E}-NLS-myc, in comparison with 36 ± 3 min in the original system. In the work developed in this chapter, we developed a chemical biology approach in which exogenous modules can be functionally implemented in heterologous model. These modules can be modified by introduction of mutations or protein variants, in an ever-optimizing approach.

Supplement

3.5 Development of the AID methodology for generic application in mammalian cells

3.5.1 Development of a shorter AID tag

3.5.1.1 Motivation

Thus far, we have been reusing the AID sequence originally implemented for the Auxin Inducible Degron methodology by Kanemaki *et al.* (Nishimura, 2009). In this strategy, the AID sequence is the full length *At*Aux/IAA17, a 229 amino-acid and 25 kDa protein[20], a size comparable to EGFP (238 amino-acid). Whether fusion of such protein tags with POI preserves the structure and activity of the POI is an important issue in analyzing cellular responses to perturbation techniques (Snapp, 2010). Therefore, development of shorter protein tags might be useful for a generic method.

3.5.1.2 Identification of essential functionalities in AID and construction of a short degron

As a member of the IAA transcription factor family, *At*Aux/IAA17 is composed of four domains, as explained on **Fig. 3.16.a**; domains I is responsible for the co-transcriptional repression activity, whereas domains III and IV mediates homo and heterodimerization with ARF proteins (Villalobos, 2012). Domain II has been identified as responsible for the interaction with TIR1, through a hexapeptide sequence VGWPPV which binds TIR1 through the interaction with auxin (Tan, 2007). A 17 peptide from domain II is sufficient to bind TIR1 in presence of auxin in immunoprecipitation experiments (Villalobos, 2012). Therefore, we wondered whether deletions introduced in

[20] Which can be fused at the N-ter or the C-ter of the POI (Nishimura, 2009).

*At*Aux/IAA17, preserving domain II sequence, might give functional short AID (shAID) degron.

No crystallographic structure of proteins of the Aux/IAA family had been described by this time (a structure was recently released (Han, 2014)). Using sequence alignments (Blast) between different proteins of the Aux/IAA family and secondary structure prediction software (Baldwin), we identified that domains II and III were separated by an unstructured sequence and postulated that they were functionally independent. We deleted the terminal domains III and IV of *At*Aux/IAA17 to build a short shAID degron (pAG47, *Os*TIR1-9cMyc-IRES-EGFP-shAID-NLS) (**Fig 3.16.b**).

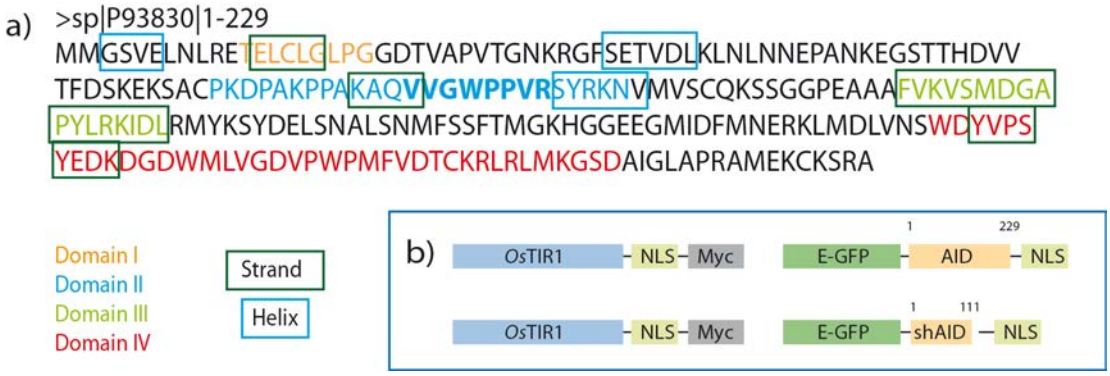

Fig. 3.16: **(a)** Structure of full-length *At*Aux/IAA17 protein with identified domains I to IV, and predicted strand and helix regions. **(b)** Graphical map of the heterologous proteins expressed in pAG47 (bottom) compared to pAG38 (top).

3.5.1.3 The short AID is functional but less efficient than full-length AID

We first assessed that the new construction was functional for auxin-dependent degradation: significant depletion of shAID-GFP-NLS was observed in immunoblotting analysis after incubation with 500 µM IAA for one hour in HEK293 cells expressing *Os*TIR1, although to a lesser extent than full length AID in similar conditions (**Fig. 3.17.a**).

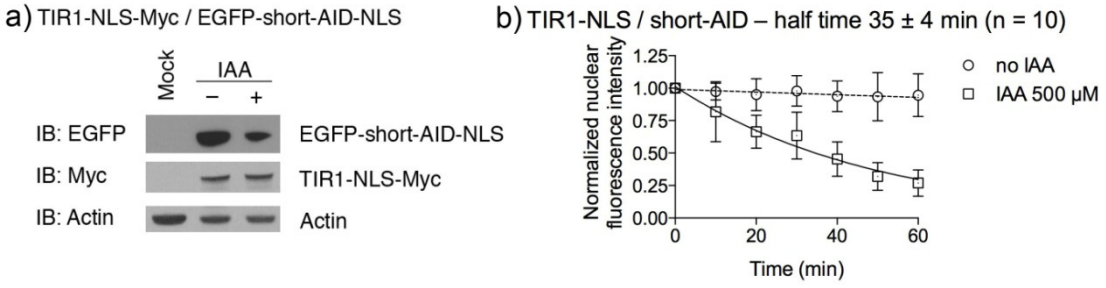

Fig. 3.17: **(a)** HEK293 cells co-expressing EGFP-shAID-NLS and *Os*TIR1-NLS-Myc were incubated with (+) or without (–) 500 µM IAA for 1 hour. Cell lysates were analyzed by immunoblotting (IB) with the indicated antibodies. **(b)** The nuclear fluorescence of HEK293 cells co-expressing EGFP-shAID-NLS and *Os*TIR1-NLS-Myc were quantified by confocal microscopy at various times after 500 µM IAA addition (square). Plots show the normalized nuclear fluorescence intensity in function of time (mean ± SD, n = 10). Least squares fits (lines) gave the half-lives of EGFP-AID-NLS. Control experiments without IAA (circle) are shown.

To confirm that the shAID was functional, the kinetics of degradation of AID-GFP-NLS in single HEK cells expressing *Os*TIR1 were quantified by the decay of the EGFP signal in time-lapse microscopy. In presence of 500 µM IAA, we observed a half-life of 35 ± 4 min (**Fig. 3.17.b**). This slower degradation rate was coherent with immunoblotting experiments.

3.5.1.4 Discussion

These observations confirmed that an auxin-conditional degradation can be obtained with a degron half-shorter than the reported AID sequence (Nishimura, 2009). However, this functionality is associated to a twofold loss in degradation rate. Although this prevents generic implementation to the classical AID methodology, shAID might however provide a degron tool in contexts where POI expression or functionality is sensitive to fusion with large protein tags[21] (Moravska, 2013).

3.5.1.5 Validation in literature

Convergently, a similar strategy to develop a shorter degron was reported in yeast (Havens, 2012). The authors assessed the contributions of residues outside the domain II of Aux/IAA protein to AFB proteins binding, by monitoring the depletion kinetics of Aux/IAA truncations in yeast heterologous systems. As a complex combinatorial properties between AFB proteins and Aux/IAA proteins (19 members in *Arabidopsis*), domain deletion can induce differential kinetic effect, although general trends can be outlined. Contrary to depletion of domain I, deletions of domains III and IV do not lower the depletion rate, and even accelerates it in some case. This study allowed to identify essential residues outside the domain II for auxin-induced degradation, and to engineer a minimal 40 residue degron that can be useful in contexts where full-length AID fusion is an issue. These results where later confirmed by (Yu, 2013). Furthermore, (Villalobos, 2012) measured the auxin-binding affinities of truncated versions of *At*Aux/IAA7 to *At*TIR1: versions containing Domains I and II displayed the same affinity as the WT protein, whereas versions with truncation limited to Domain II had an affinity one order of magnitude lower. However, to our knowledge, no application was reported to this date in mammalian cells.

[21] Under the same transfection conditions, basal EGFP-shAID-NLS expression was significantly higher than basal EGFP-AID-NLS, whereas the F-box adaptor *Os*TIR1 expression is the same in both conditions. This relative shAID overexpression might imply a saturation of the UPS degradation system relying on endogenous ubiquitin Ligase components. Slower degradation rate might be observed, as AID polyubiquitination is a limiting step, Confirming this, (Moravska, 2013) reported that fusion of full-length AID considerably reduced Rad53 protein levels to undetectable levels, whereas higher expression are observed with truncated versions of AID fusion tags. A solution to this issue might be to reduce the overexpression of AID by modifying the strength of the IRES sequence to lower the expression of the shAID-tagged protein; other strategies are discussed in note **B2**.

3.5.2 Use of esterase-sensitive auxin for enhanced permeability

3.5.2.1 Motivation

Due to its anionic carboxylate, the natural auxin IAA is poorly cell permeable at pH 7.4. This feature, which is important for the diffusion model of this phytohormone in plants[22], is a constraint for the AID depletion system which relies on conditional intracellular delivery of auxin, which is limited by the slow membrane diffusion process. Consequently, high external concentrations (500 µM) of auxin are added in the medium for fast depletion, although efficient degradation is observed at slower rates for lower concentrations (up to 5 µM) (see **Fig. 1.4**).

Alternatively, we used a commercial Methyl-ester version of IAA (Me-IAA) (**Fig. 3.18.a**). In *Arabidopsis*, the phytohormone IAA can be converted to Me-IAA by endogenous enzymes as a supplementary level of regulation of auxin patterns (see section **1.4.2.3**) (Yang, 2008). Esterification of carboxylate by methanol is a classical strategy in chemical biology for the intracellular delivery of poorly-permeable molecules. Endogenous esterases in the cytoplasm hydrolyze the esters, liberating the bioactive molecule (Tian, 2012).

3.5.2.2 Me-IAA can trigger AID depletion in mammalian cells

The kinetics of degradation of AID-GFP-NLS in single HEK293 cells expressing *Os*TIR1 were quantified in time-lapse microscopy. Upon addition of 500 µM Me-IAA, a half-life of 17 ± 2 min was observed (**Fig. 3.18.b**), comparable with the depletion kinetics induced by free IAA. This validated that Me-IAA could efficiently trigger AID depletion.

We investigated whether Me-IAA could be more efficient than free IAA at lower concentrations. We monitored the depletion of AID-GFP-NLS by immunoblotting in HEK293 cells expressing *Os*TIR1-NLS after one hour incubation with IAA or Me-IAA at various concentrations. Indeed, Me-IAA seems to be associated with a higher depletion than IAA at lower concentrations (**Fig. 3.20.c/d**).

[22] Neutral IAAH possesses a permeability of 4.10^{-3} cm.s$^{-1,}$ six orders of magnitude higher than the charged carboxylate IAA^-. This discrepancy can explain the differential diffusion of protonated auxins across plant plasma membrane, from the cell wall (pH < 5) into the cytoplasm (pH > 7), where it is deprotonated. Charged IAA^- efflux are highly regulated by permeases such as PIN and AUX1, whose highly regulated differential spatial distribution segregate auxin patterns. (Teale, 2006) This process allows diffusion of auxin through cells as fast as 15 mm/h (DeRybel, 2009).

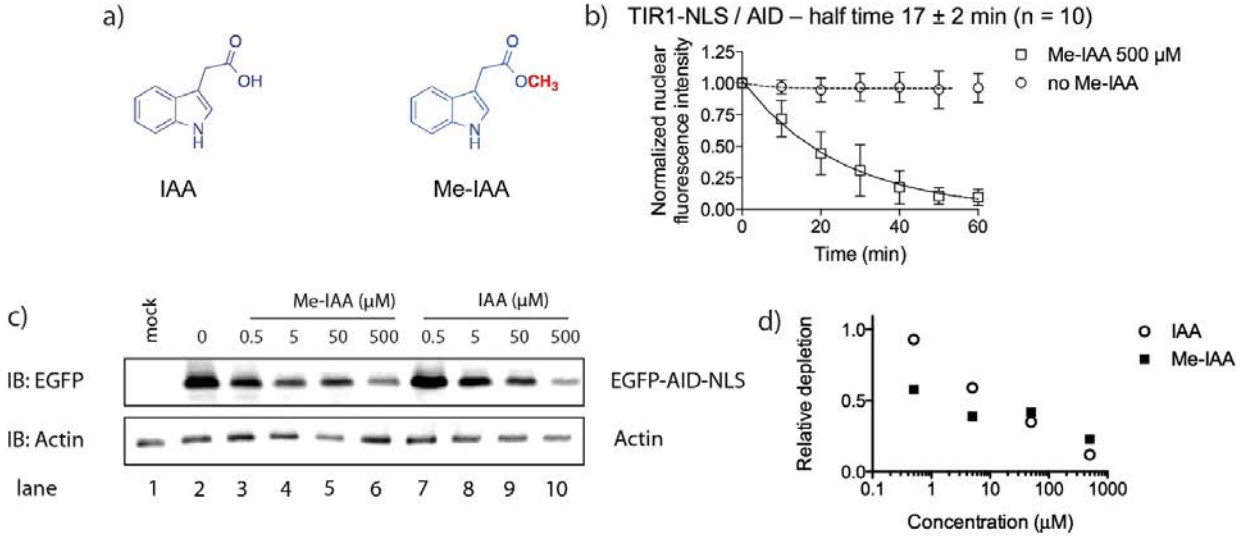

Fig. 3.18: **(a)** Structure of IAA and Me-IAA **(b)** The nuclear fluorescence of HEK293 cells co-expressing EGFP-AID-NLS and *Os*TIR1-Myc were quantified by confocal microscopy at various times after 500 µM Me-IAA addition (square). Plots show the normalized nuclear fluorescence intensity in function of time (mean ± SD, n = 10). Least squares fits (lines) gave the half-lives of EGFP-AID-NLS. Control experiments without IAA (circle) are shown. **(c)** HEK293 cells co-expressing EGFP-AID-NLS and *Os*TIR1-Myc were incubated with (+) or without (–) 500 µM MeIAA for 1 hour. Cell lysates were analyzed by immunoblotting (IB) with the indicated antibodies. **(d)** Quantification with non-incubated sample (**0,** lane 2) as reference.

We thus approved that intracellular delivery could be enhanced kinetically by methyl-esterification; however, we did not interrogate the differential kinetics at low concentrations. Auxin ester derivatives might provide an interesting tool in contexts where cells are sensitive to high amount of external metabolites, or for deep penetration of auxin in multicellular layers, such as in tissue or a small animal.

3.5.3 Development of cytoplasmic AID depletion is hindered by the nuclear localization of AID

The AID methodology, as described in (Nishimura, 2009) is *a priori* generic to any POI and applicable to various cellular contexts. In particular, degradation of cytoplasmic POI is highly desirable, as many essential regulation processes take place in this compartment. Two examples of conditional AID depletion of cytoplasmic POI were reported since in mammalian cells ((Holland, 2012), see **table 1.2**). In this section, we will discuss whether we can implement cytoplasmic AID depletion with an AID-tagged fluorescent reporter.

3.5.3.1 Heterologous AID-EGFP fusions are adressed to the nucleus in HEK293 cells

In a first attempt to implement cytoplasmic auxin-dependent degradation, we removed the NLS sequence present at the C-ter of AID protein of all our precedent constructions. We fused the complete AID sequence N-terminally to a mCherry red fluorescent reporter protein under the dependence of a CMV promoter (pAG36, CMV-mCherry-AID). However, HEK293 cells transiently transfected with pAG36 displayed a strong nuclear fluorescence, indicating that endogenous nuclear addressing sequences were present in mCherry-AID (**Fig. 3.19**).

3.5.3.2 Endogenous NLS sequences are present in AID

The AID degron corresponds to the complete sequence of *At*Aux/IAA17, which is a nuclear transcriptional repressor in its native plant context. A bipartite NLS, localized between domain I and II, has been identified in *Os* and *At*Aux/IAA17 (Jain, 2006). As nuclear addressing can vary between plant and mammalian cells, we analyzed whether the heterologous AID sequence contained specific addressing signals in mammalian cells. Strong NLS sequences were predicted (cNLS mapper) between domains I and II, and in domain IV. Together, these features can explain the identical nuclear addressing of AID and AID-NLS fused to reporter fluorescent proteins.

Fig. 3.19: **(a)** AID sequence (*At*Aux/IAA17), highlighting NLS sequences described in functional context in plants and predicted in mammalian cells **(b)** HEK293 cells expressing heterologous EGFP-AID-NLS or mCherry-AID imaged in confocal microscopy.

The strength of the endogenous NLS is a limitation to the genericity of the AID methodology applied to non-nuclear POI[23]. Alternatively, we embraced the reported examples of AID-tagged cytoplasmic POI that we will describe on chapter **6**.

[23] It was reported that intracellular context might affect the depletion efficiency in methodologies based on small-molecule conditional stabilization ((Sellmyer, 2012), see section **1.2.2.2**).

Chapter 4

Design of photo-activatable auxins

*The work reported in part **4.2.3** was realized in collaboration with Dr Isabelle Aujard (permanent researcher in our group), wheras the work reported in parts **4.2.4**, **4.3.1** and **4.3.2** was realized in collaboration with Chenge Li (master student in our group).*

4.1 Introduction: structural analysis of auxin perception by TIR1 enables the rational design of caged auxins

4.1.1 Auxin perception in plants

In 2007, a molecular mechanism for auxin perception by TIR1 was proposed, as a crystallographic structure of a ternary *At*TIR1**:IAA:**Aux/IAA7 was published (Tan, 2007) (section **1.4.1.2**). TIR1 has a mushroom-shape with LRR domains responsible for auxin perception and Aux/IAA7 substrate recruitment. At the top surface of TIR1, a pocket contains a promiscuous hydrophobic binding site able to accommodate planar structures such as the Indole-ring of natural auxin IAA[24] (**Fig. 4.1.a**).

Benzene region of indole ring interacts with two-hydrophobic residues in TIR1 (Phe79 and Phe82), whereas the carboxylic group of IAA binds to Arg403 and Ser 438 residues[25] (**Fig. 4.1.b**). Insertion of auxin docks the hydrophobic pocket, allowing the insertion of the coiled IAA7 peptide on the upper part of the pocket, through a short hydrophobic domain II WPPV motif. The aromatic ring of

[24] An inositol 1,2,3,4,5,6-hexakisphosphate (InsP6) cofactor is also bound at the core of TIR1.

[25] Synthetic auxins 1-NAA and 2,4-D also bind TIR1 through their common carboxyl group although their hydrophobic ring structures are different (but mimic the indole ring binding to the TIR1 hydrophobic cavity).

IAA displays hydrophobic interactions with the close tryptophan and second proline residues in Aux/IAA7 on one side, with Phe82 in TIR1 on the other side (**Fig. 4.1.c**). Aux/IAA thus forms a co-receptor with TIR1, with auxin acting as"molecular glue", enhancing hydrophobic interactions (**Fig. 4.1**). Neither binding of auxin or of IAA7 peptide affects however the structure of the TIR1-LRR domain. Rational design based on the crystal structure led to the development of specific auxin antagonists[26].

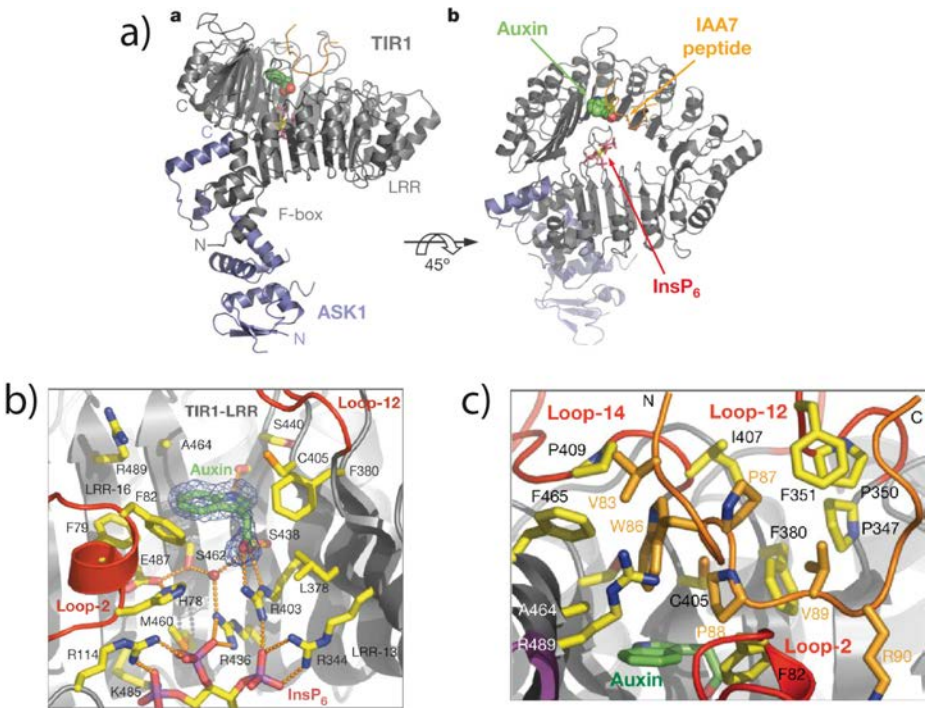

Fig. 4.1: Crystal structure of TIR1:IAA:Aux/IAA7 (Tan, 2007). **(a)** Overall structure of the TIR1 complex with auxin and degron IAA7 peptide **(b)** detail zoom on the hydrophobic pocket in TIR1 binding IAA. The auxin molecule (IAA) is shown as a green stick model. The TIR1 residues surrounding auxin and right underneath the auxin-binding site are shown as a yellow stick model. Essential residues Phe82, Arg403 and Ser438 are displayed. (**c**) A close-up side view of the central GWPPV motif in the IAA7 peptide upon binding to TIR1. Interacting residues of the substrate peptide and TIR1 are shown as orange and yellow stick models, respectively. Auxin is shown as a green stick model.

[26] The first reported works led to the development of specific α –alkyl substituted auxin antagonists which insert the binding site of TIR1, perturbing Aux/IAA interaction due to steric hindrance with Pro residues in Aux/IAA (Hayashi, 2008). Further development based on *in silico* screening led to the development of auxinole-based-antagonists. Phenyl ring of stack with Phe82, enhancing the affinity of IAA-antagonists (Hayashi, 2012).

4.1.2 Caged auxins in plants

Caged auxin methodologies were reported for single cell studies in plants[27] (Kosuka, 2009). The carboxylic group common to three different auxins Indole Acetic Acid (IAA), Naphtalene Acetic Acid (NAA) and 2,4 Dichlorophenoxyacetic (2,4-D) were esterified with *ortho*-nitrobenzyl (NB) alcohol caging group (classically used in mammalian cells) (**Fig. 4.2**). *In vitro*, these caged auxins were stable in the dark, and efficiently released upon UV light illumination, as assessed by HPLC. However, *in vivo* studies indicated that the caged auxins were biologically unstable in the dark.

Endogenous plant serine esterases were suspected to be responsible of this background release in the dark. Consequently, the authors developed esterase-insensitive auxins by addition of bulky-groups phenyl derivatives to NB caging groups, in order to block access to catalytic serine residues in esterase active sites. This resulted in a global enhanced stability in dark conditions, without affecting the photo-liberation kinetics[28]. In particular, 2,4 dimethoxyphenyl-2-nitrobenzyl (DMPNB) caged auxin were stable in the dark, but short (2s) UV light pulses allowed manipulation of auxin levels in single cells (uncaging quantum yield Φ= 0.04). This caged molecule was later used in another study to probe the complex interaction of auxin with the actin cytoskeleton (Maisch, 2009).

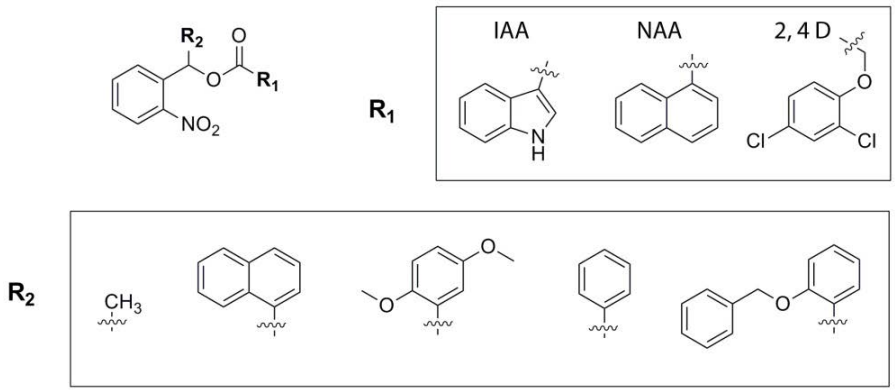

Fig. 4.2: Caged auxins developed by (Kosuka, 2009).

Based on these studies, we identified the carboxylic group as a potential target for protection; addition of a large caging group must hinder the carboxylic group involved in the interaction with TIR1, therefore preventing the auxin-dependent interaction of TIR1/AID in heterologous systems.

[27] Auxin control many physiological processes in plants, such as cell division, elongation or differentiation. As local gradients of auxin form complex and yet not fully understood patterns, plants biologists were interested in the fast release of auxin in high spatiotemporal control offered by caging approach (DeRybel, 2009). Free auxin is often quantified using a reporter gene under the control of an auxin-dependent promoter in Arabidopsis (Kosuka, 2009).

[28] However, diminution of solubility by introduction of hydrophobic groups could be an issue.

4.2 Development of carboxylate-conjugated DMNB caged auxin

4.2.1 First-generation

4.2.1.1 Motivation

The 2-nitrobenzyl caging group used for auxin protection in (Kusaka, 2009) is efficiently cleaved at 280-300 nm, a toxic wavelength range for mammalian cells. Alternatively, we chose the 4,5-dimethoxy-2-nitrobenzyl (DMNB) as a caging platform which is widespread for biological studies[29]. This group is known to be efficiently cleaved upon illumination within the 350-400 nm range. Moreover, caged DMNB-molecules were reported to be stable in the dark in mammalian cells (Ouyang, 2010). We thus proposed to synthesize DMNB-caged auxins NAA and IAA.

4.2.1.2 Synthesis

The caged auxin DMNB-NAA **1N** and DMNB-IAA **1I** were obtained with 92% yield (resp. 40%) by coupling NAA (resp. IAA) with (4.5-dimethoxy-2-nitrophenyl) methanol in presence of dicyclohexylcarbodiimide (DCC) and dimethylaminopyridine (DMAP) (Steglich esterification) in dichloromethane at room temperature overnight (**Fig. 4.3**).

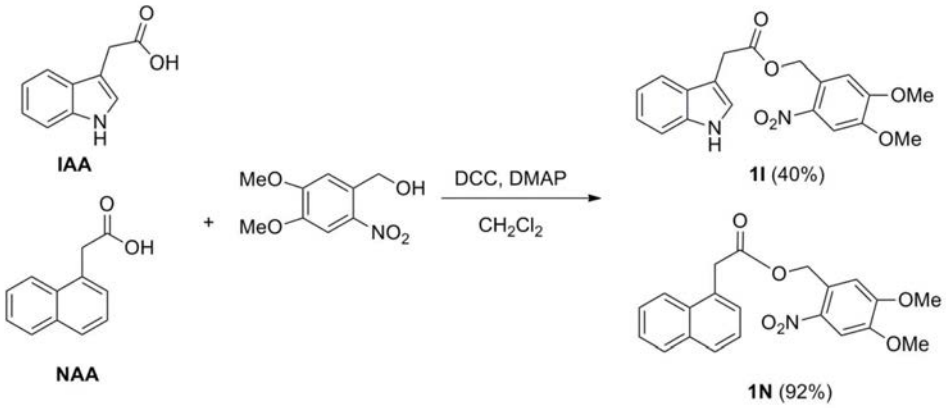

Fig. 4.3: Synthetic scheme of **1N** and **1I.**

4.2.1.3 Photochemical characteristics

UV spectra of the caged molecules exhibit a large band at 365 nm, characteristic of the DMNB caging group (**Fig. 4.4.a**). Interestingly, while both free NAA and IAA are fluorescent (with resp. max. emission at 324 and 354 nm), this was not the case for their DMNB-caged analogs, hypothetically due to intramolecular quenching introduced by the caging group. This property was

[29] This caging platform had been previously used and further developed in our laboratory (see section **2.2.1.2**).

used to characterize the uncaging of **1N** (resp. **1I**) by following the extent of NAA (resp. IAA) release upon UV illumination [30] in fluorometry at its maximum emission wavelength. The corresponding results are displayed for **1N** in **Fig. 4.4.a**. The quantum yields of photolysis for **1I** and **1N** were evaluated to resp. 5.9×10^{-4} and 5.6×10^{-4}**.**

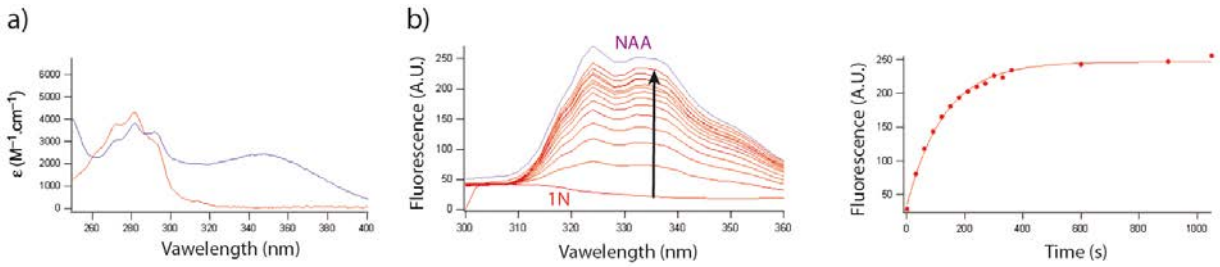

Fig. 4.4: **(a)** Absorption spectrum of **1N** (violet) and NAA (red); Temperature: 20°C, Solvent water/acetonitrile 1:1 (v:v)**. (b)** Fluorescence emission spectrum of **1N** (red) (excitation 280 nm) after various duration of 365 nm illumination compared to NAA (violet) at 10 µM concentration in solvent water/acetonitrile 1:1 (v:v), Temperature: 20°C**. (c)** Quantification of fluorescence emission at 339 nm at various times under 365 nm illumination (excitation 280 nm).

4.2.1.4 *In vivo* stability

We next evaluated whether caged auxin **1N** and **1I** were stable in mammalian cells in the dark, which is an essential parameter for physiological studies as background release would liberate constitutively the active compound. The stability of the caged auxin candidates in the dark was evaluated indirectly by monitoring the depletion extent of EGFP-AID-NLS in CHO cells expressing *Os*TIR1-myc incubated with various concentrations of **1N** or **1I. Fig.4.5** displays the results for both caged auxins **1I** and **1N** and their respective free auxin equivalent IAA and NAA. Liberation of free auxin by hydrolysis would trigger interaction of *Os*TIR1-myc and EGFP-AID-NLS, leading to the polyubiquitination of EGFP-AID-NLS and its subsequent proteasomal degradation.

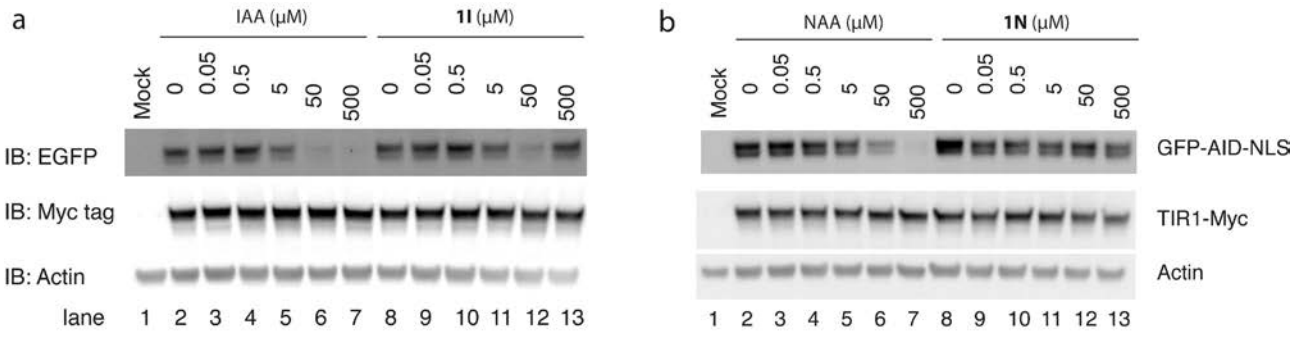

Fig 4.5: Mammalian cells co-expressing EGFP-AID-NLS and *Os*TIR1-myc were incubated with **(a) 1I** and its free auxin equivalent IAA, or **(b) 1N** and its free auxin equivalent NAA at various dilutions and incubated in the dark for 1 h. Cell lysates were analyzed by immunoblotting (IB) with indicated antibodies.

[30]The UV illumination power was evaluated by monitoring nitrone photoconversion (protocol section **10**).

We observed a depletion of the EGFP-AID-NLS protein level (monitored by the EGFP epitope) in presence of the caged molecules in the dark, even at low concentrations, compared to the standard level incubated with DMSO. We concluded that the candidates **1N** and **1I** were not stable *in vivo.*

4.2.2 Discussion

DMNB-caged auxin incubation leads to a background degradation activation, indicating that these caged molecules are not stable *in vivo.* Although esters-based caging groups are often less stable than amides or carbamates (Carrie, 2005), these results are contrasting with the relative stability of reported DMNB-conjugated examples in mammalian cells. For example, Abscissic acid conjugated to simple DMNB group by its carboxylic group was reported to be stable at 10 μM in HEK293 cells (Wright, 2015).

One can therefore hypothesize that the self-hydrolysis of the caged ester is due to enzymatic recognition of auxin-based moiety rather than the caging group, unlike methyl- or ethyl- derived esters recognized by specific esterases *in vivo* (Tian, 2012). Although IAA esterases are present in plants, we did not find equivalents in mammalian cells (BLAST). However, an interesting candidate is the pancreatic enzyme chymotrypsin, which hydrolyses terminal aromatic residues in peptides. It was reported that chymotrypsin processes aromatic carboxyl esters (Sawyer, 1975) [31].

4.2.3 Second generation

4.2.3.1 Synthesis

In order to address the background activation of DMNB-auxins in the dark and enhance the stability of the caged auxin *in vivo*, we developed a bulky version of DMNB (or equivalent 4, 5- methylene-dioxy-2-nitrophenyl), by incorporating Methyl or Tribromomethyl substituents on the connecting carbon atom (see (Klan, 2014) for a recent review). These substitutions have been previously described to be efficiently cleaved upon illumination *in vivo* (resp. (Allan, 1998) and (Aujard, 2006)). Addition of the bulky groups might hinder the ester from active site of endogenous esterases. These bulky DMNB groups were conjugated to IAA by Steglich esterification (*vide* **4.2.1.2**).

[31] Although this enzyme is not expressed in HEK293 cells (Human Protein Atlas), others enzymes present chymotrypsin-like activity, such as cathepsin in the lysosome or proteasome subunit β-type 5 in cytosol and nucleus. Proteasomal chymotrypsin-like activity enabled the development of ester-based inhibitors (Kuhn, 2004). As proteasome particles are highly present in HEK 293 cells, a possible explanation for the background hydrolysis of DMNB-IAA might be the low-affinity degradation by inner-core proteasome particles.

Resulting caged auxins candidates **2I** and **3I** are displayed on **Fig. 4.6** with their synthetic yield.

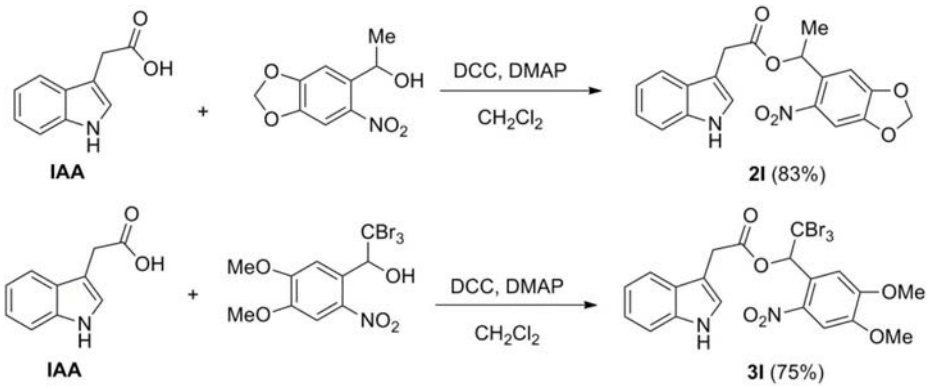

Fig. 4.6: Synthetic scheme of **2I** and **3I.**

4.2.3.2 Stability

As in *vivo* stability was a determinant specification for the development of caged auxins in section **4.2.1.4**, we first evaluated the stability of the caged candidates *in vivo* in the dark prior further photophysical analysis. The depletion extent of EGFP-AID-NLS was monitored in HEK293 cells expressing *Os*TIR1-myc incubated with **2I** and **3I** at a concentration of 50 µM (duplicate experiments). Cells incubated with **2I** displayed significant EGFP depletion, although less than cells incubated with **1I** or free-auxin IAA at the same concentration. Cells incubated with **3I** showed depletion at a lesser extent (**Fig. 4.7**). We hypothesized that the large tribromomethyl group present in **3a** hindered background hydrolysis by endogenous esterases. We chose to continue this strategy by addition of larger bulky groups.

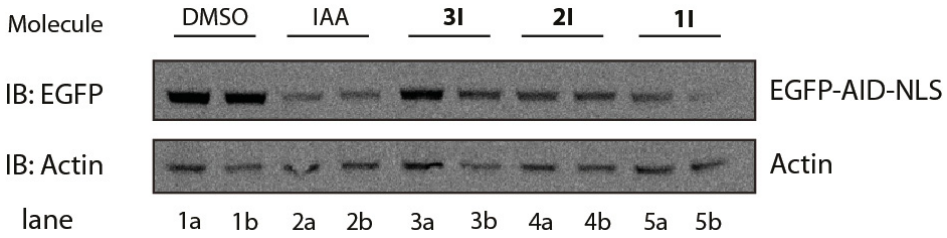

Fig. 4.7: HEK293 cells co-expressing EGFP-AID-NLS and *Os*TIR1-myc were incubated with candidate caged auxins **1I**, **2I** and **3I** at 50 µM and incubated in the dark for 1 h. Negative and positive controls (cells incubated with resp. **DMSO** or **IAA** at 50 µM) are displayed. Cell lysates were analyzed by immunoblotting (IB) with indicated antibodies.

4.2.4 Third generation

4.2.4.1 Synthesis

We developed bulky versions of the DMNB by incorporating an extra 2, 5-dimethoxyphenyl group on the connecting carbon atom. 4,5-dimethoxy-2-nitrobenzaldehyde was reacted with the commercial 2,5-dimethoxy-phenyl (DMP) Grignard reagent in THF at –15°C for 30 minutes to yield the alcohol with 82% yield. This bulky PNB-OH group was conjugated to IAA and NAA by Steglich esterification (*vide* section **4.2.1.2**) (**Fig. 4.8**). Resulting caged auxins candidates **4I** to **4N** were obtained with respectively 89 % and 85 % yield.

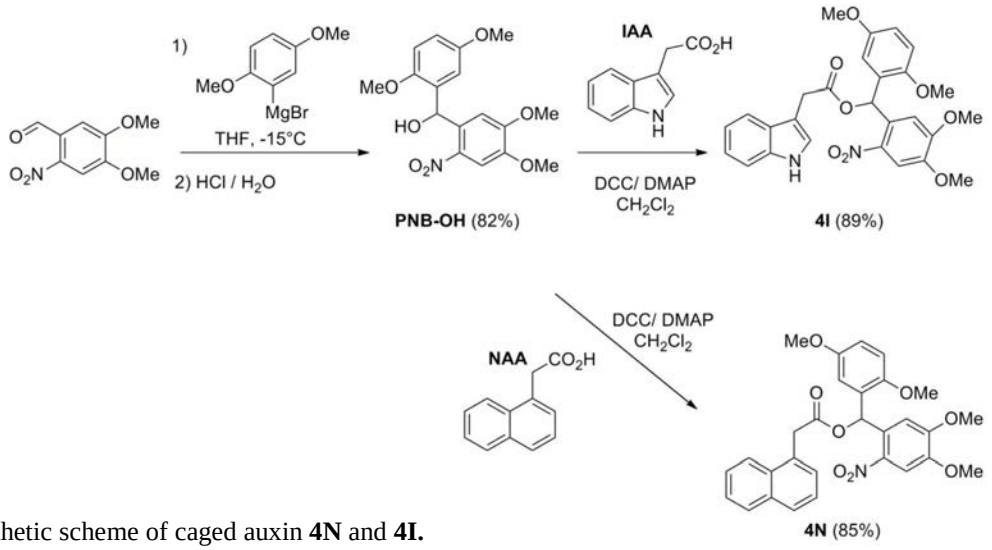

Fig. 4.8: Synthetic scheme of caged auxin **4N** and **4I.**

4.2.4.2 Photochemical characterization

4I and **4N** displayed the expected absorption properties (**Fig. 4.9**). As characterized by HPLC titration, both **4I** and **4N** were stable in the dark in aqueous media. Moreover, both **4I** and **4N** were quantitatively photocleaved at 350 nm with respective uncaging quantum yield $\Phi = 0.012$ and $\Phi = 0.007$ (**Fig. 4.10**). These values are in accordance with previous reports on similar light-removable protecting groups (Aujard, 2006).

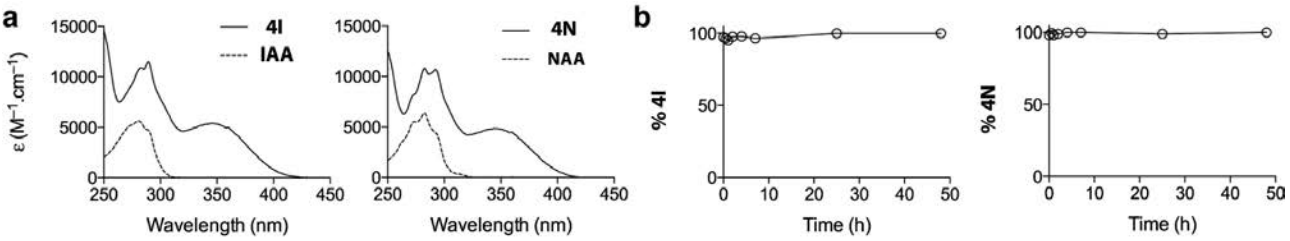

Fig. 4.9: (**a**) Absorption spectra of **4I** (solid line) and **IAA** (dashed line). Absorption spectra of **4N** (solid line) and **NAA** (dashed line). Temperature: 20°C, solvent: acetonitrile/ 20 mM Tris buffer 1:1 (pH 7.5). (**b**) Stability of **4I** (a) and **4N** (b) in aqueous media in darkness. Solutions (25 µM) were kept in the dark for various times: plots show the percentage of caged auxin (determined by HPLC) in function of time. Solvent: 20 mM Tris pH 7.5 / acetonitrile 1:1 (v:v).

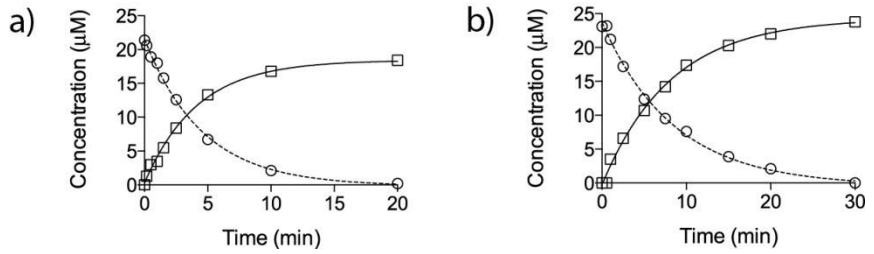

Fig. 4.10: Auxin release upon photolysis of photoactivatable auxins. **(a)** Photolysis of **4I**. Solutions of **4I** (400 µL at 21 µM) were illuminated at 350 nm (light intensity ~ 10^{-8} Ein.s^{-1}, pathlength of the light beam 1 cm). Plots show the concentrations of **4I** (circle) and IAA (square) in function of time. **(b)** Photolysis of **4N**. Solutions of **4N** (400 µL at 25 µM) were illuminated at 350 nm (light intensity ~ 10^{-8} Ein.s^{-1}, pathlength of the light beam 1 cm). Plots show the concentrations of **4N** (circle) and NAA (square) in function of time.

4.2.4.3 In vivo stability

The depletion of EGFP-AID-NLS was monitored in HEK293 cells expressing *Os*TIR1-myc. No significant EGFP depletion was observed upon incubation of **4I** and **4N** up to 200 µM concentration.

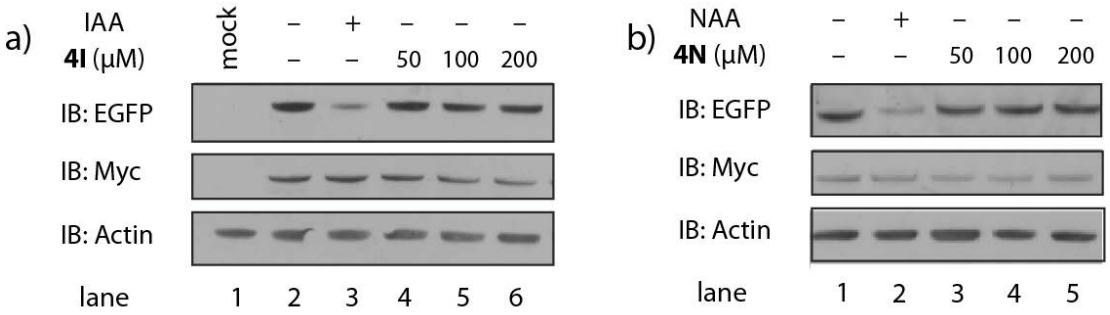

Fig. 4.11: HEK293 cells co-expressing EGFP-AID-NLS and *Os*TIR1-myc-NLS were incubated with **4I (a)** and **4N (b)** at various dilutions and incubated in the dark for 1 h. Positive control displays cells incubated with 500 µM of corresponding auxin. Cell lysates were analyzed by immunoblotting (IB) with indicated antibodies.

However, **4N** was poorly soluble in water. This feature might prevent the efficient intracellular delivery of **4N**. Therefore, **4N** was not further characterized in cells.

4.2.5 Conclusion

Eventually, our approach allowed us to select a caged auxin candidate **4I** that meet the specifications mentioned in section **2.2.2**. First candidate caged molecules **1I** and **1N** were not stable *in vivo* (section **4.2.1.4**). We addressed this issue by a strategy designed to hinder the DMNB caging group from endogenous esterases, by addition of substituent groups. As a general trend, caged auxins were more stabilized with the addition of bulkier substituents (section **4.2.3.2**). However, a limit to the addition of large substituent is that it can lower the solubility, as in the case of **4N** (section **4.2.4.3**). Eventually, **4I** appears a potential candidate for photo-activation of IAA, as

it is stable in the dark *in vitro* and *in vivo*, and is efficiently cleaved by UV illumination with reasonable action cross-section efficiency. However, we investigated whether use of other caging groups might allow the development of caged auxins with enhanced photochemical properties.

4.3-Alternative strategies for the development of caged auxins

4.3.1 Coumarin-based caging groups

As an alternative strategy we proposed to conjugate the carboxylic group of IAA with a [(7-(diethylamino)-coumarin-4-yl]-methyl (DEACM) caging group, which is known to be efficiently cleaved upon illumination within the 350-400 nm range (Fournier, 2013).

Based on the instability of DMNB caged auxin reported on section **4.2.1**, we chose at first to develop bulky version of DCEAM by incorporating an extra 2,5-dimethoxyphenyl group on the connecting carbon atom, to hinder the ester function from endogenous esterases. We called the resulting caging group **PCM** (2,5-dimethoxyphenyl-7-diethylamino-coumarin-4-methyl). 7-(diethylamino)-2-oxo-2H-chromene-4-carbaldehyde was reacted with the commercial 2,5-dimethoxyphenyl Grignard reagent in THF at –15°C for 2 hours and then reacted at room temperature overnight to yield the alcohol PCM-OH with 66% yield. The caged auxin **5I** was obtained with 96% yield by coupling IAA with PCM-OH in presence of DCC and DMAP (section **4.2.1.2**) in dichloromethane at room temperature overnight (**Fig. 4.12**).

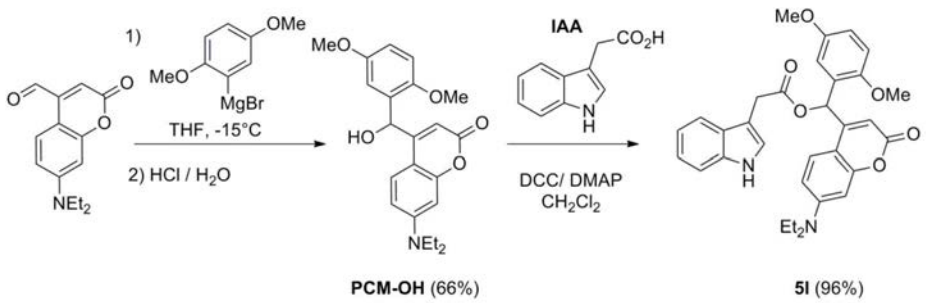

Fig. 4.12: Synthetic scheme of caged auxin **5I.**

5I displayed the expected absorption properties (**Fig. 4.13.a**) and was stable in the dark (**Fig. 4.13.b)**. The stability in aqueous media in darkness and uncaging upon light illumination of **5I** were characterized by HPLC titration. The photolysis reaction displayed first-order kinetics. **5I** was photocleaved faster than **4I** with a quantum yield of ~ 0.03 and a corresponding action cross-section

of ~ 100 $m^2.mol^{-1}$. This 10-fold increase in photolysis action cross-section results from the convolution of a higher quantum yield of photolysis and a larger cross-section of absorption.

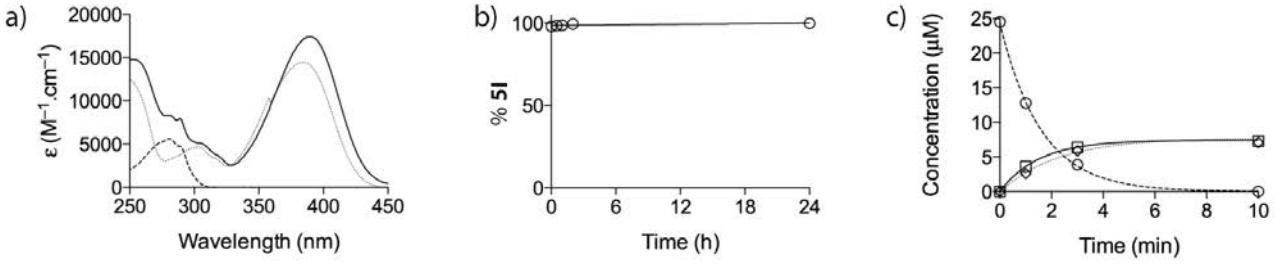

Fig. 4.13: (**a**) Absorption spectra of **5I** (solid line), IAA (dashed line) and **PCM**-OH (dotted line). Temperature: 20°C, solvent: acetonitrile/ 20 mM Tris buffer 1:1 (v:v) (pH 7.5). (**b**) Stability of **5I** in aqueous media in darkness. Solutions (25 µM) were kept in the dark for various times: plots show the percentage of caged auxin (determined by HPLC) in function of time. Solvent: 20 mM Tris pH 7.5 / Acetonitrile 1:1 (v:v). (**c**) Photolysis of **5I**. Solutions of **5I** (400 µL at 25 µM) were illuminated at 390 nm (photon rate 4 $nmol.s^{-1}$, pathlength of the light beam 1 cm). Plots show the concentrations of **5I** (circle), IAA (square) and **PCM**-OH (diamond) in function of time. Temperature: 20°C, solvent: acetonitrile/ Tris buffer 1:1 (v:v) (pH 7.5).

Although quantitative **5I** degradation was observed upon 390 nm illumination, only about 30 % IAA was released (**Fig. 4.13.c**). A likely explanation to this partial release is the competitive formation of an unreactive side-product through a rearrangement reaction. As such side-reaction could prevent reliable photorelease of IAA in cells; we abandoned this strategy which did not allow quantitative photolysis, an important specification for caged auxin development.

4.3.2 NH-protection strategy

4.3.2.1 Motivation

Alternatively, we proposed to cage other positions than the carboxylic acid in auxins. As we hypothesized that the *in vivo* instability of caged auxins **1X** to **3X (X = I** or **N)** resulted from hydrolysis of the ester linkage by endogenous esterases (section **4.2.3.2**), we expected that caging other positions with non-ester linkage might enhance the *in vivo* stability.

An important specification is that the introduction of the caging group prevents interaction with TIR1 (see section **4.1.1**). The NH Indole ground in IAA displays an important interaction with the amide group of Leu439 in TIR1 (Tan, 2007). This was further proved by development of auxin-antagonists (see note **B.25**), in which N-alkylation of IAA dramatically reduced affinity to TIR1. Thus, we next evaluated strategies to cage the NH group of IAA with an N-caging group.

4.3.2.2 Model for reactivity

We chose to evaluate the experimental parameters for conjugation of the NH group using a simple model reaction: IAA was activated upon deprotonation with a base and subsequent alkylation with a halide derivative (1-bromopropane) (**Fig. 4.14**). Different bases and solvents were tested. IAA reaction with 1-bromopropane in anhydrous dimethylformamide (DMF) with sodium hydride (NaH) leads to two by-products (O-alkylated IAA and N,O-dialkylated IAA), but not to the expected N-alkylated IAA (**Na-I**)). Reactions performed in THF solvent rather than DMF do not work, likely due to solubility issues. To prevent activation of the carboxylic group of IAA by NaH, we used a methyl ester derivative (MeIAA). MeIAA in the same conditions led to the expected N-alkylated MeIAA (**Na-MeI**) and two by-products (N, O-dialkylated IAA **BP-1** and O-alkylated IAA **BP-2**) resulting from trans-esterification.

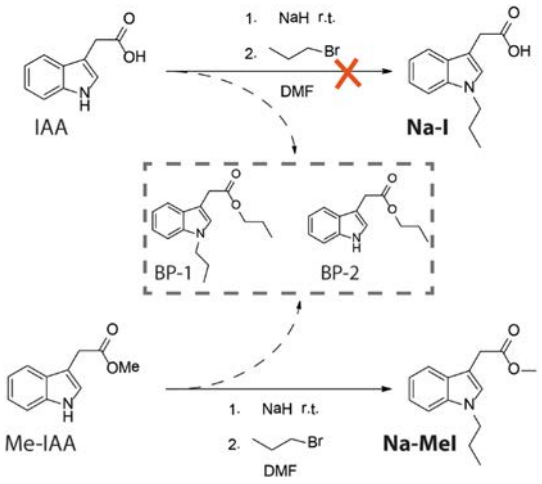

	reactant	base	solvent	products
1	MeIAA	NaH	THF	
2	MeIAA	NaH	DMF	**Na-MeI**, BP-1, BP-2
3	IAA	NaH	DMF	BP-1, BP-2
4	MeIAA	BuLi	THF	

Fig. 4.14: Exploration of the experimental condition for IAA/Me-IAA N-conjugation with a model alkylating reaction.

This preliminary study indicated that the synthetic condition **4** might enable the caging of MeIAA. Eventually, caged methyl IAA could either be processed by ester hydrolysis to obtain the N-caged IAA, or incubated directly in cells. In section **3.4.2**, we showed that Me-IAA mediated AID-degradation in HEK293 cells with rate similar rate to IAA, indicating that it is efficiently cleaved by endogenous esterases.

4.3.3 NH-protection with DMNB

4.3.3.1 Synthesis

We first assessed the possibility to use DMNB as a protecting group of the NH group in Me-IAA.

To synthesize DMNB-N-caged Me-IAA (**6-MeI**), 1-(bromomethyl) -4,5-dimethoxy-2-nitrobenzene in DMF was reacted with MeIAA deprotonated with NaH to yield the DMNP-MeIAA with only 10% yield (**Fig. 4.15**). The major product was the product of the trans-esterification (56%).

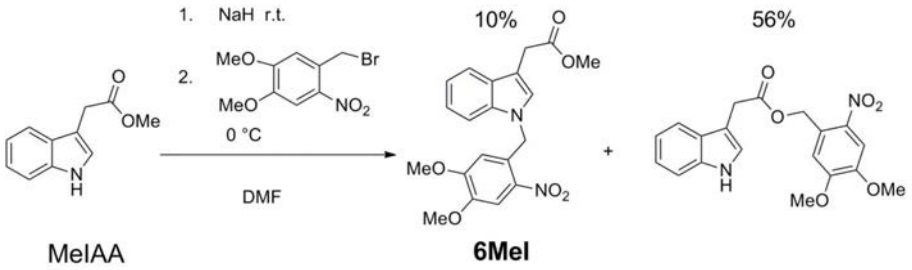

Fig. 4.15: Synthetic scheme of caged auxin **6MeI**.

4.3.3.2 Photochemical evaluation

Light illumination of **6MeI** led to its fast disappearance with first-order kinetics. However, accumulation of intermediate molecule and slow release of Me-IAA were observed in HPLC (data not shown). A thermally-driven step within the uncaging process is likely rate-limiting. This slow release of auxin prevents further use of this caged compound for cellular photoactivation.

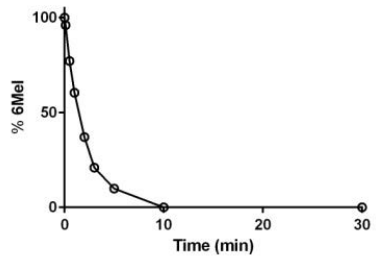

Fig. 4.15: Photolysis of **6MeI**. Solutions of DMNB-MeIAA (400 µL at 25 µM) were illuminated at 350 nm (light intensity ~ 2×10^{-8} Ein.s^{-1}, pathlength of the light beam 1 cm). Plots show the relative concentrations of **6MeI** in function of time.

4.4 Conclusion

In this part, we described the synthesis and characterization of caged auxin candidates to identify a potential photo-activatable auxin that meets reasonably the specifications listed on section **2.2.2**. Based on a described structure of auxin interaction with receptor TIR1, we proposed that the carboxylic group common to natural auxin IAA or synthetic auxin NAA could be targeted for inactivation by conjugation with a caging group.

DMNB-ester caged auxins were sensitive to hydrolysis *in vivo*, leading to background activation in the dark. This issue was addressed by introduction of bulky-substituted caging groups, which led to the identification of caged auxin **4I** as a potent candidate. Alternative strategies lead to the development of caged auxin candidates **5I** and **6MeI** that did not allow efficient photorelease.

	λ_{max} (nm)	k_1 (min^{-1})	k_2 (min^{-1})	I_0 ($Ein.s^{-1}$)	$\sigma\phi$ ($m^2.mol^{-1}$)	ε ($M^{-1}.cm^{-1}$)	σ ($m^2.mol^{-1}$)	ϕ
4I	350	0.22	0.23	1.1×10^{-8}	14	5160	1187	0.012
4N	350	0.12	0.12	9.7×10^{-9}	8	5080	1168	0.007
5I	390	0.65	0.70	3.9×10^{-9}	116	17420	4007	0.029
6MeI	350	0.51	-----	1.8×10^{-8}	------	4420	1017	------

Table 4.2. Photolysis parameters of the photoactivatable auxins. The wavelength λ_{max} of maximal absorption, the kinetic constant of caged auxin disappearance k_1, the kinetic constant of auxin appearance k_2, the light intensity of the lamp I_0, the action cross-section of photolysis $\sigma\phi$, the molar absorption coefficient ε, the molar absorption cross-section σ and the quantum yield of photolysis ϕ are given for the different photoactivatable auxins.

Therefore, **4I** was chosen for photo-controlling auxin liberation, and will from now on be dubbed **PA-IAA** for Photo-Activatable IAA. We will assess in Chapter **5** the possibility to trigger protein depletion in living cells by **PA-IAA** photocontrol.

Chapter 5

Photo-induced protein degradation in living cells

In chapter **3**, we described the optimization process for an auxin-dependent degradation platform, and selected *Os*TIR1^{D170E} as an optimized heterologous F-box protein. Then, in chapter **4**, we described the synthesis and selection of a caged auxin candidate PA-IAA. In this part, we will discuss the possibility of implementing the degradation of a POI through light-control by combining the two tools detailed in the previous chapters, as summarized on **Fig 5.1.**

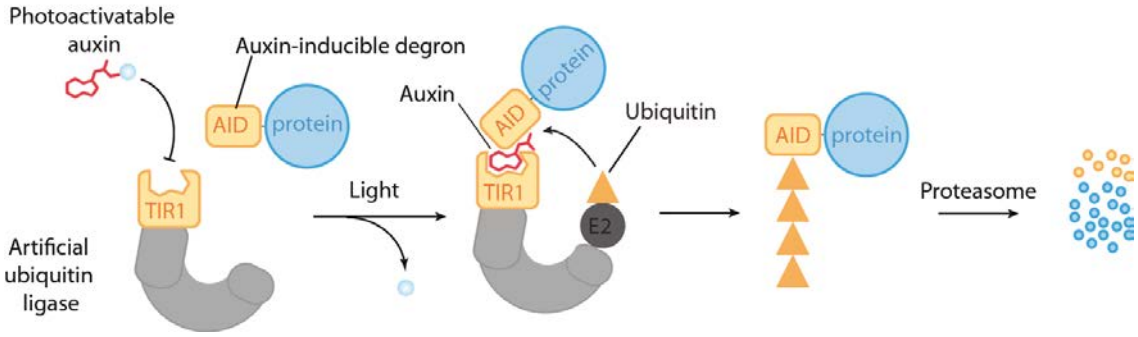

Fig. 5.1: Overview of a light-controlled AID for conditional depletion of POI in mammalian cells. PA-IAA is inactive in the dark, whereas its photolysis by UV illumination mediates the direct interaction between heterologous POI-AID and F-box *Os*TIR1, leading to the subsequent polyubiquitination and degradation of the POI-AID.

5.1 Validation of the protein depletion strategy triggered by PA-IAA photocontrol by immunoblotting

5.1.1 Description of the protocol for global UV illumination

Using the optimized degradation system described on chapter **3**, we next tested our ability to globally promote protein depletion in HEK293 cells grown on culture dish by photoliberation of PA-IAA. Besides giving a validation of the approach, this allowed us to adjust the parameters of illumination. HEK293 cells co-expressing *Os*TIR1^{D170E}-NLS and EGFP-AID-NLS were incubated in presence of PA-IAA in complete medium, illuminated at 365 nm with a hand UV lamp (**Fig. 5.2)**.

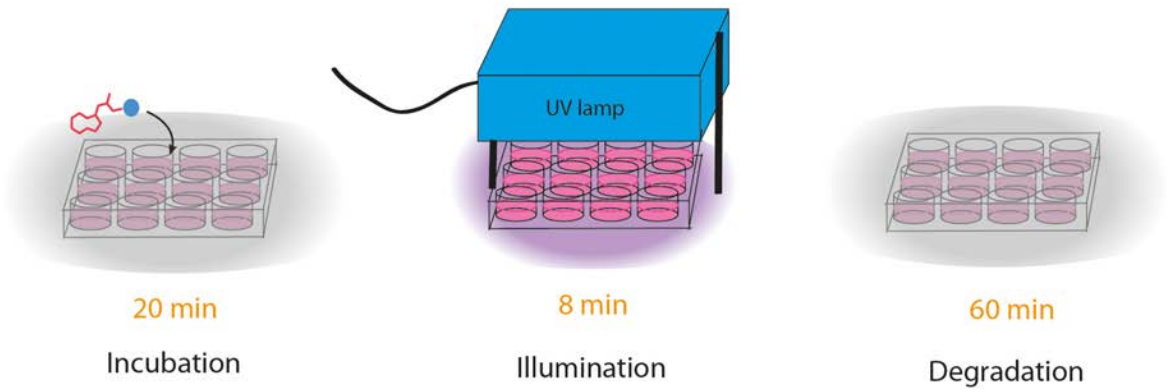

Fig 5.2: Overview of the illumination protocol. HEK293 cells were cultivated in 12-wells dishes, and transfected with pAG72 for 24h before manipulation. Cells were then incubated with PA-IAA for 20 min in the dark, illuminated with a hand UV lamp for 8 min and left in the dark at 37°C for one to two hours.

The hand UV-lamp delivered a measured photon flux I = 100 µmol.s^{-1}.m^{-2}. Using the uncaging cross-section $\varepsilon.\Phi$ = 6 m^2.mol^{-1} determined for PA-IAA in section **4.2.4.2**, the half-time for photorelease was evaluated to 500 s, according to equation **(5.1)**:

$$t_{1/2} = \frac{\ln(2)}{2.3\ \varepsilon.\Phi\ I} \quad \textbf{(5.1)}$$

Post-illumination, the cells were left in the dark at 37°C for various times. Cells lysates were analyzed by immunoblotting to monitor the EGFP-AID-NLS depletion.

5.1.2 Optimization of the PA-IAA concentration

The photo-activation strategy *in vivo* necessitates optimizing the concentration of PA-IAA used, which has to be:

- high enough for a genuine biological effect. IAA has a reported dissociation constant K_D for *At*TIR1 below 100 nM (Dharmasiri, 2005); therefore, a low amount of IAA might be sufficient to trigger the heterodimerization of TIR1 and Aux/IAA; however, sufficient amount of activatable PA-IAA has to accumulate intracellularly before illumination. It is expectable that protection with a caging group might enhance the diffusibility of the poorly-permeable IAA, based on our observations with methyl-ester IAA reported on section **3.4.2**.

- below a limit concentration where hydrolysis or auto-activity become non-negligible, to avoid a background effect in the dark.

We tested various concentrations of PA-IAA in HEK293 cells co-expressing EGFP-AID-NLS and *Os*TIR1^{D170E}-NLS, in the dark or illuminated by a UV-lamp for 8 min, which corresponds to the half-life for photorelease. The corresponding results are displayed on **Fig 5.3:**

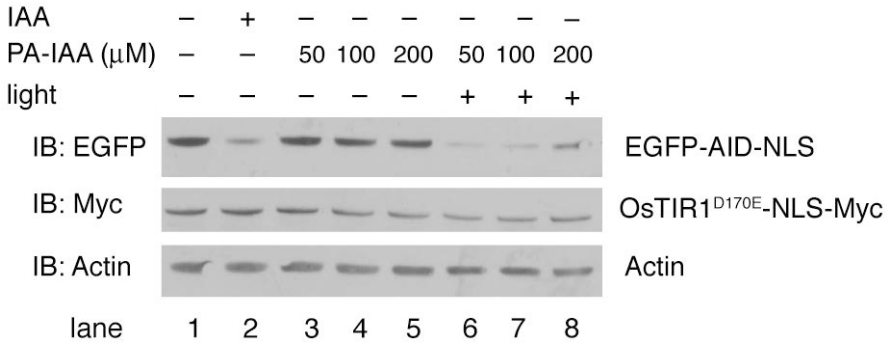

Fig. 5.3: HEK293 cells co-expressing EGFP-AID-NLS and *Os*TIR1^{D170E}-NLS were incubated with PA-IAA in a range from 50 to 200 µM for 20 min in the dark at 37°C, then illuminated (+) or not (-) at 365 nm with a photon flux of 100 µmol.s^{-1}.m^{-2} for 8 min and finally left in the dark for 1 hour at 37°C. Cell lysates were analyzed by immunoblotting (IB) with the indicated antibodies. HEK293 cells co-expressing EGFP-AID-NLS and *Os*TIR1^{D170E}-NLS were used for controls. Negative control (lane 1, untreated cells) displays the initial EGFP-AID-NLS immunoblotting level. Positive control (lane 2, cells treated for 2 h with 500 µM IAA) displays the free-auxin induced depletion in identical time.

We deduce from variations of the EGFP-AID-NLS level (assessed by EGFP immunoblotting) that:

- As previously reported on section **4.2.4.3**, EGFP-AID-NLS is stable for PA-IAA concentrations up to 200 µM.
- Significant protein depletion was observed for each concentration following illumination.

Although it might be possible that even lower concentrations could be as effective, we thus chose 50 µM as a working concentration of PA-IAA for the following experiments.

5.1.3 Optimization of the UV-illumination time

We next assessed the UV illumination time necessary to significantly photoliberate the caged product. We tested various illumination times from 0 to 8 min in HEK293 cells co-expressing EGFP-AID-NLS and *Os*TIR1^{D170E}-NLS incubated with the previously determined 50 µM PA-IAA concentration. The corresponding results are displayed on **Fig 5.4.** The EGFP-AID-NLS depletion increases with illumination time. Efficient depletion is observed for 8 min illumination, corresponding to the half-life of photoliberation. Although we assume that no cytotoxic effects[32] are associated with this range of illumination, longer UV exposure would not however be desirable.

[32] This corresponds to delivering a photon irradiation of 48 µmol.m^{-2} (or 0.25 J.m^{-2}), which is below the reported phototoxicity for UV-A in mammalian culture cells (Sun, 2010).

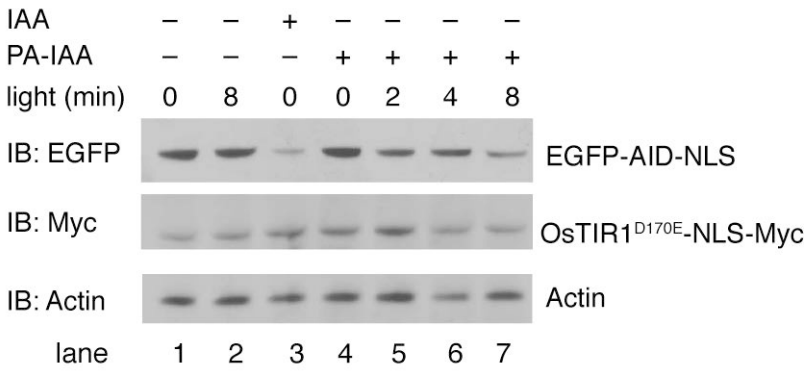

Fig. 5.4: HEK293 cells co-expressing EGFP-AID-NLS and *Os*TIR1^{D170E}-NLS were incubated with 50 µM PA-IAA for 20 minutes in darkness, then illuminated at 365 nm with a photon flux of 100 µmol.s^{-1}.m^{-2} for 0, 2, 4 or 8 min, and finally incubated in the dark for 2 h (lanes 4-7). Cell lysates were analyzed by immunoblotting (IB) with the indicated antibodies. HEK293 cells co-expressing EGFP-AID-NLS and *Os*TIR1^{D170E}-NLS were used for controls. Negative controls display the initial EGFP-AID-NLS immunoblotting level (lane 1, untreated cells), and the UV-induced depletion at maximal illumination (lane 2, cells exposed to 365 nm with a photon flux of 100 µmol.s^{-1}.m^{-2} for 8 min). Positive control (lane 3, cells treated for 2 h with 500 µM IAA) displays free-auxin induced depletion in identical time.

We then validated that the parameters previously determined allowed light-dependent conditional-degradation in three independent experiments in HEK293 cells co-expressing EGFP-AID-NLS and *Os*TIR1^{D170E}-NLS. The corresponding results are displayed on **Fig. 5.5:**

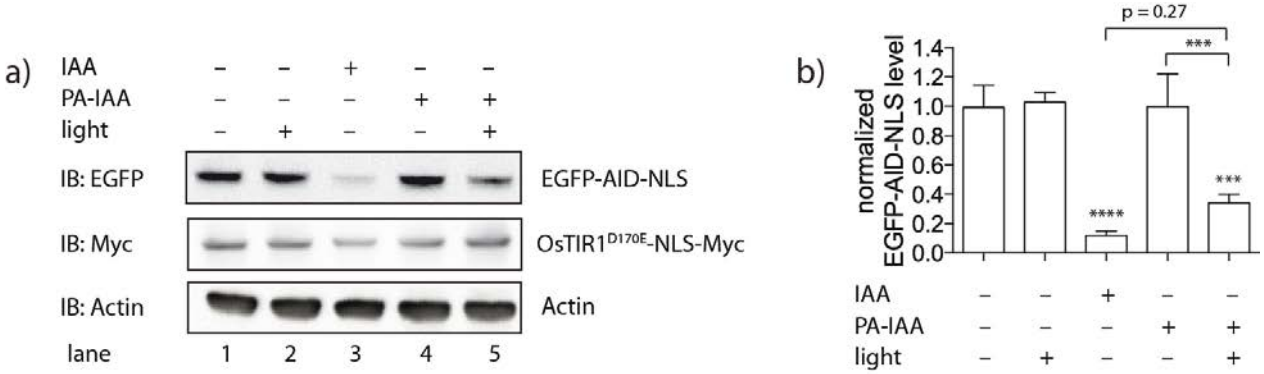

Fig. 5.5: **(a)** HEK293 cells co-expressing EGFP-AID-NLS and *Os*TIR1^{D170E}-NLS were incubated with (+) or without (–) 50 µM PA-IAA for 20 minutes in darkness, then illuminated (+) or not (–) at 365 nm with a photon flux of 100 µmol.s^{-1}.m^{-2} for 8 min, and finally incubated in the dark for 1 h (lanes 2, 4 and 5). Cells lysates were analyzed by immunoblotting (IB) with the indicated antibodies. Negative control experiments display the initial EGFP-AID-NLS **IB** level (lane 1, untreated cells), and the UV-induced depletion at maximal illumination (lane 2, cells exposed to 365 nm with a photon flux of 100 µmol.s^{-1}.m^{-2} for 8 min). **(b)** Western blot quantification. Plots represent the mean ± SD of 3 independent experiments. Data represent the EGFP-AID-NLS level normalized by the Os-TIR1^{D170E}-NLS level. The statistical significance was evaluated by a one-way analysis of variance (*** p value < 0.001, **** p value < 0.0001).

This series of three independent experiments confirmed that PA-IAA in these conditions met the specifications of a caged-auxin candidate:

- no significant depletion of AID-EGFP-NLS was observed in cells illuminated in absence of PA-IAA, nor in cells incubated with 50 µM PA-IAA in the dark.
- significant protein depletion of AID-EGFP-NLS was observed in cells incubated with 50 µM PA-IAA and illuminated at 365 nm.

These experiments confirmed that specific photocontrol of the cellular stability of POI fused to AID was possible by photolysis of PA-IAA, using the parameters determined on section **5.1.1**. However, immunoblotting displays averaged results in a global system, and is therefore inefficient to interrogate the degradation dynamics in individual cells. We next tested whether we could induce local photo-induced degradation by monitoring fluorescence depletion in confocal microscopy.

5.2 Monitoring of protein depletion triggered by PA-IAA photocontrol in confocal microscopy

We next tried to photolyse PA-IAA in HEK293 cells at 365 nm, using a microscope metal-halide lamp equipped with a DAPI filter as light source. HEK293 cells were grown on individual microscopy dishes and were illuminated on a surface of 0.1 mm^2 with a 63 × objective (NA 1.4).

5.2.1 Evaluation of the local illumination parameters

A method to quantify the local surfacic illumination power was necessary to estimate the illumination conditions necessary for significant uncaging of PA-IAA. This implies the setup of a protocol monitoring optical changes varying linearly with UV light illumination intensity. Classically, the photoliberation of a caged fluorophore can be used for calibration[33].

5.2.1.1 Kikume Green/Red can be used as a local illumination reporter

We however chose another strategy by using a fully genetically encoded Kikume Green/Red (Kik G/R) reporter protein, developed for regional tracking in cells, as explicated on **Fig. 5.6**. KikG/R is a photo-switchable protein able to irreversibly convert from green to red fluorescence when illuminated by UV or violet light (Tsutsui, 2005). However, the excitation lights used to elicit red or

[33] Such as PA-Fluoresceine, with a DMNB caging group. Caged fluoresceine is uncolored, whereas free fluoresceine exhibit a strong green fluorescence. Assuming that the photophysical properties of PA-IAA and PA-Fluoresceine are comparable, following the photoliberation of PA-Fluoresceine might be a good reporter of the UV illumination power.

green fluorescence do not induce the photoconversion. The green to red ratio can be calculated and reports directly to the power of UV illumination.

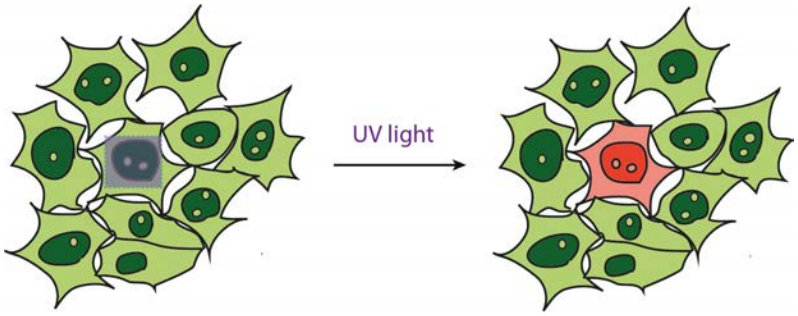

Fig. 5.6: Principle of single cell-tracking by KikG/R photoconversion from Green to Red upon UV illumination.

5.2.1.2 Validation of local illumination by KikG/R

KikG/R was expressed in HEK293 cells using a commercial plasmid under a CMV promoter. Positive transfected cells grown in dark conditions exhibit a strong cytoplasmic fluorescence in the green range, but not in the red range. We photoconverted KikG/R in HEK293 cells on a surface of 0.1 mm^2, using a microscope metal-halide lamp equipped with a DAPI filter as light source. Quantitative photoconversion of fluorescence from green to red was observable upon 10 s UV illumination (**Fig. 5.7**). As KikG/R and PA-IAA cross-sections are comparable (resp. 8 and 6 $m^2.mol^{-1}$) (Tsutsui, 2005), this confirmed that significant photoliberation of PA-IAA is expected within seconds using this illumination protocol. Consistently, the illumination photon flux I_0 was evaluated to 100 $mmol.s^{-1}.m^{-2}$ using a powermeter.

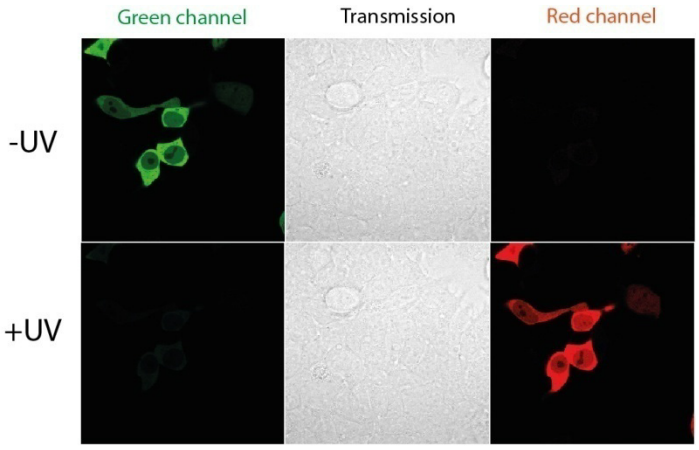

Fig. 5.7: KikG/R expressed in HEK293 cells accumulate as a green fluorescent cytoplasmic protein. Green to red photoconversion is observed upon 10s UV illumination with a metal halide lamp and a 63 × objective (NA 1.4, photon flux at specimen plan ~ 100 $mmol.s^{-1}.m^{-2}$).

5.2.2 Implementation of protein degradation by a photoliberation protocol

5.2.2.1 Description of the protocol for global UV illumination

We next characterized the kinetics of degradation of EGFP-AID-NLS co-expressed with *Os*TIR1^{D170E}-NLS in HEK293 cells upon photorelease of IAA. EGFP fluorescence was used as a reporter of EGFP-AID-NLS protein level and quantified by time-lapse confocal microscopy. PA-IAA absorbance is negligible beyond 425 nm (see section **4.2.4.2**); therefore, EGFP could be excited at 488 nm without activating PA-IAA photolysis. With an uncaging cross-section $\varepsilon\Phi$ = 6 $m^2.mol^{-1}$, the half-life of PA-IAA under an illumination power I_0 =100 $mmol.s^{-1}.m^{-2}$ was evaluated to 0.5 s (equation (**5.1**)). Therefore, quantitative photoliberation is expected with a 12 s illumination time. No major cytotoxic effects are associated with these illumination parameters (see note **B32**).

5.2.2.2 Optimization of the illumination protocol for PA-IAA release

However, first attempts to trigger PA-IAA in HEK293 cells co-expressing *Os*TIR1^{D170E}-NLS and EGFP-AID-NLS did not lead to significant EGFP fluorescence depletion. We suspected that the presence of serum in the incubation medium might affect the effective PA-IAA concentration. Indeed, addition of serum is known to deplete hydrophobic molecules from medium due to adsorption to serum proteins such as albumin (Fasano, 1975). We therefore replaced the complete D-MEM medium (containing fetal calf serum), by OptiMEM (a serum-free, phenol-red free synthetic medium supplemented with growth factors). However, in HEK293 cells co-expressing *Os*TIR1^{D170E}-NLS and EGFP-AID-NLS incubated with 50 µM PA-IAA, we monitored limited depletion (25% in one hour) after a single UV pulse (12 s) (**Fig. 5.8.a**).

We next addressed the timing of UV illumination, to assess whether, for identical light illumination, multiple frequent pulses were more efficient than one single pulse. In HEK293 cells co-expressing *Os*TIR1^{D170E}-NLS and EGFP-AID-NLS, we successively monitored the depletion induced:

- first, by a single UV illumination (12s) for one hour.
- second, by several pulses of 1s illumination every 5 min (12×1s) for one hour.

We measured differential relative depletion kinetics within one hour (**Fig. 5.8.b**): 25 ± 2 % for single UV pulse, compared to 73 ± 23 % for several pulses. Thus, a protocol based on multiple short illumination pulses spaced apart by darkness periods every 5 min was chosen. Further UV illumination might be toxic for cells. Relying on the light calibration on section **5.2.1.2**, 1s illumination pulse should convert 75% of intracellular PA-IAA into active IAA every 5 min.

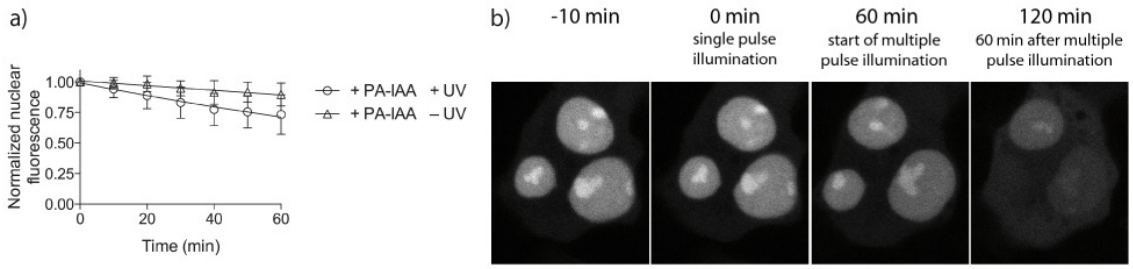

Fig. 5.8: **(a)** Normalized nuclear fluorescence intensity in function of time (mean ± SD, n = 10 cells). HEK293 cells co-expressing EGFP-AID-NLS and *Os*TIR1^{D170E}-NLS were incubated from t = -30 min with 50 µM PA-IAA min in dark. Imaging started at t= -10 min. At t = 0 min, cells were illuminated for 12 s at 365 nm (photon flux at the specimen plane ~ 100 mmol.s^{-1}.m^{-2}) (+PA-IAA +UV). Also displayed are control experiments where cells were not illuminated (+PA-IAA -UV). **(b)** Confocal micrographs of HEK293 cells co-expressing EGFP-AID-NLS and *Os*TIR1^{D170E}-NLS were incubated with 50 µM PA-IAA from t = -20 min in the dark and imaged from t = -10 min. At t = 0 min, cells were illuminated for 12 s at 365 nm. From t = 60 min, cells were illuminated for 1 s at 365 nm every 5 min for 1 hour. Photon flux at the specimen plane ~ 100 mmol.s^{-1}.m^{-2}.

5.2.2.3 EGFP fluorescence robustly reports for EGFP-AID-NLS level upon UV illumination

However, quantification of the photobleaching induced by UV illumination was necessary to ensure that the observed depletion in the EGFP fluorescence signal was not due to photobleaching. EGFP fluorescence was monitored in individual HEK293 cells co-expressing EGFP-AID-NLS and *Os*TIR1^{D170E}-NLS following the UV illumination and imaging protocol used for photoactivation. The results are displayed on **Fig. 5.9.a**. Loss of fluorescence was below 10% within one hour.

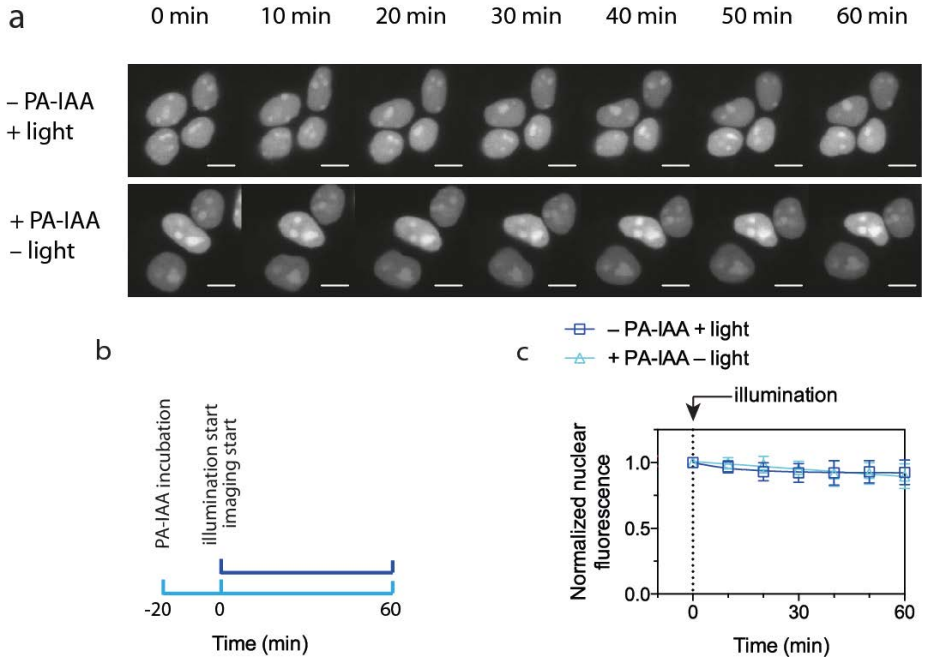

Fig. 5.9: (a) HEK293 cells co-expressing EGFP-AID-NLS and *Os*TIR1^{D170E}-NLS were imaged in following conditions: **(i)** cells were incubated with 50 µM PA-IAA for 20 min in the dark (t=-20 min) and imaged from t= 0 min. (+PA-IAA -light); **(ii)** from t = 0 min, cells were illuminated for 1 s at 365 nm (photon flux at the specimen plane ~ 100 mmol.s^{-1}.m^{-2}) every 5 min for 1 hour. (-PA-IAA +light). **(b)** Kinetic summary of the experimental conditions. **(c)** Normalized nuclear fluorescence intensity in function of time (mean ± SD, n = 10 cells).

Another specification for PA-IAA was to be stable in the dark. Although global PA-IAA stability was evaluated previously in immunoblotting (section **4.2.4.3**), we monitored EGFP fluorescence in control cells incubated with 50 µM PA-IAA (**Fig. 5.10.a**.) Loss of fluorescence was below 10% within one hour.

5.2.3.4 Significant, rapid protein depletion following PA-IAA photoliberation

Therefore, the photoliberation of IAA by UV-light pulses was tested. In HEK293 cells co-expressing *Os*TIR1^{D170E}-NLS and EGFP-AID-NLS pre-incubated with 50 µM PA-IAA, we observed significant depletion within 1 hour by flashing at 365 nm for 1s every 5 min (**Fig. 5.10**). We determined a protein half-life of 20 ± 3 min, in accordance with the degradation kinetics observed with free IAA.

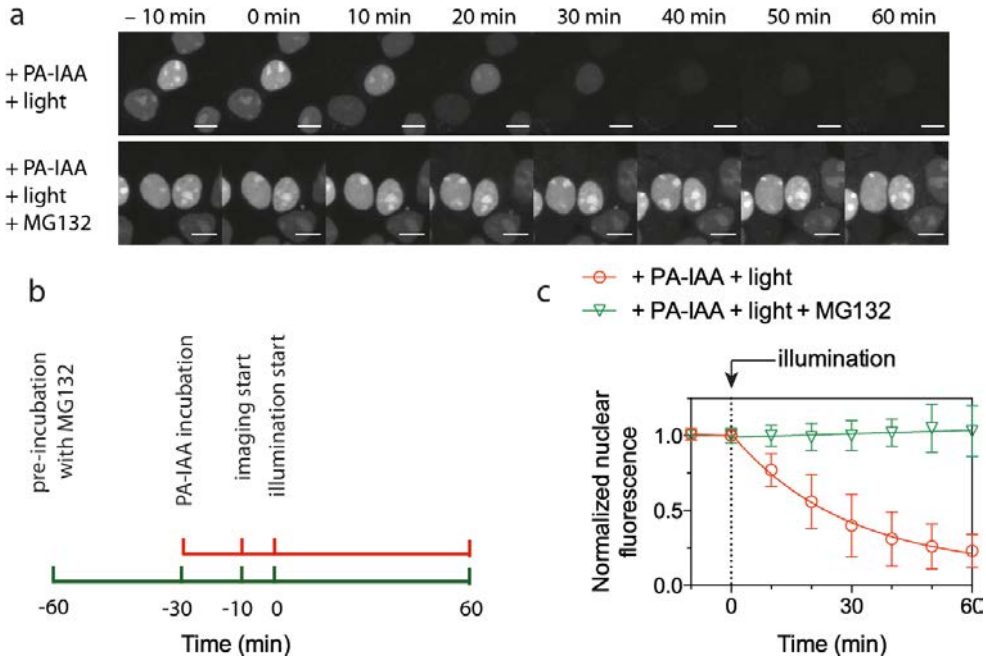

Fig. 5.10 (a) HEK293 cells co-expressing EGFP-AID-NLS and *Os*TIR1^{D170E}-NLS were imaged in following conditions:

- cells were incubated with 50 µM PA-IAA for 20 min in the dark (t=-30 min) and imaged from t= -10 min. From t = 0 min, cells were illuminated for 1 s at 365 nm (photon flux at the specimen plane ~ 100 mmol.s^{-1}.m^{-2}) every 5 min for 1 hour (+PA-IAA +light).
- cells were pre-treated for 1 hour with 50 µM MG132 (t= -60 min), and then incubated with 50 µM PA-IAA for 20 min in the dark (t=-30 min) and imaged from t= -10 min. From t = 0, cells were illuminated for 1 s at 365 nm (photon flux at the specimen plane ~ 100 mmol.s^{-1}.m^{-2}) every 5 min for 1 hour (+PA-IAA +light +MG132).

(b) Kinetic summary of the experimental conditions. **(c)** Normalized nuclear fluorescence intensity in function of time (mean ± SD, n = 10-30 cells).

5.2.3.5 The light-induced protein depletion is a proteasomal degradation

The observed depletion cannot be explained by the convolution of both PA-IAA background hydrolysis and photo-bleaching, as indicated by control experiments in **5.2.2.3** and **5.2.3.1**. However, we also confirmed that the observed fluorescence depletion was not due to the release of reactive species produced by PA-IAA photoactivation. In control cells pre-treated with the proteasome inhibitor MG132, no degradation was observed upon photoactivation of PA-IAA[34] (**Fig. 5.10**), showing that the observed EGFP loss upon IAA photorelease was indeed due to proteasome degradation and not to inactivation by reactive oxygen species.

5.2.4 Discussion

To sum up, we setup a methodology to trigger protein degradation by UV-light short pulses. Parameters were adjusted, such as PA-IAA concentration, and UV light pulse intensity, but also frequency. Interestingly, we observed that a protocol based on multiple short illumination pulses spaced apart by darkness periods was more efficient for maintaining efficient degradation than one single initial pulse. We will now discuss on the origin of this discrepancy.

5.2.4.1 Possibility of auxin-catabolism in HEK293 cells

A first hypothesis to address the relative inefficiency of single UV pulse to trigger depletion is that the active IAA is metabolized by HEK293 endogenous enzymes. As IAA is closely related to the Tryptophan amino-acid, we first postulated that IAA might be degraded by one of the two major pathways[35] for tryptophan catabolism existing in human cells (**Fig. 5.11**):

- Indoleamine 2, 3-dioxygenase (IDO1) catalyses the oxydative opening of the indole ring, which is the first step of the kynurenine pathway. However, it is not expressed in HEK293 cells (Human Protein Atlas).
- Tryptophan hydroxylase (THP) catalyses the hydroxylation of C5 in tryptophan, the first step of the serotonin formation pathway. THP2 is expressed at low levels in HEK cells (Human protein atlas), although it is highly abundant in kidney[36].

[34] An actual increase of GFP fluorescence of 10% was observed, indicating that heterologous EGFP-AID-YFP is degraded by the UPS in HEK293 at corresponding rates.

[35] Another reported degradation pathway in human cells is the generation of cytotoxic species by oxidation of IAA catalyzed by horseradish peroxidase has been reported as a potential cancer therapy (Jeong, 2010).

[36] HEK cells were originally assumed to originate from an adenovirus transformed fibroblastic or epithelial embryonic

Consequently, it is improbable that neither of these mechanisms is sufficient to explain the rapid depletion of active IAA observed after PA-IAA photorelease.

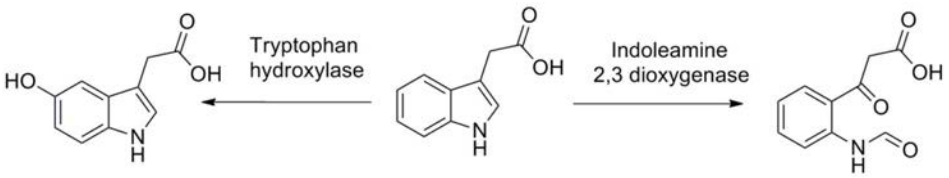

Fig 5.11: Overview of two hypothetical catabolic pathways for IAA degradation in mammalian cells, based on the described tryptophan pathway : **(a)** Tryptophan hydroxylase, first enzyme involved in serotonin synthesis pathway ; **(b)** Indoleamine 2,3 dioxygenase catalyzing oxidative opening of the Indole-ring.

5.2.4.2 Possibility of export of photo-liberated IAA in HEK293 cells

Another hypothesis is that the active IAA is externalized out of the cells by porines or permeases. Geisler *et al.* observed a net efflux of radiolabeled auxins in HeLa cells, in a few minutes timescale. Heterologous expression of plant auxin-transporter enhances this efflux effect (Geisler, 2005).

A first hypothesis for auxin efflux in mammalian cells is the existence of human homologs of plant auxin-transport proteins. Multi-drug resistance (MDR) gene MDR/TAP1 presents the highest homology in sequence alignment with plant MDR transporter *At*PGP1 (BLAST). MDR/TAP1 is expressed at a medium level in HEK293 cells (5 times higher than in HeLa cells), but not in other human cell lines, such as MCF-7 (Human Protein Atlas). Indeed, auxin efflux processes in HeLa cells were reduced by using plant and mammal MDR inhibitors, but not totally, indicating that an MDR-independent background efflux exists in mammalian cells (Teale, 2006), (Geisler, 2005).

Another possibility involves amino-acid transporters[37], which play important roles in kidney physiology and have been extensively reviewed in mammalian cells (Palacin, 1998). One can suspect *SLC16A10*/TAT1 (Tyrosine and Tryptophan Amino-acid transporter) (Mariotta, 2012) as the possible actor of auxin efflux. TAT1, a Na^+ and H^+-independent uniport, allows net efflux and influx of aromatic amino acids with low-affinity (K_D from 3 to 6 mM), but also recognizes N-methylated derivatives of amino-acids and monocarboxylates (Broer, 2006). SLC16A10 is expressed at a medium level in HEK293 cells, contrary to other cells lines such as HeLa where it is absent (Human Protein Atlas). This feature would allow net efflux of the high-concentration of free auxin liberated by PA-IAA illumination.

kidney tissues. Recent studies rather related HEK cells to immature neurons or adrenal cells (Shaw, 2002).

[37] In contrast to other transporters, such as the broad heteromeric transporter of neutral amino-acid transporter 4F2hc/LAT2 found at the basolateral membrane in kidney. This is not however the major hydrophobic amino-acid efflux pathway in kidney, but rather an exchanger with intracellular Cys (Liu, 2006).

Eventually, one can propose a model to explain the inefficiency of single pulses, as the liberated IAA can be rapidly inactivated by a cellular process, either catabolism, or more likely export by porines. This mechanism is summarized in **Fig. 5.12.**

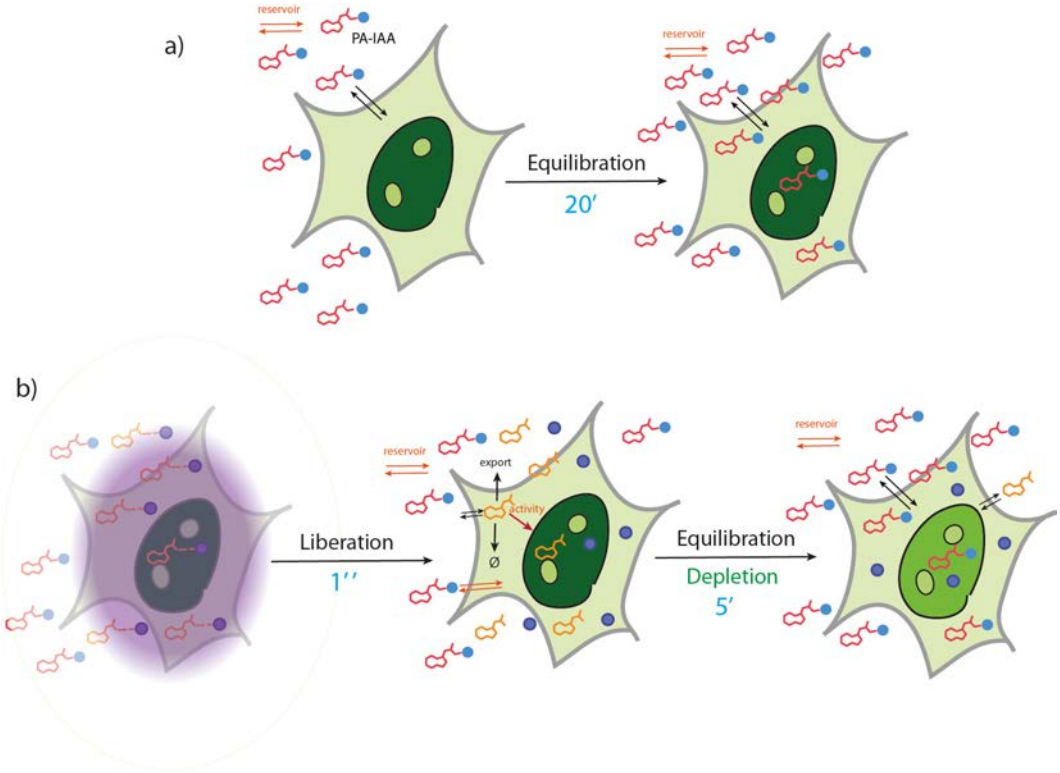

Fig. 5.12: Overview of the hypothetical mechanism reporting the IAA apparent de-activation post UV-liberation: **(a)** addition of PA-IAA in the dark for 20 min leads to the equilibration within extra and intracellular media. **(b)** UV-light pulses (1 s) liberate free IAA within the illumination area. Active auxin can induce the TIR1-dependent AID degradation; however, either catabolic degradation or porine export leads to the depletion of free IAA within minutes. PA-IAA accumulates again due to equilibrium exchange with the reservoir.

5.2.5 Conclusion

In this part, we showed that local photo-control of protein degradation could be obtained with the conditional release of a caged effector molecule. Although this protocol necessitates several pulses, it can be easily implemented and convenient for manipulators. The actuation timescale is comparable to free auxin addition (half-life of target protein < 20 min). One major advantage of caged molecules is to allow high spatial resolution for active molecule photorelease[38]. The specific control of degradation in individual cells by local photorelease, down to the single cell level, is thus highly desirable, and will be discussed in the next section.

[38] For example this feature is of particular interest for the precise release of neurotransmitters such as L-glutamate in neurons (Specht, 2006), (Matsuzaki, 2010).

5.3 Protein depletion with single-cell resolution triggered by PA-IAA resolution

5.3.1 Evaluation of the local illumination parameters

Next, we assessed the possibility to trigger spatially-controlled POI degradation using local photorelease of IAA using a commercial confocal microscopy laser setup. Local photolysis of PA-IAA was achieved using a laser diode at 405 nm, a wavelength at which PA-IAA still absorbs enough for efficient uncaging (section **4.2.4.2**), using a bleaching procedure of the confocal observation Software (Zen Zeiss). A rectangular region of interest (ROI) of 200 μm^2 was defined and illuminated (protocol in section **10.2**). The photon flux was adjusted by photoconverting heterologous KikG/R expressed in single HEK293 cells on a ROI, as displayed on **Fig. 5.13**.

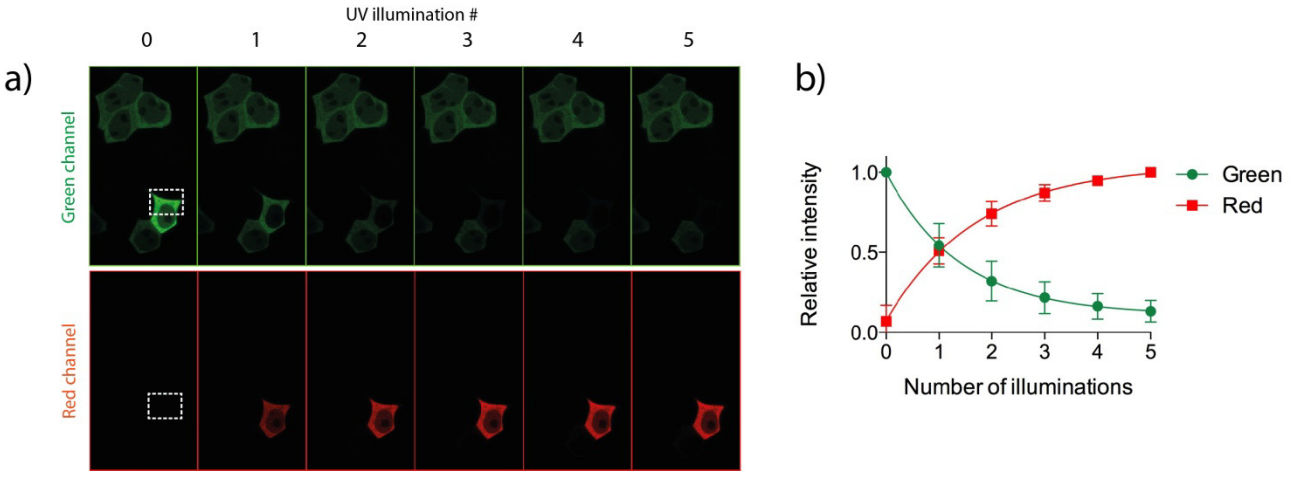

Fig. 5.13: **(a)** Single-cell highly specific photoconversion of KikG/R heterologously expressed in HEK293 cells can be achieved upon 405 nm illumination. **(b)** Evolution of the green and red fluorescence upon 405 nm illumination. Quantitative conversion is observed upon 5 sequences of illumination.

Five consecutive illumination events were sufficient to achieve complete photoconversion, with a highly specific single-cell resolution. This comforted us in the fact that spatial control of photo-illumination pattern can be achieved with 405 nm laser illumination. As a single series of illumination enabled 50% photoconversion, and to avoid high illumination powers, a protocol based on single 405 nm illumination every 10 min was selected.

5.3.2 Significant selective protein depletion induced by patterned illumination

5.3.2.1 Specific protein depletion in single-cell

We next characterized whether we could induce specific degradation of EGFP-AID-NLS cells upon specific photorelease of IAA. HEK293 cells co-expressing EGFP-AID-NLS and *Os*TIR1^{D170E}-NLS were pre-incubated in the dark for 20 minutes with 50 µM PA-IAA in OptiMEM buffer. Regions of interest (ROI) of 200 µm^2 were delimited within individualized cells. IAA bursts localized to ROI were generated by flashing repeatedly every 10 min with the 405 nm laser. Consequently, specific EGFP fluorescence depletion was observed in ROI, as exemplified on **Fig. 5.14**: cells #1 and #2, which were included in the illuminated ROI displayed at 75% loss within one hour.

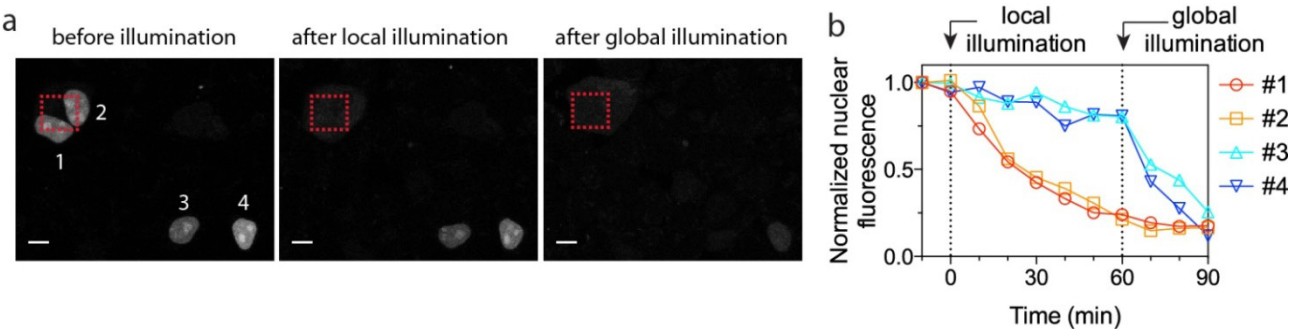

Fig. 5.14: **(a)** Summary of confocal micrographs of cells before illumination (t = 0 min), after local illumination at 405 nm (t = 60 min) and after global illumination at 365 nm (t = 90 min). The red square shows the region of interest (ROI) illuminated at 405 nm. Scale bars 10 µm. **(b)** Normalized nuclear fluorescence of cells 1-4 in function of time. The arrows successively indicate beginning of local illumination and of global illumination.

To show that photobleaching was not involved in EGFP fluorescence depletion specifically observed in the illuminated area, systematic picture acquisition before and after illumination was performed, as shown in **Fig. 5.15**. In the series of experiment shown, the relative fluorescence difference before and after a single illumination event was evaluated to 0.27 ± 0.9 % for UV-illuminated cells (n=12), and 0.12 ± 0.8 % for non illuminated-cells (n=12), showing that local depletion cannot be attributed to photobleaching.

5.3.2.2 Spatial selectivity in protein depletion

Local photorelease of IAA enabled to induce proteolysis with high spatial resolution, as shown on **Fig. 5.14**. Cells #3 and #4, distant of 60 µm to the ROI display less than 20% fluorescence loss in one-hour post-illumination. Finally, global illumination at 365 nm, using a microscope metal-halide lamp led to global EGFP depletion in the illuminated field, at timescales comparable to those reported on section **5.2.2**.

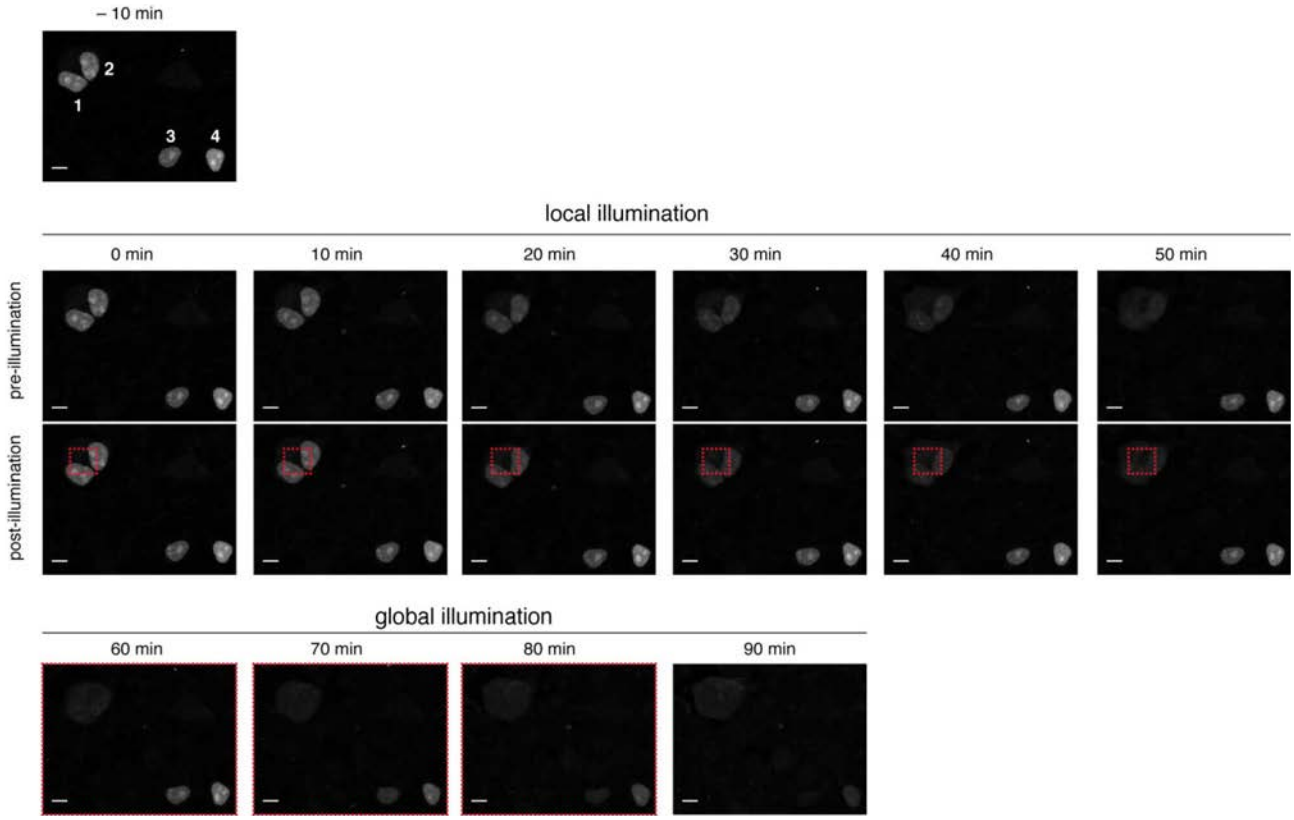

Fig. 5.15: Global time-lapse of locally-induced protein degradation summarized in **Fig. 5.14.a**. For each time point, pre- and post-illumination images are shown to evidence that the loss of fluorescence is not due to photobleaching.

However, statistical analysis showed that EGFP-AID-NLS depletion following illumination was not strictly limited to the ROI, but also affected surrounding cells. To monitor the spatial selectivity of PA-IAA uncaging, we related the fluorescence EGFP loss in one hour in individual cells to their distance to the illuminated ROI (**Fig. 5. 16**). Specific depletion was restricted to cells immediately surrounding the ROI at a distance shorter than 20 µm, whereas no significant difference was observed further, compared to non-incubated cells.

In conclusion, specific EGFP fluorescence depletion was observed in the uncaging ROI and immediately surrounding cells at a distance shorter than 20 µm. This indicates that local photorelease of IAA could enable the control of protein degradation at the single cell level.

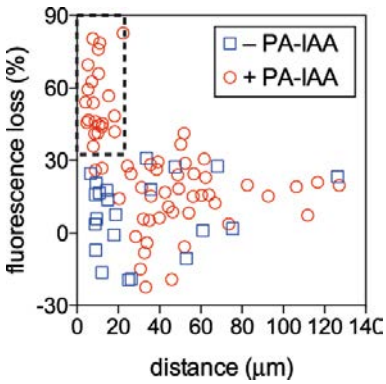

Fig 5.16: Percentage of fluorescence loss in individual cells 60 min after local illumination in function of their distance to the illuminated spot (red circles; n =66 cells from 12 experiments). In control experiments, cells were illuminated and imaged in the same conditions but in absence of PA-IAA (blue squares; n = 26 cells from 6 exp.).

5.3.3 Modelization of IAA diffusion following single-cell PA-IAA photoliberation

In a simple model of auxin diffusion, one can consider a punctual source of free IAA which diffuses following a 3D diffusion **(7.2)** distribution along the distance *r* in the time *t*:

$$c(r,t) = \frac{1}{(4\pi Dt)^{3/2}} . e^{-\frac{r^2}{4Dt}} \quad \textbf{(7.2)}$$

We took 700 µm^2.s^{-1} for D, the diffusion coefficient of IAA (Hetherington, 2008). **Fig. 5.17** reports the predicted IAA distribution at various distances from the source (computed with Matlab). Following illumination (t=0 s), short (< 1 s) bursts of auxin are observable at 5 and 10 µm, rapidly decreasing with distance. Almost no effective concentration of IAA is *seen* in regions beyond 10 µm.

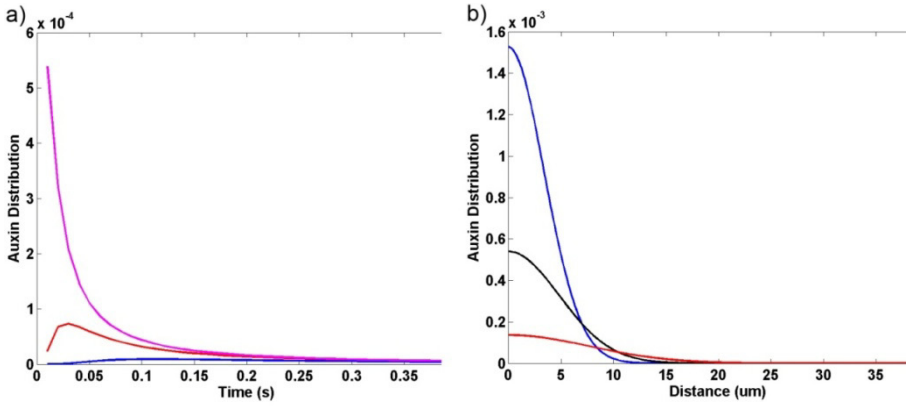

Fig 5.17: **(a)** Predicted temporal evolution of active IAA distribution at various distances after PA-IAA photoliberation: 5 µm (violet), 10 µm (red), 20 µm (blue) **(b)** Predicted distribution profiles of active IAA diffusion at various times: 0.01 s (blue), 0.02 s (black), 0.05 s (red) following PA-IAA photoliberation.

This simplified model can be compared to our observations. PA-IAA illumination creates an active auxin pattern that rapidly dissipates in space and time, although the mechanism is not determined[39]. Free auxin is poorly permeable due its anionic carboxylate and high concentrations of auxin are necessary to trigger AID degradation in mammalian cells (Nishimura, 2009), see also Fig **3.1.3**. Membrane permeation might be a kinetic determinant step.

5.4 Conclusion

This set of experiments showed the possibility to implement light-activated protein depletion of AID-tagged protein upon photorelease of IAA in individual cells, down to the single-cell level with multiple short light pulses; although this protocol is more constraining than activation by single pulse, it does not necessitate continuous light-illumination contrary to other reported methods for light-induced degradation, which will be further discussed on part **7.1**.

[39] Further refinements would include the suspected efflux of intracellular auxin discussed on **5.2.3**. However, diffusion would also induce rapid dissipation of auxin, so that subsequent depletion might be limited to surrounding regions.

Chapter 6
Photo-induced protein degradation of a cytoplasmic protein in living cells

So far in previous chapters, a nuclear AID-EGFP reporter has been used as a model for auxin-induced degradation. Application to actual POI is an important specification for the development of a generic protein depletion methodology. The generic AID methodology can be *a priori* applied to any POI, regardless of their cellular context (Nishimura, 2009). This potentiality has been illustrated in mammalian culture cells with six different POI targets, including two cytoplasmic proteins, which were conditionally degraded by auxin addition (Holland, 2012). Thus, development of the AID methodology in a cytoplasmic context is desirable. We will address this question in this chapter.

6.1 CyclinB1 is a cytoplasmic target for conditional AID degradation

In section **3.4.3**, we reported that endogenous sequences present in AID may prevent in some cases the cytoplasmic localization of fusion proteins. To implement light-inducible protein degradation in a cytoplasmic context, we focused on cytoplasmic AID-fusion proteins previously reported.

6.1.1 Heterologous Cyclin B1-AID is addressed to cytoplasm in mammalian cells

*Hs*Cyclin B1 fused to AID was reported as an example of cytoplasmic POI[40]. Fluorescence microscopy confirmed that the fusion protein Cyclin B1-AID-YFP colocalized in the cytoplasm with endogenous Cyclin B1 (Holland, 2012). This implied that the nuclear addressing driven by endogenous sequences in AID is balanced by cytoplasmic addressing signals in Cyclin B1.

[40] Plk4 (Polo Kinase 4) was also described as cytoplasmic POI target. AID-YFP-Plk4 was degraded upon auxin addition with a half-life of 9 min. These two cytoplasmic proteins however differ by their sub-localization: Plk4, which regulates the centriole duplication, is punctually associated with centrosome.

6.1.2 Heterologous Cyclin B1-AID is conditionally degraded by auxin addition

Cytoplasmic Cyclin B1-AID-YFP transiently transfected in HEK293 cells stably expressing *Os*TIR1-myc, was rapidly degraded by auxin addition (half-life of 17 min) (Holland, 2012). Last, fusion with AID-YFP did not prevent interaction with Cyclin B1 endogenous substrate CDK1, as assessed by pull down experiments. These features identified Cyclin B1-AID-YFP as a candidate for both cytoplasmic degradation and functional light induced perturbation implementation.

6.2 Light-controlled degradation of Cyclin B1-AID in HEK293 cells

6.2.1 Cyclin B1-AID-YFP degradation can be controlled by light-activation

6.2.1.1 Motivation

Consequently, we used the Cyclin B1-AID-YFP plasmid (Courtesy of Dr Cleveland) to test our ability to control the degradation of a functional cytoplasmic POI with light, in the strategy reported in **Fig.6.1.** In their original paper, Holland et al. constructed mammalian cell lines stably expressing *Os*TIR1, in which Cyclin B-AID-YFP was transiently transfected (Holland, 2012). We chose an alternative strategy by constructing a plasmid expressing *Os*TIR1-myc under the dependence of a CMV promoter. Co-expression of the two plasmids in HEK293 cells at a 1:1 ratio allowed the co-expression of Cyclin B-AID-YFP and *Os*TIR1-myc, which are both cytoplasmic[41].

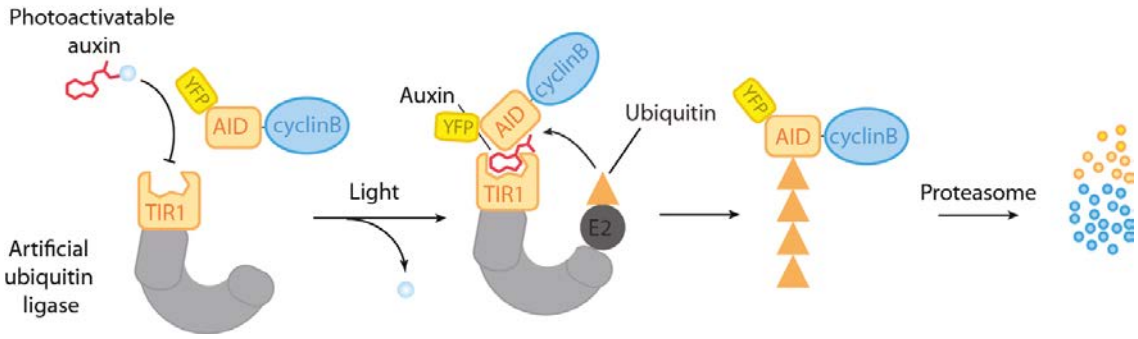

Fig. 6.1: Overview of photoactivation process for Cyclin B1-AID-YFP degradation in HEK cells. UV-light illumination of a photoactivatable auxin liberates free auxin, which induces the dimerization of heterologous Cyclin B1-AID-YFP and artificial ubiquitin ligase SCF^{OsTIR1}, leading to the polyubiquitination of Cyclin B1-AID-YFP and its eventual proteasomal degradation.

6.2.1.2 Local PA-IAA photo-activation triggers CyclinB1-AID-YFP degradation

We thus assessed whether the protocol elaborated on **5.2** could be used for CyclinB1-AID-YFP to

[41] CyclinB-AID-YFP: **Fig. 6.2**; *Os*TIR1myc: **fig. 6A** in (Holland, 2012) and section **3.2.2** in this dissertation.

locally induce light-activated degradation using a microscope metal-halide lamp setup equipped with a DAPI filter as light source. We monitored the depletion by time-lapse confocal microscopy. However, to simplify the protocol of acquisition compared to section **5.2.3**, a period of 60 min of incubation with PA-IAA in the dark preceded the light-activation of depletion. Therefore, background activation control and depletion monitoring post-photorelease were coupled. HEK293 cells co-expressing Cyclin B1-AID-YFP and *Os*TIR1myc were incubated with 20 µM PA-IAA in OptiMEM in the dark. No depletion of Cyclin B1-AID-YFP was observed after one hour in the dark, as shown on the time-lapse in **Fig. 6.2.a.** Subsequently, we illuminated the observation field by flash illumination at 365 nm for 1s every 5 min spaced apart by darkness periods. A significant depletion was observed within one hour, with a characterized half-life of 18 ± 4 min.

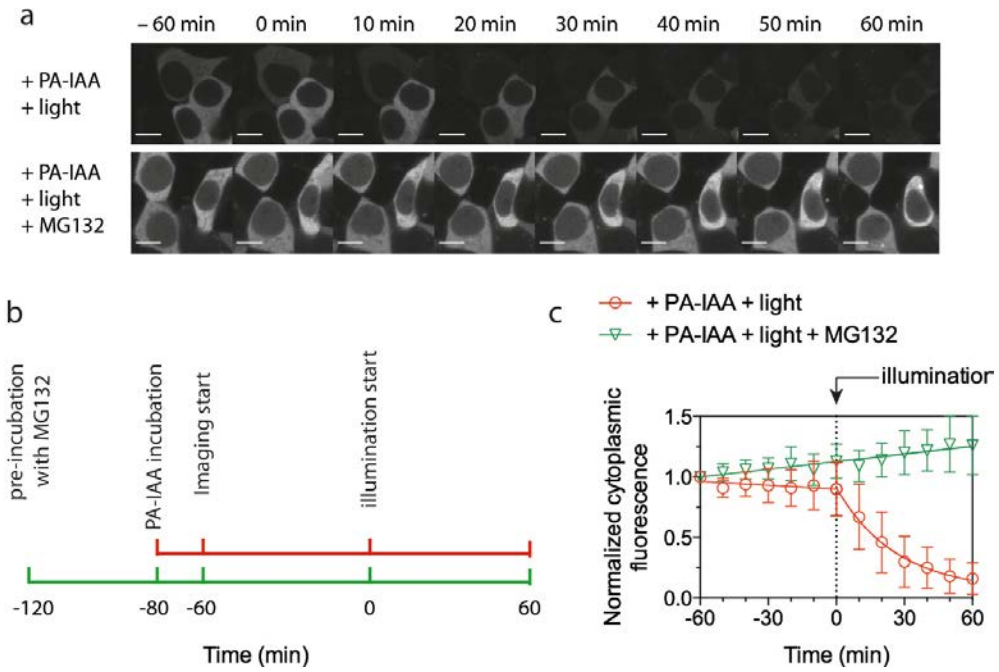

Fig. 6.2: (a) HEK293 cells co-expressing Cyclin B1-AID-YFP and *Os*TIR1^{D170E}-NLS were imaged in conditions:

- cells were incubated with 20 µM PA-IAA from t= -80 min in the dark. Imaging started at t = -60 min. From t = 0 min, cells were illuminated for 1 s at 365 nm every 5 min for 1 hour. (+PA-IAA +light).
- cells were pre-treated for 1 hour with 50 µM MG132 (t= -120 min) cells were incubated with 20 µM PA-IAA from t= -80 min in the dark. Imaging started at t = -60 min. From t = 0 min, cells were imaged for 1 s at 365 nm (photon flux at the specimen plane ~ 100 mmol.s^{-1}.m^{-2}) every 5 min for 1 hour. (+PA-IAA +light +MG132).

(b) Kinetic summary of the experimental conditions. **(c)** Normalized fluorescence intensity in function of time of experiments **a**) (mean ± SD, n = 10-15 cells).

This timescale is in good accordance with the value (17 min) reported in the literature for IAA-induced Cyclin B1-AID-YFP degradation (Holland, 2012). It is also consistent with timescales determined in chap. **1** and **3** for the optimized nuclear degradation, induced resp. by addition of free IAA or photoliberation of PA-IAA (resp. 15 ± 1 min and 20 ± 3 min). This confirmed that PA-IAA, stable in dark, can be liberated by short UV pulses, inducing rapid Cyclin B1-AID-YFP depletion.

6.2.1.3 PA-IAA dependent Cyclin B1-AID-YFP degradation is a proteasomal process

We confirmed that the PA-IAA + light-dependent POI degradation was indeed mediated by the proteasome. We repeated the previous experiment in the presence of proteasome inhibitor MG132 (pre-incubated 1 h before PA-IAA addition). No significant fluorescence depletion[42] was observed in presence of PA-IAA in one hour, neither in the dark nor with UV illumination **(Fig. 6.2)**, confirming that the observed depletion is not due to photobleaching. This set of experiments showed that we could induce proteasome-dependent depletion of cytoplasmic AID-tagged POI upon photorelease of IAA, on a time-scale comparable to our reported observations for nuclear proteins (part **5.2.3)**.

6.2.2 PA-IAA dependent Cyclin B1-AID-YFP degradation is spatially controlled

Then, as for nuclear GFP-AID-NLS protein in previous chapter (section **5.3.2**), we demonstrated that we could induce specific protein degradation at the single cell level by local photorelease of IAA using the parameters described on section **5.3.1**. HEK293 cells co-expressing Cyclin B1-AID-YFP and *Os*TIR1 were pre-incubated in the dark for 20 minutes with 20 µM PA-IAA in OptiMEM buffer. Regions of interest (ROI) of 200 μm^2 were chosen. ROI-localized IAA bursts were generated by flashing repeatedly every 10 min with the 405 nm laser.

Consequently, specific YFP fluorescence depletion was observed in ROI, as shown on **Fig. 6.3**: cell #1 included in the illuminated ROI displayed a 60% YFP fluorescence loss in the hour timescale, unlike cells #2, #3 and #4 (distance from the ROI > 20 µm). Global illumination starting at t=60 min led to significant degradation in these cells.

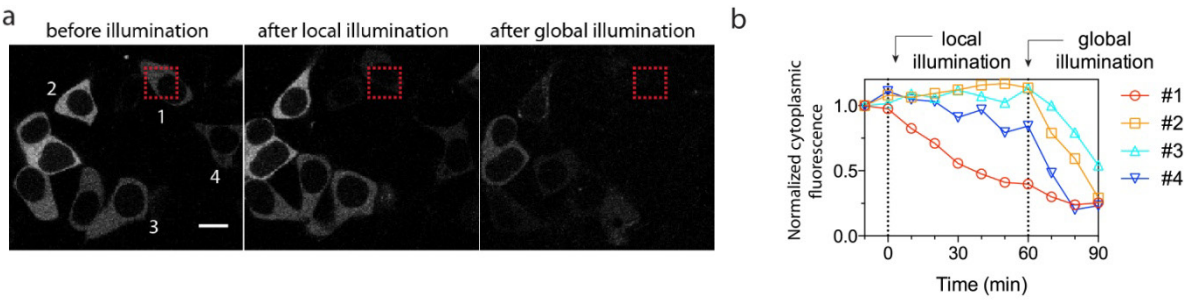

Fig. 6.3 (a) Summary of confocal micrographs of cells before illumination (t = 0 min), after local illumination at 405 nm (t = 60 min) and after global illumination at 365 nm (t = 90 min). The red square shows the region of interest (ROI) illuminated at 405 nm. Scale bars 10 µm. **(b)** Normalized cytoplasmic fluorescence of cells # 1-4 in function of time. The arrows successively indicate beginning of local illumination and of global illumination.

[42] An actual increase of YFP-fluorescence of 10% per hour was observed, indicating that heterologous Cyclin B1-AID-YFP is degraded by the UPS in HEK293 at corresponding rates.

6.2.3 PA-IAA photo-activation can trigger degradation of nuclear-activated Cyclin B1-AID-YFP

During the experiments described on section **6.2.1.2**, on a single event, we were able to activate the degradation of a nuclear-translocated Cyclin Bl-AID-YFP. This process, linked to the activation of CyclinB-Cdk in mitosis, will be presented in section **9.1**.

In cell #1 in **Fig. 6.4**, cytoplasmic Cyclin B1-AID-YFP was imported to the nucleus between t= -10 min and t= 0 min (before light activation), concomitant with the Nuclear Envelope Breakdown (NEB) (**Fig. 6.4.b/c**). At t= 0 min, PA-IAA was photo-activated, leading to the subsequent degradation of global (cytoplasmic + nuclear) Cyclin B1-AID-YFP in cell #1, at rates comparable to neighboring cells displaying cytoplasmic Cyclin B1-AID-YFP localization (**Fig. 6.4.d**).

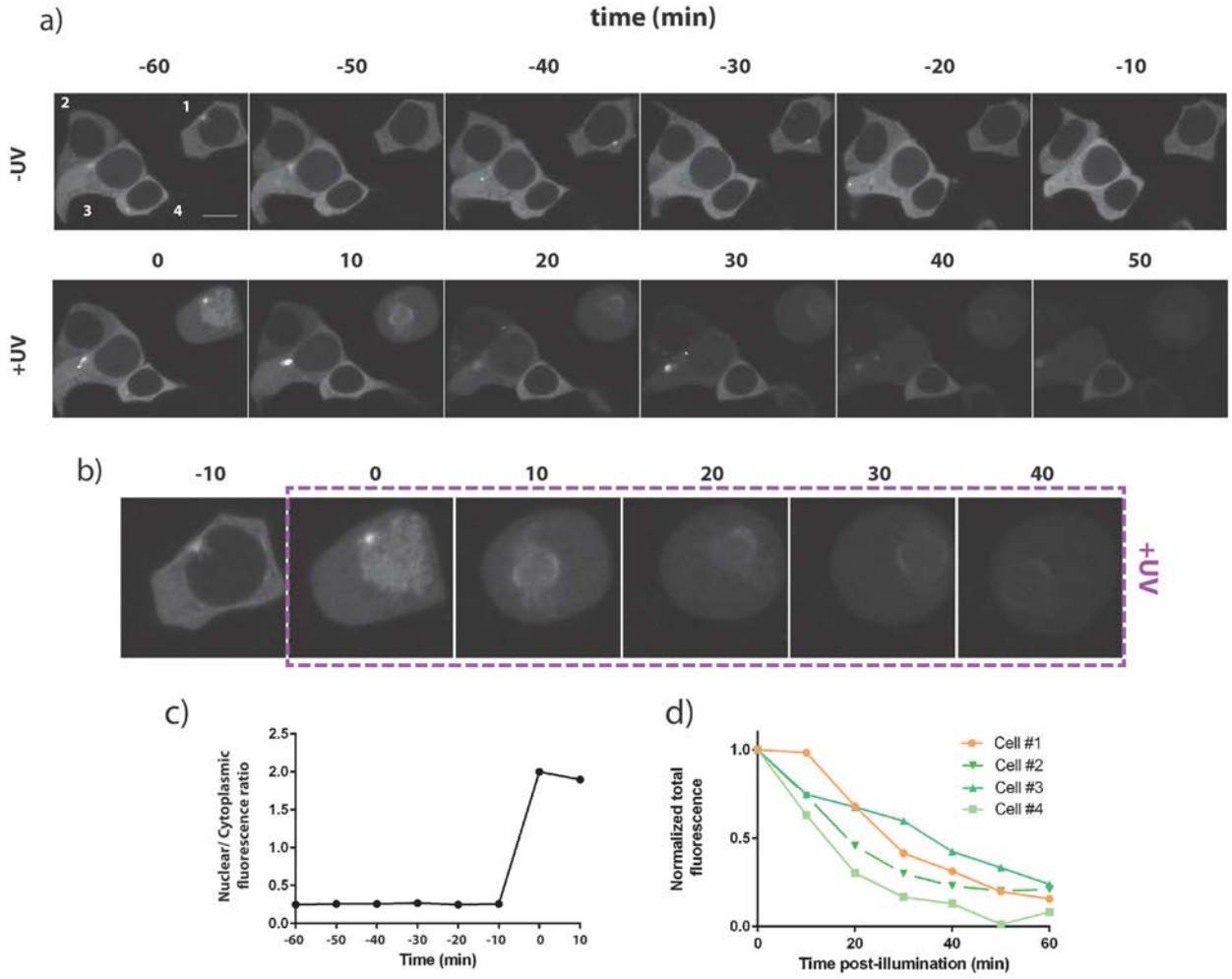

Fig. 6.4: **(a)** HEK293 cells co-expressing Cyclin B1-AID-YFP and *Os*TIR1^{D170E}-NLS were incubated with 20 µM PA-IAA from t= -80 min in the dark. Imaging started at t = -60 min (-UV). From t = 0 min, cells were imaged for 1 s at 365 nm every 5 min for 1 hour (+UV). **(b)** Zoom on cell #1 between times t=-10 and 40 min, showing nuclear import from t=-10 min and light-activated degradation from t=0 min. **(c)** Quantification of nuclear import in **b**): Normalized nuclear/cytoplasmic fluorescence intensity ratio between times t= -10 and t= 40min in cell #1. **d)** Normalized total fluorescence intensity in function of light-induced degradation experiment reported between t = 0 and 60 min in **a**).

Moreover, an intriguing phenomenon was observed from t= 90 min (30 min after photoactivation start), a time by which 55% of initial Cyclin Bl-AID-YFP had been depleted. The mitotic spindle, easily identifiable in transmission microscopy **(Fig. 6.5.a)**, was off-centered; moreover, radial rotation of the spindle was observed, at constant angular speed, as displayed (**Fig. 6.5.b/c)**.

A series of micrographs illustrates this process, highlighting positions of the spindle at various times starting at t=120 min. Complete revolution around the cell in direct sense is observed within 5 minutes, a process observed consecutively several times. Auto-rotation of the spindle was observed, so that it sometimes oriented perpendicular to the surface (as between t = 120 to 160 s in **Fig. 6.5.a**).

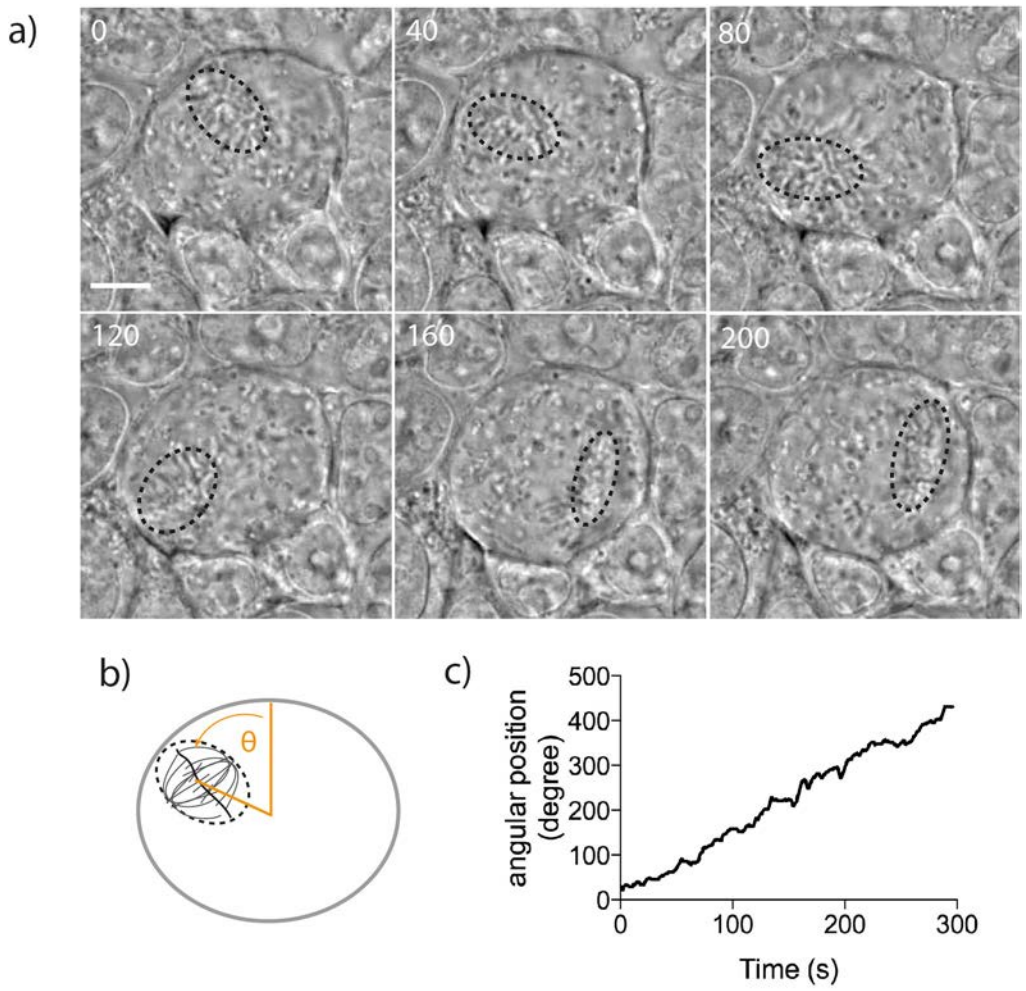

Fig. 6.5: **(a)** Transmission micrographs of cell #1 from **Fig. 6.4** at various times (in seconds). The dotted circle shows the spindle **(b)** Model for spindle position quantification. **(c)** Quantification of the angular position of the spindle relative to the definition in **(b).**

Implications of these observations on the possibility to control the degradation of active Cyclins at different phases of the cell-cycle will be further discussed on section **9.1.3**.

6.3 Conclusion: PA-IAA photo-activated degradation of AID-tagged POI is a generic perturbation method

This series of experiments confirmed further that the light-induced degradation methodology elaborated on nuclear reporter in chapter **5** was extendable to cytoplasmic targets, with possible high spatial resolution ; more generally, it illustrates that the Auxin-Inducible Degradation method is *a priori* generic, associated to important potentialities for POI targeting in various cellular contexts. AID has also been implemented with reticulum, mitochondrial or plasma membrane proteins. An essential condition is that AID degron is exposed to the cytoplasm (Nishimura, 2009).

PART C
DISCUSSION
PERSPECTIVES

L'objet matérialise l'intention préexistante qui lui a donné naissance et sa forme s'explique par la performance qui en était attendue avant même qu'elle s'accomplisse. Rien de tel pour le fleuve ou le rocher, que nous savons ou pensons avoir été façonnées par le libre jeu de forces physiques auxquelles nous ne saurions attribuer aucun projet. Ceci tout au moins si nous acceptons le postulat de base de la méthode scientifique : à savoir que la Nature est objective et non projective. C'est donc par référence à notre propre activité projective, c'est parce que nous sommes nous-mêmes fabricants d'artefacts, que nous jugeons du « naturel » ou de l'« artificiel » d'un objet quelconque[1].

Jacques Monod, Le Hasard et le Nécessité

[1] The artifact materializes the pre-existent intention that gave birth to it, and its forms can be explained by the performances that were expected even before their realization. There is nothing equivalent for the river or the rock, which we know, or think to know, to result from the free interplay of physical forces to which we cannot attribute any project. This at least if we accept the basic postulate of the scientific method, that is that Nature is objective, but not projective. Thus, it is in reference to our own projective activity, because we make artifacts ourselves, that we assess the natural or artificial nature of a given object (Jacques Monod, Chance and Necessity).

Le hasard et la nécessité, Essai sur la philosophie naturelle de la biologie moderne, POINTS ESSAIS, p 19. First edition: Editions du Seuil, 1970.

Chapter 7

Discussion

In Chapter **1**, we reviewed the existing methodologies to control the stability of a given POI by UPS degradation. Based on the endogenous mechanisms controlling the stability of proteins *in vivo*, POI can be constitutively destabilized. Conditionality can be introduced as a refinement of this constitute perturbation approach, as the transition between a stable and an unstable state of the degron-POI can be driven by a controllable perturbation. We identified light as a potential perturbation method and reviewed the existing methodologies for photo-actuation in Chapter **2**. In this part, we will compare our work with alternative approaches for photo-induced POI depletion.

7.1 Photo-activatable degradation systems enable light-control of Protein degradation

7.1.1 Light control of POI degradation by PA-IAA

In this work, we presented an approach for the control of POI stability by light. We developed a caged auxin (PA-IAA, see section **4.2.3**), which acts as a photo-activatable inducer of the auxin inducible degradation AID platform, a generic method enabling the conditional degradation of POI upon auxin addition. IAA mediates the heterodimerization between AID-tagged POI and an artificial SCF^{OsTIR1} E3 Ubiquitin Ligase (see section **3.3**), eventually leading to POI polyubiquitination and degradation by the proteasome.

We observed that active IAA can be locally released by the photolysis of PA-IAA with short UV light pulses. With this strategy, we were able to promote the efficient protein degradation in mammalian cells within an hour timescale, with a half-life of 19 min (section **5.2**). This method, first developed with nuclear proteins, can be extended to cytoplasmic POI (section **6.2**)

7.1.2 Alternative strategies for POI degradation by blue-light sensitive degradation modules

7.1.2.1 Design of blue-light sensitive degradation modules

In 2013, the team of C. Taxis applied the photosensitive domains described in section **2.1** to the development of a blue-light conditional degradation module dubbed photosensitive degron (psd) in yeast cells. The C-terminal Jα-helix LOV2 domain of *At*Phototropin1 was fused to a degron derived from the murine Ornithine Decarboxylase (ODC), a 23 amino-acids unstructured peptide with a Cys-Ala motif recognized as a degron in eukaryotes[2] (**Fig. 7.1**). This motif is designedly inactivated in the dark due to the helical fold interaction with the core LOV2 domain, whereas it is activated by Jα helix unfolding.

Using a similar approach, the team of T. Wandless developed a Blue Light Inducible Degradation (B-LID) technique in vertebrates (Bonger, 2014). A small peptide degron (RRRG), inducing fast-proteasomal degradation in mammalian cells, was fused to the C-terminal alpha helix of the *As*LOV2 full domain or truncations.

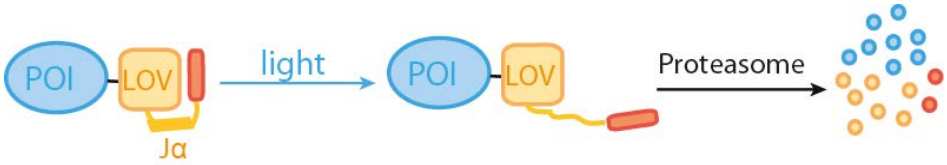

Fig. 7.1: Photosensitive LOV-domain based strategies for light-controlled of proteasomal degradation of POI developed in (Renicke, 2013) and (Bonger, 2014). A degron fused to a LOV domain is sequestered in the dark; Blue-light illumination mediates an unfolding mechanism leading to the degron presentation and proteasomal degradation.

7.1.2.2 Modulation of the properties of blue-light sensitive degradation modules

General trends are identifiable in the development process of C-terminal B-LID and psd domains. In both cases, the engineered light-actuator must meet the two following specifications:

[2] Actually, this process is proteasome-dependent but ubiquitin-independent (see section **1.1.4**).

a) stabilization in the dark due to cryptic sequestration of the degron by the interaction of the Jα terminal helix with the LOV core domain.

b) destabilization in blue-light due to degron exposure by dissociation of the Jα helix, leading to proteasomal degradation.

In both cases, several initial constructions did not meet these specifications. Two limit phenotypes were observed: first, the candidate exhibited excessive constitutive degradation in dark, meaning an insufficient sequestration or excessive strength of the degron. Alternatively, the candidate was stable in the dark and upon light exposure, where no significant degradation was observed. Various modifications can be introduced to modulate the activity of the fusion protein:

- Variation of insertion locus relative to the Jα helix or variation of the linker length
- Variation of the degron length and strength, to prevent constitutive degradation or enhance lit-state degron recognition
- Introduction of mutations that either :

  1) stabilize closed-conformation in the dark to prevent unwanted constitutive degradation by thermal exposition of the cryptic degron .

  2) stabilize the open-conformation in the lit-state, increasing the time of degron exposure, or increase the dissociation of the Jα helix.

Candidate module exhibiting a satisfactory balance between strong stabilization in the dark and degron exposure upon blue-light illumination were selected as B-LID or psd domain, respectively in mammalian cells and yeasts.

7.1.2.3 psd module enables blue light-mediated efficient degradation in yeast cells

In yeast cells, constant blue-light exposure dramatically affects the life-time of a Red Fluorescent Protein (RFP)-tagged psd from 157 min to 21 min, allowing an almost quantitative depletion within two hours (Renicke, 2013). A second series of psd degron in yeasts was later reported with extended range of sensitivity towards blue light induced degradation for the fine tuning of protein stability[3] (Usherenko, 2014

[3] Combination of site-directed or random mutagenesis and variations on the degron sequence generated psd variants whose characteristics were assessed *in vivo* and *in silico*. In most cases, low-stability in darkness correlated with short half-life under blue-light exposure, so that compromise has to be made between stability and degradation efficiency. However, psd candidates optimizing the dark/light ratio and short half-life upon light-illumination were selected.

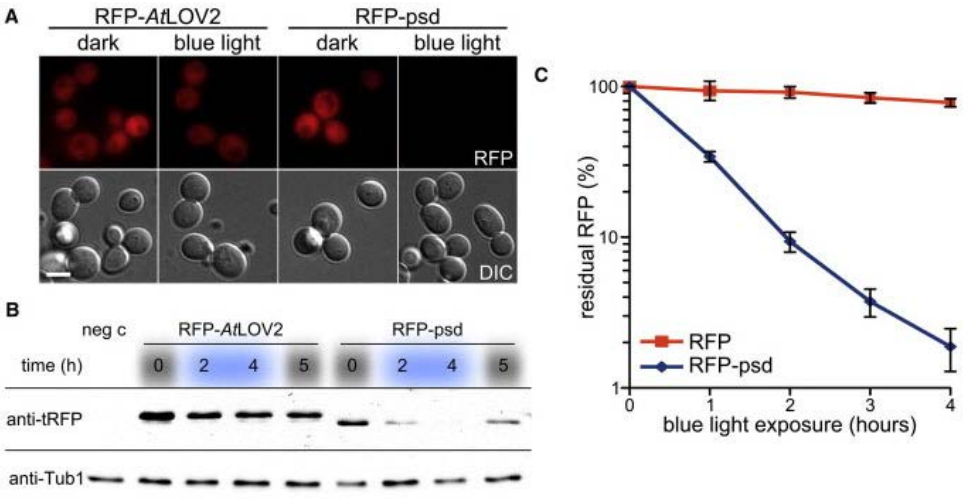

Fig. 7.2: Photosensitive LOV-domain based strategies for light-controlled of proteasomal degradation of POI developed in (Renicke, 2013). (A) Fluorescence micrographs of yeast cells expressing a reporter RFP protein fused either to *At*LOV2 (control) or psd in the dark or under blue light illumination. (B) Immunoblotting of yeast cells expressing RFP-*At*LOV2 or RFP-psd incubated with reported times in the dark or under blue light illumination. (C) Quantification of Blue-Light induced depletion of RFP-psd by immunoblotting. Control RFP is displayed (Renicke, 2013).

7.1.2.4 B-LID module enables blue light-mediated efficient degradation in vertebrates

Similarly, illumination with blue-light induced a significant depletion of a reporter protein fused to the B-LID domain in NIH3T3 culture cells with an estimated half-life of 30 minutes (Bonger, 2014). This blue-light induced protein depletion methodology was extended to the small transparent, Zebrafish embryo by injecting mRNA coding for a B-LID domain fused to a reporter fluorescent protein. Significant depletion in fluorescence was observed under blue light illumination. This work constitutes a proof-of-principle of the potential of the B-LID domain for the optical destabilization of POI in mammalian culture cells and vertebrate small organisms.

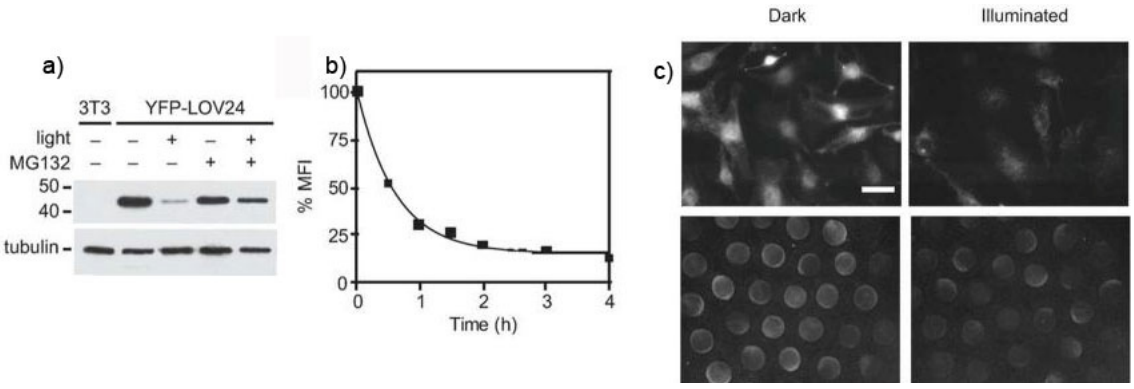

Fig. 7.3: Photosensitive LOV-domain based strategies for light-controlled of proteasomal degradation of POI developed in (Bonger, 2014). (a) NIH3T3 culture cells expressing YFP-B-LID treated with either vehicle or proteasome inhibitor MG132 were kept in the dark or irradiated under blue-light for 2 hours (b) NIH3T3 culture cells expressing YFP-B-LID were illuminated for various time. Mean fluorescence Intensity (MFI) was monitored with flow cytometry (c) NIH3T3 culture cells (top) or Zebrafish embryos (bottom) expressing mCherry-B-LID incubated in the dark or under constant blue-light illumination (resp. for 2 and 6 hours) (Bonger, 2014).

7.1.3 Comparison of the described photo-activatable degradation systems

7.1.3.1 Conditional degradation methods enable rapid and efficient depletion

The half-life and depletion extent of various POI in mammalian cells upon either small-molecule addition or light-illumination are reported on Table **7.1**. Consistently, these values range between 15 and 30 min. Although even faster degradation kinetics have been reported for heterologous POI (Holland, 2012), these results might indicate that the perturbation induction is not a rate-limiting step in conditional degradation.

POI target	GFP-AID-NLS			CyclinB-AID-YFP			B-LID-POI
Perturbation method	auxin	UV light		auxin	UV light		Blue light
POI half-life (min)	15	20		17	19		30
Residual POI after 1h	<10%	<20%		<5%	<20%		20%
Ref.	Section **3.3.2**	Section **5.2.2**		Holland, 2012	Section **6.2.1**		Bonger, 2014

Table 7.1: Comparison of three conditional degradation methods in mammalian cells, in which the stability of a POI can be controlled either by small molecule or light illumination. The half-life of POI after perturbation and residual POI monitored one hour after perturbation are reported.

In section **5.2.2** we reported that significant depletion is observed upon illumination.[4] We determined a half-life of 19 min. 20% of residual fluorescence was observed after one hour, consistent with other reports (Bonger, 2014). As we did not measure further the depletion induced by illumination after one hour, it not possible to determine whether this decay will continue, or if an asymptotic regime is attained. Bonger *et al.* reported that the fluorescence signal is stabilized at 20% from one to four hours post-illumination in the B-LID degradation methodology (Bonger, 2014).

Renicke *et al.* developed a kinetic model to explain the discrepancies observed between half-lives of heterologous proteins expressed with different strengths (Renicke, 2013). This model is presented on **Fig. 7.4.b**, and complemented with the equivalent for our methodology (**Fig. 7.4.a)**. At steady-state, depending on transcription rates, protein neo-synthesis might compensate the degradation, possibly explaining the remnant POI signal upon photolysis. This can be modulated by using constitutive promoters with variable strengths, or inducible promoters (Renicke, 2013).

[4] The increase of cytoplasmic fluorescence observed during experiment by the release a free EGFP, according to the model developed in section **3.2.2.3** was taken in account during in the quantification process.

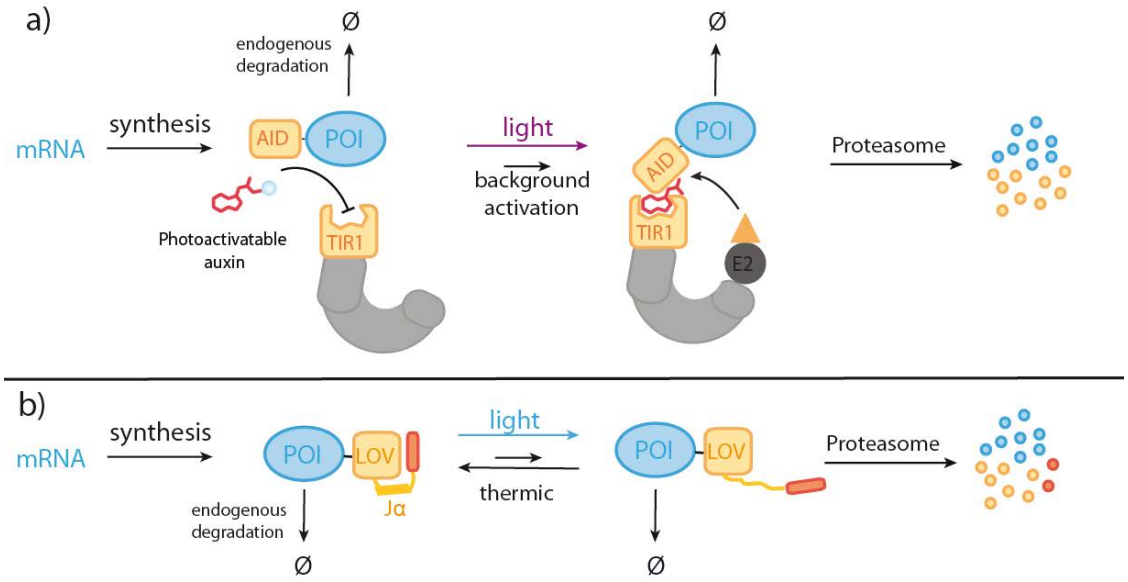

Fig. 7.4: Kinetic model for POI level modeling. Remnant level of POI at steady-state under perturbation can be explained by the balance between neo-synthesis accumulating POI and light-dependent or independent degradation mechanisms.

7.1.3.2 Light conditional degradation requires either constant blue light or UV pulses

Comparison of the illumination strategies are recapitulated on table **7.2**.

Method	**AID/PA-IAA**	**AID/PA-IAA**		**B-LID**		**Psd (yeasts)**
	Global	Local				
Light wavelenght	365 nm	365 nm		465 nm		465 nm
Illumination mode	8 min pulse	1s frequent pulses		continuous		continuous
Light irradiance	100 µmol.m^{-2}.s^{-1}	100 mmol.m^{-2}.s^{-1}		20 µmol.m^{-2}.s^{-1}		30 µmol.m^{-2}.s^{-1}
Cumulated irradiance in 1h	50 mmol.m^{-2}	1 mol. m^{-2}		60 mmol. m^{-2}		110 mmol. m^{-2}
Reference	Section **5.1**	Section **5.2**		Bonger, 2014		Renicke, 2013

Table **7.2**: Comparison of the illumination parameters for light induced degradation methods in eukaryotes.

Both B-LID and the PSD systems require long-term constant blue light illumination to maintain the LOV-domain in an active state for complete degradation. In contrast, our photo-activation system requires short pulses of UV light[5] every 5 or 10 min for significant degradation. This protocol can be easily implemented by manipulator, and is compatible with EGFP monitoring. Blue light is reputed less-toxic that long length UV light, although it was reported that it can induce phototoxic effects in mitochondria (Godley, 2005). However, neither of both wavelengths used at the reported rates are associated with phototoxicity according to literature (see note **B.32**).

[5] Contrary to other protocols for uncaging in vivo, the physiological function (proteasomal degradation) cannot be controlled by a single UV pulse, hypothetically due to active IAA efflux (see section **5.2.2**).

7.1.3.3 Light conditional degradation enables spatial control of depletion

The psd module allows macroscopic monitoring of blue light illumination: in yeasts cells expressing RFP-psd reporter protein, a direct inverted dependency links the RFP fluorescence to blue light illumination, allowing the creation of macroscopic fluorescence patterns by applying a simple illumination mask (Renicke, 2013). In both psd and B-LID methodologies, the spatial control of protein degradation was proved macroscopically; however, local photolysis up to the single-cell level is theoretically possible. In our work (section **5.3**), we showed that local photolysis of PA-IAA enabled to control protein degradation down to the single cell level, opening perspectives for spatial control of POI stability in complex biological structures.

7.1.3.4 Light conditional degradation is intrinsically limited by diffusion

The subcellular control of biological mechanisms with light is a highly desirable feature. However, spatial resolution is competed by diffusion processes which are rapid at the cellular scale. We estimate the timescale of auxin diffusion in the cytoplasm of HEK293 cells by applying the simple diffusion power law **7.1**:

$$D\tau = \frac{R^2}{6} \quad \textbf{(7.1)}$$

where D is a diffusion coefficient for intracellular auxin, evaluated to 700 $\mu m^2.s^{-1}$, and R is a typical length scale (13 μm for the typical diameter of HEK293 cells[6]). Using these parameters, we find a timescale τ = 40 ms for significant diffusion through the cytoplasm, four orders of magnitude lower than the half-life of conditional degradation methods in mammalians cells (15 min). Even in the fastest yeast-degradation systems, several minutes are necessary to ubiquitinate and degrade a substrate protein[7]. The spatial inhomogeneity induced by the photo-controlled liberation of free auxin is relaxed during the time necessary for ubiquitination and degradation. Similarly, for a photosensitive protein with an estimated diffusion coefficient of 30 $\mu m^2.s^{-1}$, we find a timescale τ = 0.9 s. This estimation implies that subcellular spatiotemporal control of protein degradation is not applicable to free-diffusing POI using photo-activatable methodologies[8].

[6] These numbers were found in *Bionumbers*, a very complete data base run by Pr. R. Philips, for biological parameters estimation (http://bionumbers.hms.harvard.edu/).

[7] The half-life of POI fused to destabilizing degron can be as low as two minutes for application of the N-end rule and typically range from 5 to 20 minutes.

[8] In 2011, Toettcher proposed to generate spatial patterns of activation for proteins that can be activated and inactivated by illumination at different wavelength, by coupling local activation and global inactivation (Toettcher, 2011).

7.1.4 Conclusion

Both PA-IAA and LOV domain-based tools (B-LID in vertebrates, psd in yeast cells) enable light conditional degradation of POI, with comparable kinetics and depletion extent. However, these classes of techniques rely on different endogenous proteasomal degradation pathways (resp. specific substrate recognition by SCF E3 ubiquitin ligase and quality control degron recognition), and on different light actuation mechanisms (caged small effector *vs* LOV-based light sensitive protein modules). It is therefore difficult to fully compare their implementation.

In this study, we implemented light actuation by manipulating a small phytohormone, auxin, in an heterologous dimerization system. The development of methodological tools adapted from plant hormones illustrates the potentialities offered by adaptation of molecular features to orthogonal species using a chemical biology approach. Several examples have been described recently. In the next part, we will focus on Gibberellic acid (GA)- and Abscissic acid (ABA)-based heterodimerization systems and their caged-equivalent for light control, in comparison to our work.

7.2 Development of caged phytohormone-based systems: a chemical biology approach

7.2.1 Development of photo-controlled Chemically-Induced Dimerization based on phytohormone

Concomitant to the publication of our work this year (Delacour, 2015), two papers reported light control of Chemically-Induced Dimerization (CID) systems based on plant hormones (Gibberellic acid and Abscissic acid) in mammalian cells. Interestingly, these studies present several similarities with our reported work; therefore, critical comparison of the three strategies for introducing light control in a heterologous system is an interesting perspective.

The phytohormone Gibberellic acid (GA) binds to plant protein GID1 and mediates a conformational change inducing dimerization with GAI. Similarly, Abscissic acid (ABA) controls the dimerization of proteins PYL and ABI. These plant systems were derivatized into orthogonal

CID in mammalian systems, allowing control of POI heterodimerization by addition of a small molecule (resp. (Lin, 2013) and (Liang, 2011)).

In both reported systems, chemical biology approaches allowed optimization of the CID. This included enhanced permeation of GA by carboxylate conjugation to esterase-sensitive groups, and reduction of GID1 sequence for the GA-based CID (Miyamoto, 2013). Similarly, PYL protein was engineered to inactivate the phosphatase activity, preventing toxicity in heterologous systems (Liang, 2011).

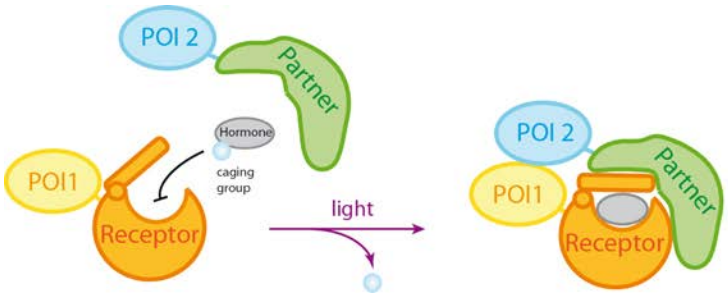

CID name	ABA	GA
Hormone	Abscissic Acid	Gibberellic Acid
Receptor	**PYL**	**GID1**
Partner	**ABI**	**GAI**

Fig. 7.5: Principle of Photo-controlled CID exemplified with the development of caged GA. Protection of an essential carboxylate by a caging group prevents its interaction with receptor GID1. UV light illumination liberates GA, which binds to GID1, inducing a conformational change allowing the heterodimerization of GID1 to GAI.

7.2.2 Photo-activatable phytohormones enable photo-control of dimerization

Caged-GA and caged-ABA for the development of light conditional dimerization were reported this year (resp. (Schelkle, 2015) and (Wright, 2015)) (**Fig. 7.5**). Rational caging strategy was in both cases based on crystal structure of the heterodimer receptor**:**phytohormone and plant physiology databases; these studies convergently identified a key carboxylic group. In both cases, this position was conjugated to various 2-nitrophenyl-based caging groups.

Both caged-GA and caged-ABA were efficiently liberated by UV light *in vitro*, as assessed by HPLC. In culture cells, they both mediated light-dependent heterodimerization of their respective receptors fused to reporter FPs, although much faster in the case of caged-ABA activation[9]. 10 µM caged-ABA were used for photo-control, comparable to our reported parameters (20 to 50 µM), whereas lower concentrations (1 µM) were necessary for caged-GA, with no background activation

[9] The illumination parameters for caged-ABA were: 120s illumination with peak excitation at 365 nm (power density: 23 mW.cm^{-2}), whereas these parameters were however not described for caged-GA in (Schelkle, 2015).

of either caged-dimerizer in the dark. However, neither study reported quantum yield values.

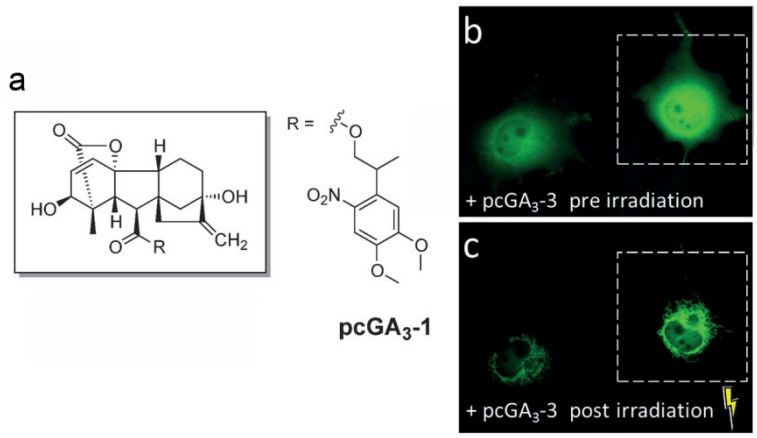

Fig. 7.6: (**a**) Structure of caged GA. (**b-c**) Epifluorescence micrographs of COS-7 cells expressing EGFP-GID1 and mCherry-GAI addressed to the mitochondria (TOM10-mCherry-GAI). 10s UV light liberation of GA induces the redistribution of the nuclear EGFP-GAI by GA-induced heterodimerization with mitochondrial GAI (Schelkle, 2015).

Furthermore, caged-ABA photo-liberation controlled heterodimerization of a split transcriptional activator, inducing gene expression in HEK293 and CHO cells (Wright, 2015). Spatial selectivity of light induced dimerization can be restricted to single (albeit individualized) cells using a 405 nm laser in the case of caged-GA (Schelkle, 2015), but not caged-ABA which is not efficiently cleaved in these conditions. Therefore, the DMNB caging group in caged-ABA was replaced by a coumarin-based caging group ([7-(diethylamino)-coumarin-4-yl] methyl group (DEACM)). This allowed efficient photo-control in vivo at 405 nm; however, spatial selectivity was not addressed in (Wright, 2015)[10].

Finally, conjugation of GA to a 2-(*o*-nitro-phenyl)-propyl derived caging group[11] enabled the two-photon photocontrol of GA-induced heterodimerization *in vivo* in COS7 cells. As two-photons allow deep-tissue penetration and high spatial resolution, this opens the way to new perspectives for CID control in small animals and tissues.

7.2.3 Comparison: photocontrolled CID and PA-IAA methodologies allow light induced depletion

[10] The authors seem to indicate that ABA diffuses outside cells post-liberation, although not detailing it.

[11] 2-(*o*-nitro-phenyl)-propyl caging group with a π-extended diphenylacetylene core structure bearing a functionalized dialkylamino moiety in *para*-position.

Caged ABA and GA offer methodologies for photocontrolled CID, with applications to sequestration of POI, which can be seen as a rapid conditional method for functional POI depletion[12] (DeRose, 2012), an alternative to light-activated degradation addressed in this work. Interestingly, convergent approaches were set to introduce photo-control and address the limitations met during the development of the methodology. These phytohormone-based CID methodologies, allow rapid, reversible, non-toxic heterodimerization controlled by a cheap small molecule and therefore offer interesting alternatives to reported photocontrolled CID systems based either on caged rapamycin (Umeda, 2010) or on caged bi-functional synthetic dimerizers (Ballister, 2014).

In conclusion, these two systems offer an interesting comparison with the work presented in this dissertation; in each case, a functional plant module heterologously expressed in mammalian culture cells could be photo-controlled by introduction of a photocaging group in a key carboxylic residue of the molecular inducer. They also illustrate the potentialities of phytohormones for chemical biology approaches, to be compared with fully-encoded CID tools presented on part **2.1.2**.

[12] For example, significant addressing of a nuclear transcription factor to the plasma membrane by CID leads to global genetic inactivation (Haruki, 2008).

Chapter 8: Perspectives

Strategies for photocontrol of protein stability

Having reviewed the existing methodologies for modulation of protein stability on chapter **1**, and for light actuation on chapter 2, we will now adopt the same approach to speculate on new strategies that could be used to implement protein degradation by light[13].

8.1 Strategies for the light control of proteins degradation by fusion of photo-sensitive protein domains

8.1.1 FP Dronpa might enable development of reversible photo-activatable degradation tools

8.1.1.1 Motivation: FP Dronpa monomeric state is reversibly controllable by light

On section **2.1.2.4**, we described the strategy developed by the group of Lin to control the association state of FP Dronpa variants with light (Zhou, 2012). Mutants 145N and 145K associate into a dimer in the dark. This dimer dissociates upon a 500 nm illumination, but is reformed either by thermal return or 400 nm illumination. This elegant approach allows a reversible photoactivation process, although protein engineering, with Dronpa fusion at each end can be challenging, and sometimes impossible ; therefore, it would be highly desirable to design generic Dronpa-controlled effectors designed as tools for the control of downstream target POI stability (LaBella, 2013), rather than engineering POI themselves with Dronpa.

[13] In 2013, while listing the existing strategies for conditional protein depletion, LaBella proposed various speculative possibilities to implement light control of protein degradation (LaBella, 2013). Some of these are discussed here.

8.1.1.2 Light modulation of protease activity by Dronpa

Interestingly, light control of the activity of Hepatitis C protease fused to Dronpa was reported (Zhou, 2012)[14]. This method might be extended to Tobacco-Etch Virus (TEV) protease, for reversible control of the activation of the TIPI degradation platform (blue light), or inactivation (violet light or thermal return) (see section **1.2.1.2**). As presented in Fig **8.2**, Dronpa-TEV-Dronpa fusion might be engineered with the following requirements:

- « native » protein is inactive due to Dronpa dimerization masking the TEV active site
- 500 nm light dissociates the Dronpa dimer, exposing the active site
- The Dronpa dimer is reformed by thermal return or 400 nm light, inhibiting TEV protease.

These specifications should be met by variation on the linker sizes, or the use of Dronpa variants. Alternatively, a TIPI variant method based on a hepatitis C cleavage site could be developed using the readily-described photo-controlled protease.

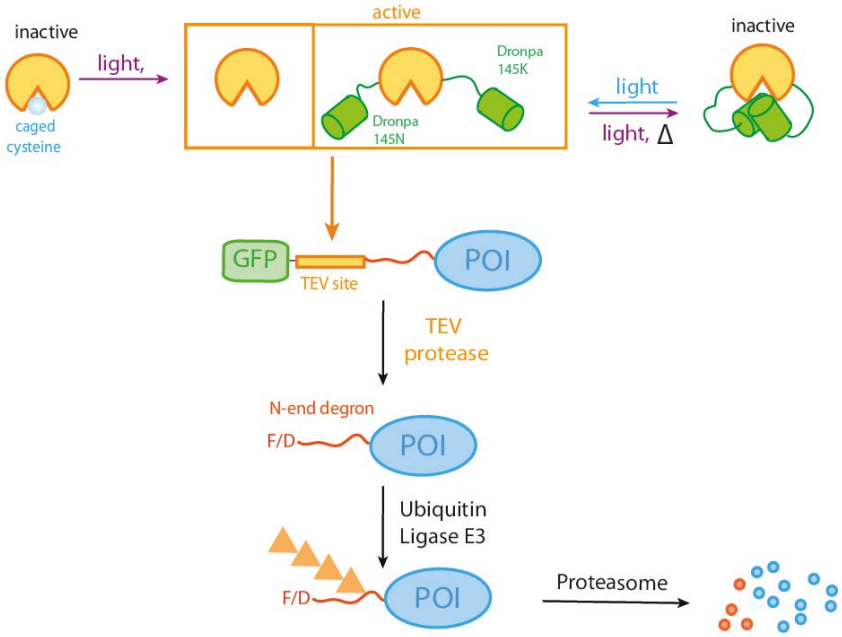

Fig. 8.1: Strategy for light controlled protease activation controlling the stability of a POI. The active-site of a TEV protease can be hindered by fused Dronpa variants (right). Blue light illumination dissociates the Dronpa dimer, liberating the active TEV protease. Alternatively, TEV protease can be modulated by photocaging of a key cysteine residue (left) **(8.3.1.2)**. Light activated TEV can condition the exposition of a degron sequence fused to a POI by selective cleavage of a TEV sequence in a TIPI strategy (see section **1.2.1.2**).

[14] Chimeric Dronpa-protease-Dronpa activation following blue light illumination within one hour was monitored by a Fluorescent Protein fused to a membrane-addressing tag separated by hepatitis C target sequence.

8.1.2 Development of artificial SCF Ubiquitin Ligase for optical dimerization

8.1.2.1 Motivation: Light induced dimerization can control ubiquitination of SCF substrates

As a general trend described in section **1.3.1**, physical proximity of a substrate with catalytic E2 Ubiquitin Transferase mediated by SCF complexes can be sufficient to induce their polyubiquitination. Modular F-box adapter allow specificity of substrate selection *in vivo*. This principle was adapted into the design of F-box artificial adapters targeting a specific POI, or the synthesis of bifunctional PROTACs addressing POI to endogenous F-Box.

Several examples of optical dimerizers were presented on section **2.1.2** as methodological tools for the control of heterodimerization of POI. A general strategy for the light control of protein degradation (**Fig. 8.3)** would be to engineer an artificial F-box protein with an optical dimerizer protein (e.g. F-box-Cry2, see **2.1.2.2**) (**Fig. 8.3)**. Differential affinity for a binding partner fused to a POI (e.g. CIB1-POI) would be triggered by light illumination and would result in the polyubiquitination and subsequent proteasomal degradation mediated by the close UCE E2.

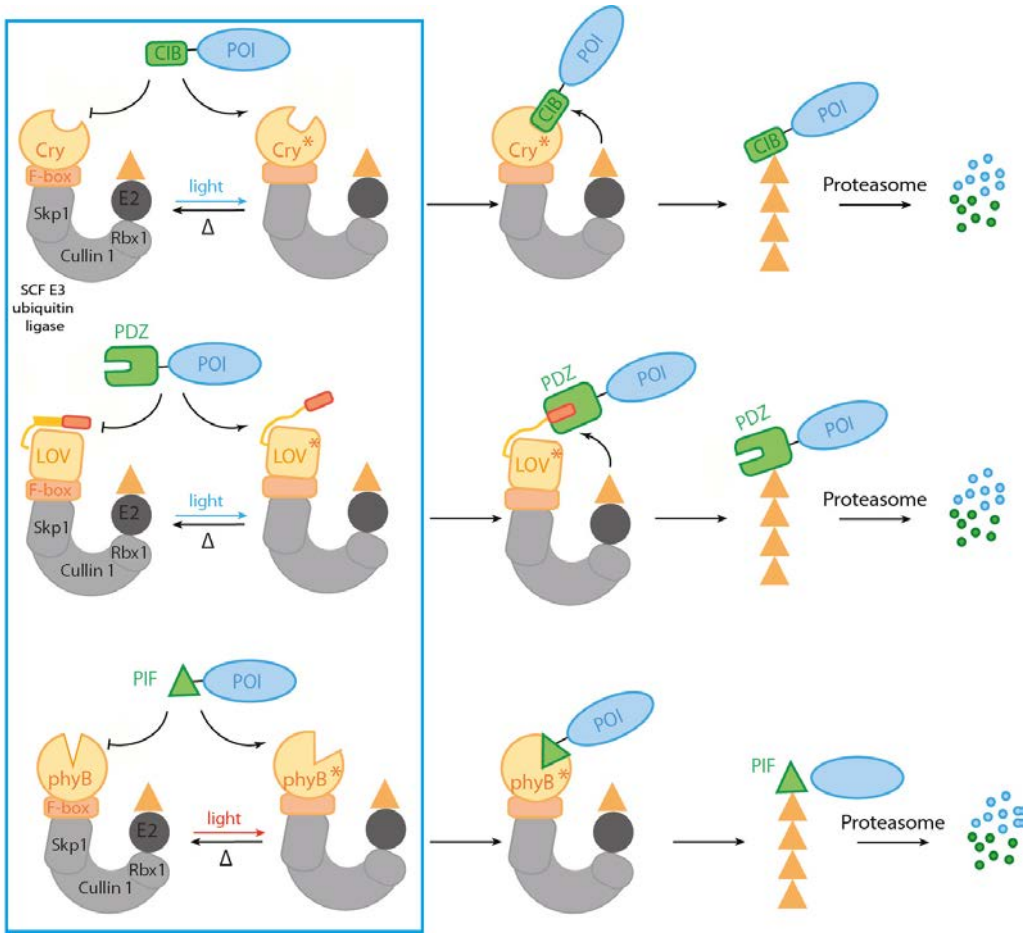

Fig. 8.3: Strategy for light-controlled ubiquitination of a POI. Artificial SCF adapter can be engineered by fusion of an F-box sequence to a light conditional dimerizing partner (see section **1.3.1**) This heterologous protein can interact with endogenous components to form an artificial SCF complex, which conditionally binds to an interacting partner fused to a POI upon selective light illumination. We present here possible examples based on the description in section **2.1.2**.

One important issue would be to prevent the auto-ubiquitination of the artificial F-box protein. This process has been described for endogenous F-box proteins (see note **A.27**) and might be due to accessibility of F-box proteins Lys residues to ubiquitination by spatially-close E2 enzyme.

8.1.2.2 Comparison of various optical dimerization systems

Development of optical dimerization relies on the choice of efficient light activatable platform. Recently, Pathak et al. compared the potentialities of three optical dimerizer systems (which have been further described on part **2.1.2**) using heterologous yeast transcriptional assay[15] (Pathak, 2014):

- Cryptochrome CRY2 and its binding partner CIB1
- TULIPs LOV2-domain-based with a peptide tag at the C-ter of the Jα-helix, binding upon light excitation to a engineered (ePDZ) domain
- Phytochrome-based phyB and its binding partner PIF.

The authors outlined that the phyB/PIF3 system combined low background activation and reversible control with far-red reversible control and the highest light activation over the four systems. Moreover, red light allows high tissue penetration and low toxicity in contrast to blue light. Drawbacks of this system however are the large size of the PIF domain, the required supplementation with 10 µM phycocyanobilin (PCB) fluorophore and the extreme light sensitivity which might be a constraint for users to prevent unwanted activation during manipulation.

In contrast, the two blue-light regulated systems CRY2/CIB and TULIPs offer lower-fold activation upon light illumination, and can present higher background-activation in the dark. Some TULIPs were also reported to be toxic in yeasts cells. These small systems offer high photo-switching dynamic range; however, they often require considerable adjustment dependent on each context to avoid background activation or slow kinetics upon light illumination.

8.1.2.3 Development of Dronpa-based SCF Ubiquitin Ligase for optical dimerization

Alternatively, the light-dependent dimerization of Dronpa monomer could be developed in already reported ubiquitination systems based on conditional dimerization. For example, an artificial F-box bipartite protein might be engineered by fusioning an F-box domain and a 145K Dronpa variant, separated by a linker. Upon blue light illumination, this artificial F-box could interact with and degrade a POI fused to a 145N Dronpa, with a light-reversible control (**8.1.1.2)**.

[15] Yeast two-hybrid using Gal4-BD-POI1 and Gal4AD-POI2 fusions controling the expression of a gene reporter (ß-galactosidase in this case) are widely used system for monitoring dimerization process. They have been presented on part **3.3.1.1** for the evaluation of auxin-dependent dimerization of AFB/Aux-IAA proteins.

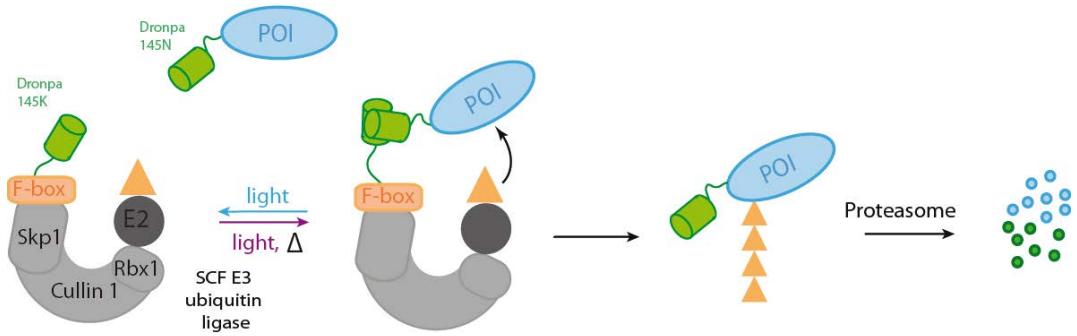

Fig. 8.2: Strategy for light-controlled degradation. Artificial SCF adapter can be engineered by fusion of an F-box sequence to Dronpa 145K (section **2.1.2.4**) This heterologous protein can interact with endogenous components to form an artificial SCF complex, which conditionally binds to a Dronpa145N fused to a POI upon selective light illumination.

8.2 Genetically encoded strategies for the light control of auxin inducible degradation

In this work, we implemented light-control over the AID protein degradation methodology presented in section **1.4.2.** Auxin triggers the direct interaction between F-Box protein TIR1 and an AID degron, forming a tertiary complex TIR1::auxin::AID. The small molecule auxin was conjugated with a caging protecting group (chapter **2**). Free-auxin can be liberated by light illumination, leading to the interaction of AID-tagged POI with SCF^{TIR1}, leading to the eventual proteasomal degradation of AID-POI. Alternatively, we will discuss in this part the possibility to control the activity of the two other partners TIR1 and AID by light.

8.2.1 Genetically encoded caged protein for the light control of AID degradation

8.2.1.1 Motivation

On section **2.2.1.3**, we described the methodologies for genetic incorporation of unnatural amino-acid, which led to the development of caged-proteins, whose activity can be controlled by light illumination, which photolyses the native residue and restores the initial activity of the protein. In this section, we will describe potential strategies for light controlled degradation of a POI. Implementing a caged-protein strategy to control auxin-conditional degradation implies to identify a key residue in either TIR1 or AID whose conjugation to a caging group affects the auxin-dependent heterodimerization. This strategy is summarized on **Fig. 8.4**. Compared to the PA-IAA liberation strategy described in this work which necessitated frequent short light pulse, a single light pulse would be sufficient to irreversibly activate TIR1 or AID, although the implementation of this approach might be complex.

8.2.1.2 Strategies for TIR1 light modulation by caged residues

As a first strategy, TIR1 activity could be controlled by light by conjugating an identified essential residue with a caging group. The structural mechanism of auxin-dependent heterodimerization of TIR1 and Aux/IAA was presented in section **4.1.1**. Auxin enhances the affinity of Aux/IAA by docking a hydrophobic LRR-pocket in TIR1. Outlined essential residues were Phe82 and Arg 403. However, no genetically-encoded caged-versions of these residues exist. Other close residues in the auxin-binding pocket include Ser 462 and Cys 405, for which strategies for incorporation of caged derivative have been described in section **2.2.1.3**. However, one should be aware that addition of a caging aromatic group might mimic the action of auxin by docking the hydrophobic pocket of TIR1, resulting in background heterodimerization with Aux/IAA17.

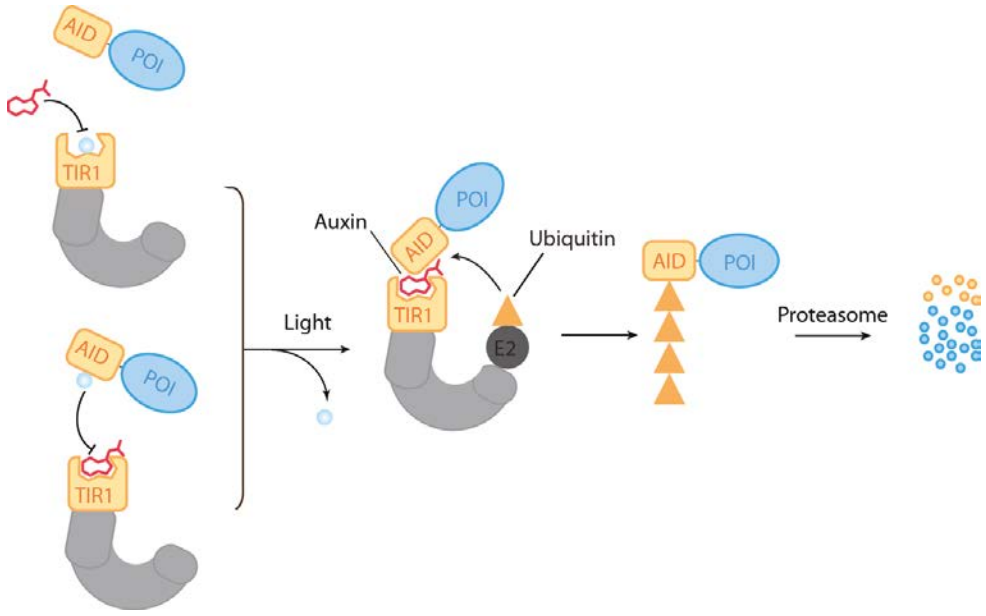

Fig. 8.4: Strategies for light controlled of the auxin-dependent dimerization of TIR1 and AID-POI proteins. Introduction of caged amino-acids replacing of residues critical for interaction, either in TIR1 or in AID sequence can hinder the interaction site; UV light illumination liberates the active site for interaction; leading to the polyubiquitination and eventual proteasomal degradation of AID-POI.

Alternatively, the K35A mutation was reported to abolish the TIR1-auxin interaction, although it is not located on the auxin-binding pocket nor on the interaction surface with Aux/IAA (Kepinski, 2005). The K35 position in TIR1 could be inactivated by incorporation of a genetically encoded caged-Lys a.a.; the full-activity might be recovered upon UV illumination, liberating active Lys[16].

[16] Lys 485 controling insertion of Inositol 6-P is another potential residue for a caging strategy. Adjacent S462E mutation is sufficient to abolish auxin enhanced binding, but does not inhibit basal binding to TIR1 (Tan, 2007).

8.2.1.3 Control of the auxin-dependent interaction by AID caging

Another possibility would be to introduce photo-control by caging of residues in the AID protein[17]. This involves the identification of essential residues whose conjugation to a photosensitive caging group globally inactivates AID function. Two distinct features can be identified in AID degradation:

a) Auxin-dependent heterodimerization

AID/TIR1 heterodimerization is directly mediated by auxin, through hexapeptide hydrophobic motif VGWPPV in domain II (see section **4.1.1**). However, no genetically-encoded caged-versions of these residues have been yet described. Implementation of this strategy would require the new developments in the unnatural mutagenesis technology.

b) AID polyubiquitination

An alternative strategy would be to identify preferred sites for Lys ubiquitination (section **1.1.2**) and to inactivate them by conjugation with a caging group. A similar approach allowed, for example, the photocontrol of nuclear import of POI by photocaging essential Lys residues in NLS (Gautier, 2010).

K35Q (Villalobos, 2012) and K37Q (Droher 2006) mutations diminished the auxin-binding by resp. 50% and 70%, but do not quantitatively inactivate the protein function. A systematic analysis was recently led in Aux/IAA1 (Gilkerson, 2015): Lys to Arg mutations were introduced to interrogate the role played by each of the 16 Lys residues. None of these modifications significantly prevented auxin-dependent[18] degradation, or nuclear addressing and auxin-dependent association with TIR1. Surprisingly, mutations of all Lys residues to Arg did not prevent the rapid degradation of Aux/IAA, although at slightly lower rates. This results indicate that ubiquitination of Aux/IAA17 upon auxin addition might take place at non Lys sites, such as N-end amine, Ser/Thr hydroxyl or Cys thiols. In the current model description, Lys residues are the preferential acceptors of ubiquitination: but neighboring residues can be efficient redundant sites for Ub conjugation in their absence.

However, even if complete inactivation of the degron sequence can be achieved by essential Lys residue photocaging, another issue is that Lys residue present in POI fused to AID could be

[17] Although the domain DII has been identified as essential for interaction with TIR1, other sequences are required for rapid degradation. (Villalobos, 2012) The AID sequence can be reduced to 40 a. a. in yeast without affecting the degradation kinetics, contrasting with our reports using similar methodology in mammalian cells (cf section **1.4.2**).

[18] The Aux/IAA1 variants were still rapidly degraded upon auxin degradation. The authors first hypothesized that the 3 conserved Lys residues in Aux/IAA variants were preferentially polyubiquitinated, but no specific degradation inhibition was observed upon K to R mutation.

ubiquitinated due to the plasticity of SCF E3 Ubiquitin-Ligase (see section **1.3.1.1**). It would thus be necessary to ensure that no Lys residues in POI are structurally close to E2, which would limit the development of generic degradation tools.

8.2.2 LOV domains-based systems for allosteric presentation of a degron

8.2.2.1 Motivation: development of LOV2-based degradation modules

In section **2.1.2.1**, we presented the *At*LOV2-based domain modules and their applications. In these modules, the conformational change induced by blue light illumination lead to the dissociation and unfolding of the Jα helix. This light-driven process paves the way for a chemical biology approach for the control of proteasomal degradation. In section **7.1.2**, we presented the strategies developed by the groups of Taxis and Wandless for light-controlled degradation, resp. in yeasts and vertebrates. In these approaches, a chimeric protein can be engineered by fusion and directed evolution of a light-sensitive LOV-derived module and a degron sequence fused to the Jα helix. Instability can be conferred by differential presentation of a degron driven by blue light illumination.

8.2.2.2 Development of LOV2-based conditional AID degradation

This strategy might be extended to AID-based systems. As presented in section **1.4.1.2**, a hexapeptide sequence in Domain II of AID sequence interacts with TIR1**::**auxin. Although the sequence of domain II alone is sufficient for dimerization in crystal structure, its affinity for TIR1::auxin is ten-fold lower than the full-length AID. A 40 residue short version of AID, containing Domain II and adjacent residues was however as efficient as full-length AID (see section **3.5.3**).A first strategy presented would be to fuse a minimal AID degron to the Jα helix in C-ter of a *As*LOV2 domain (**Fig. 8.5**).

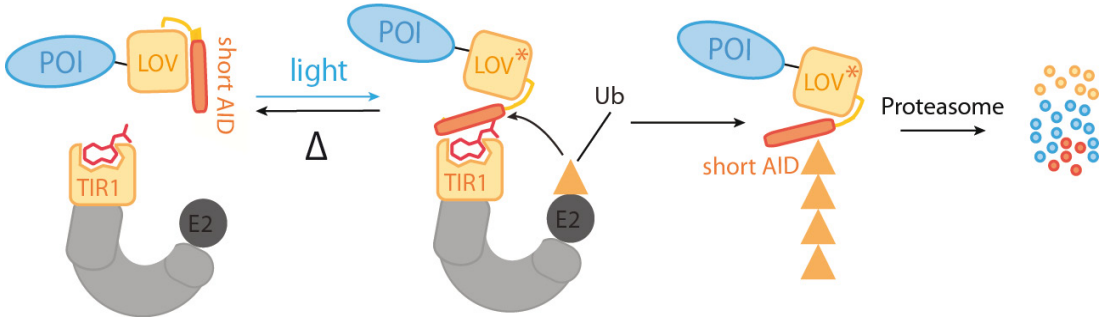

Fig. 8.5: Strategy for blue-light-control of the degradation of a POI. A functional short AID tag is fused at the C-ter to the Jα-helix of a LOV-domain. In the dark, the interacting hexapeptide is hindered by the LOV-core domain. Blue-light activation undocks the AID which dimerizes with a heterologous SCF^{TIR1} in presence of auxin, leading to its polyubiquitination and proteasomal degradation.

In this approach, the hydrophobic hexapeptide in domain II would be hindered by interaction with the LOV2 core domain, whereas blue-light illumination would result in the presentation of the degron, interacting with TIR1 in presence of auxin, leading to the polyubiquitination and eventual proteasomal degradation of a POI fused to LOV-short AID domain.

8.3 Alternative strategies for the light-control of protein degradation

8.3.1 Caged cysteines for the control of enzymatic-dependent proteolysis

8.3.1.1 Motivation

The ability to implement caged-cysteine modified POI provides interesting perspectives for the photo-control of cellular pathways, as key cysteine residues are involved in several important enzymatic pathways[19] including UAE E1 and UCE E2 enzymes (see section **1.1.2.2**).

8.3.1.2 Caged cysteine for photocontrol of TIPI degradation

A photo-activatable Tobacco Etch Virus (TEV) protease engineered by directed evolution of the PylRS/$tRNA_{CUA}$ to incorporate photocaged cysteine was recently reported (Nguyen, 2014). In HEK293 cells, 365 nm illumination can induce the fast activation of the caged TEV protease (80% within 15 min), as monitored by the FRET signal of fusion reporter proteins composed of two Fluorescent Proteins separated by a TEV cleavage site. This photoinducible TEV protease could be inserted into the TIPI system described in section **1.2.1.2** for light-control of POI cleavage and degron exposure (**Fig. 8.2**). A single light pulse might be sufficient to irreversibly activate the TEV protease, in contrast to the reversible Dronpa-based methodology proposed on section **8.1.1.2**.

8.3.2 Caged small molecules modulating protein stability

8.3.2.1 Caged Rapamycin

An efficient strategy for the subcellular control of dimerization by a caged-rapamycin[20] has been reported (Umeda, 2010). UV illumination releases a macromolecule tethered to rapamycin C40

[19] Genetically encoded strategies applied to phosphorylation, Intein control, or Caspases controlling apoptosis using caged Cys were reported (Baker, 2014).

[20] Another reported strategy involves direct caging with a bulky group at the C40 hydroxyl position of Rapamycin (Karginov, 2011) However, the caged-rapamycin itself is active, requiring introduction of a modified FKBP dimerizer.

hydroxyl group by a light-sensitive linker. Enhanced subsequent permeability of rapamycin allows its entry into NIH3T3 cells where it can trigger the heterodimerization of heterologous FRB and FKBP-POI. This strategy was used to control the subcellular localization of the small GTPase Rac. A photoactivatable rapamycin could conditionally control the interaction of a POI-FRB and an artificial FKBP-F-box protein functionally inserted into an SCF complex (**Fig. 8.6**).

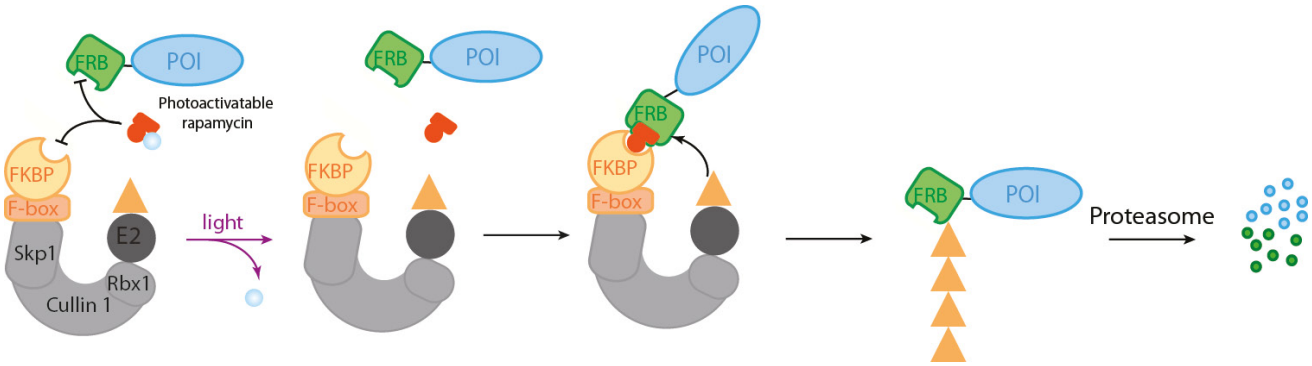

Fig. 8.6: Strategy for light-conditional control of addressing of a POI by a Chemically Inducible Dimerization (CID) system. An artificial SCF adapter can be engineered by fusion of an F-box sequence to FKBP. This heterologous protein can interact with endogenous components to form an artificial SCF complex, which can conditionally bind an interacting partner fused to a POI upon rapamycin addition. Free-Rapamycin disponibility can be controlled by light using a described caged –version of rapamycin.

Alternatively, introduction of a caged rapamycin methodology would allow photocontrol of the strategies reported on chapter **1** for rapamycin-conditional POI degradation. These included:

- direct addressing to proteasome, mediated by FRB-Rpn10 (section **1.1.1.2**)
- conditional stabilization of a constitutively degraded POI fused to an unstable FRB variant (section **1.2.2.2**)
- conditional control of Split Ubiquitin processing to release a constitutively degraded POI (section **1.2.1.2**).

8.3.2.2 Caged Trimethoprim

As described on section **1.2.2.2.a,** Trimethoprim (TMP), a small-inhibitor of *E. coli* protein Dihydrofolate Reductase protein (*ec*DHFR) has been reported as stabilizing the ^{ts}DHFR degron upon temperature-shift. Recently, a caged TMP was described for light-conditional interaction between TMP and *ec*DHFR[21] (Ballister, 2014). This tool might allow combination of light and temperature-control for the conditional stabilization of ^{ts}DHFR-based degrons.

[21] TMP diaminopyrimidine ring was caged using a nitroveratryl-carbamate coupling strategy. This caging inhibited the binding with ecDHFR. Photorelease by 387 nm illumination led to the rapid (15s) but reversible (by addition of free TMP) recruitment of *ec*DHFR-FP to centromeres in HeLa cells.

8.4 Conclusion

In this section, we proposed alternative strategies for light-control of protein degradation, based on the combination of conditional destabilization methods strategies described in chapter **1**, and the tools developed for light-actuation described on chapter **2**.

Methodological development of light-inducible degradation techniques with different characteristics might constitute a useful “toolkit” for biologists. These techniques could be implemented in a chemical biology approach, depending on the experimental specifications. For example, light actuation can be triggered at different wavelengths. Phytochrome-based modules or two-photon uncaging strategies allow red and far red activation, an interesting alternative to widely used UV and blue light actuation methods. Fully encoded methodologies, such as caged-amino acids or photosensitive proteins modules can be particularly efficient strategies in systems such as yeasts which can be easily genetically modified.

Consequently, the choice of a photoactuation method depends on experimental specifications and on several parameters, including the organism, the developmental stage, the target POI or the illumination tolerated. In the next chapter, we will propose two biological contexts in which the implementation of light-induced degradation methodologies might be an interesting approach.

Chapter 9: Perspectives

Light-activatable degradation could be a relevant perturbation method in various contexts

We next discuss applications of light-activatable degradation methodologies, which can be potential approaches to monitor the activity of a given POI. We identified two biological systems in which UPS degradation plays an essential regulation role by controlling the stability of various substrates. We thus discuss here the possibility of implementing on-demand artificial ubiquitin ligase for the spatio-temporal control of protein target stability in these contexts.

9.1 Cyclins are potential POI for further understanding the cell-cycle progression through spatio-temporal perturbative methods

9.1.1 Cyclin B stability is regulated during the cell-cycle

In chapter **6**, we have been considering Cyclin B1 as a reporter fusion protein for cytoplasmic degradation, without evaluating the physiological perturbation triggered by the light-activated degradation of exogenous Cyclin B1-AID-YFP. However, in a single event (see section **6.2.3**), degradation of a nuclear-translocated Cyclin B1-AID-YFP by PA-IAA photoactivation led to an intriguing oriented rotation of the mitotic spindle.

In this part, we will discuss more precisely on the biological role of Cyclin B and the possibility to monitor direct cellular changes in responses to a light-induced degradation, which is one of our initial motivation.

9.1.1.1 Cyclin B activity regulates early mitotic events

The eukaryotic cell-cycle is a highly time-regulated process (Alberts, 2007, chap. 17). Cyclin-dependent protein kinases (CDKs) control cell-cycle events by phosphorylation of key substrates, requiring activatory subunits called cyclins. These regulators are expressed in a cell-cycle dependent manner and mediate downstream activation.

In human cells, cyclin B/cdk activation has been historically described as the major event controling the mitotic state entry. Coherent with its name, the Cyclin B level oscillates during the cell-cycle: most of Cyclin B is synthesized over the G2 phase, and peaks during early mitosis. During S and G2 phase, Cdk1:Cyclin B is located in the cytoplasm[22], and inactive due to phosphorylation of the Cdk1 subunit, which is mediated by a complex balance of phosphatases (Burgess, 2010). This regulation prevents premature entry into mitosis. In early mitotic events, the active complex is translocated into the nucleus, where it regulates essential steps of cell cycle progression during early mitosis: chromosome condensation, assembly of the mitotic spindle and Nuclear Envelope Breakdown (NEB) (Tuck, 2013) (**Fig. 9.1**).

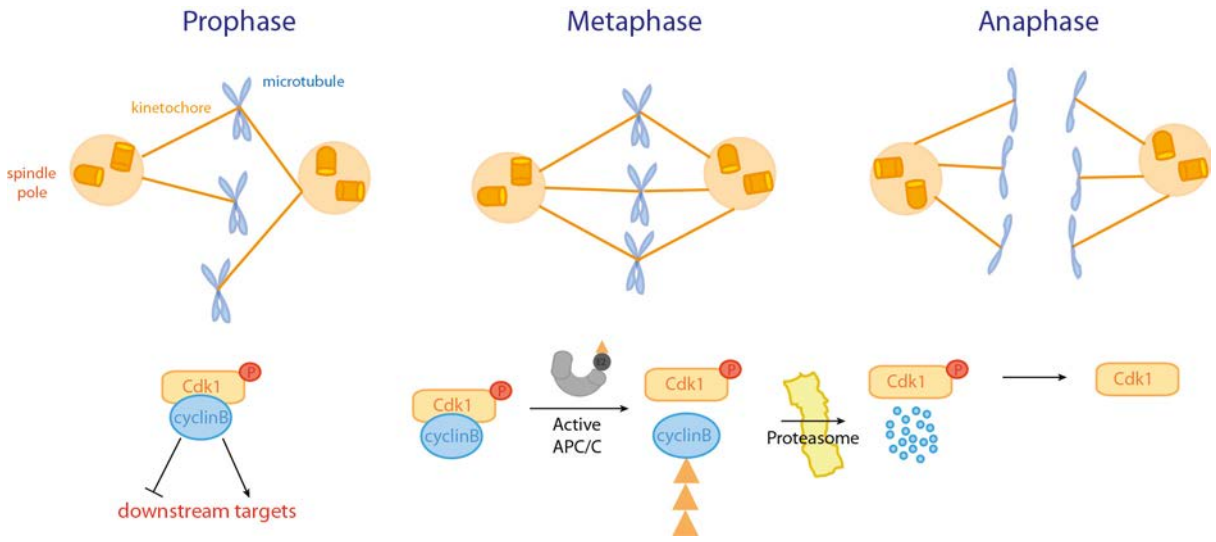

Fig. 9.1: Model for Cyclin B role in early mitotic steps. In (**prophase**) Cyclin B forms an active complex with phosphorylated Cdk1, controling various downstream targets; in (**metaphase**) Spindle Activation Checkpoint (SAC) inhibition as chromosomes are properly aligned at the metaphatic plane activates E3 ubiquitin ligase APC/C, targeting Cyclin B for proteasomal degradation. In (**anaphase**) Cdk1 is inactive in absence of Cyclin B, concomitant with chromosome separation and cytokinesis.

[22] Cyclin B-Cdk1 is targeted for ubiquitination in the nucleus by SCF^{NIPA} to prevent early activation until late G2, where NIPA activity is silenced by phosphorylation, enabling nuclear accumulation of Cyclin B (Bassermann, 2005).

9.1.1.2 Cyclin B degradation is concomitant to mitotic progression

Eventually, Cyclin B is degraded at anaphasis by an E3 ubiquitin ligase Anaphase Promoting Complex (APC/C) with a fine temporal control. APC/C is inactive until Spindle Assembly Checkpoint (SAC); resulting in Cyclin B polyubiquitination and its rapid proteasomal degradation[23] (see Chen, 2014 for a recent complete model). Consequently[24], in telophase, mirror phenomenons are observed compared to pro- and metaphase: chromosome decondensation, spindle disassembly and nuclear envelope reconstitution, concomitant with reduced CDK activity.

9.1.1.3 Cyclin degradation is a general strategy for cell-cycle regulation

CDK oscillations are generated by complex regulatory networks at the transcriptional, translational and post-transcriptional level, such as proteolysis and phosphorylation control. However, contrary to the latter, UPS dependent degradation is an irreversible process, ensuring unidirectionality. Therefore, it allows the precise spatial and temporal proteolysis of the main components of the cell cycle machinery. Overexpression of a non-degradable mutant of Cyclin B in HeLa cells induces mitotic arrest and rapid cell death in G1 phase (Eichhorn, 2014), indicating that the time-controlled degradation of Cyclin B is an essential process for cell survival.

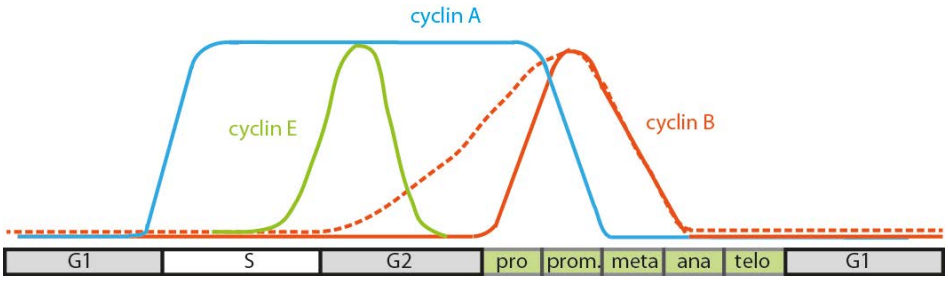

Fig. 9.2: Activities of Cyclin A, B and E along the cell-cycle. The total Cyclin B (inactive and active protein) is represented in red dotted lines

Others cyclins have different temporal activation patterns (**Fig. 9.2**): Cyclin E/Cdk2 activation starts in late G1 phase, initiates the DNA replication in S-phase and is degraded by the SCF as the cells progress through S and G2 phases. Similarly, Cyclin A/Cdk2 is involved in the G2/M transition. While both mitotic Cyclin A and Cyclin B are ubiquitinated by the APC/C, their temporal

[23] However in prometaphase, APC/C^{Cdc20} enhances Cyclin B activity by degrading specific inhibitor p21.

[24] A direct link exists as mitotic Cyclin:Cdk inhibit Separase controlling sister chromatide separation. Separase is above all inhibited by its interaction with the chaperone Securin, which is degraded upon APC/ C activation, leading to Cohesin degradation and chromatide segregation. Cyclin B degradation also activate Cdh1, an APC/C substrate adapter inactivated by phosphorylation in early mitosis.

degradation profile is different: cyclin A is degraded in prometaphase, whereas cyclin B degradation starts in metaphase/anaphase transition [25]. Therefore, temporal control of this degradation is important to prevent mitotic defects.

9.1.2 Cyclin B is targeted for degradation by APC/C

The E3 ubiquitin ligase APC/C is structurally related to the SCF complex, although with a more complex description due to the higher number of components. Two co-activators: Cdc20 and Cdh1, conferring substrate specificity (comparable to F-box protein in SCF) associate with the APC/C core at differential stages during cell cycle during cell-cycle progression. Activated at the end of metaphase, the APC/C thus coordinates the late mitosis progression (APC/C^{Cdc20}), and exit (APC/C^{Cdh1}) to establish a stable G1 phase (Sarikas, 2011).

Prior to anaphase, APC/C is inhibited by the Spindle Assembly Checkpoint (SAC), an essential mitotic mechanism regulating the correct attachment of kinetochores to the spindle fibers and the alignment of chromosomes on the metaphase plate. Mitotic checkpoint proteins such as Bub3 and Mad2 sequester Cdc20 in a Mitotic Checkpoint Complex (MCC), inactivating APC/C^{Cdc20}.

A complex interplay exists between APC/C and SCF based E3 ubiquitin ligases. Illustrating this, APC/C^{Cdh1} targets cell-cycle progression promoter F-box Skp2 (see part **3.2.3**) for degradation; consequently, inactivation of APC/C^{Cdh1} in late G1 allows the accumulation of SCF^{Skp2}, promoting cell-cycle progression through degradation of specific regulators. As a general trend APC/C and SCF complexes have antagonist activities during the cell-cycle and might constitute a regulatory loop. This dual repression system between ubiquitin ligases can account for the time control of cell-cycle transitions. It also illustrates the complex regulation of UPS components which are themselves targeted for degradation.

[25] Intringuingly, Cyclin A is degraded in early mitosis, a stage at which its specific ubiquitin ligase APC/C should be inhibited by active spindle checkpoint; this process might involve an APC/C independent process (van Leuken, 2008).

9.1.3 Cyclin B is a potential POI for further understanding of the cell cycle progression through spatio-temporal perturbative methods

9.1.3.1 Motivation: perturbation of the spindle positioning by light-induced degradation

In Chapter **6**, we described the implementation of an artificial $SCF^{TIR1,}$ mimicking APC/C^{Cdc20} for the light-conditional degradation of Cyclin B1; however, contrary to the latter, this on-demand degradation system can be activated at any cell cycle state.

On a single event (section **6.2.3**), we observed that the light-induced depletion of nuclear-translocated Cyclin B1 led to a global perturbation of the mitotic spindle positioning. Oriented rotation of the spindle around the cell was observed. We will now discuss this observation by comparison with reports from the literature.

9.1.3.2 Cyclin knockdown perturbates mitotic progression and spindle positioning

Cyclin B knockdown by siRNA (Yuan, 2004) and conditional stabilization by Shield1 ((Chu, 2009), see section **1.2.2.2**) was reported. Significant depletion of Cyclin B led to G2/M arrest in mammalian culture cells. However, depletion was achieved on a day timescale and the temporal evolution of individual cells upon Cyclin B depletion was not addressed.

Complete depletion of Gwl (Greatwall), a critical Ser/Thr kinase phosphorylating Cyclin B-Cdc2, by siRNA for 48h arrests human cells in G2 (Burgess, 2010). However, partial depletion by a lower siRNA dose induced multiple defects in spindle assembly and mitosis. Consistently, severe cytokinesis defects were observed in a large number of cells, in a siRNA dose-dependent manner. In some cases, dynamical rotation of the spindle within the cell was visible. Alternatively, defects in chromosome congression or segregation were observed. Interestingly, no metaphase rotation was observed upon introduction of a non-degradable form of Cyclin B1.

Even more dramatic effects are associated with Cyclin A knockdown in HeLa cells (Beamish, 2009). Off-centering and dynamic rotation of the incomplete metaphase plate were often observed, along with chromosome impairment in anaphasis[26]. This rotation was hypothetically linked to the inactivation of Cyclin A/Cdk. Consistently, similar rotation was observed with siRNA knockdown of Cdc25B, an activator of cyclin A/cdk2.

[26] The metaphase plate orientates to allow subsequent division along the longest axis of the cell; a limited rotation of the metaphase plane might be consequently observed for the ajustement of this positioning (O'Connell, 2000).

9.1.3.3 Perturbation of the spindle positioning can be associated with spindle rotation

Using cells grown on adhesive micro patterns, Fink et al. showed that specific adhesion geometry might control mitotic spindle orientation (Fink, 2011). Slight rotation of mitotic spindles (10° –15°) was observed between late prometaphase and metaphase in control cells. Laser ablation of retraction fibers, or external forces applied on mitotic cells can trigger significant spindle rotation. Nocodazole, a microtubule-depolymerizing drug inhibits the spindle rotation in anaphase, indicating that astral microtubules are required for this process.

Selective small-molecule inhibitor of CDK1 RO-3306 has been identified, which reversibly arrest human cells at the G2/M (Vassilev, 2006), preventing mitotic entry or inducing mitotic exit. Upon low doses of molecule RO-3306 (a Cdk1-specific inhibitor), a minority of spindle rotation and lagging chromosome are observed upon incubation (McCloy, 2014). However, CDK1 interacts with several Cyclin partners other than cyclin B along the cell-cycle, so that RO-3306 might globally affect the spindle positioning.

9.1.3.4 Perspective: ecchronic degradation of Cyclin as a cell-cycle perturbation method

Cell division control is essential for cell-fate or organism development; proper division geometry or equirepartition of chromosomes are regulated by endogenous mechanisms such as the SAC. UPS degradation is an important effector of spatio-temporal control. Targeting of cell cycle effectors such as Cyclin B by E3 ubiquitin ligases APC/C^{Cdc20} at specific states can trigger their functional depletion, resulting in differential physiological outputs. The ubiquitin ligases themselves are temporally regulated, with a complex regulatory network between SCF and APC/C-based Ubiquitin-Ligase. APC/C is activated after SAC inactivation in late metaphase, leading to Cyclin B degradation (Sarikas, 2011).

In Chapter **6**, we described an artificial SCF^{TIR1}, mimicking APC/C^{Cdc20} for the light-conditional degradation of Cyclin B1; however, contrary to the latter, this on-demand degradation system can be activated at any cell-cycle state, with a timescale much smaller than siRNA depletion. This perturbative approach might be relevant to interrogate the activity of Cyclin B, as well as regulation of cellular processes by APC/C, by degrading Cyclin B at times such as prophasis when APC/C is normally inactive. This process can be extended to other cyclins which also present a differential activity or sensitivity to degradation along the cell cycle. It might also be relevant for better understanding the complex interplay between various cyclins[27].

[27] Slow cyclin A destruction is associated with delayed cyclin B destruction, which might be explained by SAC

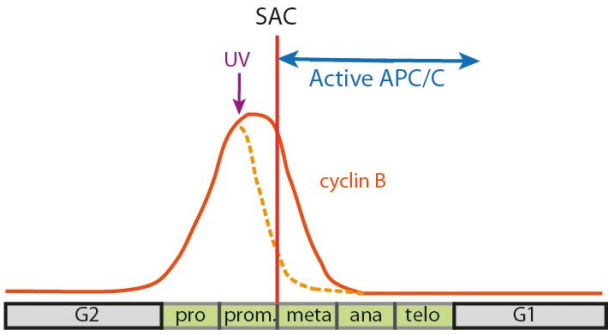

Fig. 9.3: Expected activity profile upon light-triggered premature degradation of Cyclin B before SAC by an artificial APC/C-like ubiquitin-Ligase.

In 2013, Renicke *et al.* proposed to implement cell cycle control by light-induced degradation (Renicke, 2013). Dominant-active versions of regulators of Cdc28 were fused to a psd module, including Cyclin B/Cdc28 inhibitor Sic1 lacking its degradation sequence. Therefore, regulation of the stability of effectors is set by light-modulation instead of the endogenous cell cycle mechanisms. This allows ecchronic modulation of the degradation of cell cycle effectors by illumination, resulting in significant visible phenotype alteration. This confirms that light-activatable degradation can be a functional tool for the generation of conditional mutants and the analysis of cell cycle mechanisms.

9.2 Light-induced degradation can be relevant to study the generation of spatio-temporal pattern of morphogens in living systems

9.2.1 Morphogen distribution generate developmental patterns

9.2.1.1 Motivation

The generation of spatio-temporal patterns in living systems by diffusible morphogen molecules is a fascinating example of interplay between theoretical prediction and experimental observations[28].

inactivation, or perturbation of the APC/C activation (Di Fiore, 2010).

[28] The hypothesis that gradients of morphogenic chemical substances can explain the patterns observed in multicelular organisms roots in previous embryological observations (Wartlick, 2009); in particular, the Spemann organizer discovery in the 1920s suggested that local groups of cells were able to release signals control the differentiation of surrounding cells. This mechanism was formalized by Alan Turing in 1952, who proved reaction diffusion models were able to generate spatial patterns of morphogen concentration. This formalism led to the « French Flag model » by Wolpert in 1969: morphogen secretion by source cells (and degradation by a sink) creates a gradient of concentration, which itself generates a spatial pattern of gene expression in response to differential thresholds. This model was later

Morphogen gradients can generate precise positional information, which determines downstream developmental decisions. In the classical « French flag » model, differential distribution of a transcription factor along the embryonic axis induces differential genetic pattern due to transcriptional activation.

Quantitative approaches are necessary to study the molecular mechanisms controlling the formation of these gradients. In this part, we will focus on the protein Bicoid in *Drosophila*, the paradigmatic example of a morphogen gradient. Other morphogen gradients examples (mostly in *Drosophila* and *Danio* embryos) are listed in (Kicheva, 2012), along with their diffusion coefficient and their characteristic lengthscales.

9.2.1.2 The Bicoid morphogen controls the Antero-posterior polarity in *D. melanogaster*

Bicoid is a homeodomain transcription factor responsible for the acquisition of the antero-posterior (AP) polarity in *Drosophila melanogaster* (Hecht, 2009). Maternal *bicoid* mRNA is localized at the anterior pole of the oocyte[29]; egg deposition initiates the synthesis of Bicoid and its diffusion through the embryo; this results in the formation, in 2 hours, of a Bicoid gradient along the AP axis (in cycles 10-14) (**Fig. 9.4**).

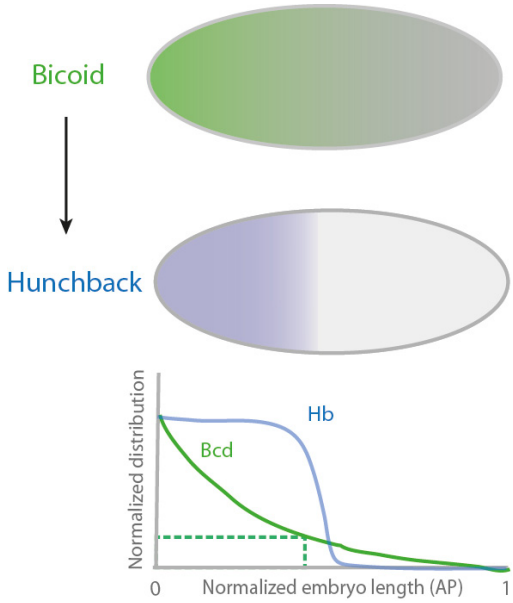

Bicoid controls the highly robust expression of downstream effectors, such as Hunchback (Hb)[30]; this simple model can explain the reproducible acquisition of the segmentation in the body plan of the embryo.

Fig. 9.4: Overview of Bicoid gradient in Drosophila embryo. Diffusion of Bicoid along the Antero-Posterior (AP) axis creates a gradient which modulate Hunchback expression

validated experimentally with the identification of the paradigm morphogen Bicoid as a regulator of the Antero Posterior (AP) identity (Frohnhofer, 1986).

[29] However, restricting the source of Bicoid production to a single point is an idealized approximation. More elaborate models can include the distribution of the *bcd* mRNA profile (Liu, 2011 II).

[30] An accuracy of 10% of Bcd gradient reproducibility is observed between embryos while 10% precision is observed in the readout of Bcd by Hb (Gregor, 2007). The precise mechanism of Bcd-activated transcription is not yet fully known.

9.2.2 Evaluation of a morphogen activity in development

9.2.2.1 Morphogen activity can be assessed by perturbative methods

Perturbative methods can be applied to the study of morphogen gradients formation. Genetic inactivation or overexpression methods offer powerful tools to understand the specific roles of given genes (e.g. the morphogen Dpp receptor gene (Nellen, 1996)). Recently, Staller et al. published an all-cell expression atlas of 13 patterning genes following maternal Gal 4shRNA depletion of Bicoid (Staller, 2015). However, poor spatio-temporal actuation resolution can be obtained, which prevents fine analysis of these highly dynamical processes.[31]

Morphogen gradients can be experimentally measured directly by fusion with fluorescent protein reporters[32] (see (Kicheva, 2012) for a review). This enables the estimation of gradient kinetic parameters by Fluorescence Correlation Spectroscopy (FCS), or by perturbation of the steady-state fluorescence. The latter can be achieved by photobleaching experiments (Kicheva, 2007), or photoactivation. These experiments offer excellent spatio-temporal selectivity for the determination of diffusion mechanisms, but only affect the fluorescence distribution, not the activities of the POI.

9.2.2.2 Modelization of a Morphogen activity in a developing organism

In 2005, Gregor et al. thus used a GFP-Bicoid reporter and modelled the gradient formation by integrating a simple diffusion-degradation equation[33]:

$$\frac{\partial C(x,\ t)}{\partial t} = D\Delta.C(x,t) - k.C(x,t) \quad (9.1)$$

where *C* is the concentration of Bicoid, D the diffusion coefficient of Bicoid in embryo, and k the degradation rate. Assuming k is a constant parameter, integration of equation **9.1** at steady-state gives a simple exponential decay profile along the AP axis.

$$C(t) = C_0 e^{-\frac{x}{\lambda}} \qquad \lambda = (\mathrm{D}/\mathrm{k})^{\frac{1}{2}} \quad (9.2)$$

The amplitude C_0 and the characteristic length λ both depend on the degradation constant k. This

[31] An interesting alternative was the application of temperature sensitive-degrons to study the role of dynamin-dependent endocytosis in gradient formation (Entchev, 2000). Unlike mammalian, insect cells support temperature-shift, although they can highly alter the developmental response.

[32] However, these last options require complex calibration and normalization procedures to ensure linearity of the measurement. Other options include immunostaining or indirect observations through target gene expression domains.

[33] Morphogen gradients can be described in two ways: discrete models explicit the molecular mechanisms at a cellular resolution, whereas continuum models offer low resolution and continuous morphogen concentration changes, capturing the essential biological processes.

model was applied to direct monitoring of Bicoid-EGFP fluorescence in fly embryos (Gregor, 2005). Although this diffusive model can explain the Bicoid gradient formation, it is insufficient to explain biological features, such as the length scaling between different embryos. Other mechanisms are likely to be involved, such as dynamical exchanges between nuclei, or cytoplasmic fluid flows (Liu, 2011). Although the value of the diffusion coefficient D has been much discussed, the degradation rate k has often been considered constant in time and space[34]. However, the precise degradation mechanism phenomenologically modeled by k was often not explicated.

9.2.3 Control of the activity of a morphogen by UPS degradation

9.2.3.1 Bicoid is targeted for UPS degradation by the SCF

In 2011, it was proved that Bicoid can be degraded in a UPS-dependent manner. The F-Box protein Fates-shifted (Fsd) was identified as the specific SCF adapter for the ubiquitination of Bicoid. Polyubiquitinated Bicoid is degraded by the proteasome. It is thus relevant to wonder whether UPS-dependent degradation is involved in the shaping of the Bicoid gradient.

Indeed, perturbation of Bicoid degradation in *fsd* knock-out embryos results in alteration of the Bicoid gradient profile, resulting in a higher value of characteristic length λ. This observation implied that controlled degradation could be important for the Bicoid gradient formation and shaping (Liu, 2011). Moreover, it was also observed that the lifetime of the embryos varies during the early stages on Bicoid gradient formation (around 15 min during the first two hours[35], more than 40 min after) (Liu, 2011, II), implying that the degradation rate k is not constant in time and space.

9.2.3.2 Light-activatable degradation of Bicoid can be a relevant perturbation method for evaluation of morphogen activity

We propose thus to replace the constant degradation parameter *k* by *k(x,t)* variable in space and time in the simple diffusion-reaction equation **9.3** (Gregor, 2005)[36].

[34] A model for the formation of a stable Bicoid gradient in absence of degradation was proposed (Coppey, 2007), which involves nuclear trapping.

[35] This high degradation process contrasts with others gradient formation models, and might shed new lights on controversies on the diffusion coefficient value *D* (Coppey, 2007) (Abou-Arish, 2010).

[36] Non-linear degradation mechanisms have been described in Drosophila for Hedgehog (Hh) which enhances its own degradation by a feedback mechanism with its receptor Patched (Ptc). This affects the gradient nature (see (Wartlick, 2009) for an extensive model).

$$\frac{\partial C(x,\ t)}{\partial t} = D\Delta.C(x,t) - k(x,t).C(x,t) \quad (9.3)$$

To assess the importance of non-linear degradation in the Bicoid gradient formation, we propose to implement an artificial Fsd-like ubiquitin Ligase to control the degradation of heterologous Bicoid fused to a controllable degron. This strategy could be implemented with either the photo-activatable AID methodology developed in this work, or one of blue-light sensitive degradation modules (psd in yeasts cells (Renicke, 2013); or B-LID in mammalian cells or *Danio* embryos, see section **7.1.2)**. Validation of these methodologies in *Drosophila* would be a first requirement to implement a light-controlled protein degradation strategy.

This would constitute an interesting approach to investigate the stability and the robustness of the gradient: controllable depletion would allow identifying developmental stages and locations in which UPS dependent degradation is determinant for the shaping of the Bicoid gradient, in different contexts:

– *fsd* embryos where the gradient phenotype is altered
– Embryos over-expressing ectopic Bicoid-degron

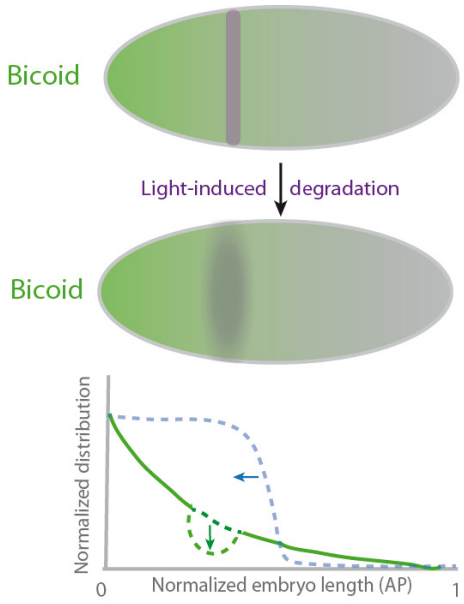

In these two contexts, the Bicoid gradient phenotype would be altered (a longer characteristic length is expected). Conditional rescue of the phenotype, either during the gradient formation, or with a steady-state gradient, might provide valuable informations on the Bicoid gradient formation.

Fig. 9.5: Overview of a light-induced strategy for the perturbation of Bicoid activity in Drosophila embryo. Photo-activatable Bicoid can be implemented by fusion with light-sensitive degradation modules (such as B-LID, psd or AID/PA-IAA) along the Antero-Posterior (AP) axis creates a gradient which modulate Hunchback expression.

Chapter 10
Materials and Methods

10.1 Chemistry part

10.1.1 General

Commercially available reagents were used as obtained. ^{1}H and ^{13}C NMR spectra were recorded at room temperature on Bruker AM 300 spectrometers; chemical shifts are reported in ppm with protonated solvent as internal reference ^{1}H, $CHCl_3$ in $CDCl_3$ 7.26 ppm, CHD_2COCD_3 in CD_3COCD_3 2.05 ppm, CHD_2OD in CD_3OD 3.35 ppm; ^{13}C, $^{13}CDCl_3$ in $CDCl_3$ 77.0 ppm, $^{13}CD_3COCD_3$ in CD_3COCD_3 29.9 ppm, $^{13}CD_3OD$ in CD_3OD 48.8 ppm; coupling constants *J* are given in Hz. Mass spectra (chemical ionization and electronic impact with NH_3 or CH_4, or high resolution) were performed by the Service de Spectrométrie de Masse de Chimie ParisTech (Paris, France) or the Service de Spectrométrie de Masse IMAGIF/ICSN de Gif-sur-Yvette (France). Column chromatography was performed on silica gel 60 (0.040- 0.063 nm) Merck. Analytical thin-layer chromatography (TLC) was conducted on Merck silica gel 60 F254 precoated plates. The UV−vis absorption spectra were recorded at 20°C on an Agilent Cary 300 spectrophotometer equipped with 1 × 1 Peltier cell holders. Molar absorption coefficients were extracted while checking the validity of the Beer−Lambert law. High pressure liquid chromatography (HPLC) was carried out on Agilent 1260 infinity equipped with a column (poroshell 120, C18, 27mm).

10.1.2 Photolysis quantification

Solutions of caged auxins (400 µL at 25 µM) in Acetonitrile / TRIS buffer pH 7.5 were illuminated at 350 nm or 390 nm with a mercury lamp equipped with a monochromator

(pathlength of the light beam 1 cm) using a LPS 220 spectrofluorometer (PTI, Monmouth Junction, NJ), equipped with a TLC50 cuvette holder (Quantum Northwest, Liberty Lake, WA) thermoregulated at 20°C. Solution concentration was adjusted so that optical density at max. Absorption was between 0.1 and 0.15. Measures were carried out on 0.4 mL samples in quartz cuvettes 1.0 × 0.2 cm^2 (l =1cm). Solutions were illuminated for various times and the concentrations were quantified by HPLC or fluorometry. For each caged-auxin, the action cross-section of photolysis σΦ was extracted from the temporal evolution of the concentration *C* of photoactivatable auxin by fitting with the following equation (Aujard, 2006) :

$$\frac{C(t)}{C_0} = e^{-\sigma\Phi\frac{I_0.l.t}{V}}$$

where C_0 is the initial concentration of the photoactivatable auxin, σ is the molar absorption cross-section at maximal absorption wavelength, Φ is the quantum yield of photolysis, *V* is the solution volume, *l* is the pathlength of the light beam and I_0 the light intensity or photon rate (in $mol.s^{-1}$). I_0 was determined following previously reported protocol (Aujard, 2006).

10.1.3 First generation of carboxylate-DMNB caged auxins (section 4.2.1)

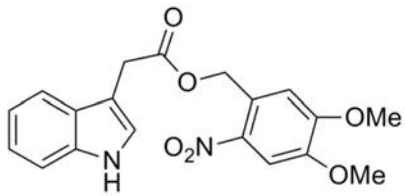

(4,5-dimethoxy-2-nitrophenyl)ethyl 2-(1H-indol-3-yl)acetate 1I

Indole Acetic Acid (IAA) (100 mg, 0.571 mmol), (4,5-dimethoxy-2-nitrophenyl)methanol (DMNBA, 122 mg 0.571 mmol) and dimethylaminopyridine (DMAP, 69.7 mg, 0.571 mmol) were added and dissolved in 10 mL anhydrous dichloromethane. Dicyclohexycarbodiimide (DCC, 118 mg, 0.571 mmol) was added at 0 °C to the stirred solution under nitrogen. After 10 min, ice was removed and the reaction was left overnight at room temperature. Reaction was checked on TLC (cyclohexane/dichloromethane 70/30). The reaction mixture was filtered over a Buchner with dichloromethane, then washed twice with 10 mL HCl 1.2 M and twice with 10 mL saturated $NaHCO_3$. The remaining organic phase was then dried over $MgSO_4$, filtered with a filter paper and evaporated. The product was purified on a flash chromatography (cyclohexane/ethyl acetate 70/30). 35 mg of **1I** was obtained as a yellow powder (0.095 mmol, yield 40 %). ^{1}H NMR (300 MHz, $CDCl_3$, δ in ppm): 3.14 (s, 3H), 3.82 (s, 3H), 3.86 (s, 2H), 5.52 (s, 2H), 6.47 (s, 1H), 7.29 (d, 1H), 7.61 (d, 2 H), 8.10(s, 1H). ^{13}C

NMR (75 MHz, $CDCl_3$, δ in ppm) : 26.7, 31.7, 55.5, 56.2, 63.1, 76.6, 77.1, 77.6, 107.8, 108.8, 111.3,118.7, 119.7, 122.2, 123.6, 127.6, 136.1, 147.8, 153.6, 171.2, 206.6. MS (CI, NH_3): m/z 388.15 $[M+NH_4]^+$, calcd mass for $[C_{19}H_{22}N_3O_6]^+$: 388.15.

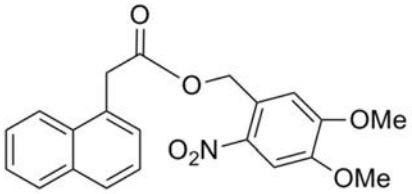

(4,5-dimethoxy-2-nitrophenyl)ethyl 2-(1H-naphtalen-yl)acetate <u>1N</u>

Naphtalene Acetic Acid (NAA, 106.3 mg, 0.571 mmol), (4,5-dimethoxy-2-nitrophenyl)methanol (DMNBA, 122 mg, 0.571 mmol) and dimethylaminopyridine (DMAP, 69.7 mg, 0.571 mmol) were added and dissolved in 5 mL anhydrous dichloromethane. Dicyclohexycarbodiimide (DCC, 118 mg, 0.571 mmol) was added at 0 °C to the stirred solution under nitrogen. After 10 min., ice was removed and the reaction was left overnight at room temperature. Reaction was checked on TLC (cyclohexane/dichloromethane 70/30). The reaction mixture was filtered over a Buchner with dichloromethane, then washed twice with 10 mL HCl 1.2 M and twice with 10 mL saturated $NaHCO_3$. The remaining organic phase was then dried over $MgSO_4$, filtered with a filter paper and evaporated. The product was recrystallised twice in cyclohexane by adding ethyl acetate at 85°C. 98 mg of **1N** was obtained as a white powder (0.25 mmol, yield 85%). ^{1}H NMR (300 MHz, $CDCl_3$, δ in ppm): 3.12 (s, 3H), 3.81 (s, 3H), 4.14 (s, 2H), 5.46 (s, 2H), 6.28 (s, 1H), 7.17 (s, 1H), 8.01 (d, 1H, J = 9 Hz). ^{13}C NMR (75 MHz, $CDCl_3$, δ in ppm) = 24.7, 25.6, 34.0, 39.5, 55.6, 56.6, 63.5, 76.6, 76.9, 77.5, 108.0,108.7, 123.7, 125.7, 126.2, 126.6, 128.2, 128.4, 128.7, MS (CI, NH_3): m/z 382.13 $[M+H]^+$, calcd mass for $[C_{21}H_{20}NO_6]^+$: 382.13.

10.1.4 Second generation of carboxylate-DMNB caged auxins (section 4.2.3)

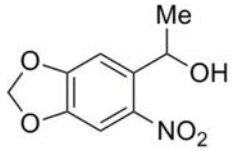

1-(4,5-Methylenedioxy-2-nitrophenyl)ethan-2-ol

was prepared according to literature procedures (Teague, 1996): To a solution of 6-nitropiperonal (1.95 g, 10 mmol) in dry methylene chloride (60 ml) was added dropwise at

0°C trimethylaluminium (2M in hexane, 11 ml, 2.2 eq). The reaction mixture was stirred at room temperature for 4h, then cooled to 0°C and quenched with an aqueous hydrochloric acid solution (1.2M, 100 ml). Extraction with dichloromethane, drying and evaporation gave a yellow solid which was purified by silica column chromatography (cyclohexane/ethyl acetate: 7/3, v/v; 0.46 g, 85 %). ^{1}H NMR (300MHz, $CDCl_3$, δ in ppm): 7.38 (s, 1H), 7.20 (s, 1H), 6.05 (s, 1H, *J* =1.2 Hz), 6.04 (s, 1H, *J* =1.2Hz), 5.38 (q, 1H, *J* = 6.3 Hz,), 2.26 (s, 1H), 1.46 (d, 3H, *J* = 6.3 Hz,).

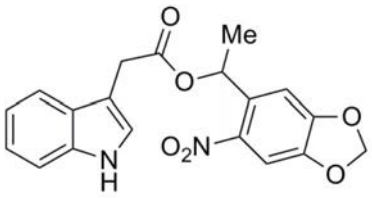

1-(5-Nitrobenzo[1,3]dioxol-6-yl)ethyl 2-(1H-indol-3-yl)acetate 2I

Dicyclohexycarbodiimide (47 mg, 0.23 mmol, 1 eq.) was added at 0°C under nitrogen to a stirred solution of 2-(1H-indol-3-yl)acetic acid (40 mg, 0.23 mmol), 1-(4,5-Methylenedioxy-2-nitrophenol)ethan-2-ol (50 mg, 0.23 mmol, 1 eq.) and 4-dimethylaminopyridine (33 mg, 0.23 mmol,1 eq.) in anhydrous dichloromethane (10 mL). The mixture was stirred for 10 min at 0°C and for 12h at 20°C. The organic phase was washed with 1.2 M hydrochloric acid (2 x 10 mL) and with saturated aqueous solution of sodium hydrogen carbonate (2 x 10 mL). It was subsequently dried over magnesium sulfate and evaporated. The resulting residue was purified by silica column chromatography (cyclohexane/ethyl acetate: 7/3, v/v) then suspended in methanol. The precipitate was filtered, washed with cold methanol and dried under reduced pressure to give **2I** as a yellow powder (70 mg, 83%). ^{1}H NMR (300MHz, Acetone-d_6, δ in ppm): 10.05 (s,1H), 7.53 (d, 1H, J=8.1 Hz), 7.43 (s, 1H), 7.38 (d, 1H, *J* =8.1 Hz), 7.27 (d, 1H, *J* =2.1 Hz), 7.13-6.98 (m, 2H), 6.92 (s, 1H), 6.25 (q, 1H, *J* =6.3 Hz), 6.18 (d, 1H, *J* =1 Hz), 6.15 (d, 1H, *J* =1 Hz), 3.82 (d, 1H, *J* =0.6 Hz), 3.81 (d, 1H, *J* =0.6 Hz), 1.42 (d, 3H, *J* =6.3 Hz); MS (ESI): m/z 367.4 (calcd av. mass $C_{19}H_{15}N_2O_6$: 367.3).

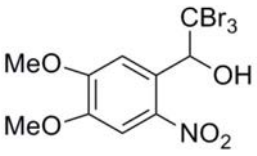

2,2,2-Tribromo-1-(4,5-dimethoxy-2-nitrophenyl)ethanol

was prepared according to literature procedures (Aujard, 2006): Tribromoacetic acid previously recrystallised in chloroform (1.05 g, 3.55 mmol, 1.5 equiv) was added to a solution of 4,5-dimethoxy-2-nitrobenzaldehyde (500 mg, 2.36 mmol) in freshly distilled dimethyl

sulfoxide (12.5 mL). The mixture was stirred for 1 h at room temperature under nitrogen. Then it was poured into ice-cold water (125 mL). The solution was extracted with ether. The organic phase was washed with sodium hydrogenocarbonate solution (5% m/m), and dried over magnesium sulfate. After solvent evaporation, the product was obtained as a yellow solid (962 mg, 88%). ^{1}H NMR (400 MHz, $CDCl_3$, δ in ppm): 7.63 (s, 1 H), 7.53 (s, 1 H), 6.61 (s, 1 H), 4.01 (s, 3 H), 3.96 (s, 3 H), 3.65 (s, 1 H).

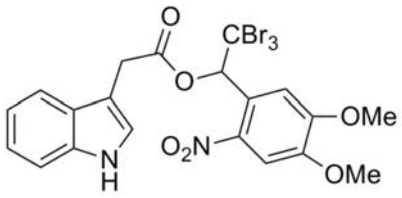

2,2,2-Tribromo-1-(4,5-dimethoxy-2-nitrophenyl)ethyl 2-(1H-indol-3-yl)acetate <u>3I</u>

Same as for **2I** with Dicyclohexycarbodiimide (16 mg, 0.08 mmol, 1 eq.), 2-(1H-indol-3-yl)acetic acid (13 mg, 0.08 mmol), 2,2,2-Tribromo-1-(4,5-dimethoxy-2-nitrophenyl)ethanol (35 mg, 0.08 mmol, 1 eq.), 4-dimethylaminopyridine (10 mg, 0.08 mmol,1 eq.). **3I** was obtained as a yellow powder (35 mg, 75%). ^{1}H NMR (300MHz, acetone-d_6, δ in ppm): 10.26 (s,1H), 7.79 (s, 1H), 7.73 (d, 1H, *J* =7.8 Hz), 7.63 (s, 1H), 7.42 (d, 1H, *J* =7.8 Hz), 7.37 (d, 1H, *J* =2.4 Hz), 7.15-7.02 (m, 2H), 7.09 (s, 1H), 3.92 (s, 6H), 3.36 (s, 2H).

10.1.5 Third generation of carboxylate-DMNB caged auxins (section 4.2.4)

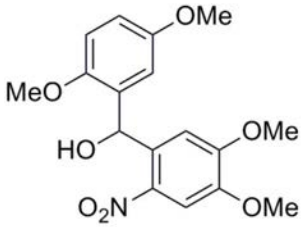

[(4,5-dimethoxy-2-nitrophenyl)(2,5-dimethoxyphenyl) methanol] <u>PNB-OH</u>

To a stirred solution of 4,5-dimethoxy-2-nitrobenzaldehyde (500 mg, 2.4 mmol) in dry THF (12 mL) was slowly added (2,5-dimethoxyphenyl) magnesium bromide (9.5 ml, 4.8 mmol, 2.0 eq.) at –15°C. The solution was stirred for 15 min at –15°C. HCl (0.2 N, 25 mL) was added to quench the reaction and then the aqueous layer was separated and extracted with EtOAc (3 × 100 mL). The combined organic extracts were washed with an aqueous saturated NH_4Cl solution and brine, dried over anhydrous magnesium sulfate, filtered, and concentrated *in vacuo* to afford the crude residue, which was purified by flash chromatography on silica gel

with cyclohexane/EtOAc (7/3, v/v). Compound PNB-OH is obtained as an orange powder (682 mg, 82% yield). ^{1}H NMR (300 MHz, $CDCl_3$, δ in ppm) : δ 7.61 (s, 1H), 7.20 (s, 1H), 6.83 (d, *J* = 8.9 Hz, 1H), 6.77 (dd, *J* = 8.9, 2.9 Hz, 1H), 6.72 (s, 1H), 6.61 (d, *J* = 2.9, 1H), 3.96 (s, 3H), 3.90 (s, 3H), 3.79 (s, 3H), 3.71 (s, 3H); ^{13}C NMR (75 MHz, $CDCl_3$, δ in ppm): 153.6, 153.3, 151.0, 147.8, 140.6, 132.9, 131.9, 113.6, 112.6, 111.5, 110.5, 107.7, 66.79, 56.4 (2C), 56.0, 55.7; MS (CI, NH_3): m/z 366.99 $[M+NH_4]^+$, calcd mass for $[C_{17}H_{23}N_2O_7]^+$: 367.15; HRMS (ES): m/z 332.1122 $[M+H–H_2O]^+$, calcd mass for $[C_{17}H_{18}NO_6]^+$: 332.1134.

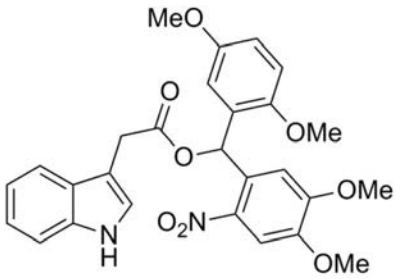

(4,5-dimethoxy-2-nitrophenyl)(2,5-dimethoxyphenyl) methyl 2-(1H-indol-3-yl)acetate] 4I

A solution of compound PNB-OH (100 mg, 0.29 mmol), indole 3-acetic acid (IAA, 60 mg, 0.34 mmol, 1.2 eq.), N,N'-dicyclohexylcarbodiimide (DCC, 71 mg, 0.34 mmol, 1.2 eq.) and 4-dimethyl aminopyridine (42 mg, 0.34 mmol, 1.2 eq.) in CH_2Cl_2 (5 mL) was stirred at room temperature overnight. After the addition of an aqueous saturated NH_4Cl solution (10 ml), the aqueous layer was separated and extracted with CH_2Cl_2 (3 × 30 mL). The organic layer was washed with brine, dried over anhydrous Na_2SO_4, filtered, and concentrated in vacuo. The residue was purified by flash chromatography on silica gel with cyclohexane/EtOAc (7/3, v/v). Precipitation in MeOH yielded to **4I** (130 mg, 89% yield) as gray yellow powder. ^{1}H NMR (300 MHz, Acetone-d_6, δ in ppm) : 10.23 (s, 1H), 7.79 (s, 1H), 7.66 - 7.60 (m, 2H), 7.42 (d, *J* = 8.1 Hz, 1H), 7.35 (m, 1H), 7.13 (t, *J* = 8.1 Hz, 1H), 7.02 (t, *J* = 8.0 Hz, 1H), 6.95 (d, *J* = 8.9 Hz, 1H), 6.88 – 6.81 (m, 2H), 6.44 (d, *J* = 3.0 Hz, 1H), 3.92 (s, 3H), 3.90 (s, 1H), 3.89 (s, 1H), 3.75 (s, 3H), 3.53 (s, 3H), 3.41 (s, 3H); ^{13}C NMR (75 MHz, Acetone-d_6, δ in ppm) : 171.0, 154.7, 154.5, 152.6, 149.6, 141.6, 137.9, 130.1, 129.8, 128.7, 125.2, 122.7, 120.1, 120.0, 114.7, 114.7, 113.2, 112.6, 111.3, 109.2, 108.7, 69.1, 56.8, 56.8, 56.4, 55.98, 32.43; MS (CI, NH_3): m/z 524.02 $[M+NH_4]^+$, calcd mass for $[C_{27}H_{30}N_3O_8]^+$: 524.20; HRMS (ES): m/z 529.1585 $[M+Na]^+$, calcd mass for $[C_{27}H_{26}N_2O_8Na]^+$: 529.1587.

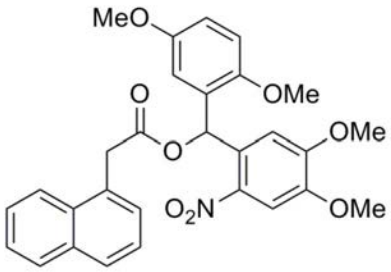

(4,5-dimethoxy-2-nitrophenyl) (2,5-dimethoxyphenyl) methyl 2-(naphthalen-2-yl) acetate 4N

A solution of compound PNB-OH (100 mg, 0.29 mmol), 1-Naphthaleneacetic acid (NAA, 64 mg, 0.34 mmol, 1.2 eq.), N,N'-dicyclo hexylcarbodiimide (DCC, 71 mg, 0.34 mmol, 1.2 eq.) and 4-dimethylaminopyridine (DMAP, 42 mg, 0.34 mmol, 1.2 eq.) in CH_2Cl_2 (5 mL) was stirred at room temperature overnight. After the addition of aqueous saturated NH_4Cl solution (10 ml), the aqueous layer was separated and extracted with CH_2Cl_2 (3 × 30 mL). The organic layer was washed with brine, dried over anhydrous Na_2SO_4, filtered, and concentrated in vacuo. The residue was purified by flash chromatography on silica gel with cyclohexane /EtOAc (7/3, v/v). Precipitation in MeOH yielded to **4N** (127 mg, 85% yield) as yellow solid. ^{1}H NMR (300 MHz, Acetone-d_6, δ in ppm) : 8.11 (m, 1H), 7.94 (m, 1H), 7.88 (d, J = 8.1 Hz, 1H), 7.79 (s, 1H), 7.61 (s, 1H), 7.57 - 7.44 (m, 4H), 6.93 (d, J = 8.9 Hz, 1H), 6.86 – 6.82 (m, 2H), 6.45 (d, J = 3.0 Hz, 1H), 4.27 (s, 2H), 3.93 (s, 3H), 3.70 (s, 3H), 3.58 (s, 3H), 3.57 (s, 3H); ^{13}C NMR (75 MHz, Acetone-d_6, δ in ppm) : 170.6, 154.7, 154.4, 152.5, 149.7, 141.7, 135.2, 133.4, 132.0, 129.7(2C), 129.5, 129.4, 129.0, 127.4, 126.9, 126.7, 125.2, 114.8, 114.6, 113.1, 111.4, 109.2, 69.3, 56.8(2C), 56.7, 56.0, 39.7; MS (CI, NH_3): m/z 535.04 $[M+NH_4]^+$, calcd mass for $[C_{29}H_{31}N_2O_8]^+$: 535.21; HRMS (ES): m/z 540.1610 $[M+Na]^+$, calcd mass for $[C_{29}H_{27}NO_8Na]^+$: 540.1634.

10.1.6 Coumarin-based caged auxins (sections 4.3.1)

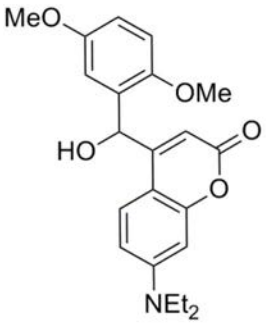

[7-(diethylamino)-4-((2,5-dimethoxyphenyl)(hydroxy)methyl)-2H-chromen-2-one] PCM-OH

To a stirred solution of 7-(diethylamino)-2-oxo-2H-chromene-4- carbaldehyde (130 mg, 0.5 mmol) in dry THF (1.5 mL) was slowly added (2,5- dimethoxyphenyl) magnesium bromide

(2.0 ml, 1.0 mmol, 2.0 eq.) at –15℃. The solution was stirred for 2 hours at –15℃, then at room temperature overnight. HCl (1 N, 1 mL) was added to quench the reaction and then aqueous layer was separated and extracted with EtOAc (3×25 mL). The combined organic extracts were washed with an aqueous saturated NH_4Cl solution and brine, dried over anhydrous magnesium sulfate, filtered, and concentrated in vacuo to afford the crude residue, which was purified by flash chromatography on silical gel with dichloromethane /acetone (96/4, v/v). PCM-OH was obtained as a yellow brown solid (133 mg, 66% yield). ^{1}H NMR (300 MHz, $CDCl_3$, δ in ppm) 7.34 (d, J = 9.3 Hz, 1H), 6.89 (d, *J* = 8.9 Hz, 1H), 6.82 (dd, *J* = 8.9, 3.0 Hz, 1H), 6.74 (d, *J* = 3.0 Hz, 1H), 6.51 (s, 2H), 6.37 (s, 1H), 6.32 (d, *J* = 3.0 Hz, 1H), 3.90 (s, 3H), 3.69 (s, 3H), 3.37(q, *J* = 7.2 Hz, 4H), 1.17 (t, *J* = 7.2 Hz, 6H). ^{13}C NMR (75 MHz, $CDCl_3$, δ in ppm) 162.7, 156.3, 156.2, 153.8, 150.5, 150.1, 129.5, 125.8, 114.1(2C), 111.9, 108.4, 106.6, 106.36, 97.5, 66.5, 56.1, 55.6, 44.6 (2C), 12.4(2C). MS (CI, NH_3): m/z 384.27 $[M+H]^+$, calcd mass for $[C_{22}H_{26}NO_5]^+$: 384.18; HRMS (ES): m/z 384.1815 $[M+H]^+$, calcd mass for $[C_{22}H_{26}NO_5]^+$: 384.1111.

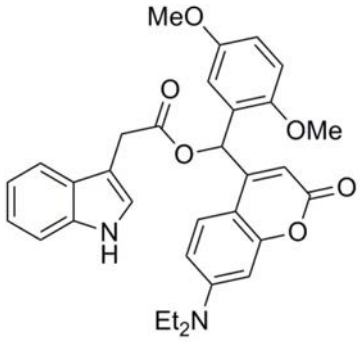

[(7-(diethylamino)-2-oxo-2H-chromen-4-yl)(2,5-dimethoxy phenyl)methyl 2-(1H- indol-3-yl)acetate] <u>5I</u>

A solution of PCM-OH (95mg, 0.25 mmol), indole 3-acetic acid (44 mg, 0.30 mmol, 1.2 eq.), N,N'-dicyclohexylcarbodiimide (DCC, 62 mg, 0.11 mmol, 0.30 eq.) and 4-dimethyl aminopyridine (37 mg, 0.30 mmol, 1.2 eq.) in CH_2Cl_2 (4.5 mL) was stirred at room temperature for 5h. After the addition of an aqueous saturated NH_4Cl solution (10 ml), the aqueous layer was separated and extracted with CH_2Cl_2 (3×30 mL). The organic layer was washed with brine, dried over anhydrous Na_2SO_4, filtered, and concentrated in vacuo. The residue was purified by flash chromatography on silica gel with dichloromethane /acetone (96/4, v/v). **5I** was obtained (130 mg, 96% yield) as a red brown solid. ^{1}H NMR (300 MHz, $CDCl_3$, δ in ppm) 8.24 (s, 1H), 7.55 (d, *J* = 7.8 Hz, 1H), 7.45 (s, 1H), 7.35 (m, 2H), 7.14 (m, 3H), 6.82 (m, 2H), 6.74 (s, 1H), 6.48 (s, 1H), 6.43 (s, 1H), 6.06 (s, 1H), 3.88 (s, 2H), 3.77 (s, 3H), 3.59 (s, 3H), 3.35 (q, *J* = 7.0 Hz, 4H), 1.16 (t, *J* = 7.0 Hz, 6H). ^{13}C NMR (75 MHz, Acetone-d_6, δ in ppm) 171.2, 161.5, 157.3, 154.8, 154.4, 151.6, 151.2, 137.6, 128.4, 126.9,

126.5, 124.9, 122.3, 119.8, 119.6, 115.6, 115.0, 113.4, 112.3, 109.8, 108.2, 107.2, 107.0, 98.5, 67.5, 56.7, 55.8, 45.4(2C), 31.8, 12.7(2C). MS (CI, NH_3): m/z 541.30 $[M+H]^+$, calcd mass for $[C_{32}H_{33}N_2O_6]^+$: 541.23; HRMS (ES): m/z 541.2337 $[M+H]^+$, calcd mass for $[C_{32}H_{33}N_2O_6]^+$: 541.2339.

10.1.7 DMNB N-caged auxin (section 4.3.2)

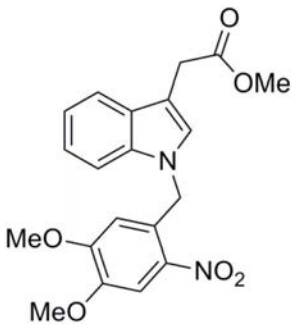

Methyl 2-(1-(4,5-dimethoxy-2-nitrobenzyl)-1H-indol-3-yl)acetate (DMNB-MeIAA) 6MeI

Methyl 2-(1H-indol-3-yl) acetate (50 mg, 0.26 mmol) was added to a solution of NaH (60% suspension in mineral oil) (12 mg, 0.29 mmol, 1.1 eq.) in DMF (1 ml), and the mixture was stirred at room temperature for 15m. After being cooled to 0℃, 1-(bromomethyl)-4,5 dimethoxy-2-nitrobenzene (80 mg, 0.29 mmol, 1.1 eq.) was added slowly. The solution was stirred for 2 hours at 0℃, then continued stirring at room temperature overnight and H_2O (5 ml) was added. the aqueous layer was separated and extracted with EtOAc (3×50 mL). The organic layer was washed with brine, dried over anhydrous $MgSO_4$, filtered, and concentrated *in vacuo*. The residue was purified by flash chromatography on silica gel with dichloromethane which yielded to the desired **6MeI** (10 mg, 10% yield) as brown oil. ^1H NMR (300 MHz, $CDCl_3$, δ in ppm): 7.77 (s, 1H), 7.63 (m, 1H), 7.16 (m, 4H), 5.75 (s, 2H), 5.68 (s, 1H), 3.93 (s, 3H), 3.82 (s, 2H), 3.70 (s, 3H), 3.40 (s, 3H). MS (CI, NH_3): m/z 402.25$[M+NH_4]^+$, calcd mass for $[C_{20}H_{24}N_3O_6]^+$: 402.17.

10.2 Biology part

10.2.1 Cloning

The plasmids used in this study are listed in **table 10.1.** pNHK60 (kind gift from M. Kanamaki) and derived plasmids IRES-containing bicistronic vector were used for co-expression of Protein A: F-box-(NLS)-Myc (NLS: PKKKRKVPKKKRKV) and Protein B:EGFP-AID-NLS. Sequences were verified by sequencing. Sequences were verified by DNA sequencing. pcDNA5-FRT-TO-CyclinB-AID-YFP (kind gift from D. Cleveland) was used together with pAG122 for the co-expression of OsTIR1-Myc and CyclinB1-AID-YFP. Restriction enzymes were supplied by New England Biolabs. Phusion polymerase (New England Biolabs) was used for Polymerase Chain Reaction amplification.

Plasmid	Protein A	Protein B	from
pNHK60	*Os*TIR1-9cMyc	EGFP-AID-NLS	(Nishimura, 2009)
pAG1	*Os*TIR1-9cMyc	HA-EGFP-AID-NLS	pNHK60
pAG36	mCherry-AID		pNHK60
pAG38	*Os*TIR1-NLS-3cMyc	HA-EGFP-AID-NLS	pAG1
pAG39	*Hs*SKP1-*Os*TIR1-9cMyc	HA-EGFP-AID-NLS	pAG1
pAG40	*Hs*SKP1-*Os*TIR1-NLS-3cMyc	HA-EGFP-AID-NLS	pAG38
pAG47	*Os*TIR1-NLS-3cMyc	HA-EGFP-shAID-NLS	pAG38
pAG52	*At*AFB2-NLS-9cMyc	HA-EGFP-AID-NLS	pAG1
pAG53	*Os*AFB2-NLS-9cMyc	HA-EGFP-AID-NLS	pAG1
pAG72	*Os*TIR1^{D170E}-NLS-3cMyc	HA-EGFP-AID-NLS	pAG38
pAG73	*Os*TIR1^{M473L}-NLS-3cMyc	HA-EGFP-AID-NLS	pAG38
pAG74	*Os*TIR1$^{D170E/M473L}$-NLS-3cMyc	HA-EGFP-AID-NLS	pAG38
pAG75	*At*AFB2^{D170E}-NLS-9cMyc	HA-EGFP-AID-NLS	pAG52
pAG76	*At*AFB2^{M473L}-NLS-9cMyc	HA-EGFP-AID-NLS	pAG52
pAG77	*At*AFB2$^{D170E/M473L}$-NLS-9cMyc	HA-EGFP-AID-NLS	pAG52
pAG122	*Os*TIR1-9cMyc		pAG1

Table 10.1:List of plasmids used in this study.

pAG1 was obtained from pNHK60. The IRES sequence was amplified with the primers ag7/ag2. The EGFP sequence was amplified with the primers ag3/ag4. The two fragments were then assembled by PCR using the primers ag7/ag4. The resulting fragment contained the sequence coding for an HA tag flanked by *Pvu* I and *EcoR* I upstream the sequence coding for EGFP. After digestion with *Xma I* and *BsrG I*, this fragment was inserted in pNHK60 between *Xma I* and *BsrG I* restriction sites.

pAG36 was obtained from a modified pIRES vector by inserting the sequence coding for mCherry-LYKGAGAGAGAGAGP-AID into *Bgl* II and *Not* I restriction sites.

pAG38 was obtained from pAG1. The sequence coding for the 9×Myc-tag in pAG1 was replaced by a sequence coding for NLS-3×Myc (amplified from pAG1 using primers ag49/ag50) using *Sal I* and *Xma I* restriction sites.

pAG39 and **pAG40** were obtained respectively from pAG1 and pAG38. The sequence coding for *Hs*SKPI-GGGSGGGSTR-*Os*TIR1(1-39) was synthesized by Eurofins, and subcloned into pAG1 and pAG38 using *Eco47* III and *Blp* I.

pAG47 was obtained from **pAG38**. The sequence encoding shortAID-NLS was generated by digesting pAG38 with *Age* I and *Mfe* I and subsequently inserting a synthetic sequence (obtained from Eurofins) containing (a) the coding sequences for the C-term of short-AID and the nuclear localization signal (NLS) and (b) a sequence identical to the 3'-UTR of pAG38 located upstream *Mfe* I.

pAG52 and **pAG53** were obtained from pAG38. The sequence coding from respectively *At*AFB2-NLS-9×Myc and *Os*AFB2-NLS-9×Myc were synthesized by Eurofins and subcloned into pAG38 using *Bgl* II and *Xma* I restriction sites.

pAG72, **pAG73**, **pAG74** were obtained from pAG38 by site-directed mutagenesis.

pAG75, **pAG76**, **pAG77** were obtained from pAG52 by site-directed mutagenesis.

pAG122 was obtained from pAG1. The sequence coding for HA-EGFP-AID-NLS was removed by digestion using *EcoR* I and *Mfe* I restriction sites. Ligation of the digested vector gave pAG122 (Note: *EcoR* I and *Mfe* I have compatible cohesive ends).

Primer lists:

ag2: aatctggaacatcgtatgggtacgatcgcatggttgtggccatattatc

ag3: atacgatgttccagattacgctgaattcgtgagcaagggcgaggagctg

ag4: ggaagaccaagacacagctcag

ag7: ggaacgatcattcaagagatccc

ag49:atcctactcgagggtgctggcgcccccaagaagaaaagaaaggtccctaaaaagaaacgtaaggtttccggttctgctgctagtg

ag50: gcggatcccggggatctcttg

10.2.2 Cell culture and protein quantification

Mammalian cell culture Chinese Hamster Ovarian (CHO) cells were grown at 37°C in 5% CO_2 atmosphere in DMEM (GIBCO) complemented with 10% fetal bovine serum (FBS, GIBCO), 1% non-essential amino-acids (GIBCO) and 1% penicillin / streptomycin (Life technologies). Human embryonic kidney 293 cells were grown at 37°C in 5% CO_2 atmosphere in DMEM with GlutaMAX-1 (GIBCO) complemented with 10% fetal bovine serum (FBS, GIBCO) and 1% penicillin / streptomycin (Life technologies). Cells were transiently transfected with Genejuice (Merck) according to the manufacturer's protocol.

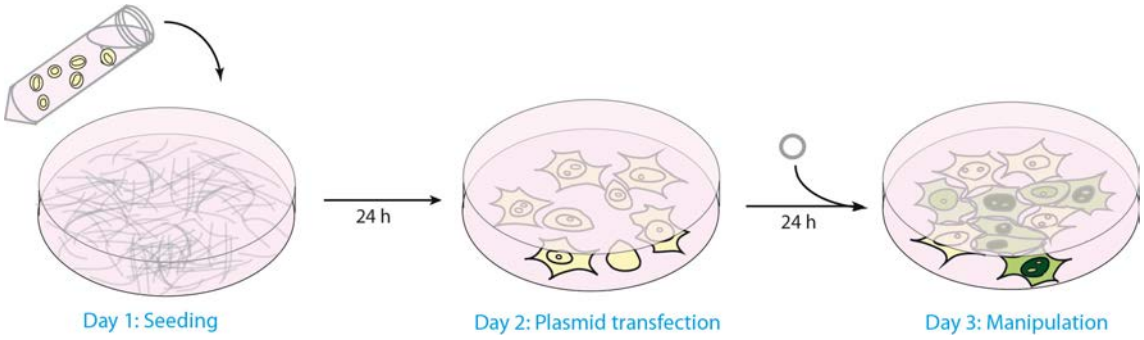

Fig. 10.1: Overview of transient expression protocol in mammalian culture cells. Cells are seeded on culture wells pre-coated with poly-lysine polymer and grown for 24 h, after which cells were transfected at 50-70% density for 24h.

For experiments with auxins (or caged auxins in the dark), medium was replaced with fresh complete medium supplemented with the auxin at indicated concentration and incubated for the indicated duration. The supplemented medium contained 1% DMSO (Sigma). For the microscopy experiments with PA-IAA (**4I)**, medium was replaced with serum-free

DMEM/OPTI-MEM (GIBCO) (1:1) supplemented with the photoactivatable auxin at the indicated concentration and incubated for 20 min in darkness before photolysis. The supplemented medium contained 1% DMSO.

Immunoblotting.

Cells were washed with ice-cold phosphate buffer saline (PBS, GIBCO), then lysed with ice-cold lysis buffer (Sigma) supplemented with protease inhibitors cocktail (Roche). Samples were boiled with 2% β-mercaptoethanol-containing SDS-loading buffer (BioRad). Samples were then resolved using Novex Nupage 4-12% bis-Tris gels (Life technlogies) and transferred on nitrocellulose membrane (GE Healthcare). Membranes were blocked with 5% dried non-fat milk in TBS buffer containing 0.1% Tween-20 (Sigma), and then incubated with the appropriate antibodies for subsequent detection by standard chemoluminescence methods. For immunoblotting analysis, the following antibodies were supplied by Cell Signaling: actin (rabbit, 1:2,000), Myc (rabbit, 1:2,000), GFP (rabbit, 1:4,000, monoclonal (D5.1)).

Immunostaining. Cells were washed with ice-cold phosphate buffer saline (PBS), and fixed with 5 % paraformaldehyde (PFA, Sigma) in PBS. Nuclear membrane was permeated through treatment with Triton X100 0.25%. Cells were incubated with 1% BSA in PBS for blocking, then incubated with a solution of rabbit anti-Myc antibody (1/50), washed, and incubated with the Alexa-633-conjugated secondary anti-rabbit antibody (1/50).

10.2.3 Illumination protocols and microscopy imaging

Global photolysis in cells

Cells grown in 12-well plates and treated as described were globally illuminated at 365 nm (photon flux 100 $\mu mol.m^{-2}.s^{-1}$ or 3 $mW.cm^{-2}$) with a hand lamp (Vilber Lourmat VL-6L 6W) placed above the plate for the indicated duration, then incubated in darkness at 37°C in 5% CO_2 atmosphere for the indicated duration. Cells were then harvested for immunoblotting analysis. The photon flux was measured using a Nova II powermeter (Laser Measurement Instruments).

Live cell imaging

Live cells grown in μ-Dish (Ibidi) were imaged at 37°C with an inverted Zeiss LSM 710 Laser Scanning Microscope equipped with a Plan Apochromat 63 ×/1.4 oil immersion objective. EGFP and YFP were excited with a 488 nm argon laser, and emission was collected between 497-797 nm. The mean nuclear fluorescence intensities were quantified using ImageJ software.

Photolysis with the metal halide lamp

Photolysis was performed at a 63× magnification with an EXFO X-Cite 120 XL System employing a 120 W metal halide lamp with a UV filter (filter setting– excitation G 365, beam splitter FT 395, emission BP 445/50). The illumination area was 0.1 mm^2. The photon flux in the specimen plane (100 $mmol.m^{-2}.s^{-1}$) was estimated using a Nova II powermeter (Laser Measurement Instruments). Pulses of 1s every 5 minutes were used in the presented experiments.

Photolysis with the 405 nm laser diode

Photolysis at the single cell level was performed at a 63× magnification using a 405 nm laser diode. Using the bleaching procedure of the Zeiss Zen Software, a rectangular region of interest (ROI) of 200 μm^2 was defined and illuminated with 50 iterations using the 405 nm laser diode at 1% power. We adjusted roughly the photon flux by comparing with the photon flux enabling the photoswitching of KikGR, a fluorescent protein switching for green to red upon UV-violet excitation and possessing an action-cross section of photoswitching close to the action-cross section of PA-IAA photolysis. Pulses every 10 minutes were performed in the presented experiments.

Bibliography

Abel, S., & Theologis, A. Odyssey of auxin *Cold Spring Harb. Perspect. Biol.*, **2** (10) (2010).

Aghajan, M. *et al.* Chemical genetics screen for enhancers of rapamycin identifies a specific inhibitor of an SCF family E3 ubiquitin ligase *Nat. Biotechnol.*, **28,** 738–742 (2010).

Ahmed, I. & Fruk, L. The power of light: photosensitive tools for chemical biology *Molecular BioSystems*, **9**, 565–570 (2013).

Alberts, B., Johnson, A., Lewis J., Raff M., Roberts K., Walter P. Molecular biology of the cell *Garland Science,* **5th Ed.** (2008).

Allen, G. J., Kuchitsu, K., Chu, S. P., Murata, Y., & Schroeder, J. I. Arabidopsis abi1-1 and abi2-1 phosphatase mutations reduce Abscisic acid – induced cytoplasmic calcium rises in guard cells *Plant Cell*, **11**, 1785–1798 (1999).

Andley, U. P., Lewis, R. M., Reddan, J. R. & Kochevar, I. E. Action spectrum for cytotoxicity in the UVA- and UVB-wavelength region in cultured lens epithelial cells *Investig. Ophtamol.*, **35** (2), 367–373 (1994).

Asher, G., Bercovich, Z., Tsvetkov, P., Shaul, Y. & Kahana, C. 20S proteasomal degradation of ornithine decarboxylase is regulated by NQO1 *Mol. Cell*, **17,** 645–655 (2005).

Audas, T. E., Jacob, M. D. & Lee, S. Immobilization of proteins in the nucleolus by ribosomal intergenic spacer noncoding RNA *Mol. Cell*, **45,** 147–157 (2012).

Aujard, I., Benbrahim, C., Gouget, M., Ruel, O., Baudin, J.-B., Neveu, P., & Jullien, L. *o*-nitrobenzyl photolabile protecting groups with red-shifted absorption: syntheses and uncaging cross-sections for one- and two-photon excitation *Chemistry*, **12** (26), 6865–6879 (2006).

Bachmair, A., Finley, D., Varshavsky, A. *In vivo* half-life of a protein is a function of its amino-terminal residue *Science,* **234**, 179-186 (1986).

Baker, A. S. & Deiters, A. Optical control of protein function through unnatural amino acid mutagenesis and other optogenetic approaches *ACS Chem. Biol*., **9**, 1398-1407 (2014).

Ballister, E. R., Aonbangkhen, C., Mayo, A. M., Lampson, M. A. & Chenoweth, D. M. Localized light-induced protein dimerization in living cells using a photocaged dimerizer *Nat. Commun.,* **5,** 1–9 (2014).

Banaszynski, L., Liu, C. W. & Wandless, T. J. Characterization of the FKBP-rapamycin-FRB ternary complex *J. Am. Chem. Soc.*, **127,** 4715–4721 (2005).

Banaszynski, L., Chen, L. C., Maynard-Smith, L. & Wandless, T. J. A rapid, reversible, and tunable method to regulate protein function in living cells using synthetic small molecules *Cell,* **126,** 995–1004 (2006).

Banaszynski, L. A. & Wandless, T. J. Conditional control of protein function review *Chem. Biol.,* **13,** 11–21 (2006).

Bargmann, B. O. R. & Estelle, M. Auxin perception: in the IAA of the beholder *Physiol. Plant.,* **151,** 52–61 (2014).

Basserman, M. The ubiquitin proteasome system – Implications for cell cycle control and the targeted treatment of cancer *Biochim. Biophys. Acta.,* **1843** (1) (2014).

Beamish, H., de Boer, L., Giles, N., Stevens, F., Oakes, V., and Gabrielli, B. Cyclin A/cdk2 regulates adenomatous polyposis coli-dependent mitotic spindle anchoring *J. Biol. Chem.,* **284** (42), 29015–29023 (2009).

Bedford, L., Lowe, J., Dick, L. R., Mayer, R. J. & Brownell, J. E. Ubiquitin-like protein conjugation and the ubiquitin-proteasome system as drug targets *Nat. Rev. Drug Discov.,* **10,** 29–46 (2011).

Bence, N.F., Bennett, E. J., Kopito, R. R. Application and analysis of the GFPu family of ubiquitin-proteasome system reporters *Methods Enzymol.,* **399** (33) (2005).

Bennett, E. J., Bence, N. F., Jayakumar, R. & Kopito, R. R. Global impairment of the ubiquitin-proteasome system by nuclear or cytoplasmic protein aggregates precedes inclusion body formation *Mol. Cell,* **17,** 351–365 (2005).

Bernstein, J. G., Garrity, P. A. & Boyden, E. S. Optogenetics and thermogenetics technologies for controlling the activity of targeted cells within intact neural circuits *Curr. Opin. Neurobiol.,* **22,** 61–71 (2012).

Bett, J. S., Cook, C., Petrucelli, L. & Bates, G. P. The ubiquitin-proteasome reporter GFPu does not accumulate in neurons of the R6/2 transgenic mouse model of Huntington' s disease *PLOS One,* **4,** 4 (2009).

Binari, R., Gocha, T., Dasgupta, R. & Perrimon, N. PAPTi : A Peptide Aptamer Interference Toolkit for perturbation of protein-protein *Sci. Rep.*, **3 (**1156), 1–8 (2012).

Bioquı, D. Molecular biology of mammalian plasma membrane amino acid transporters *Physiol.Rev.,* **78,** 969–1054 (1998).

Bochet, C. G. Orthogonal photolysis of protecting groups. *Angew. Chem. Int. Ed.*, **40**, 2071-2073 (2001).

Bonger, K. M., Chen, L., Liu, C. W. & Wandless, T. J. Small-molecule displacement of a cryptic degron causes conditional protein degradation *Nat. Chem. Biol.,* **7,** 531–537 (2011).

Bonger, K. M., Rakhit, R., Payumo, A. Y., Chen, J. K., & Wandless T., J.. A general method for regulating protein stability with light *ACS Chem. Biol*., **9** (1), 111–115 (2015).

Boyd, M. T., Vlatkovic, N., & Rubbi, C. P. The nucleolus directly regulates p53 export and degradation *J. cell biol.*, **194** (5), 689–703 (2011).

Brauchle, M. *et al.* Protein interference applications in cellular and developmental biology using DARPins that recognize GFP and mCherry *Biology Open*, **3**, 1252–1261 (2014).

Buckley, D. & Crews, M. Small molecule control of intracellular protein levels through modulation of the ubiquitin-proteasome system *Angew. Chem. Int. Ed.*, **53,** 2312–2330 (2015).

Burgess, A. *et al.* Loss of human Greatwall results in G2 arrest and multiple mitotic defects due to deregulation of the cyclin B-Cdc2/PP2A balance *Proc. Natl. Acad. Sci. U. S. A.*, **107,** 12564–12569 (2010).

Cambridge, S. B., Geissler, D., Calegari, F., Anastassiadis, K., Hasan, M. T., Stewart, A., Huttner, W., Hagen, V. & Bonhoeffer, T. Doxycycline-dependent photoactivated gene expression in eukaryotic systems *Nat. Meth.*, **6**, 527 - 531 (2009).

Cardozo, T. & Pagano, M. The SCF ubiquitin ligase: insights into a molecular machine *Nat. Rev. Mol. Cell Biol.*, **5,** 739–751 (2004).

Caussinus, E., Kanca, O. & Affolter, M. Fluorescent fusion protein knockout mediated by anti-GFP nanobody *Nat. Struct.Mol. Biol.*, **19,** 117–121 (2011).

Chaulk, S. G. & Macmillan, A. M. Synthesis of oligo-RNAs with photocaged adenosine *Nat. Prot.*, **2,** 1052–1058 (2007).

Chen D., Gibson E.S., Kennedy M.J. A light-triggered protein secretion system. *J. Cell Biol.*, **201**, 631–640 (2013).

Chen, J. & Liu, J. Spindle assembly checkpoint *Nat. Commun.*, **5,** 1–13 (2014).

Cho, U. *et al.* Rapid and tunable control of protein stability in *Caenorhabditis elegans* using a small molecule *PLoS One*, **8,** e72393 (2013).

Colas, P., Cohen, B., Ferrigno, P. K., Silver, P. A., & Brent, R. Targeted modification and transportation of cellular proteins *Proc. Natl. Acad. Sci. U. S. A.*, **98** (26), 14418–14420 (2001).

Cong, F., Zhang, J., Pao, W., Zhou, P. & Varmus, H. A protein knockdown strategy to study the function of β-catenin in tumorigenesis *BMC Mol. Biol.*, **11,** 1–11 (2003).

Cornish Carmony, K., Kim, K. PROTAC-induced proteolytic targeting *Meth. Mol. Biol*., **832**:627-638 (2012).

Corrie, J. E. T. Photoremovable protecting groups used for the caging of biomolecules *Dynamic Studies in Biology*, Wiley (1999).

Crefcoeur, R.P., Yin, R., Ulm, R. and Halazonetis, T.D. Ultraviolet-B-mediated induction of protein–protein interactions in mammalian cells *Nat. Commun.*, **4**, 1779 (2013).

Crews, C. M. Targeting the Undruggable Proteome: The small molecules of my dreams *Chem. Biol.,* **17,** 551–555 (2011).

Dantuma, N. P., Lindsten, K., Glas, R., Jellne, M. & Masucci, M. G. Short-lived green fluorescent proteins for quantifying ubiquitin / proteasome- dependent proteolysis in living cells *Nat. Biotech.,* **18,** 538-543 (2000).

Dantuma, N. P. & Lindsten, K. Stressing the ubiquitin-proteasome system *Cardiovasc. Res.,* **85,** 263–271 (2010).

Davis J. H., Baker T. A., and Sauer R. T. Small-molecule control of protein degradation using split adaptors *ACS Chem. Biol.*, **6** (11), 1205–1213 (2011).

De Bie, P. *et al.* Ubiquitination of E3 ligases: self-regulation of the ubiquitin system via proteolytic and non-proteolytic mechanisms *Cell Death Differ.*, **18,** 1393–1402 (2011).

Deisseroth, K. Optogenetics *Nat. Meth.,* **8** (1)**,** 26–29 (2011).

Deiters, A. Principles and applications of the photochemical control of cellular processes *ChemBioChem.*, **11,** 47–53 (2010).

Delacour Q., Li C., Plamont M.A., Billon-Denis E., Aujard I., Le Saux T., Jullien L., Arnaud Gautier A. Light-Activated Proteolysis for the Spatiotemporal Control of Proteins *ACS Chem. Biol.*, **10** (7), 1643–1647 (2015).

Derose, R., & Inoue, T. Manipulating signaling at will chemically -inducible dimerization (CID) techniques resolve problems in cell biology *Eur. J. Physiol.,* **10**.1007 (2013).

DeRybel, B. *et al.*, The past, present and future of chemical biology in auxin research *ACS Chem Biol.*, **4,** 987–998 (2009).

Dharmasiri, N., Dharmasiri, S., Estelle, M. The F-box protein TIR1 is an auxin receptor *Nature*, **435** (7041), 441-445 (2005).

Dikic, I., Wakatsuki, S., Walters, K.J. Ubiquitin-binding domains - from structures to functions *Nat Rev. Mol. Cell Biol.,* **10**, 659-671 (2009).

Do, S., Kim, K., Lee, H., Kim, H., Do, T., Yun, J., Kim, D., Chae, S., Park, Y., Park, C., Sohn, J., Min, K., Pyo, J. Aberrant expression pattern and location of cullin 1 are associated with the development of papillary carcinoma in thyroid and cyclin D1 expression *Endocr. Pathol.,* **3**, 282-287 (2014).

Dohmen, R.J., Wu, P., Varshavsky, A. Heat-inducible degron: a method for constructing temperature-sensitive mutants *Science,* **263**, 1273-1276 (1994).

Dougan, D. A., & Truscott, K. N. The N-end rule pathway From recognition by N-recognins, to destruction by AAA + proteases *BBA - Mol. Cell Res.,* **1823,** 83–91 (2012).

Driever, W., & Nu, C. The bicoid Protein determines position in the *Drosophila* embryo in a concentration-dependent manner *Cell*, **54**, 95–104 (1988).

Duda, D. M., Borg, L. A., Scott, D. C., Hunt, H. W., & Schulman, B. A. Structural insights into NEDD8 activation of Cullin-RING ligases: conformational control of conjugation *Cell*, **134** (6), 995–1006 (2008).

Dugué, G. P., Akemann, W. & Knöpfel, T. A comprehensive concept of optogenetics *Progress in Brain Research*, **196,** 1–28 (2012).

Eichhorn, J. M., Kothari, A. & Chambers, T. C. Cyclin B1 overexpression induces cell death independent of mitotic arrest *PLoS One*, **9,** e113283 (2014).

Eletr, Z. M., Wilkinson, K. D. Regulation of proteolysis by human deubiquitinating enzymes *Biochim. Biophys. Acta*., **1843,** 1–30 (2014).

Emond, M., Sun, J., Grégoire, J., Maurin, S. , Tribet, C. and Jullien, L. Photoinduced pH drops in water. *Phys. Chem. Chem. Phys.*, **13**, 6493-6499 (2011).

Engels J, Schlaeger E.J. Synthesis, structure, and reactivity of adenosine cyclic 3',5'-phosphate benzyl trimesters. *J. Med. Chem.*, **20**, 907 (1977).

Farrar, M.A., Olson, S.H., Perlmutter, R.M. Coumermycin-induced dimerization of GyrB-containing fusion proteins *Methods Enzymol.*, **327**, 421-429 (2000).

Fasano, M. *et al.* Critical review: the extraordinary ligand binding properties of human serum Albumin *Life*, **57,** 787–796 (2005).

Fink, J. *et al.* External forces control mitotic spindle positioning *Nat. Cell Biol.*, **13,** 771–778 (2011).

Foe, I. T. & Toczyski, D. P. Ubiquitin ligases: Taming the APC *Nat. Chem. Biol.*, **8,** 323–324 (2012).

Folcher, M., Oesterle, S., Zwicky, K., Thekkottil, T., Heymoz, J., Hohmann, M., Christen, M., *et al*. Mind-controlled transgene expression by a wireless-powered optogenetic designer cell implant. *Nat. Commun.*, **5**, 5392 (2014).

Fournier, L., Aujard, I., Le Saux, T., Maurin, S., Beaupierre, S., Baudin, J.B., Jullien, L. Coumarinyl-methyl caging groups with redshifted absorption *Chemistry*, **19** (51), 17494-17507 (2013).

Fredrickson, E. K. & Gardner, R. G. Mediated protein quality control degradation *Semin. Cell. Dev. Biol.*, **23,** 530–537 (2013).

Gastaldello, S., D'Angelo, S., Franzoso, S., Fanin, M., Angelini, C., Betto, R., & Sandon, D. Inhibition of proteasome activity promotes the correct localization of disease-causing alpha-sarcoglycan mutants in HEK-293 cells constitutively expressing beta-, gamma-, and delta-sarcoglycan *Am. J. Path.*, **173** (1), 170–181 (2008).

Gautier, A., Nguyen, D.P., Lusic, H., An, W., Deiters, A. & Chin, J.W. Genetically encoded photocontrol of protein localization in mammalian cells.*J. Am. Chem. Soc.*, **132**, 4086-4088 (2010).

Gautier, A., Deiters, A. & Chin, J.W. Light-activated kinases enable the temporal dissection of signaling networks in living cells. *J. Am. Chem. Soc.*, **133**, 2124-2127 (2011).

Gautier, A. *et al.* How to control proteins with light in living systems *Nat. Chem. Biol.*, **10,** 533–541 (2014).

Geisler, M. *et al.* Cellular efflux of auxin catalyzed by the Arabidopsis MDR / PGP transporter AtPGP1 *Plant J.*, **44**, 179–194 (2005).

Genschik, P., Sumara, I. & Lechner, E. The emerging family of CULLIN3-RING ubiquitin ligases (CRL3s): cellular functions and disease implications *EMBO J.*, **32,** 2307–2320 (2013).

Gibson, M. C. Bicoid by the numbers: quantifying a morphogen gradient *Cell*, **130,** 14–16 (2007).

Gilon, T., Chomsky, O. & Kulka, R. G. Degradation signals for ubiquitin system proteolysis in Saccharomyces cerevisiae *EMBO J.*, **17,** 2759–2766 (1998).

Godley, B. F., Shamsi, F. a., Liang, F.-Q., Jarrett, S. G., Davies, S., & Boulton, M. Blue light induces mitochondrial DNA damage and free radical production in epithelial cells *J. Biol. Chem.*, **280** (22), 21061–21066 (2005).

Goguen, B. N. & Imperiali, B. Chemical tools for studying directed cell migration *ACS Chem. Biol.*, **6,** 1164–1174 (2012).

Goldberg, A. L. Protein degradation and protection against misfolded or damaged proteins *Nature*, **426,** 895–899 (2003).

Goldenberg, S. J., Marblestone, J. G., Mattern, M. R. & Nicholson, B. Strategies for the identification of ubiquitin ligase inhibitors *Biochem. Soc. Trans.*, **38,** 132–136 (2010).

Gosink, M. & Vierstra, R. Redirecting the specificity of ubiquitination by modifying ubiquitin-conjugating enzymes *Proc. Natl. Acad. Sci. U. S. A.*, **92**, 9117–9121 (1995).

Gregor T., Wieschaus E. F., McGregor A. P., Bialek W., and Tank D. W. Stability and nuclear dynamics of the Bicoid morphogen gradient *Cell*, **130** (1), 141–152 (2008).

Gurney, A. M. Flash photolysis of caged compounds *Fluorescent and Luminescent Probes for Biological Activity (Second Edition)*, Academic Press, 389–406 (1993).

Hagai, T., Tóth-Petróczy, Á., Azia, A. & Levy, Y. The origins and evolution of ubiquitination sites *Mol. Biosyst.*, **8,** 1865-1877 (2012).

Halestrap, A. P. The monocarboxylate transporter family--Structure and functional characterization *IUBMB life*, **64** (1), 1–9 (2012).

Hansen, M. J., Velema, W. A., Bruin, G. De, Overkleeft, H. S. & Feringa, B. L. Proteasome inhibitors with photocontrolled activity *ChemBioChem.,* **15**, 2053 Chapter 5 (2014).

Havens, K. A. *et al.* A synthetic approach reveals extensive tunability of auxin signaling *Plant Physiol.,* **160,** 135–142 (2012).

Hayashi, K. *et al.* Small-molecule agonists and antagonists of F-box protein – substrate interactions in auxin perception and signaling *Proc. Natl. Acad. Sci. U. S. A.,* **105** (14) 5632-5637 (2008).

Hayashi, K. *et al.* Rational design of an auxin antagonist of the SCF *ACS Chem. Biol.,* **7**, 590-598 (2012).

Hecht, I., Rappel, W.-J. & Levine, H. Determining the scale of the Bicoid morphogen gradient *Proc. Natl. Acad. Sci. U. S. A.,* **106,** 1710–1715 (2009).

Hemphill, J., Chou, C., Chin, J. W. & Deiters, A. Genetically encoded light-activated transcription for spatio- temporal control of gene expression and gene silencing in mammalian cells *Proc. Natl. Acad. Sci. U. S. A.,* **135,** 13433–13439 (2014).

Hines, J., Gough, J. D., Corson, T. W. & Crews, C. M. Posttranslational protein knockdown coupled to receptor tyrosine kinase activation with phosphoPROTACs **110** (22), 8942-8947 (2013).

Holland, A. J., Fachinetti, D., Han, J. S. & Cleveland, D. W. Inducible, reversible system for the rapid and complete degradation of proteins in mammalian cells *Proc. Natl. Acad. Sci. U. S. A.,* **109,** E3350–3357 (2012).

Houser, J. R. *et al.* An improved short-lived fluorescent protein transcriptional reporter for S. cerevisiae *Yeast,* **29,** 519–530 (2013).

Hwang, C., Shemorry, A., Auerbach, D. & Varshavsky, A. The N-end rule pathway is mediated by a complex of the RING-type Ubr1 and HECT-type Ufd4 ubiquitin ligases *Nat. Publ. Gr.,* **12,** 1177–1185 (2010).

Idevall-Hagren, O., Dickson, E. J., Hille, B., Toomre, D. K., & Camilli, P. Optogenetic control of phosphoinositide metabolism, *Proc. Natl. Acad. Sci. U. S. A.,* **109** (35), 2316-2323 (2012).

Inobe, T., Fishbain, S., Prakash, S. & Matouschek, A. Defining the geometry of the two-component proteasome degron *Nat. Chem. Biol.,* **7,** 161–167 (2011).

Inobe, T. and Matouschek, A. Paradigms of protein degradation by the proteasome *Curr Opin Struct Biol*., **24,** 156-164 (2014).

Iwamoto, M., Björklund, T., Lundberg, C., Kirik, D. & Wandless, T. J. A general chemical method to regulate protein stability in the mammalian central nervous system *Chem. Biol.,* **17,** 981–988 (2010).

Iyer, L. M., Burroughs, a M. & Aravind, L. The prokaryotic antecedents of the ubiquitin-signaling system and the early evolution of ubiquitin-like beta-grasp domains *Genome Biol.*, **7** (7)**,** R60 (2006).

Jain, M. *et al.* Structure and expression analysis of early auxin-responsive Aux/IAA gene family in rice (*Oryza sativa*) *Funct. Integr. Genomics*, **6,** 47–59 (2006).

Jankovics, F. *et al.* Functional analysis of the drosophila embryonic germ cell transcriptome by RNA interference *PLoS One*, **9** (6) (2014).

Janse, D. M., Crosas, B., Finley, D., & Church, G. M. Localization to the proteasome is sufficient for degradation *J. Biol. Chem.*, **279** (20), 21415–21420 (2004).

Jin, J. *et al.* Systematic analysis and nomenclature of mammalian F-box proteins *Genes Dev.*, **18,** 2573–2580 (2004).

Johnson, E. S. A proteolytic signal that recognizes ubiquitin as a degradation signal *J. Biol. Chem.,* **270** (29)**,** 17742-17456 **(**1995).

Jungbluth, M., Renicke, C. & Taxis, C. Targeted protein depletion in Saccharomyces cerevisiae by activation of a bidirectional degron *BMC Syst. Biol.,* **4,** 176 (2010).

Kao **,** J. P.Y. Caged molecules: principles and practical considerations. *Current Protocols in Neuroscience*, UNIT **6**.20 (2006).

Kaplan JH, Forbush B, Hoffman JF. Rapid photolytic release of adenosine 5'-triphosphate from a protected analogue: utilization by the Na:K pump of human red blood cell ghosts. *Biochemistry*, **17**, 1929 (1978).

Kanemaki, M. T. Frontiers of protein expression control with conditional degrons *Nat. Meth.*, **6** (12), 419–425 (2013).

Kanke, M. *et al.* Auxin-inducible protein depletion system in fission yeast *BMC Cell Biol.*, **12,** 8 (2011).

Kennedy, M. J., Hughes, R. M., Peteya, L. A., Schwartz, J. W., Ehlers, D., & Tucker, C. L. Rapid blue light induction of protein interactions in living cells. *Nat. Meth.*, **7** (12), 973–975 (2011).

Kepinski, S. & Leyser, O. The Arabidopsis F-box protein TIR1 is an auxin receptor *Nature*, **435,** 446–451 (2005).

Kicheva, A., Bollenbach, T., Wartlick, O., Jülicher, F. & Gonzalez-Gaitan, M. Investigating the principles of morphogen gradient formation: From tissues to cells *Curr. Opin. Genet. Dev.*, **22,** 527–532 (2012).

Kim, D. S., Jeon, S. E., Park, K.C. Oxidation of indole-3-acetic acid by horseradish peroxidase induces apoptosis in G361 human melanoma cells *Cell Signal.,* **16** (1), 81-88 (2004).

Kim, B. & Lin, M. Z. Optobiology : optical control of biological processes via protein engineering *BioChem. Soc. Trans.*, **41**, 1183–1188 (2013).

Kitada, T., Asakawa, S., Hattori, N., Matsumine, H., Yamamura, Y., Minoshima, S., Yokochi, M., Mizuno, Y., Shimizu, N. Mutations in the parkin gene cause autosomal recessive juvenile parkinsonism *Nature*, **392**(6676), 605-608 (1998).

Kipreos, E. T. & Pagano, M. The F-box protein family *Genome Biol.*, **1** (5) (2000).

Klán, P., Šolomek, T., Bochet, C. G., Blanc, A., Givens, R., Rubina, M., Popik, V. Photoremovable protecting groups in chemistry and biology: reaction mechanisms and efficacy *Chem. Rev.*, **113**(1), 119–191 (2014).

Kobayashi, Y., Imamura, S., Hanaoka, M. & Tanaka, K. A tetrapyrrole-regulated ubiquitin ligase controls algal nuclear DNA replication *Nat. Cell Biol.*, **13,** 483–487 (2011).

Kramer, R. H., Chambers, J. J. & Trauner, D. Photochemical tools for remote control of ion channels in excitable cells *Nat. Chem. Biol.*, **1,** 360–365 (2005).

Kramer, E., Draye, M., & Bennett, M. J. Modelling root growth and development *Practical Systems Biology*, Volume **61,** Ch. 10 (2008).

Krauss, U., Minh, B. Q., Losi, A., Gärtner, W., Eggert, T., Von Haeseler, A., & Jaeger, K.-E. Distribution and phylogeny of light-oxygen-voltage-blue-light-signaling proteins in the three kingdoms of life. *J. bacterial.*, **191** (23), 7234–42 (2009).

Kreidenweiss, A., Hopkins, A. V. & Mordmüller, B. 2A and the auxin-based degron system facilitate control of protein levels in *Plasmodium falciparum*, *PLoS One* **8,** 2–7 (2013).

Kruse, K., Pantazis, P., Bollenbach, T., Jülicher, F., & González-Gaitán, M. Dpp gradient formation by dynamin-dependent endocytosis: receptor trafficking and the diffusion model *Development*, **131** (19), 4843–4856 (2004).

Kusaka, N., Maisch, J., Nick, P., Hayashi, K. & Nozaki, H. Manipulation of intracellular auxin in a single cell by light with esterase-resistant caged auxins *ChemBioChem.*, **10**, 2195–2202 (2009).

Labella, M. L., Sigrist, S. & Jorgensen, E. M. 7 Putting genetics into optogenetics : knocking out proteins with light *Optogenetics*, **Dahlem Workshop Reports**, Ed. by Hegemann, P. & Sigrist, S., de Gruyter (2013).

Lange, A., Mills, R. E., Lange, C. J., Stewart, M., Devine, S. E., & Corbett, A. H. Classical nuclear localization signals: definition,function, and interaction with Importin α *J. Biol. Chem.*, **282** (8), 5101–5105 (2007).

Lee, S. *et al.* Defining binding efficiency and specificity of auxins for SCF *ACS Chem. Biol.*, **9**, 673-682 (2014).

Lemoine, D., Habermacher, C., Martz, A., Méry, P. & Bouquier, N. Optical control of an ion channel gate *Proc. Natl. Acad. Sci. U. S. A.,* **110** (51), 20813-20818 (2013).

Leong, H. S. *et al.* Imaging the impact of chemically inducible proteins on cellular dynamics in vivo *PLoS One*, **7** (1)**,** e30117 (2012).

Lester, H. A. and Nerbonne, J. M. Physiological and pharmacological manipulations with light flashes, *Ann. Rev. Biophys. Bioeng*., **11**, 151–175, (1982).

Levskaya, A., Weiner, O.D., Lim, W.A. and Voigt, C.A. Spatiotemporal control of cell signalling using a light-switchable protein interaction *Nature*, **461**, 997–1001 (2009).

Liang, F., Qi Ho, W., and Crabtree, G. R. Engineering the ABA plant stress pathway for regulation of induced proximity *Sci. Signal.*, **4** (164), (2011).

Lipkowitz, S. and Weissman, A. M. RINGs of good and evil: RING finger ubiquitin ligases at the crossroads of tumour suppression and oncogenesis *Nat. Rev. Cancer.*, **11** (9), 629-643 (2013).

Liu, J., He, F. & Ma, J. Morphogen gradient formation and action: insights from studying Bicoid protein degradation *Fly,* **5,** 242–246 (2011).

Liu J. and Ma J. Fates-shifted, a novel F-box protein that targets Bicoid for degradation, regulates developmental fate determination in Drosophila embryos *Nat. Cell. Biol.*, **13** (1), 22-29 (2011).

Long, M. J. C., Gollapalli, D. R. & Hedstrom, L. Inhibitor mediated protein degradation *Chem. Biol.,* **19,** 629–637 (2012).

Loria, P. M., Duke, A., Rand, J. B. & Hobert, O. Two neuronal, nuclear-localized RNA binding proteins involved in synaptic transmission *Curr. Biol.,* **13,** 1317–1323 (2003).

Lydeard, J. R., Schulman, B. & Harper, J. W. Building and remodelling Cullin-RING E3 ubiquitin ligases *EMBO Rep.,* **14,** 1050–61 (2013).

Mao, P., Meas, R., Dorgan, K. M. & Smerdon, M. J. UV damage-induced RNA polymerase II stalling stimulates H2B deubiquitylation *Proc. Natl. Acad. Sci. U. S. A.,* **111** (35), 12811-12816 (2014).

Marín, I. Animal HECT ubiquitin ligases: evolution and functional implications *BMC Evol. Biol.,* **10,** 56 (2010).

Matsuzaki M., Hayama T., Kasai H., and Ellis-Davies G. C.R. Two-photon uncaging of γ-aminobutyric acid in intact brain tissue, *Nat. Chem. Biol.*, **6** (4), 255–257. (2014).

Mariotta, L., Ramadan, T., Singer, D., Guetg, A., Herzog, B., Stoeger, C., Palacín, M., *et al.* T-type amino acid transporter TAT1 (Slc16a10) is essential for extracellular aromatic amino acid homeostasis control *J. Physiol.*, **590,** 6413–6424 (2012).

Matouschek, a. & Finley, D. An ancient portal to proteolysis *Science,* **337,** 813–814 (2012).

Metzger, M. B., Pruneda, J. N., Klevit, R. E. & Weissman, A. M. RING-type E3 ligases: Master manipulators of E2 ubiquitin-conjugating enzymes and ubiquitination *Biochim. Biophys. Acta,* **1843,** 47–60 (2014).

Mills, E., Chen, X., Pham, E., Wong, S. and Truong, K. Engineering a photoactivated caspase-7 for rapid induction of apoptosis *ACS Synth. Biol.*, **1**, 75–82 (2012).

Miesenböck G., Optogenetic control of cells and circuits. *Annu. Rev. Cell. Dev. Biol*., **27**, 731–758 (2011).

Miyamoto, T., DeRose, R., Suarez, A., Ueno, T., Chen, M., Sun, T., Wolfgang, M.J., Mukherjee, C., Meyers, D.J., Inoue, T. Rapid and orthogonal logic gating with a gibberellin-induced dimerization system *Nat. Chem. Biol*., **8**, 465–470 (2012).

Möglich, A. & Hegemann, P. Programming genomes with light *Nature*, **500**, 406–408 (2013).

Morawska, M., & Ulrich, H. D. An expanded tool kit for the auxin-inducible degron system in budding yeast *Yeast*, **30**, 341–351 (2013).

Morin, X., Daneman, R., Zavortink, M., & Chia, W. A protein trap strategy to detect GFP-tagged proteins expressed from their endogenous loci in Drosophila *Proc. Natl. Acad. Sci. U. S. A.*, **98** (26), 15050-15055 (2001).

Muller, K., Weber, W. Optogenetic tools for mammalian systems *Molecular BioSystems*, **9**, 596–608 (2013).

Muller,K.,Engesser,R.,Schulz,S.,Steinberg,T.,Tomakidi,P.,Weber, C.C., Ulm, R., Timmer, J., Zurbriggen, M.D. and Weber, W. Multi-chromatic control of mammalian gene expression and signaling *Nucleic Acids Res.*, **41** (12), e124 (2013).

Murakami, Y., Matsufuji, S. & Hayashi, S. Degradation of Ornithine decarboxylase by the 26S proteasome *Biochem. Biophys. Res. Comm*., **267,** 1–6 (2000).

Nagy, V. & Dikic, I. Ubiquitin ligase complexes: From substrate selectivity to conjugational specificity *Biol. Chem.*, **391,** 163–169 (2010).

Nakayama, K. I. & Nakayama, K. Ubiquitin ligases: cell-cycle control and cancer *Nat. Rev. Cancer,* **6,** 369–381 (2006).

Nawaz, H. M. , Blomberg, K. E. , Lindvall, J. M. , Kurosaki, T., Smith, C. I. Expression profiling of chicken DT40 lymphoma cells indicates clonal selection of knockout and gene reconstituted cells *Biochem. Biophys. Res. Commun*, **377**(2), 584-588 (2008).

Neefjes, J. & Dantuma, N. P. Fluorescent probes for proteolysis: tools for drug discovery *Nat. Rev. Drug Disc.*, **3,** 58-69 (2004).

Neklesa, T. K. *et al.* Small-molecule hydrophobic tagging-induced degradation of HaloTag fusion proteins *Nat. Chem. Biol.,* **7,** 538–543 (2011).

Nellen, D., Affolter, M., Basler, K. Receptor serine/threonine kinases implicated in the control of Drosophila body pattern by decapentaplegic *Cell,* **78** (2):225-237 (1994).

Nichols, C. G., Lederer, W. J. Modulation of ATP-sensitive potassium channel activity by flash-photolysis of 'caged-ATP' in rat heart cells. *Pflugers Arch.,* **415** (4), 510-512 (1990).

Niopek, D., Benzinger, D., Roensch, J., Draebing, T., Wehler, P., Eils, R., Di Ventura, B. Engineering light-inducible nuclear localization signals for precise spatiotemporal control of protein dynamics in living cells. *Nat. Comm.,* **5,** 4404-4411 (2014).

Nishimura, K., Fukagawa, T., Takisawa, H., Kakimoto, T. & Kanemaki, M. An auxin-based degron system for the rapid depletion of proteins in nonplant cells *Nat. Methods,* **6,** 917–922 (2009).

Noguchi, E., Ansbach, A. B., Noguchi, C. & Russell, P. Assays used to study the DNA replication checkpoint in fission yeast *Methods Mol. Biol.,* **521,** 493–507 (2009).

Novatchkova, M., Tomanov, K., Hofmann, K., Stuible, H. P. & Bachmair, A. Update on sumoylation: Defining core components of the plant SUMO conjugation system by phylogenetic comparison *New Phytol.,* **195,** 23–31 (2012).

Ouyang, X. & Chen, J. K. Synthetic strategies for studying embryonic development *Chem. Biol.,* **17,** 590–606 (2010).

Palacín, M., Estévez, R., Bertran, J., Zorzano, A. Molecular biology of mammalian plasma membrane amino acid transporters *Physiol Rev.,* **78** (4), 969-1054 (1998).

Park, E. C., Finley, D., Szostak, J. W. A strategy for the generation of conditional mutations by protein destabilization *Proc. Natl. Acad. Sci. U. S. A.*, **89**, 1249–1252 (1992).

Park, Y. & Yoon, S. K. The HECT domain of TRIP12 ubiquitinates substrates of the ubiquitin fusion degradation pathway *Journ. Biol. Chem.,* **284**, 1540-1549 (2009).

Park, A., Won, S. T., Pentecost, M., Bartkowski, W. & Lee, B. CRISPR/Cas9 allows efficient and complete knock-in of a destabilization domain-tagged essential protein in a human cell line, allowing rapid knockdown of protein function *PLoS One,* **9,** 1–8 (2014).

Pathak, G. P., Strickland, D., Vrana, J. D. & Tucker, C. L. Benchmarking of optical dimerizer systems *ACS Synth. Biol.,* **3**, 835-838 (2014).

Peterson-Kaufman, K. J., Carlson, C. D., Rodríguez-Martínez, J.& Ansari, A. Z. Nucleating the assembly of macromolecular complexes *ChemBioChem.,* **11,** 1955–1962 (2010).

Petroski, M. D. & Deshaies, R. J. Function and regulation of cullin-RING ubiquitin ligases *Nat. Rev. Mol. Cell Biol.,* **6,** 9–20 (2005).

Pierre-Jerome, E., Jang, S. S., Havens, K., Nemhauser, J. L. & Klavins, E. Recapitulation of the forward nuclear auxin response pathway in yeast *Proc. Natl. Acad. Sci. U. S. A.,* **111,** 9407–9412 (2014).

Pinheiro, A. V., Baptista, P., & Lima, J. C. Light activation of transcription: photocaging of nucleotides for control over RNA polymerization. *Nucleic acids research*, **36** (14), e90 (2008).

Polstein, L. R., & Gersbach, C. A. Light-inducible spatiotemporal control of gene activation by customizable Zinc finger transcription factors, *J. Am. Chem. Soc.*, **13**, 16480-16483 (2012).

Portnoff, A. D., Stephens, E. A., Varner, J. D. & Delisa, M. P. Ubiquibodies , synthetic E3 ubiquitin ligases endowed with unnatural substrate specificity for targeted protein *J. Biol. Chem.*, **289,** 7844–7855 (2014).

Pratt, M. R., Schwartz, E. C. & Muir, T. W. Small-molecule-mediated rescue of protein function by an inducible proteolytic shunt *Proc. Natl. Acad. Sci. U. S. A.*, **104,** 11209-11214 (2007).

Qian, S., Waldron, L., Klevit, R. E., Walter, J. & Patterson, C. Engineering a ubiquitin ligase reveals conformational flexibility required for ubiquitin transfer *J. Biol. Chem.*, **284** (39), 26797-26802 (2009).

Raina, K. & Crews, C. M. Chemical inducers of targeted protein degradation *J. Biol. Chem.*, 11057–11060, **285** (15), 11057-11060 (2010).

Raina, K. *et al.* Targeted protein destabilization reveals an estrogen-mediated ER stress response *Nat. Chem. Biol.*, **10,** 957–962 (2014).

Renicke, C., Schuster, D., Usherenko, S., Essen, L. O. & Taxis, C. A LOV2 domain-based optogenetic tool to control protein degradation and cellular function *Chem. Biol.*, **20,** 619–626 (2013).

Riggsbee, C. W. & Deiters, A. Recent advances in the photochemical control of protein function *Trends Biotechnol.*, **28,** 468–475 (2011).

Robinson, M., Sahlender, D., and Foster, S. Rapid inactivation of proteins by Rapamycin-induced rerouting to mitochondria. *Dev. Cell.*, **18** (2-3), 324–331 (2010).

Rodriguez, S. and Wolfgang, M. J. Targeted chemical-genetic regulation of protein stability in vivo *Chem. Biol.*, **19** (3), 391–398 (2012).

Ryding, A. D., Sharp, M. G., Mullins, J. J. Conditional transgenic technologies *J Endocrinol.,* **171**(1), 1-14 (2001).

Saha, A. and Deshaies, R. Multimodal activation of the ubiquitin ligase SCF by Nedd8 conjugation *Mol. Cell.*, **32** (1), 21–31 (2009).

Saifee, N. H. & Zheng, N. A ubiquitin-like protein unleashes ubiquitin ligases *Cell*, **135,** 209–211 (2008).

Sakamoto, K. M. *et al.* PROTACs: chimeric molecules that target proteins to the Skp1-Cullin-F box complex for ubiquitination and degradation *Proc. Natl. Acad. Sci. U. S. A.,* **98,** 8554–8559 (2001).

Samant, R. S. & Workman, P. Molecular biology: Choose your protein partners *Nature,* **490,** 351–352 (2012).

Sarikas, A., Hartmann, T. & Pan, Z.-Q. The cullin protein family *Genome Biol.,* **12,** 220 (2011).

Sauer, M., Robert, S. & Kleinevehn, J. Auxin : simply complicated *J. Exp. Bot.,* **64** (9), 2565-2577 (2013).

Sawyer, C., Kirsch, J. Letter: Kinetic isotope effects for the chymotrypsin catalyzed hydrolysis of ethoxyl-18 O labeled specific ester substrates *J. Am. Chem. Soc.,* **97**(7), 1963-1964 (1975).

Schneekloth, J. S. & Crews, C. M. Chemical approaches to controlling intracellular protein degradation *ChemBioChem.,* **6,** 40–46 (2005).

Schrima, A. *et al.* Detecting UV-lesions in the genome: The modular CRL4 ubiquitin ligase does it best! *FEBS Lett.,* **585,** 2818–2825 (2011).

Schulman, B. a *et al.* Insights into SCF ubiquitin ligases from the structure of the Skp1-Skp2 complex *Nature,* **408,** 381–386 (2000).

Sellmyer, M. a., Chen, L. C., Egeler, E. L., Rakhit, R. & Wandless, T. J. Intracellular context affects levels of a chemically dependent destabilizing domain *PLoS One,* **7,** 1–9 (2012).

Shao, Q. & Xing, B. Photoactive molecules for applications in molecular imaging and cell biology *Chem. Soc. Rev.,* **39**, 2835–2846 (2010).

Shaw, G., Morse, S., Ararat, M., & Graham, F. L. Preferential transformation of human neuronal cells by human adenoviruses and the origin of HEK 293 cells *FASEB J.,* **1**(2) (2002).

Sheikh, M. O. *et al.* Glycosylation of Skp1 affects its conformation and promotes binding to a model F - Box protein *Biochemistry,* **53**, 1657-1669 (2014).

Shimizu-Sato, S., Huq, E., Tepperman, J.M. and Quail, P.H. A light-switchable gene promoter system *Nat. Biotechnol.,* **20**, 1041–1044 (2002).

Sinha, D. K. *et al.* Photocontrol of protein activity in cultured cells and Zebrafish with one- and two-photon illumination *ChemBioChem.*, **11**, 653–663 (2010).

Skaar, J. R., Pagan, J. K., Pagano, M. SCF ubiquitin ligase-targeted therapies *Nat Rev Drug Discov.,* **13** (12), 889-903 (2014).

Skwarczynska, M., Molzan, M. & Ottmann, C. Activation of NF-κB signalling by fusicoccin-induced dimerization *Proc. Natl. Acad. Sci. U. S. A.*, **110,** 377–386 (2013).

Snapp, E. Design and use of fluorescent fusion proteins in cell biology *Curr Protoc. Cell Biol.*, **21.4** WILEY (2005).

Specht, A, Thomann, J. S., Alarcon, K., Wittayanan, W., Ogden, D., Furuta, T., Kurakawa, Y., Goeldner, M. New photoremovable protecting groups for carboxylic acids with high photolytic efficiencies at near-UV irradiation. Application to the photocontrolled release of L-glutamate. *Chembiochem.,* **11**, 1690-1695 (2006).

Sriram, S. M., Kim, B. Y. & Kwon, Y. T. The N-end rule pathway: emerging functions and molecular principles of substrate recognition *Nat. rev. Mol.Cell Biol.,* **12,** 735–747 (2011).

Staller, M. V, Fowlkes, C. C. & Bragdon, M. D. J. A gene expression atlas of a bicoid depleted Drosophila embryo reveals early canalization of cell fate *Development,* **142**, 587–596 (2014).

Stankunas, K., Bayle, J. H., Gestwicki, J. E., Lin, Y. M., Wandless, T. J., Crabtree, G. R. Conditional protein alleles using knockin mice and a chemical inducer of dimerization *Mol.Cell.*, **12**, 1615–1624 (2003).

Stoient, J. D., & Wangt, R. J. Effect of near-ultraviolet and visiblelight on mammalian cells in culture. Formation of toxic photoproducts in tissue culture medium by blacklight *Proc. Natl. Acad. Sci. U. S. A.*, **71** (10), 3961–3965 (1974).

Strickland, D., Lin, Y., Wagner, E., Hope, C.M., Zayner, J., Antoniou, C., Sosnick, T.R., Weiss, E.L. and Glotzer, M. TULIPs: tunable, light-controlled interacting protein tags for cell biology *Nat. Meth.*, **9**, 379–384 (2012).

Sun, N., Sun, C., Lin, C., Pai, L. & Chao, C. C. K. Damaged DNA-binding protein 2 (DDB2) protects against UV irradiation in human cells and Drosophila *J. Biomed. Sci.*, **17**, 27 (2010).

Suraweera, A., Münch, C., Hanssum, A. & Bertolotti, A. Failure of amino acid homeostasis causes cell death following proteasome inhibition. *Mol. Cell*, **48,** 242–253 (2012).

Taslimi, A. *et al.* An opimized optogenetic clustering tool for probing protein interaction and function *Nat. Commun.*, **5**, 4925 (2015).

Taxis, C. Stier G., Spadaccini R.& Knop M. Efficient protein depletion by genetically controlled deprotection of a dormant N-degron *Mol. Sys. Biol.,* **5** (269), 1-7 (2009).

Teague, S.J. Facile synthesis of a o-nitrobenzyl photolabile linker for combinatorial chemistry *Tet. Lett.*, **37**, 5751-5754 (1996).

Teale, W., Paponov, I., Palme, K. Auxin in action: signalling, transport and the control of plant growth and development *Nat. Rev. Mol. Cell Biol.,* **11**, 847-859 (2006).

Terrile, C. *et al.* Nitric oxide influences auxin signaling through S-Nitrosylation of the *Arabidopsis* transport inhibitor response1 auxin receptor *Plant J.*, **70,** 492–500 (2013).

Tischer, D. & Weiner, O. D. Illuminating cell signalling with optogenetic tools *Nat. Publ. Gr.*, **15,** 551–558 (2014).

Toettcher, J. E., Voigt, C. A., Weiner, O. D. & Lim, W. A. The promise of optogenetics in cell biology : interrogating molecular circuits in space and time *Nat. Meth.*, **8,** 35–38 (2011).

Tsutsui, H., Karasawa, S., Shimizu, H., Nukina, N., Miyawaki, A. Semi-rational engineering of a coral fluorescent protein into an efficient highlighter *EMBO Rep.,* **6**, 233-238 (2005).

Tuck, C., Zhang, T., Potapova, T., Malumbres, M. & Novák, B. Robust mitotic entry is ensured by a latching switch *Biol. Open*, **2,** 924–931 (2013).

Umeda, N., Ueno, T., Pohlmeyer, C. & Nagano, T. A Photocleavable Rapamycin conjugate for spatiotemporal control of small GTPase activity *J. Am. Chem. Soc.*, **133,** 12–14 (2011).

Usherenko, S. *et al.* Photo-sensitive degron variants for tuning protein stability by light *BMC Syst. Biol.*, **8** (128) (2014).

van Leuken R., Clijsters L., Wolthuis R. To cell cycle, swing the APC/C *Biochim. Biophys. Acta.,* **1786** (1), 49-59 (2008).

Varshavsky, A. The N-end rule pathway and regulation by proteolysis *Protein Sci.,* **20,** 1298–1345 (2011).

Vassilev, L. T., Tovar, C., Chen, S., Knezevic, D., Zhao, X., Sun, H., Heimbrook, D. C., *et al.* Selective small-molecule inhibitor reveals critical mitotic functions of human CDK1 *Proc. Natl. Acad. Sci. U. S. A.,* **103** (28), 10660-10665 (2006).

Veldhuyzen, W. F., Nguyen, Q., Mcmaster, G. & Lawrence, D. S. A light-activated probe of intracellular protein kinase activity *J. Am. Chem. Soc.*, **125**, 13358–13359 (2003).

Vendruscolo, M. Protein dynamics under light control *Nat. Chem. Biol.*, **4,** 449–450 (2008).

Viappiani, C., Nonell, S. & Andreas, M. Photofunctional proteins: from understanding to engineering Engineered photoreceptors as novel optogenetic tools *Photochem. Photobiol.Sci.*, **9**, 1286-1300 (2010).

Villalobos, C. *et al.* A combinatorial TIR1/AFB–Aux/IAA co-receptor system for differential sensing of auxin *Nat. Chem. Biol.*, **8**, 477-485 (2012).

Wartlick, O., Kicheva, A. & González-Gaitán, M. Morphogen gradient formation *Cold Spring Harb. Perspect. Biol.*, **1,** 1–22 (2009).

Wend, S. *et al.* A quantitative ratiometric sensor for time-resolved analysis of auxin dynamics *Sci. Rep.*, **3** (2052), 1-7 (2013).

Wright, C. W., Guo, Z.-F. & Liang, F.-S. Light control of cellular processes by using photocaged Abscisic acid *ChemBioChem*, **16,** 254–261 (2015).

Wright, R. C. & Nemhauser, J. L. New tangles in the auxin signaling web *F1000Prime Rep.*, **7,** 1–7 (2015).

Wu, Y.I., Frey, D., Lungu, O.I., Jaehrig, A., Schlichting, I., Kuhlman, B. and Hahn, K.M. A genetically encoded photoactivatable Rac controls the motility of living cells *Nature,* **461**, 104–108 (2009).

Xu, G., Ma, H., Nei, M., & Kong, H. Evolution of F-box genes in plants : Different modes of sequence divergence and their relationships. *Proc. Natl. Acad. Sci. U. S. A.*, **106** (3), 835–840 (2009).

Yang, Y., Xu, R., Ma, C.-J., Vlot, C., Klessig, D. F., & Pichersky, E. Inactive methyl indole-3-acetic acid ester can be hydrolyzed and activated by several esterases belonging to the AtMES esterase family of Arabidopsis *Plant physiol.*, **147** (3), 1034–1045 (2008).

Yu, H. *et al.* Mutations in the TIR1 auxin receptor that increase affinity for auxin/indole-3-acetic acid proteins result in auxin hypersensitivity *Plant Physiol.,* **162,** 295–303 (2013).

Yuan, J., Yan, R., Krämer, A., Eckerdt, F., Roller, M., Kaufmann, M., & Strebhardt, K. Cyclin B1 depletion inhibits proliferation and induces apoptosis in human tumor cells *Oncogene*, **23** (34), 5843–5852 (2004).

Zhang, J., Zheng, N. & Zhou, P. Exploring the functional complexity of cellular *Proc. Natl. Acad. Sci. U. S. A.*, **100,** 14127–14132 (2003).

Zeng. X. and King. R. An APC/C inhibitor stabilizes cyclin B1 by prematurely terminating ubiquitination *Nat. Cell. Biol.* **8** (4), 383–392 (2012).

Zheng, X., Wu, S., Zhai, H., Zhou, P., Song, M., Su, L., Xi, Y., *et al. Arabidopsis* phytochrome B promotes SPA1 nuclear accumulation to repress photomorphogenesis under far-red light. *The Plant cell*, **25** (1), 115–133 (2013).

Zhou, P., Bogacki, R., Mcreynolds, L. & Howley, P. M. Harnessing the ubiquitination machinery to target the degradation of specific cellular proteins *Mol. Cell*, **6,** 751–756 (2000).

Zhou, X. X., Hokyung K., Lam A. J., and Lin M. Z. Optical control of protein activity by fluorescent protein domains, *Science*, **338** (6108), 810–814 (2012).

Zhou, W., Wei, W. & Sun, Y. Genetically engineered mouse models for functional studies of SKP1-CUL1-F-box-protein (SCF) E3 ubiquitin ligases *Cell Res.*, **23,** 599–619 (2013).

Zoltowski, B. D., Vaccaro, B. & Crane, B. R. Mechanism-based tuning of a LOV domain photoreceptor *Nat. Chem. Biol.*, **5** (11), 827-834 (2009).

Zuin, A., Isasa, M. & Crosas, B. Ubiquitin signaling: extreme conservation as a source of diversity *Cells*, **3,** 690–701 (2014).

Résumé

La régulation de la protéolyse est un outil efficace pour le contrôle de la fonction d'une protéine dans des cellules. Nous présentons dans ce travail une stratégie générique permettant d'activer la protéolyse de façon conditionnelle par la lumière, améliorant ainsi la résolution spatio-temporelle. Notre approche repose sur un système de dégradation inductible par l'auxine (AID), mis au point en transposant des composants de la voie de dégradation contrôlée par l'auxine existant chez les plantes dans des cellules de mammifères. Nous présentons une version optimisée du système AID qui a permis de diminuer de façon significative la stabilité de protéines cibles en présence d'auxine. Nous avons en parallèle développé un déclencheur de dégradation photo-activable sous la forme d'une auxine cagée. Une illumination courte et locale permet la libération efficace de l'auxine dans les cellules et induit la dégradation de protéine d'intérêt avec un bon contrôle spatiotemporel. Cette méthode générique a été utilisée dans des contextes nucléaires et cytoplasmiques.

Mots-clefs: molécules cagées, *chemical biology*, optogénetique, protéasome, ubiquitine.

Abstract

The regulation of proteolysis is an efficient way to control protein function in cells. Here, we present a general strategy enabling to increase the spatiotemporal resolution of conditional proteolysis by using light activation as trigger. Our approach relies on the auxin-inducible degradation (AID) system obtained by transposing components of the plant auxin-dependent degradation pathway in mammalian cells. We developed an optimized version of the AID which enables to significantly destabilize target proteins in presence of auxin. Parallely, we developed a photoactivatable auxin that acts as a photoactivatable inducer of degradation. Upon local and short light illumination, auxin is released in cells and triggers the degradation of a protein of interest with spatiotemporal control. This generic method was implemented in nuclear and cytoplasmic contexts.

Keywords: caged molecule, chemical biology, optogenetics, proteasome, ubiquitin.